# MICROWAVE BEHAVIOR OF SILICON CARBIDE/ HIGH ALUMINA CEMENT COMPOSITES

By

KRISTIE SUE LEISER

A DISSERTATION PRESENTED TO THE GRADUATE SCHOOL
OF THE UNIVERSITY OF FLORIDA IN PARTIAL FULFILLMENT
OF THE REQUIREMENTS FOR THE DEGREE OF
DOCTOR OF PHILOSOPHY

UNIVERSITY OF FLORIDA

2001

I would like to dedicate this dissertation to my family and friends. This could not have been accomplished without your support.

ACKNOWLEDGMENTS

I would like to thank a number of people for their support and assistance during my graduate career. I would like to thank Dr. David E. Clark for his guidance and help that allowed me to complete this study. He showed me what the real professional world might be like, and helped to show me how to succeed in it. I would also like to thank Drs. Hassan El-Shall, Christopher Batich, Joseph Simmons, and Dinesh Shah for their comments and advice. I would especially like to acknowledge the support of Dr. E. Dow Whitney for his assistance and his good-natured disposition that in the early days of my graduate career always helped brighten my days.

I would also like to thank my present and former colleagues in Dr. Clark's research group, including Robert Di Fiore, Diane Folz, Becky Schulz, Greg Darby, Duangduen Atong, Mark Moore, Attapon Boonyapiwat, and Dr. Jon West. In addition, I would like to thank my peers in the Department of Materials Science and Engineering at the University of Florida, including Kimberly Christmas, Gavin McDaniel, Gwen Clark, and Tyler Lendi. A special thanks goes to Kimberly Christmas for her help, moral support, and most especially for her urgings not to give up.

I would like to express my gratitude to my family and my long-time friend Natalie. All of my brothers (Dean, Scott and Jeff) did their best to encourage me throughout graduate school. And my sister Julie could always make me smile. Knowing

that my parents believed in me always helped me get through bad days. I would also like to thank my father for his technical advice, as well as for giving me the benefit of knowing about his own experiences in graduate school. My long-time friend Natalie was always there to support me when I needed her, even though we lived across the country from each other. I would most especially like to thank my husband, Robert, who has been there throughout the very long days and the bad temper that went with those long days. His love and support throughout this time helped to keep me focused on my goals, and helped renew my own faith in what I could accomplish.

This research was sponsored in part by a National Science Foundation Graduate Fellowship.

TABLE OF CONTENTS

ACKNOWLEDGMENTS ..... iii

LIST OF TABLES ..... vii

LIST OF FIGURES ..... ix

ABSTRACT ..... xviii

CHAPTERS

1 INTRODUCTION ..... 1
General Introduction ..... 1
Outline of Study ..... 4

2 BACKGROUND ..... 6
Microwave General Characteristics ..... 6
Microwave Theory ..... 16
Sources of Dielectric Loss ..... 16
Dielectric Loss Equations ..... 26
Dielectric Property Measurements ..... 39
Partially Filled Waveguide Methods ..... 49
Cavity Perturbation Methods ..... 49
Partially-Filled Cavity Method ..... 52
Open-Ended Coaxial Probe ..... 52
Lumped-Circuit Parallel-Plate Capacitor ..... 53
Dielectric Measurement Technique Comparison ..... 53
Microwave Heating Mechanisms ..... 54
Types of Microwave Behavior ..... 57
Temperature Measurement ..... 65

3 MATERIALS AND EXPERIMENTAL PROCEDURE ..... 69
Sample Fabrication ..... 70
Phase I ..... 73
Phase II ..... 77
Phase III ..... 78
Phase IV ..... 82
Summary of Heating Conditions ..... 85
Sample Characterization ..... 86

"Green" Sample Characterization ..... 86
Processed Sample Characterization ..... 87
Characterization Methods ..... 87
X-Ray Diffraction (XRD) ..... 87
Particle Sizing ..... 89
Scanning Electron Microscopy (SEM) ..... 90
Energy Dispersive X-Ray Spectroscopy (EDX) ..... 93
Thermogravimetric Analysis/Differential Thermal Analysis (TGA/DTA) ..... 95
Thermocouple ..... 97

4 RESULTS ..... 101
Phase I ..... 101
Phase II ..... 110
Phase III ..... 123
Phase IV ..... 142

5 DISCUSSION ..... 193
General Discussion ..... 193
Phase I ..... 193
Major Results From Phase I ..... 199
Phase II ..... 199
Major Results From Phase II ..... 203
Phase III ..... 205
Major Results From Phase III ..... 225
Phase IV ..... 225
Major Results From Phase IV ..... 236
Specific Issues ..... 237
Particle Size Behavior ..... 237
Percolation Theory ..... 245
Other Issues ..... 261

6 SUMMARY AND CONCLUSIONS ..... 264

7 SUGGESTIONS FOR FUTURE WORK ..... 269

REFERENCES ..... 270

BIOGRAPHICAL SKETCH ..... 288

LIST OF TABLES


Table 2.1. Characteristics and advantages of microwave processing of ceramics. ..... 7

Table 2.2. Challenges of microwave processing. ..... 12

Table 2.3. Obstacles to commercialization of microwave processing..... 12

Table 3.1. Composition and processing of composite samples for phase III. ..... 82

Table 3.2. Depth of focus based on magnification and divergence of the electron beam..... 93

Table 3.3. Factors that influence the TGA curve..... 96

Table 3.4. Factors that influence the DTA curve..... 98

Table 3.5. Potential causes for DTA peaks..... 98

Table 3.6. Thermocouple systems and their recommended usage environments..... 99

Table 4.1. Temperature after 270 seconds of microwave heating (°C). ..... 109

Table 4.2. Steady state microwave heating rates of susceptors (°C/sec)..... 110

Table 4.3. Compounds detected by XRD in 40 weight percent silicon carbide composite samples..... 117

Table 4.4. Steady state microwave heating rates of susceptors (°C/sec)..... 117

Table 4.5. Significance levels from ANOVA for composite samples run to 600 °C..... 125

Table 4.6. Significance levels from ANOVA for composite samples run to 1200 °C..... 125

Table 4.7. Significance levels from ANOVA for all samples combined. ..... 126

Table 4.8. Summary of heating rate behavior of composites as affected by presence of air or nitrogen, as determined from Figure 4.59 - Figure 4.67. ..... 175

Table 4.9. Heating rates of composite samples heated in flowing air depending upon temperature range. (°C/min.) ..... 186

Table 4.10. Heating rates of composite samples heated in flowing nitrogen depending upon temperature range. (°C/min.) ..... 186

Table 4.11. Significance levels of the factors for composites heated in flowing air as determined by ANOVA ..... 188

Table 4.12. Significance levels of the factors for composites heated in flowing nitrogen as determined by ANOVA. ..... 189

Table 4.13. Significance levels of the factors for all composites as determined by ANOVA. ..... 191

Table 5.1. Calculated time (min.) required to raise the temperature of "coarse", "fine" and mixed silicon carbide composites by 600 °C, depending upon sample composition. ..... 198

Table 5.2. Calculated time (min.) required to raise the temperature of α- and β-phase silicon carbide composites by 600 °C, depending upon sample composition. ..... 205

Table 5.3. Calculated heating rate equations of composites as a function of weight percent silicon carbide. ..... 236

Table 5.4. Maximum distance possible between two spherical particles of silicon carbide in a spherical composite using theoretical densities. ..... 258

Table 5.5. Maximum distance possible between two cubical particles of silicon carbide in a cubical composite using theoretical densities. ..... 258

Table 5.6. Maximum distance possible between two spherical particles of silicon carbide in a spherical composite using experimental densities. ..... 259

Table 5.7. Maximum distance possible between two cubical particles of silicon carbide in a cubical composite using experimental densities. ..... 259

LIST OF FIGURES

Figure 2.1. In a conventional furnace, the surface of the sample will be heated first, as shown. In order for the interior to be heated, the heat from the surface must be conducted to the center of the sample. Whereas, in a microwave furnace, the interior of the sample will be hottest, and the surface will tend to radiate the heat to the atmosphere, so that the surface will tend to be cooler than the interior. ..... 8

Figure 2.2. Effective loss factor as a function of temperature, where $T_c$ represents the critical temperature above which the loss factor increases extremely rapidly. See equation [2.25] for a quantitative description of $\varepsilon''_{eff}$. ..... 15

Figure 2.3. The change in the electric field between the plates of a capacitor with no dielectric (a) and with a dielectric (b). The presence of the dielectric in (b) weakens the original electric field, E, between the two plates. ..... 18

Figure 2.4. Electric dipole moment between two atoms of charge q, with separation between charges denoted by $\delta$. ..... 20

Figure 2.5. Frequency dependence of individual polarization mechanisms. ..... 23

Figure 2.6. Representation of the four different types of polarization mechanisms. ..... 24

Figure 2.7. Time dependent behavior of (a) an ideal dielectric and (b) a real dielectric when subject to a voltage. ..... 29

Figure 2.8. Phase shift, $\delta$, in the induced current caused by the time delay in real dielectric materials. ..... 30

Figure 2.9. Using the dielectric mixture equations, a variety of different curves for the calculated relative dielectric constant are obtained. ..... 33

Figure 2.10. Variation of the real part of the dielectric constant for copper particles in epoxy in relation to copper particle size. ..... 35

Figure 2.11. Frequency dependence of the relative dielectric constant ($\varepsilon_r$' or k') , and relative dielectric loss factor ($\varepsilon_r$" or k") and the loss tangent as a function of frequency. 40

Figure 2.12. Frequency dependence of the loss tangent for various silicate glasses. 41

Figure 2.13. Relationship between frequency, temperature, and dielectric constant of an aluminum oxide crystal with the applied field perpendicular to the c-axis of the crystal. 42

Figure 2.14. Relationship between frequency, temperature and dielectric constant of a soda-lime-silica glass. 43

Figure 2.15. Dielectric loss peak shift in a $Li_2O \bullet 2SiO_2$ (L2S) glass due to increasing temperature. 44

Figure 2.16. Time and temperature dependence of the frequency of the dielectric loss peak for an L2S glass heated to 500 °C. (see Figure 2.15) 45

Figure 2.17. Change in loss tangent as a function of temperature for a soda-lime-silica glass and for a fused silica glass. 46

Figure 2.18. Change in loss tangent and relative dielectric constant ($\varepsilon_r$' or k') as a function of temperature and frequency for a steatite ceramic. 47

Figure 2.19. Change in loss tangent and relative dielectric constant ($\varepsilon_r$' or k') as a function of temperature and frequency for an alumina porcelain. 48

Figure 2.20. Schematic diagram for dielectric measurements made by Roberts and von Hippel using the partially filled waveguide method. 50

Figure 2.21. Schematic diagram of apparatus used for the two-impedance method for dielectric measurements. 51

Figure 2.22. Measurement of the dielectric constant of "Type N" silicon carbide as a function of temperature at 2.45 GHz. 55

Figure 2.23. Measurement of the dielectric loss factor of "Type N" silicon carbide as a function of temperature at 2.45 GHz. 56

Figure 2.24. Illustration of types of microwave interactions with materials. The material under examination in this study falls in the category of mixed absorber. 58

Figure 2.25. Skin depth, d (or $\delta$) in a metal as a function of resistivity and wavelength in air. 60

Figure 3.1. Schematic of the experimental procedure used to make the composite samples. ..... 72

Figure 3.2. Diagram of the experimental setup used for microwave heating. ..... 76

Figure 3.3. Diagram of the experimental setup used starting in phase III of the experiment. ..... 80

Figure 3.4. Conditions for x-ray diffraction. ..... 88

Figure 3.5. Illustration of depth of field attainable in an SEM image. ..... 92

Figure 3.6. Atomic energy level diagram with characteristic x-ray emissions illustrated. ..... 94

Figure 4.1. Heating rates of the susceptors using 1000 μm low-purity "coarse" silicon carbide particles. ..... 103

Figure 4.2. Heating rates of the susceptors using 85 μm low-purity "fine" silicon carbide particles. ..... 104

Figure 4.3. Heating rates of 10 weight percent silicon carbide composite samples containing different particle sizes of silicon carbide. ..... 106

Figure 4.4. Heating rates of 30 weight percent silicon carbide composite samples containing different particle sizes of silicon carbide. ..... 107

Figure 4.5. Heating rates of 50 weight percent silicon carbide composite samples containing different particle sizes of silicon carbide. ..... 108

Figure 4.6. Heating profiles of 40 weight percent silicon carbide composite samples before and after reaction. ..... 111

Figure 4.7. X-ray diffraction spectra for 40 weight percent α-phase silicon carbide composite samples before and after reaction. ..... 113

Figure 4.8. X-ray diffraction spectra for 40 weight percent β-phase silicon carbide composite samples before and after reaction. ..... 114

Figure 4.9. Heating profiles of 10-50 weight percent α-phase silicon carbide composite samples. ..... 115

Figure 4.10. Heating profiles of 10-50 weight percent β-phase silicon carbide composite samples. ..... 116

Figure 4.11. Heating profiles of 10 weight percent alpha and beta silicon carbide composite samples. ..... 118

Figure 4.12. Heating profiles of 20 weight percent alpha and beta silicon carbide composite samples. ..... 119

Figure 4.13. Heating profiles of 30 weight percent alpha and beta silicon carbide composite samples. ..... 120

Figure 4.14. Heating profiles of 40 weight percent alpha and beta silicon carbide composite samples. ..... 121

Figure 4.15. Heating profiles of 50 weight percent alpha and beta silicon carbide composite samples. ..... 122

Figure 4.16. Forty weight percent β-phase silicon carbide composite samples heated to 1200 °C in air and nitrogen. ..... 127

Figure 4.17. Twenty weight percent α-phase silicon carbide composite samples heated to 600 and 1200 °C in nitrogen. ..... 129

Figure 4.18. Twenty weight percent β-phase silicon carbide heated to 1200 °C in air. 130

Figure 4.19. Thirty weight percent α-phase silicon carbide heated to 1200 °C in nitrogen. ..... 131

Figure 4.20. Ten weight percent β-phase silicon carbide composite samples heated to 1200 °C in nitrogen. ..... 132

Figure 4.21. Ten weight percent α-phase silicon carbide composite samples heated to 600 °C in air ..... 134

Figure 4.22. Twenty weight percent α-phase silicon carbide composite samples heated to 600 °C in air. ..... 134

Figure 4.23. Forty weight percent α-phase silicon carbide composite samples heated to 600 °C in air ..... 135

Figure 4.24. Ten weight percent α-phase silicon carbide composite samples heated to 600 °C in nitrogen. ..... 135

Figure 4.25. Fifty weight percent β-phase silicon carbide composite samples heated to 600 °C in nitrogen. ..... 136

Figure 4.26. X-ray dotmapping of 50 weight percent β-phase silicon carbide composite samples heated to 600 °C in nitrogen..... 137

Figure 4.27. Fracture surface of 50 weight percent β-phase silicon carbide composite samples heated to 600 °C in nitrogen..... 139

Figure 4.28. Fracture surface of 30 weight percent β-phase silicon carbide composite samples heated to 600 °C in air..... 139

Figure 4.29. X-ray dotmapping of crystals found in 30 weight percent β-phase silicon carbide composite samples heated to 600 °C in air. ..... 140

Figure 4.30. Forty weight percent β-phase silicon carbide composite samples heated to 1200 °C in air..... 141

Figure 4.31. Fifty weight percent α-phase silicon carbide composite samples heated to 1200 °C in air..... 141

Figure 4.32. Thirty weight percent α-phase silicon carbide composite samples heated to 1200 °C in nitrogen. ..... 143

Figure 4.33. Forty weight percent β-phase silicon carbide composite samples heated to 1200 °C in nitrogen. ..... 143

Figure 4.34. Micrograph of the α-phase silicon carbide powder from H.C. Starck. ..... 145

Figure 4.35. Micrograph of the β-phase silicon carbide powder from H.C. Starck..... 146

Figure 4.36. Micrograph of the Alfrax 66 high alumina cement powder. ..... 146

Figure 4.37. Differential thermal analysis of composite samples and their constituent materials heated in flowing air. ..... 148

Figure 4.38. Differential thermal analysis of composite samples and their constituent materials heated in flowing nitrogen. ..... 149

Figure 4.39. Differential thermal analysis of α-phase silicon carbide composite samples heated in flowing air. ..... 150

Figure 4.40. Differential thermal analysis of β-phase silicon carbide composite samples heated in flowing air. ..... 151

Figure 4.41. Differential thermal analysis of α-phase silicon carbide composite samples heated in flowing nitrogen. ..... 153

Figure 4.42. Differential thermal analysis of β-phase silicon carbide composite samples heated in flowing nitrogen. ..... 154

Figure 4.43. Differential thermal analysis of 50 weight percent α- and β-phase silicon carbide composite samples heated in flowing air. ..... 155

Figure 4.44. Differential thermal analysis of 50 weight percent α- and β-phase silicon carbide composite samples heated in flowing nitrogen. ..... 156

Figure 4.45. Differential thermal analysis of a 30 weight percent α-phase silicon carbide composite sample heated in flowing air through two heating cycles. ..... 157

Figure 4.46. Differential thermal analysis of a 30 weight percent β-phase silicon carbide composite sample heated in flowing nitrogen through two heating cycles..... 159

Figure 4.47. Forty weight percent α-phase silicon carbide composite sample gradually heated to higher temperatures in flowing air to find the microwave transition temperature. ..... 160

Figure 4.48. Twenty weight percent β-phase silicon carbide composite sample gradually heated to higher temperatures in flowing air to find the microwave transition temperature. ..... 161

Figure 4.49. Forty weight percent α-phase silicon carbide composite sample gradually heated to higher temperatures in flowing nitrogen to find the microwave transition temperature. ..... 162

Figure 4.50. Twenty weight percent β-phase silicon carbide composite sample gradually heated to higher temperatures in flowing nitrogen to find the microwave transition temperature. ..... 163

Figure 4.51. Microwave heating behavior of composite samples heated in flowing air to 550 °C..... 165

Figure 4.52. Microwave heating behavior of composite samples heated to in flowing air 700 °C..... 166

Figure 4.53. Microwave heating behavior of composite samples heated in flowing air to 1100 °C..... 167

Figure 4.54. Magnified view of microwave heating behavior of composite samples heated in flowing air to 700 °C..... 169

Figure 4.55. Magnified view of microwave heating behavior of composite samples heated in flowing air to 1100 °C. ..... 170

Figure 4.56. Microwave heating behavior of composite samples heated in flowing nitrogen to 550 °C ..... 172

Figure 4.57. Microwave heating behavior of composite samples heated in flowing nitrogen to 700 °C ..... 173

Figure 4.58. Microwave heating behavior of composite samples heated in flowing nitrogen to 1100 °C ..... 174

Figure 4.59. Ten weight percent silicon carbide composite samples heated to 550 °C in air and nitrogen. ..... 176

Figure 4.60. Thirty weight percent silicon carbide composite samples heated to 550 °C in air and nitrogen ..... 177

Figure 4.61. Fifty weight percent silicon carbide composite samples heated to 550 °C in air and nitrogen ..... 178

Figure 4.62. Ten weight percent silicon carbide composite samples heated to 700 °C in air and nitrogen. ..... 179

Figure 4.63. Thirty weight percent silicon carbide composite samples heated to 700 °C in air and nitrogen ..... 180

Figure 4.64. Fifty weight percent silicon carbide composite samples heated to 700 °C in air and nitrogen ..... 181

Figure 4.65. Ten weight percent silicon carbide composite samples heated to 1100 °C in air and nitrogen ..... 182

Figure 4.66. Thirty weight percent silicon carbide composite samples heated to 1100 °C in air and nitrogen ..... 183

Figure 4.67. Fifty weight percent silicon carbide composite samples heated to 1100 °C in air and nitrogen ..... 184

Figure 5.1. Heating rates of α-phase silicon carbide composite samples as a function of weight percent silicon carbide ..... 197

Figure 5.2. Heating rates of α- and β-phase silicon carbide composite samples as a function of weight percent silicon carbide ..... 204

Figure 5.3. Plots of interaction of type of silicon carbide with atmosphere from statistical data for composite samples heated to only 600 °C..... 207

Figure 5.4. Plots of interaction of weight percent of silicon carbide with atmosphere from statistical data for composite samples heated to only 600 °C..... 222

Figure 5.5. Plots of interaction of type of silicon carbide with atmosphere as a function of time (s) for temperature to increase a given amount from statistical data for composite samples heated to 1200 °C..... 227

Figure 5.6. Plots of interaction of type of silicon carbide with atmosphere as a function of time (s) for temperature to increase a given amount from statistical data for all composite samples..... 217

Figure 5.7. Plots of interaction of type of silicon carbide with atmosphere as a function of time (s) for temperature to increase a given amount from statistical data for all composite samples..... 219

Figure 5.8. Plots of interaction of weight percent of silicon carbide with type of silicon carbide as a function of time (s) for temperature to increase a given amount from statistical data for all composite samples..... 221

Figure 5.9. Differential thermal analysis calculation for predicted curve of 50 weight percent silicon carbide/50 weight percent Alfrax 66 composite if no interactions occurred between the phases..... 226

Figure 5.10. Plot of interaction of type of silicon carbide with atmosphere as a function of the heating rate at high temperature..... 229

Figure 5.11. Heating rates of α- and β-phase silicon carbide composite samples as a function of weight percent silicon carbide for composites heated to 550 ° in air..... 230

Figure 5.12. Heating rates of α- and β-phase silicon carbide composite samples as a function of weight percent silicon carbide for composites heated to 700 ° in air..... 231

Figure 5.13. Heating rates of α- and β-phase silicon carbide composite samples as a function of weight percent silicon carbide for composites heated to 1100 ° in air..... 232

Figure 5.14. Heating rates of α- and β-phase silicon carbide composite samples as a function of weight percent silicon carbide for composites heated to 550 ° in nitrogen..... 233

Figure 5.15. Heating rates of α- and β-phase silicon carbide composite samples as a function of weight percent silicon carbide for composites heated to 700 ° in nitrogen. ..... 234

Figure 5.16. Heating rates of α- and β-phase silicon carbide composite samples as a function of weight percent silicon carbide for composites heated to 1100 ° in nitrogen. ..... 235

Figure 5.17. Mean composite temperature calculated from equation [5.38] as a function of time as the silicon carbide particle radius, $r_p$, and resulting particle surface area, $S_p$, is varied, assuming that the embedded particles do not touch and the mass fraction is held constant..... 244

Figure 5.18. Illustration of how percolation would occur on a small randomly filled 2-dimensional lattice. A path is available from one site to another when neighboring sites are occupied, as indicated by bold lines. As more of the available sites are fille, eventually (at 40%, part d), a pathway from one side of the lattice to the other is created. The creation of this pathway represents the onset of percolation..... 247

Figure 5.19. Schematic showing how the conductivity of an insulator/conductor composite would increase as the volume fraction of conducting phase is increased when percolation occurs in the composite..... 250

Figure 5.20. Determination of percolation threshold using equation [5.40], and an arbitrary choice of A as 0.01..... 254

Figure 5.21. Conditions used for determining nearest neighbor distances as a function of volume percent silicon carbide. The volume fraction occupied by the small er particles remains constant. The particle separation, d, used for the calculations is denoted as well. ..... 256

Abstract of Dissertation Presented to the Graduate School
of the University of Florida in Partial Fulfillment of the
Requirements for the Degree of Doctor of Philosophy

MICROWAVE BEHAVIOR OF SILICON CARBIDE/
HIGH ALUMINA CEMENT COMPOSITES

By

Kristie Sue Leiser

May 2001

Chair: Dr. David E. Clark
Major Department: Materials Science and Engineering

Microwave susceptors have been fabricated from composites of silicon carbide/high alumina cement. These composites are very useful for microwave processing other materials. By using these composites for microwave hybrid heating, both ordinary and unique materials have the potential to be fabricated. The use of the susceptors can help to produce a more even temperature distribution across a material being microwave heated. This composite of silicon carbide particles embedded in high alumina cement only needed to be better characterized to enhance its applicability to more systems. This goal was accomplished in this study.

During the course of the study, the factors affecting the heating rate of the composites were identified. These factors included silicon carbide particle size, weight percent silicon carbide in the composite, silicon carbide phase, processing atmosphere, and the maximum temperature experienced by the composite. A systematic study was

cdesigned to examine the importance of factors such as these and their effects upon the heating rate of high alumina cement/silicon carbide composites. Statistical design was employed to determine the significance of the factors of interest.

The effects of these factors on the heating rate of the composites were determined. As the amount of silicon carbide in the composite increased, the heating rate tended to increase. The effects observed were explained by a combination of dielectric mixing equations, a heat transfer model and percolation theory. The silicon carbide particle size also affected the heating rate of the composites. Mathematical modeling showed that the particle size effect was a geometric effect that was dependent upon imperfect thermal contact between the silicon carbide particle and the cement matrix. The silicon carbide particle size also affected the percolation threshold of the composites. The heating rate of the composites increased when calcium carbonate present in the cement was pyrolyzed to form calcium oxide due to an increase in the thermal conductivity. A nitrogen atmosphere also tended to result in higher composite heating rates than an air atmosphere, most likely due to the suppression of oxidation of silicon carbide. In addition, beta-phase silicon carbide composites tended to heat more rapidly than alpha-phase silicon carbide composites.

# CHAPTER 1
# INTRODUCTION

## General Introduction

Conventional heating methods result in thermal profiles where the highest temperatures are observed at the surface of the sample material. To increase the temperature of the interior of a sample, heat must be conducted from the exterior surface to the interior of the sample. This can create problems including warping during processes like sintering, in which the outside of the material will densify and shrink before the interior. On the other hand, direct microwave heating tends to exhibit an inverted temperature profile, with the highest temperature being in the center of the sample material. The inverse temperature profile is mostly due to radiation losses from the surface of the sample material. However, with the inverse temperature profile produced by microwave heating, some of the warping problems experienced with conventional heating methods may be avoided.

Direct microwave heating and microwave hybrid heating of materials can provide an efficient means for creating both ordinary and unique materials. As compared to conventional heating, microwave energy has the potential to more uniformly heat materials, use less energy, and take less processing time. Microwave heating may also heat materials selectively. In some instances, such as joining, selective heating is advantageous since specific regions (the joint, in this case) can be designed to heat

without using energy on the rest of the material or shrinking the overall material to be joined.

However, that selectivity can also be a disadvantage. If the material to be processed does not absorb microwave energy, and cannot be engineered to do so, how could it be heated in a microwave? For these types of materials and others that may not absorb microwave energy until higher temperatures are reached, it is still possible to heat these materials using microwave hybrid heating.

Microwave hybrid heating may be employed to surmount the difficulties in heating low microwave absorbing ceramics. Microwave hybrid heating utilizes an additional material in the microwave cavity that readily absorbs the electromagnetic energy. This additional material is termed a susceptor, which describes any material that will produce heat when subject to microwave radiation due to absorption of the energy. In microwave hybrid heating, the susceptor will then heat the sample via radiation, conduction, convection, or a combination of these heat transfer methods.

Microwave hybrid heating may be used for both low microwave absorbing materials as well as for materials that do heat by direct microwave heating. For good microwave absorbing materials, microwave hybrid heating helps to produce a more uniform temperature profile. By the addition of a susceptor at the surface that radiates energy for the sample to absorb, a more even temperature profile may be obtained by the reduction in radiation losses. For some types of materials, the addition of a susceptor for microwave hybrid heating may also be used for assistance in heating the sample material to a temperature at which it will better absorb microwave energy.

A new generation of susceptors for microwave hybrid heating that were fabricated of a mixture of high alumina cement and silicon carbide particles is of particular interest. These materials were combined to take advantage of the formability, strength and microwave transparency of the high alumina cement and the high microwave absorption of silicon carbide at 2.45 GHz. The composites can not only be formed into nearly any shape desired, but are also cheap and reusable.

The usefulness of these particular composite susceptors has been proven in the processing of many different materials. The difficulty, however, lies in that although the composite is recognized to be very effective for assisting in microwave processing, not enough information is known about what happens within the composite that affects its performance. To use these composite susceptors more effectively for processing of other materials, the susceptors themselves need to be better understood. In order to properly choose a susceptor composition for processing a product, the microwave behavior of the susceptor must be carefully documented. The focus of this investigation is to study the microwave heating behavior of susceptors comprised of silicon carbide particles embedded in high alumina cement.

The difficulty encountered in prior use of this composite susceptor system is that the two components were combined without much attention to the details. It was known that the composite was extremely effective for microwave hybrid heating. However, questions of effects of the silicon carbide particle size, silicon carbide phase, and amount of silicon carbide in the composite were not addressed. It was also unknown what changes the composite may go through as it was heated. Therefore, a systematic study was designed to examine the importance of factors such as these and their effects upon

the heating rate of high alumina cement/silicon carbide composites. As a result of this study, better choices of composition and processing may be made when using these susceptors for microwave hybrid heating.

**Outline of Study**

In Chapter 1, a general introduction to microwave processing of materials as compared to conventional heating methods is given. The basic principles of the concept of microwave hybrid heating are described, and a useful composite susceptor material of high alumina cement mixed with silicon carbide is presented, as well as some of the questions that need to be answered for the susceptors to be used to most advantage. Chapter 2 discusses the advantages and disadvantages of microwave processing, as well as methods for overcoming some of the challenges faced in the use of microwave processing. In addition, the basics of microwave theory (including mechanisms of dielectric loss, dielectric mixture models, dielectric property measurement techniques, microwave heating mechanisms, and types of microwave behavior) are presented. Furthermore, the principles of microwave hybrid heating as well as in-situ temperature measurement are discussed in detail. Chapter 3 introduces the method employed for composite sample fabrication, and the experimental procedure used to determine the microwave heating rates. The study began by asking how much silicon carbide should be in the sample, and how large the silicon carbide particles should be (Phase I). These questions led to an additional inquiry as to the importance of the phase of silicon carbide incorporated into the composite susceptor sample (Phase II), and later the processing atmosphere (Phase III). A desire for verification of the conclusions reached in earlier phases of the experiment led to Phase IV, which again examined all of the factors from

previous phases. The characterization techniques employed and some of the critical factors that had to be considered are also presented in Chapter 3. Chapter 4 contains the experimental results of each phase of the study, as well as the statistical analysis of the results. The results of each phase of the study are analyzed and discussed in Chapter 5. Equations predicting the heating rates of a composite under a given set of conditions are also presented. The effects of critical parameters including the particle size, weight percent silicon carbide in conjunction with percolation theory, the effects of calcium carbonate, and the processing atmosphere on the heating rate of the composite susceptor samples are then discussed in more detail. Finally, Chapter 6 summarizes the major results of the study.

# CHAPTER 2
# BACKGROUND

## Microwave General Characteristics

The first question that might be asked by those unfamiliar with the subject is why microwave processing? The answer can be made simple, that microwave processing may allow novel materials to be produced, and can produce other materials in less time than an alternative method. Of course, this answer is a little simplistic, as there are both benefits and challenges to the use of microwave energy.

To start with, the list of the benefits of microwave processing is quite extensive. These are presented in Table 2.1 [Sut89]. However, it should also be considered that what can be advantageous in one experiment has the potential to be detrimental in another. Some of the characteristics of microwave processing that will be discussed are volumetric heating, rapid increase of dielectric loss above a critical temperature, control of the microwave energy, and differential microwave coupling and selective heating.

To begin with, microwave energy heats a material volumetrically. Therefore, materials tend to heat from the inside out. This is the opposite of what occurs in a conventional type of furnace. The differences in how a conventional and a microwave furnace would heat a material are illustrated in Figure 2.1 [Sut89]. In fact, due to radiation losses, the temperature profile for a material heated in the microwave tends to be the opposite of that for one heated in a conventional furnace. Therefore, in the

Table 2.1. Characteristics and advantages of microwave processing of ceramics.

| Characteristic | Advantages over Conventional Heating Processes |
|---|---|
| Direct coupling (absorbing) of microwave creates volumetric (bulk) heating | Potential to heat large sections uniformly |
| | Reversed thermal gradients: surface cooler than interior |
| | Process materials at lower surface temperatures |
| | Rapid removal of water, binders, and gases without rupture or cracking |
| | Internal stresses reduction by lower thermal gradients |
| | Heat in clean (pure) environment; air, controlled atmospheres, vacuum, or pressure |
| | Control partial pressure of reactive gases for selective oxidation/reduction of certain phases |
| | Improvement of product quality, uniformity, and yields |
| | Instantaneous response to microwave power changes |
| | Low thermal mass; precise and automated temperature control |
| Dielectric losses (and heating) accelerate very rapidly with increasing temperatures above $T_{crit}$ | Ability to heat "transparent" materials above $T_{crit}$ |
| | Very rapid processing (2 to 50 times faster than conventional) |
| | Densify materials rapidly with minimum grain growth (accelerated sintering) |
| | Reduce process costs (time, energy, labor) |
| | Ability to heat ceramics well above 2000 °C (in air, vacuum, or controlled atmospheres) |
| Microwaves are polarized and coherent; location of maximum electric and magnetic fields can be controlled | Capability of high-energy concentration in short times and in selected regions |
| | Frequency and power level optimization for given material, size, and shape |
| | Potential for process automation, flexibility, efficiency, and energy savings |
| | Precise heating of selected regions, i.e., brazing or sealing of joints, fiber drawing, and plasma generation |
| | Acceleration of sintering and diffusion due to high electrical fields; thus densification at lower temperatures |
| Differential microwave coupling of phases, additives, and constituents leads to selective heating | Synthesis of new materials and microstructures |
| | Heating of selected zones (brazing and sealing) |
| | Enhanced coupling of microwave transparent materials |
| | Use of fugitive coupling materials for preheating of otherwise transparent materials |
| | Use of microwave-coupling materials as shapes or containers to heat the more transparent materials |
| | Superior control over state of oxidation through selective heating of phases and control over oxygen partial pressure |

[Sut89]

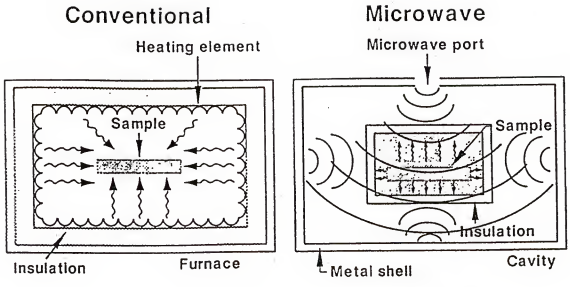


Figure 2.1. In a conventional furnace, the surface of the sample will be heated first, as shown. In order for the interior to be heated, the heat from the surface must be conducted to the center of the sample. Whereas, in a microwave furnace, the interior of the sample will be hottest, and the surface will tend to radiate the heat to the atmosphere, so that the surface will tend to be cooler than the interior. [Sut89]

microwave, a material tends to be hotter in the center of the sample than on the surface. It should be noted that even this temperature difference might be mitigated by reducing the surface radiation losses. But, volumetric heating is especially beneficial in cases where something needs to be removed from the product such as water or binders.

The volumetric heating and inverse temperature profile produced by microwaves enable processing to proceed differently than in a conventional gas or resistance furnace [Bin92]. When the sample is hottest in the center as in microwave processing, then water for example, will be removed from the center before the exterior. So, when sintering, the center of the sample will densify first using microwave heating, compared to the surface densifying first for conventional heating. If sintering is occurring at the same time, this will allow products to be more uniformly reacted and sintered, as the exterior will not seal off the interior (which may occur using conventional heating methods). One example of this is in the manufacture of $YBa_2Cu_3O_{7-x}$ superconductors, where using microwave processing, the surface will no longer seal off the interior from the needed oxygen flow [Ahm88]. In addition, volumetric heating of the product can also improve product quality by reducing the likelihood of thermal shock. When the interior and exterior temperature of the sample are more similar, fewer thermal stresses are present in the material, which not only prevents thermal shock, but can also result in a better product.

The rapid increase of dielectric losses and thus heating above a critical temperature allows for extremely rapid processing using microwave energy. Above this critical temperature, so-called "transparent" materials can also be heated. The rapidity of processing available through microwave heating saves energy, which in turn saves

money. Decreasing the amount of time to produce a product also increases the number of products that may be produced which may also increase profits. In addition, by more rapid processing, detrimental effects such as grain growth can be inhibited, thus obtaining a more uniform, fine-grained microstructure [Sut89, Ahm88, Vos91, Sut92, Kat88].

The use of microwave energy also allows much greater control over the heating of a material. With the use of single mode cavities with a standing wave pattern, the location of maximum energy can be precisely pinpointed, and thus applied to a material. Therefore, in some cases, this method could be used to selectively apply the energy to a specific part of a material. In addition, as microwaves cover a range in the electromagnetic spectrum, specific frequencies and power levels may be specified for optimum results [Sut89]. To add to the control that can be exerted with microwave processing, when the microwave power source is turned on or off, heating will start or stop. As any good chef knows, when a conventional oven is turned off, it does not always mean the meal has stopped cooking, whereas when a microwave is turned off, all cooking stops.

However, what might be considered the most intriguing characteristic of microwave processing is that of selective heating. Microwave energy will interact more with some materials than with others, depending upon the dielectric properties of the materials at specific frequencies and temperatures. Changing the frequency of the microwave energy can thus alter the degree of interaction between the microwave energy and the material. However, as a material heats, its absorption of microwave energy may also either increase or decrease. This dependency of microwave heating upon frequency and temperature can be used to great advantage.

Composite materials can be used to take advantage of this property to the utmost. Since some materials will absorb more energy than others, and thus heat more than others, selected areas of a product may be heated, with minimal effects to the remaining area. For example, a coating on a low density tile may need to be sintered, but minimal densification of the tile underneath is desired. With microwave heating and a more microwave absorbing coating, this ideal could be accomplished. This ability to selectively heat specific phases can also be very useful for joining materials without necessarily exposing the bulk to high temperatures [Dav94, DiF95a, Coz95, Coz97b, Pal88, Sil91]. In other cases, the selective heating of one phase of a composite over another has been shown to result in increased chemical bonding between the fiber reinforcement and the matrix [Drz91]. Microwave processing may also result in enhanced chemical reactions, which in some cases may be the formation of bonds, and in others the breaking of chemical bonds. The differences in these reactions are greater than those expected just from a temperature difference [Drz91, Fan91b]. And, microwave transparent materials may also be heated by adding a microwave absorbing phase [Sut89].

Unfortunately, every method available for processing will also have its downfalls, and microwave processing is no exception. Table 2.2 presents many of the challenges that may need to be overcome for microwave processing to be a viable option [Sut89, Sut92, Sut93, Cla96]. However, some of these challenges, looked at in a different light, can also be considered advantages. Some of these include difficulty in heating microwave transparent materials, development of hot spots, large temperature differences in low thermal conductivity materials, nonuniform heating, and inverted temperature

Table 2.2. Challenges of microwave processing.

| **Challenges Facing Microwave Processing** |
|---|
| Microwave transparent materials are difficult to heat |
| Development of hot spots and cracking |
| Large $\Delta T$ in low thermal conductivity materials |
| Nonuniform heating |
| Controlling internal temperature |
| Arcing, plasmas |
| Require new equipment, designs special reaction vessels |
| Equipment may be more costly and complex |
| May requires specialized equipment |
| Control of thermal runaway |
| Reactions with unwanted impurities |
| Contamination with insulation or other phases |
| Undesired decoupling during heating in certain products |
| Difficult to maintain temperature |
| Exploiting inverted temperature profiles |
| Efficient transfer of microwave energy to workpiece |
| Compatibility of the microwave process with the rest of the process line |
| Reluctance to abandon proven technologies |

[Sut89, Sut92, Sut93, Cla96]

Table 2.3. Obstacles to commercialization of microwave processing.

- Custom engineering requirement for each individual application
- Lack of equipment design standards
- Low volume sales of large industrial microwave systems
- High relative cost of microwave process equipment
- Tendency to force-fit a microwave solution to a given problem
- Lack of use confidence in new unproven process technology
- Lack of practical engineering design models
- Lack of sound economic and business decision making data
- Temperature and field measurement difficulties
- Lack of design data, e.g., inadequate dielectric property database
- Need for accurate high-temperature dielectric property measurements
- Regulatory inertia: spectrum limits, safety, environmental regulations
- Misunderstanding of the microwave-material-applicator interaction
- Lack of adequate R&D funding

[Tin93b]

profiles. Other challenges are more difficult to turn into positives in any way, but that does not make them insurmountable.

Equipment availability and temperature control can be the most difficult problems to overcome. Although the frequency of microwave energy can be tailored for a specific purpose, obtaining the equipment to allow this optimization is not necessarily so simple. Specially designed equipment may be required, which may increase complexity as well as cost [Sut89, Sut92, Sut93, Cla96]. Another "equipment" problem is that of thermal insulation. To begin with, the insulation may contaminate the sample, by reacting or bonding with it in some way. But, another common problem is that of coupling with the microwave field. Some insulation materials commonly used in conventional furnaces will absorb microwaves and therefore heat. It can be detrimental to a product if the insulation absorbs too much of the microwave energy, thus preventing the microwaves from reaching the product. However, it is also counter-productive in that the insulation is not really fulfilling its purpose when it absorbs the microwave energy. Therefore, the choice of insulation materials for microwave processing is restricted to those which do not absorb microwaves at the processing frequency.

Temperature can be difficult to control for several reasons. One is nonuniform heating, where one phase may heat preferentially over another. This can create very large temperature differentials in a sample, especially for materials in which the thermal conductivity or contact between phases is relatively low. Additionally, if the radiative heat loss is high, the internal temperature of the sample may be much higher than that of the exterior, leading to misconceptions when only the temperature of the exterior of the sample is measured.

Thermal runaway in some samples, where the loss factor increases rapidly as the temperature increases, also may prevent good control over the heating of a material. A typical curve of effective loss factor versus temperature that would characterize a material prone to thermal runaway is presented in Figure 2.2 [Met83]. As the temperature increases above the critical temperature, $T_c$, the effective loss factor increases extremely rapidly which increases the heating of the sample material correspondingly. Unfortunately, this tends to lead to a loss of control over the heating of the system. However, generally the entire material will not reach the critical temperature simultaneously, leading to the development of potentially extreme thermal gradients within the material [Fat94]. The critical temperature can be adjusted somewhat by additives [Moo93b]. In comparison to thermal runaway, in other samples, heating may drop off above a critical temperature [Sut89, Sut92, Sut93, Cla96]. And finally, there are various difficulties just in the process of temperature measurement, which will be discussed in more detail later.

However, although all of these difficulties presented in Table 2.2 may still face researchers, many of these can be overcome. For example, microwave hybrid heating has been utilized to surmount the difficulties in heating low microwave absorbing ceramics [Sut92, Cla91, Moo91, Dé91a, Ahm91]. To prevent arcing problems with thermocouple temperature measurement, possible solutions include insulation around the thermocouple [Sut92, Lei97, Lei98, Lei99], or using nitrogen gas [Sut92, Gar 96, Jan91]. Thermal runaway can be avoided or suppressed in some cases by using thermal insulation [Sut92] (which in other cases may promote thermal runaway [Koh95]), by adding a lossy material either within the material or placed in close proximity to the sample [Joh91, Fan91a], by

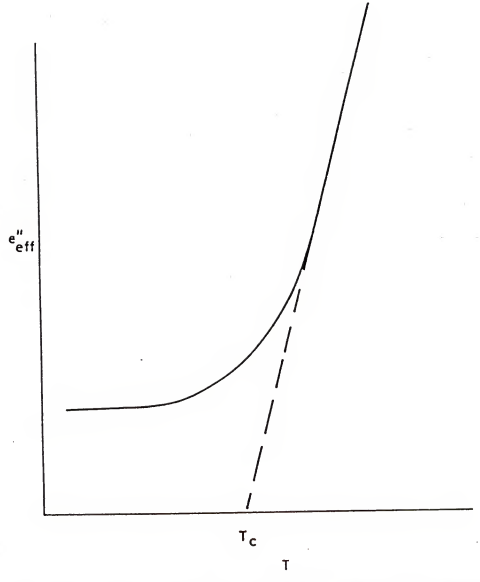


Figure 2.2. Effective loss factor as a function of temperature, where $T_c$ represents the critical temperature above which the loss factor increases extremely rapidly. See equation [2.25] for a quantitative description of $\varepsilon''_{eff}$. [Met83]

microwave hybrid heating [Ska94, Koh95], or by using high thermal conductivity sample materials [Joh91].

Irrespective of the accomplishments in overcoming these difficulties, a larger problem facing the use of microwave processing is the reluctance of industry to abandon proven technologies. Table 2.3 presents many of the obstacles towards commercialization of microwave processing as viewed by both industry and researchers [Tin93b]. A universal unit for all applications simply does not exist, so a system tends to need to be individually designed for each application. As a result, each system needs to be tested and examined to provide confidence in this new technology. Low volume industrial sales and high specialized unit costs do not assist very much in "getting the word out" so that the technology becomes more familiar. Added to this is inadequate research funding so that some of the primary industrial issues can be tackled satisfactorily [Tin93b].

## Microwave Theory

However, these issues are actually not the only challenges facing the researcher in microwave processing. The microwave community is still struggling to understand exactly what occurs in microwave processing.

### Sources of Dielectric Loss

Heating is thought to occur because of electric loss, conduction loss, and magnetic loss. Electric loss is the primary mechanism for heating at microwave frequencies [New91]. So what are the causes of electric loss? Macroscopically, we go to electromagnetic theory, where a dielectric material is defined by its dielectric constant, $\varepsilon'$, which is directly related to the electric field, E, and the electric flux density by

$$D = \varepsilon' E \quad \textbf{[2. 1]}$$

where

$$\varepsilon' = \varepsilon_o \varepsilon_r' \quad \textbf{[2. 2]}$$

where $\varepsilon_o$ is the permittivity of free space and $\varepsilon_r'$ is the relative dielectric constant* [Sol93]. Now, considering Faraday's capacitor experiments, it is known that in a vacuum, the magnitude of the charge on either plate, $Q_o$, between two parallel plates as illustrated in Figure 2.3a is

$$Q_0 = \varepsilon_o \frac{V}{d} \quad \textbf{[2. 3]}$$

where V is the voltage and d is the distance between plates. If a dielectric material with relative dielectric constant $\varepsilon_r'$ is added between these two parallel plates as in Figure 2.3b [Tip91], the charge, $Q_1$ then becomes

$$Q_1 = \varepsilon_o \varepsilon_r' \frac{V}{d} \quad \textbf{[2. 4]}$$

and the weakened electric field in the material is $E_{internal.}$ If the difference between these two charges, which may be denoted as the polarization, P, is then calculated from [2.3] and [2.4] [Sol93, Tip91],

$$Q_0 - Q_1 = P = \varepsilon_o \frac{V}{d}(\varepsilon_r' - 1) \quad \textbf{[2. 5]}$$

But, we also know that

---

* Note: $\varepsilon_r$ is also referred to in some texts as $\kappa$.

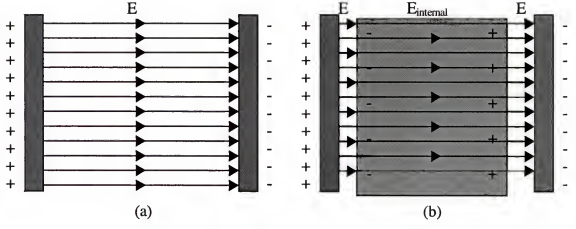


Figure 2.3. The change in the electric field between the plates of a capacitor with no dielectric (a) and with a dielectric (b). The presence of the dielectric in (b) weakens the original electric field, E, between the two plates. [adapted from Tip91]

$$V = Ed \quad \textbf{[2. 6]}$$

where E is the magnitude of the electric field. Substituting [2.6] into [2.5], we obtain the expression:

$$P = \varepsilon_o E(\varepsilon_r' - 1) \quad \textbf{[2. 7]}$$

Now this information may be taken to the microscopic level. The polarization of a material may be viewed as the relationship between a material and an electric field. Instead of looking at simply a bulk material, if we step down a level to atoms and molecules (which are made up of charged particles), we know that these charged particles will react to an electric field. In one of several ways, a dipole will be created, with a dipole moment μ, which can be defined as

$$\mu = q\delta \quad \textbf{[2. 8]}$$

where q is the total charge, and δ is the charge separation caused by the electric field, as shown in Figure 2.4 [Sol93, Met83]. Adding up all of the dipole moments, N, in the material, the polarization is once again obtained:

$$P = \sum_i^N \mu \ = \sum_i^N q\delta_i = Nq\delta = N\mu \quad \textbf{[2. 9]}$$

If it is also assumed that the electric field is low and linear, then the dipole moment may be written as

$$\mu = \alpha_T E' \quad \textbf{[2. 10]}$$

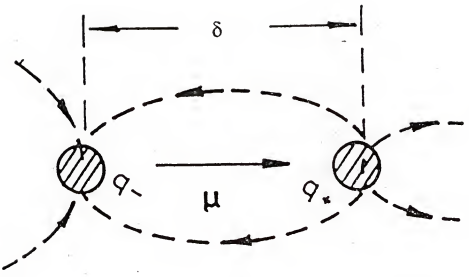


Figure 2.4. Electric dipole moment between two atoms of charge q, with separation between charges denoted by δ. [Met83]

where $\alpha_t$ is the total polarizability, and E' is the local electric field [Sol93, Met83]. E' is similar to $E_{internal}$, but E' is on the microscopic rather than macroscopic level. Then, substituting [2.10] into [2.9], the following equation is obtained:

$$P = \alpha_T N E' \textbf{ [2. 11]}$$

This equation for the polarizability [2.11] can be combined with the previously derived equation for the polarizability [2.7], to obtain a relationship between the microscopic parameters and the macroscopic parameters:

$$P = \alpha_T N E' = \varepsilon_o E(\varepsilon_r' - 1) \textbf{ [2. 12]}$$

Rewritten, this equation becomes

$$E' = E\varepsilon_o(\varepsilon_r' - 1)\frac{1}{N\alpha_T} \textbf{ [2. 13]}$$

Using the polarization phenomena, Mosotti derived a relationship between the internal and the applied electric fields. Assuming that a molecule is surrounded by an imaginary sphere, and the resulting field acting on the molecule has contributions from free charges at the electrodes, free ends of dipole chains on the cavity walls, and from nearby molecules within the sphere, the following equation is obtained [Met83, Kin76]:

$$E' = \frac{E}{3}(\varepsilon_r' + 2) \textbf{ [2. 14]}$$

It should be noted that several assumptions are made to obtain this equation, and that it only truly applies to gases and non-polar liquids, but is sometimes still used for an approximation.

The total polarizability $\alpha_T$ is made up of four components [Met83]:

$$\alpha_T = \alpha_e + \alpha_a + \alpha_d + \alpha_{MW} \quad \textbf{[2. 15]}$$

where $\alpha_e$ is the electronic component, $\alpha_a$ is the atomic or ionic component, $\alpha_d$ is the dipole rotation or reorientation component, and $\alpha_{MW}$ is the Maxwell-Wagner space charge or interfacial component. Each of these components to the total polarizability is operable over a different frequency range. As the frequency increases, some factors are unable to respond quickly enough to the stimuli to affect the polarization of the material. This is illustrated in Figure 2.5 [Kin76, Hen90, Met83]. In the microwave region, loss is primarily only affected by ionic polarization, dipolar polarization, and interfacial polarization, which are all manifestations of electric loss [New91, Met83].

Electronic polarization is associated with the motion of the electron cloud in relation to the nucleus, as shown in Figure 2.6a [Ric92]. Electrons are very small and light, and thus can respond at very high frequencies, near the ultraviolet region [Thu92]. As a result, electronic polarization causes a resonance absorption peak in the optical frequency range, leading to a dependence of the index of refraction on the electronic polarization response [Sol93, Hen90, Moo93b]. It is independent of the type of bonding in the material [Sch95]. This particular polarization mechanism is not thought to have a significant contribution in the microwave frequency range, as the total amount of polarization by this displacement is quite small, compared to other mechanisms [Ric92, New91].

Ionic or atomic polarization is the displacement of individual cations and anions in a lattice towards the oppositely charged electrode, as is shown in Figure 2.6b. It is most effective in the infrared range [Sch95, Thu92]. This type of polarization is also associated with the phenomena of pyroelectricity, piezoelectricity, and ferroelectricity

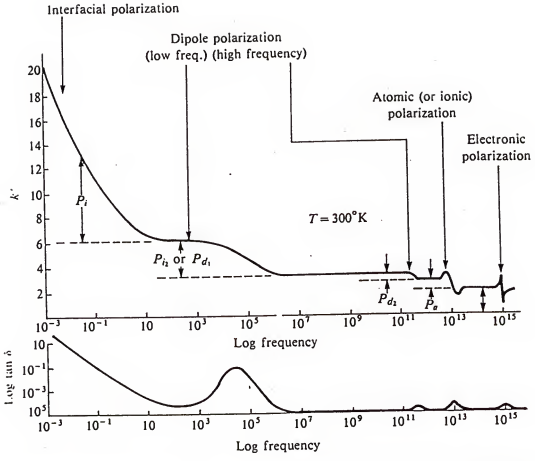


Figure 2.5. Frequency dependence of individual polarization mechanisms. [Hen90]

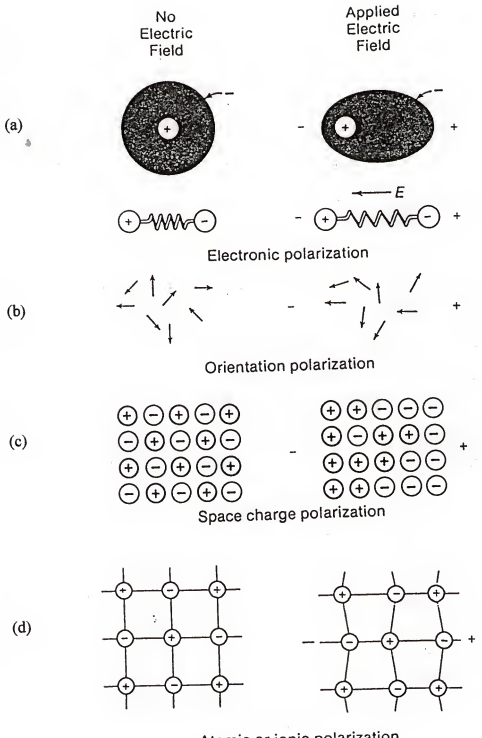


Figure 2.6. Representation of the four different types of polarization mechanisms. [Ric92]

[Ric92]. As might be expected, ionic polarization is especially effective in ionic materials [Sch95]. However, in the microwave frequency range, this mechanism does not play nearly as large a role as reorientation polarization [Met83].

Dipole rotation or reorientation polarization only affects those materials which already contain a permanent dipole. Orientation polarization is most effective at high frequencies, such as the microwave region [Sch95, Thu92]. A good example of this type of material is water, where the hydrogen atom has a small positive charge, and the oxygen atoms have a small negative charge [Ric92]. When this type of material is placed in an electric field, alignment of the molecules will occur, as shown in Figure 2.6c. The effects of orientation polarization are greater than electronic polarization, due to the greater charge displacement involved [Ric92]. Of course, it should be noted that this type of polarization is not restricted just to fluid materials, but can affect solids as well. In fact, orientation polarization is exploited in some materials, where they are aligned at high temperature, and retain this alignment after they are cooled down [Sch95]. Dipole reorientation is also thought to be the most important heating mechanism in the microwave frequency range [New91, Met83].

Interfacial polarization, also known as Maxwell-Wagner or space charge polarization, is illustrated in Figure 2.6d. This type of polarization results from charge buildup at some kind of physical barrier, and is most effective in lower frequency ranges [Sch95, Thu92]. Types of barriers include grain boundaries, phase boundaries, free surfaces and voids. Because of the barrier, localized polarization will occur due to the internal charge buildup [Sch95, Moo93b].

Heating of a dielectric can also be affected by conduction losses. A study of heating of materials with low and high conductivities indicated that higher conductivity coincided with better heating [New91, McG88]. Conduction, $\sigma$, is related to the skin depth, $\delta$, as a function of frequency, f, and permeability, $\mu$, by the equation:

$$\delta = \frac{1}{\sqrt{\pi f \mu \sigma}} \textbf{[2. 16]}$$

Skin depth is the distance into the material where the electric field has decreased to 1/e of its surface value [New91, Met83, Kat92].

Magnetic loss can slightly affect the heating of a material by microwaves, although the electric field vector is more effective [New91]. Magnetic loss is probably most important in magnetic materials with aligned spins [New91]. Some of the potential loss mechanisms include hysteresis loss, eddy current loss, dimensional resonances, magnetic resonance, and domain wall oscillations [New91, Met83].

**Dielectric Loss Equations**

Mathematically, when discussing dielectric loss, there are a number of parameters that are crucial. The first would be the dielectric constant, $\varepsilon$, which is a measure of how much the microwaves will interact with the material [Sut89]. The dielectric constant is commonly divided up into a real, $\varepsilon'$, and imaginary part, $\varepsilon''$ [Sol93]. The real term may also be referred to as the dielectric constant, and refers to the dielectric's ability to store charge. The complex term may be referred to as the dielectric loss factor, and refers to the losses of the dielectric [Met83, Sol93, Fat94]. These two terms can be derived from Maxwell's equations and rewriting the current term [Sol93]:

$$J = \sigma E \textbf{[2. 17]}$$

as

$$J - i\omega\varepsilon' E = \sigma E - i\omega\varepsilon' E = -i\omega\left(\varepsilon' + i\frac{\sigma}{\omega}\right)E \quad \textbf{[2. 18]}$$

The term enclosed in parentheses is referred to as the complex dielectric constant, where

$$\varepsilon' = \varepsilon_o \varepsilon_r' \quad \textbf{[2. 2]}$$

and

$$\frac{\sigma}{\varpi} = \varepsilon_r'' \varepsilon_o \quad \textbf{[2. 19]}$$

The dielectric constant is intimately related to the complex permittivity, $\varepsilon^*$, of the material as follows:

$$\varepsilon^* = \varepsilon' - i\varepsilon'' = \varepsilon_o\left(\varepsilon_r' - i\varepsilon_{eff}''\right) \quad \textbf{[2. 20]}$$

where $\varepsilon_{eff}''$ is the effective relative dielectric loss factor. The effective relative dielectric loss factor includes loss mechanisms due to both conduction and polarization [Sut89, Cla96, Met83, Kat92, Bru88]. The relative dielectric constant and loss factor are each related to their counterparts (dielectric constant, ε', and dielectric loss factor ε") by:

$\varepsilon' = \varepsilon_o \varepsilon_r'$ **[2. 2]** and $\varepsilon'' = \varepsilon_o \varepsilon''_r$ **[2. 21]** or $\varepsilon'' = \varepsilon_o \varepsilon''_{eff}$ **[2. 22]**

The effective relative loss factor includes a term for high frequency heating, and is related to the relative loss factor by [Coz96b]:

$$\varepsilon''_{eff} = \varepsilon''_r + \frac{\sigma}{\varepsilon_o \omega} \quad \textbf{[2. 23]}$$

The loss tangent is defined from the components of the complex dielectric constant, which is also the ratio of the loss current, $I_l$, to the charging current, $I_c$ [Sol93, Moo93b]:

$$\tan\delta \equiv \frac{\varepsilon''}{\varepsilon'} = \frac{\varepsilon_r''}{\varepsilon_r'} \textbf{[2. 24]}$$

$$\tan\delta = \frac{I_l}{I_c} \textbf{[2. 25]}$$

The loss tangent may also be referred to as the dissipation factor. As stated earlier, each polarization mechanism is frequency dependent, and thus time dependent. A real dielectric, as compared to an ideal dielectric will take time to respond to stimuli, and this is shown graphically in Figure 2.7. The loss tangent indicates the time delay between application of an electric field, and polarization of the material. This time delay causes a phase shift in the induced current in the dielectric, which is defined by the angle $\delta$, shown in Figure 2.8 [Kin76, Moo93b, Coz96b, Hen90]. The loss tangent is an energy loss due to the time requirement for polarization, and is also related to charge storage [Hen90].

This energy loss is what leads to dielectric heating. Two critical materials characteristics for dielectric heating are the relative dielectric constant, $\varepsilon_r'$, and the dielectric conductivity, $\sigma$ [Hen90]. Both of these are components of the loss tangent. If dipoles are the only significant contribution, then the dielectric conductivity is defined relative to the dielectric loss factor by [Hen90, Tin88]:

$$\sigma = \omega\varepsilon'' = 2\pi f\varepsilon'' \textbf{[2. 26]}$$

This can then be input into the equation for the dielectric loss factor to obtain:

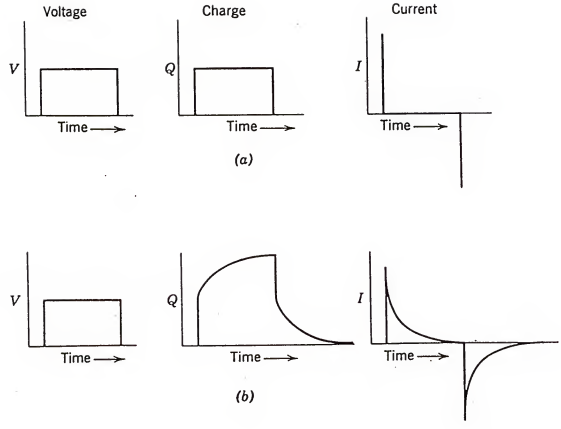


Figure 2.7. Time dependent behavior of (a) an ideal dielectric and (b) a real dielectric when subject to a voltage. [Kin76]

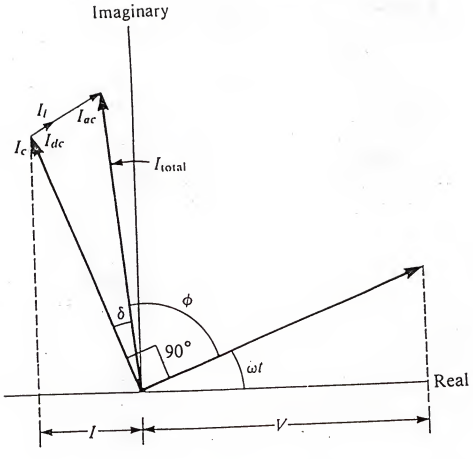


Figure 2.8. Phase shift, δ, in the induced current caused by the time delay in real dielectric materials. [Hen90]

$$\tan\delta = \frac{\varepsilon''}{\varepsilon'} = \frac{\sigma}{2\pi f\varepsilon'} \textbf{[2. 27]}$$

These equations show how frequency affects both the relative dielectric loss factor and the loss tangent.

Unfortunately, in real systems, even pure materials may have multiple phases with different dielectric properties. Many ceramics may also be composite materials, where information may be known about the individual components, but not the material as a whole. For these situations, dielectric mixture models may be useful. Most of these models are presented as two phase systems, but the general principles may be extrapolated to more phases, as well. Kingery presents the most basic mixture rules, where the relationships may correspond to either a straight volume fraction relationship:

$$\varepsilon_r' = v_1\varepsilon_{r1}' + v_2\varepsilon_{r2}' \textbf{[2. 28]}$$

$$\varepsilon_r'' = v_1\varepsilon_{r1}'' + v_2\varepsilon_{r2}'' \textbf{[2. 29]}$$

or an inverse relationship:

$$\frac{1}{\varepsilon_r'} = \frac{v_1}{\varepsilon_{r1}'} + \frac{v_2}{\varepsilon_{r2}'} \textbf{[2. 30]}$$

$$\frac{1}{\varepsilon_r''} = \frac{v_1}{\varepsilon_{r1}''} + \frac{v_2}{\varepsilon_{r2}''} \textbf{[2. 31]}$$

where $v_x$ is the volume fraction of phase x. A third dielectric mixture rule that may be used is the logarithmic mixture rule, which applies to both $\varepsilon_r'$ and $\varepsilon_r''$:

$$\log\varepsilon_r = \sum_i v_i \log\varepsilon_{ri} \textbf{[2. 32]}$$

This last rule provides a value that tends to fall in between the values from equations [2.28-2.32]. Maxwell also derived a dielectric mixture rule, where spherical particles with dielectric constant $\varepsilon_{rd}'$ are dispersed in a matrix of dielectric constant $\varepsilon_{rm}'$ given by:

$$\varepsilon_r' = \frac{v_m \varepsilon_{rm}' \left( \frac{2}{3} + \frac{\varepsilon_{rd}'}{3\varepsilon_{rm}'} \right) + v_d \varepsilon_{rd}'}{v_m \left( \frac{2}{3} + \frac{\varepsilon_{rd}'}{3\varepsilon_{rm}'} \right) + v_d} \quad \textbf{[2. 33]}$$

In addition to being used for $\varepsilon_r'$, this equation may also be used for $\varepsilon_r''$, with the appropriate substitutions. As shown in Figure 2.9, Maxwell's equation [2.33] approaches the logarithmic equation [2.32] when the dielectric constant for the dispersed phase becomes much greater than that of the matrix [Kin76]. This is characteristic of the composite material under examination in this study. However, porosity, which is also a factor in the material being studied, may cause significant departures from these equations [Kin76]. Additional assumptions which have been employed in the creation of these equations are that the electric field is uniform (not necessarily true in a multi-mode microwave oven) and that no new additional phases are formed in the material (not true for the material under study here) [Moo93b]. However, in addition to just differences in individual phases, the presence of grain boundaries and phase boundaries can affect the internal electric field in the material at these points, which will thus alter the microwave energy absorption of the material as a whole [Moo93b, Tin88].

Other researchers developed equations for particulate composites. Their studies found that for composites filled with metal particulates, the aspect ratio and correspondingly the number of particles in contact influenced the dielectric constant.

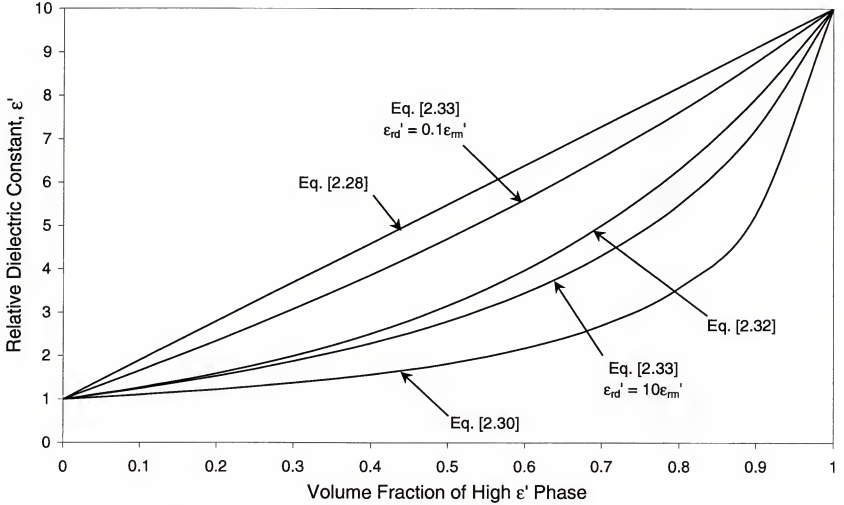


Figure 2.9. Using the dielectric mixture equations, a variety of different curves for the calculated relative dielectric constant are obtained. [adapted from Kin76]

However, with more particles, and the onset of percolation*, in some cases at a volume fraction of 0.15, these equations were less accurate. Disregarding this for the moment, the dielectric constant might be defined by Maxwell Garnett theory (MGT) by the equation:

$$\frac{\varepsilon_{rc}}{\varepsilon_{rm}} = \frac{(1+2V_f)}{(1-V_f)} \quad \textbf{[2. 34]}$$

where $\varepsilon_{rc}$ and $\varepsilon_{rm}$ are the real or complex dielectric constants for the composites and matrix respectively, and $V_f$ is the volume fraction of particles. In this case, particle size, particle size distribution and dispersion, and particle characteristics (i.e. conductivity, lossy or transparent, etc.) are disregarded. However, experimentation found that particle size has a definite effect on the dielectric constant, as seen in Figure 2.10, and that it is not simply a factor of volume percent. As a result, it cannot be applied for high volume fraction composites, or when these parameters are critical. An adaptation of this equation was developed by Wu and McCullough (WMT) to include an average particulate shape factor <h>, which would include some influence from particle contact:

$$\frac{\varepsilon_{rc}}{\varepsilon_{rm}} = \frac{\left[(1-<h>)(1-V_f)+<h>V_f\right]}{\left[(1-V_f)^2(1-<h>)\right]} \quad \textbf{[2. 35]}$$

The volume fraction was determined by adding the product of the aspect ratio and the area of particles, and then dividing this by the total area of the particles. This equation has been found to correlate to experimentation in some cases; however, it does not appear

* Rather than transport occurring throughout a material, percolation theory describes materials that have a preferred transport pathway, which tends to result in a sharp transition in transport properties being observed.

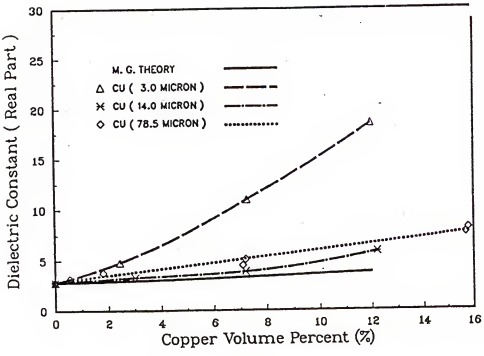


Figure 2.10. Variation of the real part of the dielectric constant for copper particles in epoxy in relation to copper particle size. [Ho88]

to sufficiently incorporate the aspect ratio, as determined by comparison with high aspect ratio experiments. The conclusion was reached that size and type of particles cannot be neglected in the determination of the dielectric properties [Ho88].

For many materials, it may be useful to take the dielectric properties to get an idea of how far the microwave energy can be expected to penetrate into the material. This has been defined in a couple of different ways as the penetration depth. One is defined as D, where the incident power has been reduced by half, and can be described by the equation [Sut89]:

$$D = \frac{3\lambda_0}{8.686\pi \tan\delta(\varepsilon_r'/\varepsilon_o)^{1/2}} \quad \textbf{[2. 36]}$$

where $\lambda_0$ is the wavelength of the incident wave. The more common definition of the penetration depth, $D_p$, describes the depth within the material at which the incident power has been reduced to 1/e, and is defined by the equation [Cla96]:

$$D_p = \frac{\lambda_0}{2\pi(2\varepsilon_r')^{1/2}}\left[\left(1+\left(\frac{\varepsilon_{eff}''}{\varepsilon_r'}\right)^2\right)^{1/2}-1\right]^{-1/2} \quad \textbf{[2. 37]}$$

If a material is low loss, meaning $\varepsilon''_{eff}/\varepsilon'_r \ll 1$, then equation [2.37] can be reduced to [Fat94, Met83]:

$$D_p \cong \frac{\lambda_0(\varepsilon_r')^{1/2}}{2\pi\varepsilon_{eff}''} \quad \textbf{[2. 38]}$$

One conclusion that can be reached from any of these equations is that as the wavelength increases or as the frequency decreases, the penetration depth will increase.

The loss tangent and the relative dielectric constant are two parameters that can be used to determine the power absorbed by the material, starting from:

$$P = \int_v \sigma |E|^2 \, dv \quad \textbf{[2. 39]}$$

If the same assumptions are made (that dipoles are the only significant contribution), we can use equation [2.26] for the conductivity, and substitute into equation [2.39]:

$$P = \int_v \omega \varepsilon_r'' |E|^2 \, dv = \int_v 2\pi f \varepsilon_r'' |E|^2 \, dv \quad \textbf{[2. 40]}$$

If we then assume that the microwave radiation is a plane wave, is uniform throughout the sample (which is not always true, especially in multi-phase samples as in this study), and that thermal equilibrium has been attained, then the integration of [2.40] is

$$\frac{P}{V} \cong 2\pi f \varepsilon_r'' |E|^2 \quad \textbf{[2. 41]}$$

This can be put in terms of the dielectric constant and the loss tangent, and then the average amount of power dissipated per unit volume, $P_{av}$, can be given by the equation:

$$P_{av} \cong \sigma |E_{internal}|^2 = 2\pi f \varepsilon_o \varepsilon_r' \tan\delta |E_{internal}|^2 \quad \textbf{[2. 42]}$$

where $|E_{internal}|$ is the magnitude of the electric field within the material [Sut89, New91, Met83, Kat92, Tin88].

However, the use of these parameters in an experimental situation is not always easy. Ideally, it would be desirable to know the values of these parameters to be able to predict the heating rate of a sample. If the average power absorbed is put into terms of heat the following equation is obtained:

$$P_{av} = \frac{Q}{t} = \frac{Mc_p \Delta T}{t} \quad \textbf{[2. 43]}$$

where Q is the heat produced in the sample, M is the mass of the sample being heated, $c_p$ is the specific heat (J/kg °C) at constant pressure, and $\Delta T$ is the amount of temperature rise [Fat94]. If equation [2.43] is multiplied by volume and combined with equation [2.42], then the heating rate can be defined as:

$$\frac{\Delta T}{t} \cong \frac{2\pi f \varepsilon_o \varepsilon_r' V \tan\delta \left|E_{internal}\right|^2}{Mc_p} \quad \textbf{[2. 44]}$$

$$\frac{\Delta T}{t} \cong \frac{2\pi f \varepsilon_o \varepsilon_r' \tan\delta \left|E_{internal}\right|^2}{\rho c_p} \quad \textbf{[2. 45]}$$

where $\rho$ is the density of the material.

Unfortunately, obtaining even this equation requires several assumptions that often are not strictly true in real life systems. To add to the problem, the measurement of the internal electric field is far from a trivial matter. In fact, it is nearly impossible, which makes the use of the above equations impractical. The situation is exacerbated by the fact that the internal electric field will not normally be constant within the material either, but will vary with location [Tin93b, Koh95, New91, Isk91, Jan92, Tin93a, Hut95a, Byk96, Cla97].

However, even putting this fact aside, these equations are not as simple as they appear. In fact, many of the equations may be further complicated in that many of the parameters such as heat capacity, dielectric constant, loss factor, loss tangent, and conductivity do not remain constant with temperature, but their values actually have a temperature dependency [Tin93a]. In addition, both frequency and temperature affect the

dielectric constant, the dielectric loss factor, and the loss tangent [Kin76, Hen90]. The frequency dependence of these parameters is shown graphically in Figure 2.11 [Hen90]. Examples of the frequency dependence of the loss tangent for several silicate glasses are shown in Figure 2.12 [Kin76]. The effects of both frequency and temperature have been experimentally verified, and examples of the shift in relative dielectric constant for aluminum oxide ($Al_2O_3$) and for a soda-lime-silica glass are shown in Figure 2.13 and Figure 2.14 [Kin76]. Measurements have been performed to determine the maximum in the loss tangent for a $Li_2O \bullet 2SiO_2$ glass as the temperature was varied, with the results shown in Figure 2.15 and Figure 2.16 [Hen90]. The temperature dependence of the dielectric loss is quite clear. Further evidence of the importance of temperature in relation to dielectric loss are represented by Figures 2.17 –2.19 [Hen90, Kin76].

**Dielectric Property Measurements**

The dielectric constant is difficult to measure at microwave frequencies. All dielectric measurements tend to fall within three categories of lumped element, resonant cavity, and transmission line techniques. Lumped element techniques measure the capacitance and conductance between two electrodes with and without the sample inserted. Resonant cavity techniques measure the shift in frequency and quality factor (Q-factor) with and without the sample inserted. Transmission line techniques measure the amplitude, phase and shape of waves transmitted or reflected by a sample. Some of the more common techniques that fall within these categories will be explained further including the partially filled waveguide methods, perturbation methods, partially filled cavity method, open-ended coaxial probe method, and lumped-circuit parallel-plate capacitor method [And91, Isk88, Ara93].

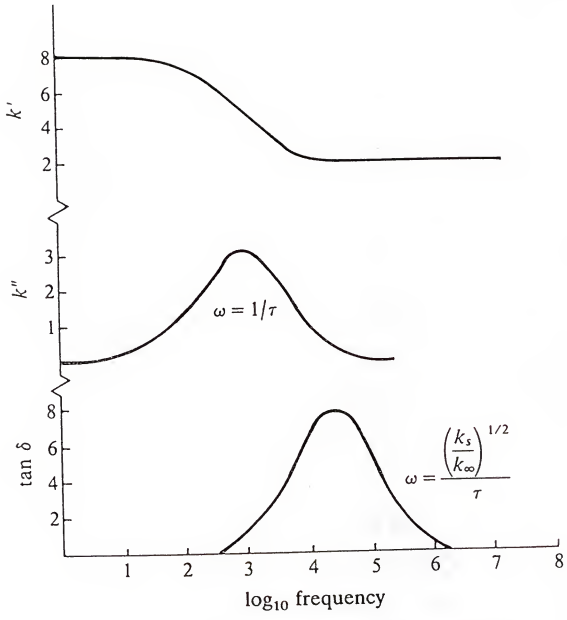


Figure 2.11. Frequency dependence of the relative dielectric constant ($\varepsilon_r'$ or k') , and relative dielectric loss factor ($\varepsilon_r''$ or k") and the loss tangent as a function of frequency. [Hen90]

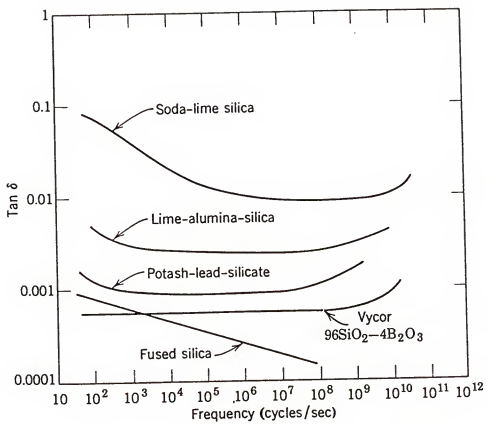


Figure 2.12. Frequency dependence of the loss tangent for various silicate glasses. [Kin76]

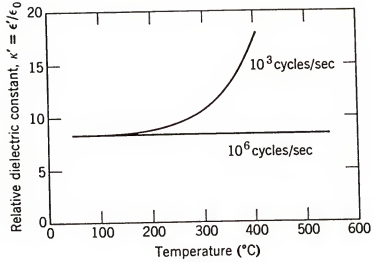


Figure 2.13. Relationship between frequency, temperature, and dielectric constant of an aluminum oxide crystal with the applied field perpendicular to the c-axis of the crystal. [Kin76]

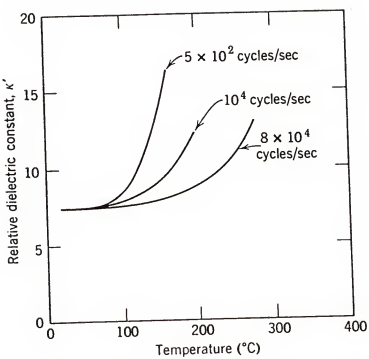


Figure 2.14. Relationship between frequency, temperature and dielectric constant of a soda-lime-silica glass. [Kin76]

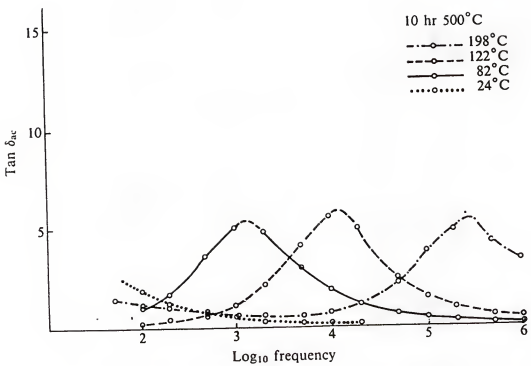


Figure 2.15. Dielectric loss peak shift in a $Li_2O{\bullet}2SiO_2$ (L2S) glass due to increasing temperature. [Kin76]

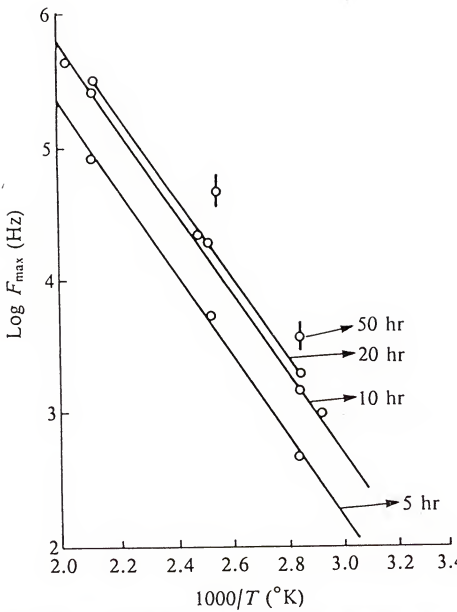


Figure 2.16. Time and temperature dependence of the frequency of the dielectric loss peak for an L2S glass heated to 500 °C. (see Figure 2.15) [Kin76]

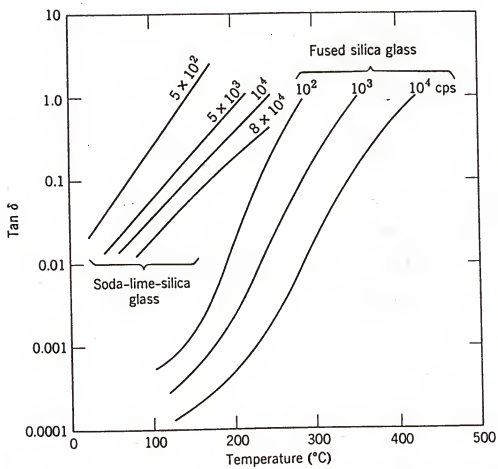


Figure 2.17. Change in loss tangent as a function of temperature for a soda-lime-silica glass and for a fused silica glass. [Kin76]

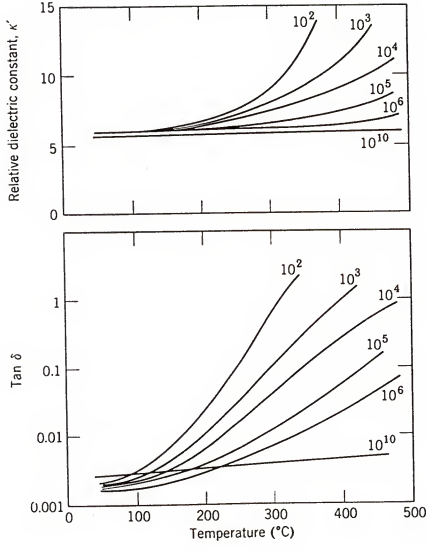


Figure 2.18. Change in loss tangent and relative dielectric constant ($\varepsilon_r'$ or k') as a function of temperature and frequency for a steatite ceramic. [Kin76]

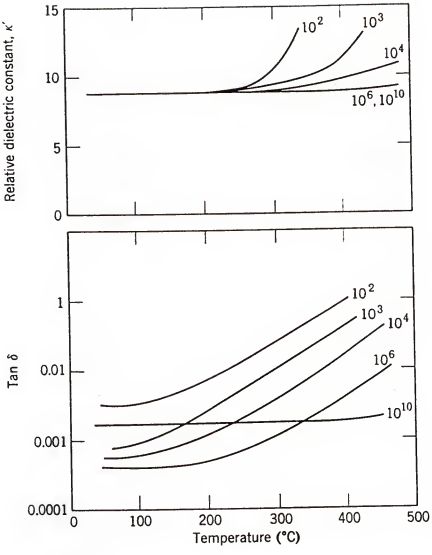


Figure 2.19. Change in loss tangent and relative dielectric constant ($\varepsilon_r'$ or k') as a function of temperature and frequency for an alumina porcelain. [Kin76]

**Partially Filled Waveguide Methods**

The first method is that of Roberts and von Hippel. This is considered a transmission line technique [Car91]. In this method, a standing wave traveling through a waveguide is analyzed when the waveguide is terminated by the sample in question compared to when it is empty. A diagram of the apparatus involved is shown in Figure 2.20 [Met83]. The wave pattern that develops from the combination of the forward and reflected waves is called a voltage standing wave ratio, or VSWR. Analysis of this data in conjunction with sample dimensions, frequency, and the characteristics of the waveguide allow the complex dielectric constant to be calculated. Further details on the equations involved in this calculation may be obtained from Metaxas or von Hippel [Met83, Rob46, And91, von54a].

A second method is a two-impedance method for liquids, which was developed by Fatuzzo. In this method, the two impedances can be calculated from the VSWR and the position of the minimum for two different positions of a variable short circuit. The complex dielectric constant may then be measured from the values of the impedances. A diagram of the setup for this measurement technique is illustrated in Figure 2.21 [And91]. This method is simplified compared to the Roberts and von Hippel method, as it requires less computation to obtain the desired values [And91, Fat64].

**Cavity Perturbation Methods**

The cavity perturbation method falls in the category of resonant cavity techniques. The cavity perturbation method requires the sample to be very small in comparison to the size of the cavity. The sample size must be small and precisely positioned so that only a small frequency shift is produced due to the insertion of the sample. In early years, this

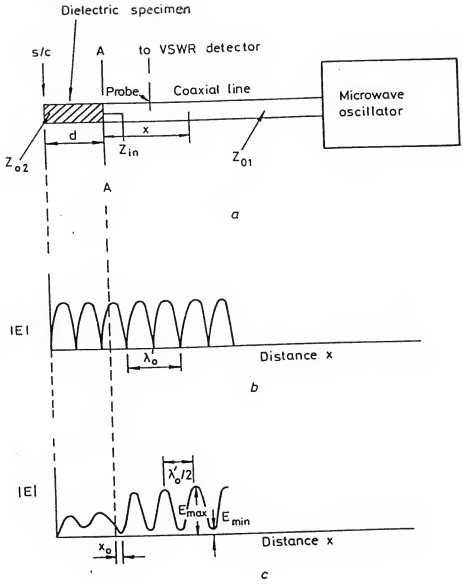


Figure 2.20. Schematic diagram for dielectric measurements made by Roberts and von Hippel using the partially filled waveguide method. [Met83]

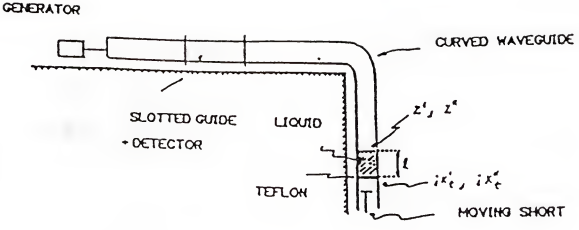


Figure 2.21. Schematic diagram of apparatus used for the two-impedance method for dielectric measurements. [And91]

method was frequently used to obtain data on low loss materials [Met83]. This method may be employed to obtain high temperature dielectric data with the additional use of a conventional furnace. Equations have been developed for both rectangular and for cylindrical cavities [Met83, And92]. This method measures the difference in the resonance frequency and the Q-factor of the cavity with and without the sample placed in the region of highest electric field [Met83, And91, And92]. With the right equipment, this technique may be utilized to obtain values of dielectric data at various frequencies as well [Hut92].

**Partially-Filled Cavity Method**

Also a resonant cavity technique, a partially-filled resonator method may be utilized when larger samples are than can be examined using the cavity perturbation technique. A single mode cavity is partially filled with the sample, and then the complex permittivity may be obtained from measurement of the resonant frequency, Q-factor, and coupling coefficient of the resonator [And91].

**Open-Ended Coaxial Probe**

A transmission line technique, the use of an open-ended coaxial probe allows a larger sample than cavity perturbation techniques, but requires a smooth flat surface on one side. This prepared surface is placed against the coaxial probe. The reflection coefficient is then measured to obtain dielectric data. However, for high temperature measurements, the thermal expansion of the probe becomes important, as the length of the probe will change, thus in effect altering the characteristics of the wave traveling down the probe. As a result, for high temperature measurements, a calibration of the probe must be performed to normalize the data [Ara93].

**Lumped-Circuit Parallel-Plate Capacitor**

This is a type of lumped element technique, and is generally used for low-frequency measurements, generally below 10 MHz. This method requires the sample to be placed in a parallel-plate capacitor, and the complex impedance to be measured. The difficulties with this technique include electrode polarization at low frequencies, and self-inductance of the sample holder at high frequencies. Possible solutions to these difficulties have been suggested, but this remains a viable technique when used properly. It has the most potential when used in conjunction with higher frequency techniques to get a better broadband picture of the dielectric properties [Isk88].

**Dielectric Measurement Technique Comparison**

It is very clear that there are many possible techniques which may be employed for the measurement of dielectric properties. The question that should then be asked is how do these methods compare to each other? It has already been mentioned that one method is better at low frequencies, another requires a very small sample size, and other factors will be important with other measurement techniques. It is also known that the values of both $\varepsilon'$ and $\varepsilon''$ are affected by temperature. In fact, $\varepsilon''$ may change by orders of magnitude between room temperature and 1000 °C [Bat95]. Therefore, values of $\varepsilon'$ and $\varepsilon''$ were measured at 915 MHz and 2.45 GHz using a variety of techniques on the same sample at different laboratories as a function of temperature.

The results were found to be dependent upon the material being examined. One material studied was aluminum oxide (alumina). Regardless of laboratory or method, all of the values found for $\varepsilon'$ were within ±5%. The measurements for $\varepsilon''$, however, were not in such good agreement. Another material that was studied was silicon carbide. In this

case, with the results shown in Figure 2.22 and Figure 2.23, the true values of ε' or ε" are difficult to conclude [Bat95]. Some laboratories were unable to even obtain values of ε' for silicon carbide. For those measurements that were successful, the range of values is from around 100 to 500. The range in values for ε" is similarly large, ranging from about 100 to 400. The conclusions that were drawn from this parallel measurement study were that agreement could be obtained for values of ε' for materials with ε'≤40. However, especially at higher temperatures, less corroboration could be obtained for ε' of lossy materials. In the case of ε", inadequate agreement between laboratories was found for both types of materials [Bat95].

However, if any further complication is needed, one can also examine the effects of size and geometry, which will also change dielectric loss measurements [Hut95a]. Porosity may also be a factor in the heating of a material [Kin76]. In any case, prediction of how much a given material will heat is very difficult in practice. To assist in this prediction, several researchers have suggested that more empirical models need to be defined in order to assist in the creation of theoretical models [Vos91, Isk93, Ste94, Gar95, Boo97].

**Microwave Heating Mechanisms**

There are several theories as to why one material will heat in the microwave frequency range and another will not. It is all based on one simple difficulty: "there appear to be no oscillations in ceramic materials with characteristic frequencies in the microwave range" [Ken91]. At one time, it was thought that microwave heating was caused by resonance. But, the frequencies of resonance vibrations are 2 to 3 orders of magnitude larger than microwave frequencies in the GHz [Ken91]. So, for resonance to

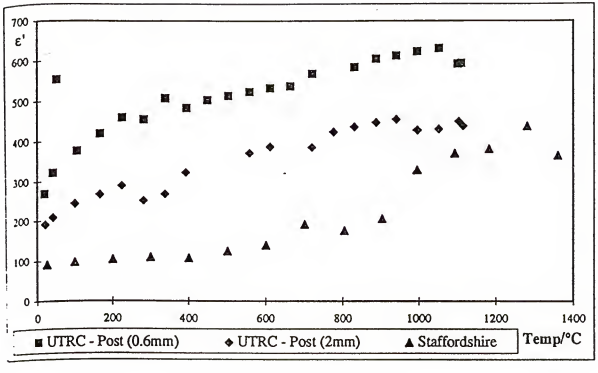


Figure 2.22. Measurement of the dielectric constant of "Type N" silicon carbide as a function of temperature at 2.45 GHz. [Bat95]

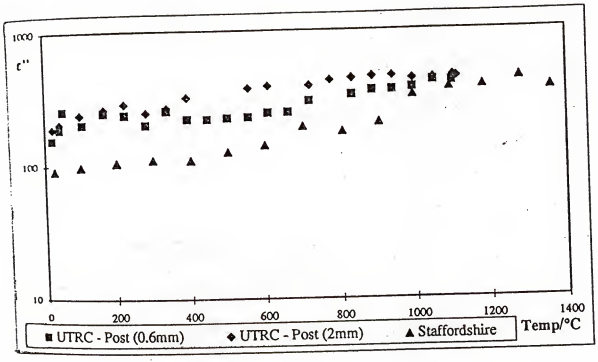


Figure 2.23. Measurement of the dielectric loss factor of "Type N" silicon carbide as a function of temperature at 2.45 GHz. [Bat95]

be the cause of microwave heating, extremely high damping forces would be required, so this idea was discarded [Ken91, Kat91]. The next theory that was submitted was that of relaxation. With this theory, scientists proposed that the Debye relaxation mechanism acting upon vacancy or interstitial motion was the microwave interaction responsible for heating at the microwave frequency range [Ken91, Kat91, Bru91, Mor91, Hut92, Men95, Hut95b, Dis97]. Unfortunately, this does not adequately explain all of the effects observed [Met83]. More recently, a new theory relating to coupled oscillators has been proposed, and further investigation of this idea is necessary to determine its validity [Wes99].

**Types of Microwave Behavior**

In any case, regardless of what exactly leads to heating at the microwave frequencies, materials may be classified into three basic categories, as shown in Figure 2.24 [Sut89]. The first is that of a transparent material, or low loss insulator, which will absorb next to no microwave energy, allowing the microwaves to fully pass through the material without significant attenuation [Sut89]. This interaction is depicted in the first diagram in Figure 2.24. An example in this category is alumina, which at least at low temperatures (and high purity) is relatively transparent to microwaves.

The second type is an opaque material, which will reflect the wave, as indicated by the second diagram in Figure 2.24 [Sut89]. Metals fall into this category, and since the material does not absorb the energy, they will usually not heat very well in the microwave. From a practical standpoint, metals may be viewed as complete reflectors. However, the microwaves will penetrate slightly into the surface, and may create surface currents which may lead to heating in very small particles [Cam92, Bes91]. This skin

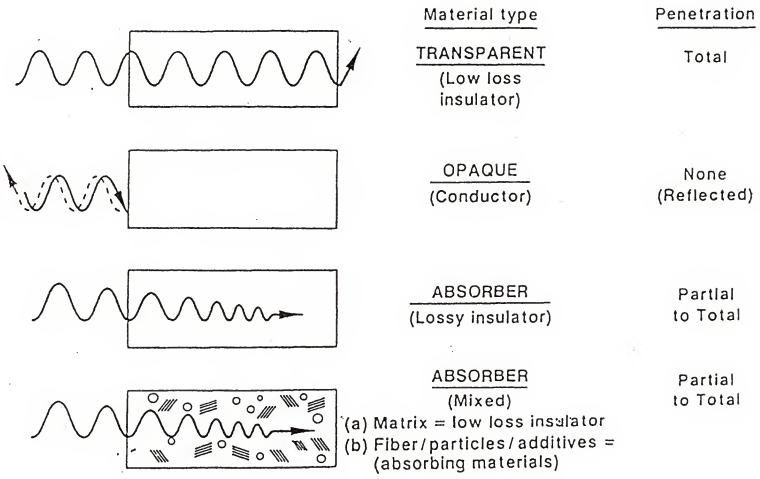


Figure 2.24. Illustration of types of microwave interactions with materials. The material under examination in this study falls in the category of mixed absorber.

depth, δ, to which these surface currents will be effective are defined by equation [2.16], and was simplified by von Hippel as:

$$\delta = 2.9 * 10^{-2} (\rho\lambda)^{1/2} \textbf{[2. 46]}$$

where ρ is the resistivity of the material, and λ is the wavelength of the incident wave [von54b, Bes91]. Most metals are conductors, which means that the resistivity would be correspondingly small, ~$1*10^{-7}$ Ω-m for platinum or iron [von54b]. As a result, it can be concluded that the skin depth would be exceedingly small, and only when the particle size gets small enough that a significant area of the metal would be included in the skin depth would a metal begin to show any significant microwave heating. Figure 2.25 gives an idea of what the skin depth would be for several common metals as a function of resistivity and wavelength in air. In addition, most metals are very good thermal conductors, which would mean that any heat generated may be quickly dissipated.

The final category of absorber has two subdivisions, as displayed in the bottom two diagrams in Figure 2.24 [Sut89]. This is the category of most interest in this study, as the susceptor material under examination falls into this category. The first subdivision within this category is that of a lossy single-phase insulator, which would include materials such as silicon carbide, carbon, boron carbide, and others. These materials will absorb the incident microwave energy by attenuating the wave. This interaction results in heating of the material. The second subdivision in this category is that of a mixed absorber, where the matrix is a low loss insulator that contains an additive that absorbs the microwave energy [Sut89]. This is exactly the type of system under examination in this study, where the matrix is low-loss high alumina cement and the reinforcement is high-loss silicon carbide particles [Lei97, Lei98, Lei99, Coz97b]. In both of these

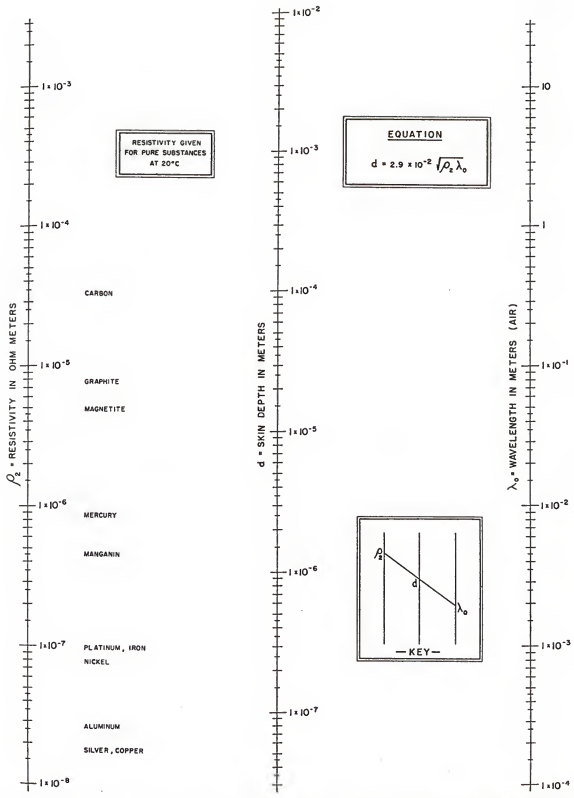


Figure 2.25. Skin depth, d (or δ) in a metal as a function of resistivity and wavelength in air.

subdivisions in the category of absorber, the radiation may pass through the material either partially or totally, depending upon the specific dielectric properties and the size of the sample.

However, what happens if we want to heat a material which at a given temperature and frequency is transparent to the incident microwave energy? In these cases, microwave hybrid heating (MHH) may be employed. The concept of microwave hybrid heating is simple: it uses an additional material (a susceptor) which will absorb the microwave energy. This additional material will then heat the sample material. This is especially useful for "jump-starting" materials which do not have much dielectric loss at low temperatures, but will heat at higher temperatures [Sut92, Cla91, Moo91, Dé91a, Ahm91]. In this manner, sample materials are heated partially by the microwave energy they themselves absorb, and partially by radiation from the susceptor. In theory, MHH could also be used for a material that might heat readily at low temperatures, but absorption drops off as temperature increases.

In addition, MHH is also useful for those materials that already sufficiently absorb microwave energy by flattening out the temperature profile. Since microwaves tend to heat a sample from the inside out, heating the material volumetrically, microwave heating tends to exhibit an inverse temperature profile with the highest temperature on the inside and the lowest temperature on the outside. This is mostly due to radiation losses [Ska94, Joh93]. Without these radiation losses, the temperature profile would be much more even throughout the sample material. However, by providing a susceptor at the surface of the sample material that radiates energy for the sample to absorb, a more even temperature profile is produced. A more even temperature profile reduces thermal

stresses, as well as producing a more uniform microstructure. The production of a more uniform microstructure is desirable in most cases because it tends to provide better mechanical properties.

It should be noted that some confusion exists in the literature with regards to terminology. The term 'casketing' may be used instead of 'microwave hybrid heating.' However, this is not always the case. The casketing of a sample refers to the enclosure in which the sample is heated within the microwave cavity. In some instances, this may be merely insulation [Por92, Vol93]. However, in other cases, the casket may also provide hybrid heating by either using a zirconia type insulation, or incorporating a susceptor material into the casket [Fre94, Sam94, Tho95, Lee95, Bru96].

The use of susceptors for various applications has been well documented. In fact several different types of susceptors have been used. One of the first types of susceptor that was suggested was boron carbide [Kat88]. Later work nearly exclusively focuses on the use of silicon carbide in one form or another to assist in microwave coupling. For example, Willert-Porada et al. used recrystallized silicon carbide for processing cermets [Por92].

Another popular design involves the use of silicon carbide rods in what is termed the 'picket fence.' This technique utilizes a number of silicon carbide rods strategically placed around the sample to assist in heating [Jan91, Kim91]. These rods are also supposed to make the electric field within the microwave cavity more uniform [Isk93, Kim91]. And, a more uniform electric field would of course provide more even heating of a material. Unfortunately, the use of these silicon carbide rods does produce some additional difficulties. One problem was arcing of the rods, although this was overcome

by a small nitrogen flow [Jan91]. This may not always be a palatable solution. Additionally, researchers encounter the question of how many rods, and where to put them [Smi92]? Modeling experiments based on the silicon carbide rod technique indicate that these rods affect the field distribution within the microwave cavity in addition to stimulating heating. As a result, they may be used to help produce more uniform heating and microstructure within a sample material [Isk93]. Unfortunately, at this point in time, techniques such as this are "considered forms of art and highly dependent on human expertise" [Smi92].

Therefore, the researcher is faced with the dilemma of too many rods may inhibit microwave heating of the sample itself if all of the energy is absorbed by the rods. Conversely, too few rods might not significantly affect the heating of the sample, and may even produce non-uniform effects [Smi92, New93]. An additional factor to consider is how far away from the sample that the rods should be placed. Finite difference time domain simulations determined that when using the 'picket fence' design, when the rods are placed at the corners and are touching the sample, it was found to heat much faster and the rods generally stay at lower temperatures. On the other hand, when the rods are moved further out, then most of the power absorbed by the silicon carbide rods is lost to the surroundings and could not sinter the sample material [Tuc92].

Another silicon carbide susceptor design that has been employed is the use of an insulating material lined on the interior with silicon carbide granules [Moo91, Dé91b, Dé91c, Coz91, Sch91, Al-A91, Al-A92, Sch93a, Sch93b, Zho93, Boo95, Boo94, Zho94, Ahm92]. The insulating material was zirconia in some cases, and in other cases an alumina refractory cement. This design has been widely used for a variety of

applications, which include: sintering alumina [Dé91b, Dé91c], processing superconductors [Coz91], processing simulated nuclear waste glass [Sch91, Sch93b], microwave joining [Al-A91, Al-A92], use with a microwave thermogravimetric analysis (MTGA) [Moo91], microwave destruction/vitrification of electronic components [Sch93a], microwave densification of porous silica gel [Zho93, Zho94], crystal growth in glass [Boo95], glass repair with a sol-gel coating [Boo94], and joining silicon carbide [Ahm92].

More recently, however, a modification of one of the above designs has been utilized. Instead of lining the alumina refractory cement with silicon carbide, the silicon carbide has been incorporated into the cement before it is shaped [Coz95, Cla94]. Consequently, a greater choice of shape of the susceptor materials is available. Nearly any castable form can be chosen, and thus the susceptor can be made to closely conform to the shape of the sample. By conforming to the shape of the sample, temperature gradients due to differences in the proximity of the sample to the susceptor can be avoided. These susceptors can also be made cheaply and easily [Lei97, Lei98, Lei99].

These particular composites have already been used to process a number of different materials. Some examples include a salt solution [Cla94], joining of zinc sulfide [DiF95a], joining of alumina [Coz95, Coz97a, Coz96a], redox ceramic-metal composites [DiF96, DiF97], decomposition of ceramic oxides [DiF98], synthesis of $TiC/Al_2O_3$ and $Ti_3SiC_2$ composites [Ato98, Kom94], and densification of $Al_2O_3$ composites [Dar96]. To truly understand what is happening within these and other systems, the susceptors used for hybrid heating need to be better understood.

**Temperature Measurement**

Difficulties with obtaining accurate temperature measurements due to arcing or other problems have been widely reported in the literature [Kat88, Sut89, Sut92, Sut93, Cla96, Jan92, Bes91, Gre93, Gre95, Coz91, Oda88, Fre93, Sch94]. Basically, several different options are available for temperature measurement in the microwave oven, and each has its own strengths and weaknesses. The commonly used techniques for temperature measurement are infrared pyrometer, optical fiber lightpipe, or thermocouple.

The infrared pyrometer examines the radiation given off by a target sample. A lower temperature limit tends to apply, since at low temperatures, materials give off very little radiation. Two different types of pyrometers are in common usage. The first is a single-color pyrometer, where the total energy of a single wavelength of emitted radiation is examined to determine the temperature. The second type is the two-color pyrometer, which examines the emitted radiation at two different wavelengths, and then determines the temperature from the energy measured at both wavelengths. This type of pyrometer tends to be more accurate than does the single-color pyrometer, as measurement errors can be eliminated somewhat by the comparison of the two energy at both wavelengths. Some of the critical parameters to the accurate determination of temperature by infrared pyrometry that are often neglected are accurate focal length, spot size, and emissivity. Depending upon the size of the sample, in some cases the temperature measured by pyrometer may include an area greater than the size of the sample, which will lead to measurement errors. In addition, proper calibration of the pyrometer with respect to emissivity is necessary. The temperature of non-graybodies may also be difficult to

measure using this method. And of especial importance for microwave hybrid heating, the infrared pyrometer may look through a sample and measure background (or susceptor) temperatures if the background is hotter than the sample [Bar95, Mer95]. However, it can be said that the pyrometer is not influenced by the presence of the electric field in the microwave cavity [Mer91].

The optical fiber lightpipe gathers emitted light, and conducts this light to a radiometer which then calculates the temperature from the amplitude of the light signal at a specific wavelength. In some cases, the tip of the optical fiber lightpipe may be coated with a thin film of a noble metal (such as platinum), which would be in thermal contact with the material. The metal film emits radiation, which is then analyzed to determine the temperature of the sample. In other cases, the optical fiber does not have a metal tip, but the tip will instead be optically polished, and will gather the energy over a conical area of ~52°. This type of probe (the metal film, if present, may couple slightly) is essentially immune to microwave energy. The response time for both types of lightpipes is extremely fast, and lightpipes may be able to withstand temperatures up to 1900 °C. They may also be manipulated to measure the temperature in difficult locations [Mer91]. The major argument in favor of this type of temperature measurement device is that since the probes are nonmetallic and nonelectric, neither the probe nor the electric field is affected by each other, so that they are capable of accurate measurements during operation of a microwave [Ber93].

The third type of temperature measurement device generally utilized is the thermocouple. Thermocouples take advantage of the Seebeck effect. The Seebeck effect involves the generation of a voltage between the joining of two dissimilar wires and the

free ends. If a voltmeter is connected to the free ends, then the temperature of the hot end, which would be in contact with a target material, could be determined from the voltage generated [Sch95]. The voltage generated for different combinations of wires have been well documented, and some types of thermocouples are effective up to 2750 °C. Unfortunately, these particular thermocouples also have very low oxidation resistance, and thus cannot be used except in inert atmospheres [Ome95].

Some authors argue that in the electromagnetic field in the microwave oven the thermocouple cannot be accurate, since they tend to couple with the microwave energy, self-heat, and have the potential to heat more than the sample itself, leading to erroneous measurements [Mer91]. Being metal, they may also perturb the electric field [Fre93]. Another difficulty previously mentioned with thermocouples is that of arcing, where the tip of the thermocouple may become superheated by the energy discharge. However, if this can be suppressed, the accuracy has been found to be within normal conventional oven parameters. Once arcing can be eliminated, studies found that thermocouple readings were reproducible, and if more than one was used, also gave very similar readings, within 2 °C throughout the entire temperature regime [Jan92, Fat93, Dar95, Gre93]. A comparison study between lightpipes, pyrometers and thermocouples found that measurements made simultaneously by the three devices were within a range of ±20 °C, similar to that within a conventional type of furnace. In fact, the pyrometer had the largest variation of the three devices. Positioning of the lightpipe was found to be critical, as the temperature reading dropped by 70 °C when at the surface of the sample as compared to when it was in a buried position within a well drilled in the sample. In fact,

the thermocouple tended to produce temperature readings that were in between that of the pyrometer and the lightpipe [Gre93].

Due to the relatively small sample size, as well as available equipment, it was decided that this study would use thermocouples as the only temperature measurement device. Much corroborating evidence is available for the validity of the measurements made by thermocouples in the microwave [Jan92, Fat91, Fan93, Gre93, Dar95, Ham97]. and they have been used extensively for temperature measurement in the microwave field [Coz95, Coz97a, Moo91, Ahm91, Lei97, Lei98, Lei99, Jan91, Fan91a, Jan92, Byk96, Dé91b, Coz91, Sch91, Sch93a, Sch93b, Boo95, DiF96, Fat91, Fan93, Gre93, Dar95, Ham97, Coz94, DiF95b, Dal90, Fat92, Jan93, Tie93, Kig93, Moo93a, Fat93, Boo93, Kig94, Gre95, Dad96].

# CHAPTER 3
# MATERIALS AND EXPERIMENTAL PROCEDURE

Using microwave energy as a high temperature processing method has many potential benefits that may be realized. However, difficulties may arise if the material to be processed does not absorb microwave energy very well at low temperatures. To overcome this, two approaches may be implemented. In either case, more information is needed to attain any kind of predictability. The first possible approach would be to shift the frequency of the incident microwave energy to one at which the sample material will absorb the energy, and thus will heat. The optimum frequency for heating will vary depending upon the material in question. Shifting the frequency is often difficult to do in practice, however, since equipment is not always commercially available (cheaply, that is) at all frequencies. And, if a variety of different materials are to be processed, it is simply not feasible to provide an oven for each frequency required. Therefore, option two is to provide a susceptor material for microwave hybrid heating that will heat the sample more readily at low temperatures and at a frequency where equipment is commercially available. This is the option under examination here.

Other studies had looked at using silicon carbide rods, or attaching silicon carbide particles to an insulation material, since silicon carbide is a lossy material that absorbs microwave energy well at 2.45 GHz. Silicon carbide is commonly and cheaply available in the form of abrasive particles. Unfortunately, it would be difficult as well as messy to

use a pile of particles as a "heating element." Aluminum oxide ($Al_2O_3$) is a material that is relatively transparent to microwave energy at low temperatures. The composites combine the benefits of the high microwave absorption of the silicon carbide particles at 2.45 GHz with the strength and formability of high alumina cement* [Sut88, Coz95, Cla96, Lei97, Lei98, Lei99, Lei00]. In this manner, the heating rate is controlled by the silicon carbide. These composites can also be formed into any castable shape, do not require any sintering, and are low cost. Beyond this, these susceptors can undergo hundreds of cycles up to 1200 °C without degradation, and many times up to 1500 °C and possibly above [Lei97, Lei98, Lei99, Lei00].

However, once the components were determined, further questions needed to be answered. Some of the questions were developed over the course of the study, as it was discovered that these factors affected the heating rates of the silicon carbide/high alumina cement composites. The factors that remained constant throughout the entire set of experiments were the general components of the composite, the fibrous refractory insulation surrounding the susceptor composites, the microwave oven in which the susceptors were heated, and the placement of the susceptor and housing within the microwave cavity.

**Sample Fabrication**

All samples for all phases were made following the same procedure. The dry weight of the samples were 60 g, and this weight was used to calculate the weight of the silicon carbide and alumina cement required to produce a composite of the desired

* High alumina cement contains approximately 95% aluminum oxide, with the remaining 5% composed of calcium compounds such as calcium oxide.

composition. The amount of silicon carbide in the composites was varied from 10 to 50 weight percent. An upper limit of 50 weight percent silicon carbide was necessary as some of the susceptors began to lose structural integrity around this composition. The high alumina cement used for all samples was Alfrax 66 manufactured by Carborundum, Refractories Division. Six different silicon carbides were used, and these will be specified later, for each individual phase of the experiment. Figure 3.1 displays a schematic of the procedure utilized to fabricate the composites.

To fabricate the samples, first the appropriate weights of silicon carbide and high alumina cement were measured to make the 60 g composite. (i.e. 6 g SiC + 54 g cement = 60 g 10 wt.% SiC composite) Then, these two dry materials were mixed together to create a uniform mixture. De-ionized water was next added to this mixture. Subsequently, as small an amount of water as possible to create a flowable mixture was added so that particle settling of the larger silicon carbide particles would be minimized. Since this cement is a hydraulic cement, as long as the amount of water is sufficient for hydration, stronger cements will be created from the addition of less water [Ric92]. Once a uniform mixture was once again obtained, it was cast into an approximately 30 mm (2") diameter polytetrafluoroethylene (PTFE) container. An indentation for the thermocouple was made in the center of the composites once they had set enough to hold the shape. This indentation was made to measure the temperature of the susceptor closer to the center of the sample. After casting, the composites were dried. The composites were first dried with a cover overnight to allow the initial setting of the cement to take place. Next, the composites were air dried with the covers removed for 24 hours. Finally, the composites were placed in a drying oven at 75-100 °C for 1-2 days to remove the

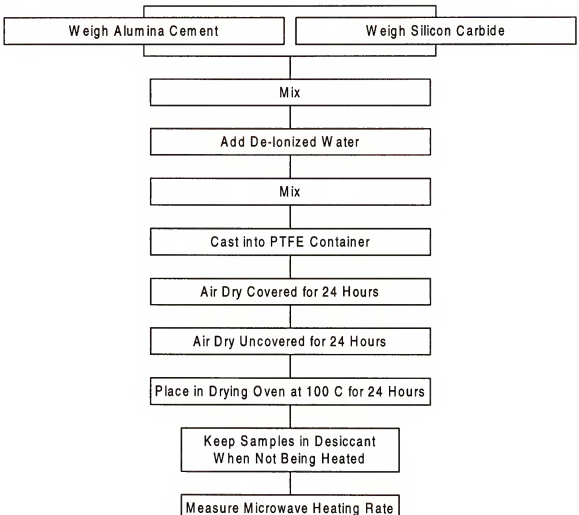
Weigh Alumina Cement
Weigh Silicon Carbide
Mix
Add De-Ionized Water
Mix
Cast into PTFE Container
Air Dry Covered for 24 Hours
Air Dry Uncovered for 24 Hours
Place in Drying Oven at 100 C for 24 Hours
Keep Samples in Desiccant When Not Being Heated
Measure Microwave Heating Rate

Figure 3.1. Schematic of the experimental procedure used to make the composite samples.

remaining unbonded water. The composites were not removed from the casting container until after the entire drying process was complete. During the final drying step, the composites tended to shrink, and the PTFE containers also tended to expand slightly away from the composites, allowing for easy removal at completion of this step.

The above procedure was found to be quite effective towards the objective of creating a strong, uncracked composite. At this point, the composites were ready to undergo heating.

**Phase I**

The first question that was postulated was how much silicon carbide, and how large should it be? This question formed the basis of the design for phase I of the experiment. In this case two types of silicon carbide were utilized, with the weight percent of silicon carbide in the composites varying from 10 to 50 weight percent. The two types of silicon carbide each had very different particle sizes, with the "coarse" silicon carbide composites using α-phase silicon carbide from Standard Sand and Silica Co., 16 GRP Carbolon Green silicon carbide, with an approximate 1000 μm particle diameter, and the "fine" silicon carbide composites using α-phase silicon carbide from Norton Company, 180 Grit Crystolon, with an approximate 85 μm particle diameter. A few combination "coarse" and "fine" composite samples were also fabricated, incorporating half of each type of silicon carbide. Both of these types of silicon carbide are low purity, abrasive grade materials comprised of approximately 97-98% silicon carbide, with the major contaminant being elemental carbon. After being cast and dried, these composites were then weighed again, and it was found that the sample weight was maintained at between 58 and 59 grams.

At this point, the composites were ready to be microwave heated. A fibrous refractory housing of LI-900* was specially shaped to conform to the samples and insulate them. This insulation is one of the few materials that has been found to be not only an extremely effective thermal insulation material, but also an effective microwave processing insulation material. Difficulties have been encountered in obtaining an insulation which does not absorb microwave energy at 2.45 GHz. When the insulation absorbs the microwave energy, its effectiveness is reduced, as the insulation will not only get hot, but this also reduces the microwave energy that can subsequently be absorbed by the sample that is desired to be heated. The top of the refractory housing contained a hole to allow a grounded tip, K-type thermocouple (Omega Engineering, Inc., XCIB-K-1-3-L) to pass through the refractory housing and come in contact with the sample, so that the temperature of the composites could be measured in-situ. A small piece of zirconia felt (Zircar) was placed in between the composite sample and the thermocouple tip to prevent arcing between the two.

To measure the microwave heating rate, samples were placed in a home model 800 watt microwave oven manufactured by JC Penney, model 5910-00-40. The microwave cavity was slightly modified to allow the insertion of the thermocouple through the outer wall of the microwave cavity. The thermocouple was well grounded to the aluminum outer wall of the cavity, which minimized charge buildup (and consequently the potential resulting erroneous temperature readings) along the Inconel sheath of the thermocouple. Within the microwave cavity, composite samples were raised off the floor of the microwave by a low temperature refractory brick being placed

*Lockheed Insulation-900, 100% $SiO_2$ fibers

on the floor of the microwave cavity, and the refractory housing containing the composite sample would be placed on top of this brick. The location of both the brick in the microwave cavity as well as that of the refractory housing on the brick was marked. This was done to ensure that further variables were not inadvertently introduced into the experiment.* A diagram of this experimental setup is demonstrated in Figure 3.2.

Composite samples were then heated for either 15 minutes (900 seconds) or until the sample reached approximately 1150 °C, whichever came first. The maximum temperature limit was imposed by the K-type thermocouple used to measure temperature, as well as to prolong the life of the refractory housing. Temperature versus time data was measured every 30 seconds for each different sample composition. After the composite samples had either reached the maximum temperature or been heated for the maximum time, they were immediately removed from the microwave cavity and refractory housing and allowed to cool as rapidly as possible in air. This was done to ensure that the composite samples underwent the harshest thermal cycling that might be experienced in production of other materials. However, in some cases, due to thermal expansion of the composite samples, they could not be immediately removed easily from the refractory housing. In these instances, the composites were allowed to cool within the housing for 3-5 minutes, at which point they would have cooled to below approximately 600-700 °C, and could then be easily removed. The experiment was repeated up to 17 times for each

* In a multimode microwave cavity, the field, and thus the modes produced, may shift by any change in the contents of the cavity. Therefore placement of the sample may in some cases subtly affect the heating rates measured. However, this effect is less pronounced for microwave ovens with a mode-stirrer such as the one employed here.

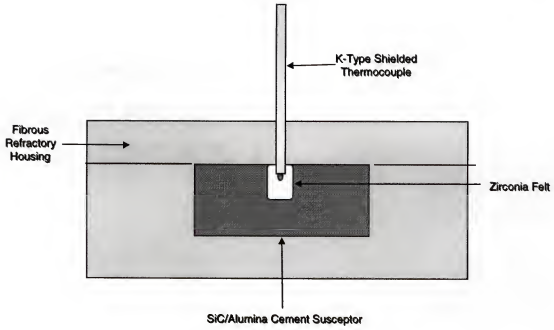


Figure 3.2. Diagram of the experimental setup used for microwave heating.

sample to prove repeatability, and even under this thermal cycling, mechanical failure (which would be caused by thermal shock) did not occur.

**Phase II**

Phase I of the experiment demonstrated that both the weight percent and particle size of the silicon carbide incorporated into the composite sample affected the heating rate. The next question that was postulated was whether or not the phase of the silicon carbide might also be a factor affecting the heating rates of the composite samples. Therefore, two more types of silicon carbide were utilized, with the weight percent of silicon carbide in the composites once again varying from 10 to 50 weight percent. However, in this case the major difference between the two types was the phase of the silicon carbide that was mixed with the high alumina cement. The composite samples were fabricated as before to make 60 g susceptors, except in this case using either 2 μm diameter particles of α-phase silicon carbide manufactured by Alfa Aesar with 99.8% purity, or 1 μm diameter particles of β-phase silicon carbide also manufactured by Alfa Aesar with 99.8% purity. Higher purity silicon carbide was used in order to remove the purity of the silicon carbide as a variable.

It was also found at this point that humidity did tend to affect the weight of the composite samples. This did not appear to significantly affect the heating rate of the susceptors, especially since any physically bonded water would be driven off during the low temperature regime of the heating cycle. However, to minimize error as much as possible, the composite samples were placed in a desiccator jar whenever they were not being run. Additionally, relative humidity was measured before each run, and heating

rates from several different days, and correspondingly several different relative humidities, were averaged together to give the results reported here.

The composite samples were heated in the same setup and insulation as was used for phase I, as is depicted in Figure 3.2. As before, the composite samples were once again heated to approximately 1150 °C or up to 15 minutes, with the temperature being measured by thermocouple every 30 seconds. Each composite sample was also heated through at least five thermal cycles, and these results were later averaged to obtain the results. Rapid cooling of the susceptors once again did not appear to have any detrimental effects on the material, either in heating, or mechanically.

**Phase III**

Indications that the phase of the silicon carbide incorporated into the composite samples affected the heating rates, especially at higher temperatures were evident from the results of phase II of the experiment. As a result, bonding of the two different particle types to the alumina cement appeared to potentially be a significant factor. It was thought that part of the reason for this difference might be caused by oxidation. Therefore, if oxidation could be inhibited, might the difference be lessened? As a very noticeable difference was still observed between low and high weight percent silicon carbide susceptors, the composition was again varied from 10 to 50 weight percent silicon carbide. In this case, the same high purity Alfa Aesar $\alpha$- and $\beta$-phase silicon carbides were used as in Phase II to fabricate the 60 g composite samples. Humidity continued to be controlled by the use of desiccators.

In order to reduce oxidation, a nitrogen atmosphere would be added to the cavity. The same LI-900 refractory housing could be employed, but other parts of the

experimental setup required adjustment. The microwave cavity required an additional minor modification to allow the atmosphere to be fed into the cavity, so a hole was drilled into the floor of the microwave, and a gas feed tube was inserted. Additionally, the atmosphere in the cavity needed to be contained in some fashion. An overturned desiccator jar (similar to a bell jar) was placed over the entire refractory housing to contain the atmosphere. This new experimental setup is drawn out in Figure 3.3.

This experimental setup did create some additional complications. Due to the increased height of the assembly, a refractory brick of approximately half the height of the one in phases I and II was used underneath the refractory housing. The location of the refractory housing was once again carefully marked on the brick, in the same location as was used previously. Also, the placement of the thermocouple became more complicated. The thermocouple now had to be threaded through the back of the microwave under the lower rim of the jar* without touching the jar or the refractory brick†, up and over to the top of the refractory housing and down to good contact with the composite sample inside. This task was not impossible, but merely difficult to achieve.

This assembly did not provide an airtight seal, but since reduction of oxidation was the primary goal of introducing atmosphere, this was not essential. However, since nitrogen is lighter than oxygen, the nitrogen should drive the oxygen out of the jar given enough time. Therefore, nitrogen was continuously flowed into the chamber at a constant

---

* The thermocouple also could not be allowed to come too close to the floor of the microwave cavity either, or arcing and the corresponding incorrect temperature readings would occur. In addition, too much arcing between the thermocouple and the cavity in a single location would also lead to the development of a hole in the cavity!

† The thermocouple also should not be in contact with the jar or refractory brick as these would normally be much cooler than the composite sample, and this would have the potential to slightly skew the temperature (continued next page)

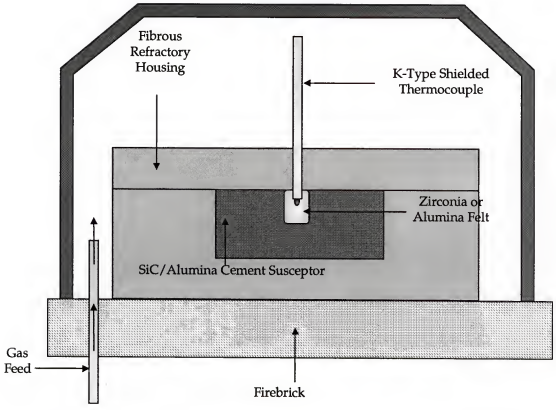


Figure 3.3. Diagram of the experimental setup used starting in phase III of the experiment.

rate throughout the experiment. To determine if the chamber had been adequately purged of oxygen, a match was lit, placed in the jar, and then watched to see if the match went out immediately. Once this had happened, the composite samples were deemed ready to be microwave heated.

Unfortunately, as previously mentioned, the change of anything within the microwave cavity may (at least subtly) affect the electric field and the modes, and thus the heating rates that would be measured might be altered by the change in the experimental setup. As a result, another set of samples was fabricated to be run in flowing air rather than flowing nitrogen. This was done to provide a set of samples that would be more directly comparable, as it used the same experimental setup, and would also have a flowing atmosphere. In addition, results from phase II of the experiment indicated that a change occurred at approximately 600 °C that altered the heating rate of the composite samples. As a result, an additional parameter was included in the experiment, so that some susceptors would only be heated to 600 °C, and others would be heated to over 1100 °C.

Due to the increase in the number of samples, a fractional factorial statistical design was employed to reduce the number of samples that needed to be microwave heated. The parameters that were included in the statistical design were silicon carbide phase, weight percent, and maximum temperature of processing. The susceptor compositions and processing tested are presented in Table 3.1. Calculations for each of

---

readings by providing a heat sink for the thermocouple. This could be more of a problem if the thermocouple were allowed to touch an additional surface for one sample, and not for others.

Table 3.1. Composition and processing of composite samples for phase III.

| Atmosphere | Nitrogen | | | | Air | | | |
|---|---|---|---|---|---|---|---|---|
| Temperature | 600 | | 1200 | | 600 | | 1200 | |
| Phase of SiC | Alpha | Beta | Alpha | Beta | Alpha | Beta | Alpha | Beta |
| Wt.% SiC | 10, 20 | 50 | 20, 30 | 10, 40 | 10, 20, 40, 50 | 20, 30 | 50 | 20, 40 |

these parameters as well as their second order interactions were performed. The use of this design allowed determination of the statistical significance of each of the parameters included in the experiment, which included atmosphere, phase of silicon carbide, weight percent of silicon carbide, and the maximum temperature experienced by the composite sample. As in phases I and II, temperature measurements were recorded every 30 seconds until the composite sample reached the maximum temperature allowed for the run. However, for these experiments, the possible time for the composite samples to reach maximum temperature was increased to 99 minutes (5940 seconds). This maximum amount of time was only necessary for the lower weight percent silicon carbide samples, which did not always reach the maximum allowable temperature even in this time period. Each experiment was repeated at least three times for each sample to ensure a good statistical sample.

**Phase IV**

Phase III of the experiment indicated that each of the parameters of processing atmosphere, weight percent silicon carbide, and phase of the silicon carbide did affect the heating rate of the composite samples. However, it was desirable to confirm that the difference in particle size of the $\alpha$- and $\beta$-phase silicon carbide was not leading to incorrect conclusions. The results from phase I hinted that as the particle size got

smaller, that the heating rate would decrease, which led to the supposition that given the same particle size of α- and β-phase silicon carbide, the difference would actually be even greater than that which was observed. Confirmation of this hypothesis was one of the goals of phase IV.

Therefore, two new types of silicon carbide were incorporated to form the composite samples. Composites were comprised of the same high alumina cement as before and either 0.64 μm α-silicon carbide manufactured by H.C. Starck with 99+% purity, or 0.68 μm β-silicon carbide also manufactured by H.C. Starck with 99+% purity. Both silicon carbides had similar impurities, and both manufacturer and on-site particle size analysis indicated that they also had similar particle size distributions. These particles were incorporated into the high alumina cement as before, with compositions varying from 10 to 50 weight percent silicon carbide. And, as before, after fabrication of the composite samples, they were stored with desiccant to eliminate as much water absorption from the atmosphere as possible.

Nearly the same experimental setup was utilized as in phase III, which is depicted in Figure 3.3, except with one alteration. The zirconia felt did not sufficiently inhibit dielectric breakdown (arcing) between the thermocouple and the sample. An alumina felt (Zircar) was then substituted for the zirconia felt, and this eliminated the problem. Experiments indicated that the addition of the alumina felt did not significantly affect the accuracy of the thermocouple readings of the composite. Also, as before when a flowing nitrogen atmosphere was used, a match test was performed to determine if the chamber had been sufficiently purged of oxygen.

However, for this phase of the study, two separate experiments were performed. Phase II indicated that a change occurred in the composite samples with heating. Phase III confirmed this change, and showed that it had a significant effect on the heating rate observed. The goal of the first experiment in this phase was to determine at what temperature this transition occurred in air and nitrogen. Silicon carbide composite samples containing 10, 30, or 50 weight percent α- or β-phase silicon carbide were all tested in the TGA/DTA to determine at what temperature regime the reaction starts to occur when using conventional heating methods. Generally, these tests indicated that with the exception of the water evaporation peak at approximately 100 °C, the first point of interest for any of these samples occurred at approximately 300 °C.

Consequently, this was decided to be the starting point for determining the temperature at which changes in heating rate might occur during microwave heating. Two sets of composite samples were fabricated, one set to be run in flowing air, and the other set to be run in flowing nitrogen, containing 20 wt.% α-SiC, 40 wt.% α-SiC, 20 wt.% β-SiC, and 40 wt.% β-SiC. These were used to identify the reaction temperature in the microwave, and were individually microwave heated to 300 °C. Then, the samples were cooled, and the composites would be heated again to a temperature 25 °C greater than the previous run. Therefore, in the second run the composite samples were heated to 325 °C, in the third run they were heated to 350 °C, and so on. This procedure was repeated until a significant change in heating rate was observed.

The transition temperature at which this change occurred was utilized in the second experiment in this phase. A full factorial statistical design was employed to determine the significance of each experimental parameter and their interactions. The

parameters that were included in the statistical design were weight percent silicon carbide, silicon carbide phase, maximum temperature of processing, and atmosphere of processing. Significance levels of each of these factors and their interactions were calculated. Five microwave heating cycles for each composite sample were performed to obtain sufficient statistical information.

In this experiment six sets of composite samples of 10, 30, and 50 weight percent $\alpha$ and $\beta$ silicon carbide were heated. Three sets were heated in flowing air, and three sets were heated in flowing nitrogen. The first set for each atmosphere was microwave heated to a temperature slightly below the temperature determined in the first experiment, the second sets were heated to a temperature slightly above this transition temperature, and the third sets were heated to 1100 °C (the near maximum temperature of the K-type thermocouples.) As in previous phases, temperature measurements were recorded every 30 seconds until the composite sample reached the maximum temperature for the set, or until it had been microwave heated for 99 minutes, whichever came first. Each composite sample was heated at least five times to provide the average heating profile.

**Summary of Heating Conditions**

In summary, silicon carbide/high alumina cement composites underwent the following heating conditions. In phase I, composite samples containing between 10 and 50 weight percent low purity 85 μm and/or 1000 μm $\alpha$-phase silicon carbide were heated to approximately 1150 °C or for a maximum of 15 minutes. In phase II, the particle size of the silicon carbide was reduced, and the purity was also greatly increased. In this case, composite samples containing between 10 and 50 weight percent of high purity 2 μm $\alpha$-phase silicon carbide or 1 μm $\beta$-phase silicon carbide were heated to 1150 °C or for a

maximum of 15 minutes. The same types of silicon carbide composite samples were heated in either flowing air or flowing nitrogen for phase III. A fractional factorial statistical design was employed, and some composite samples were heated to 600 °C, and others were heated to over 1100 °C. In this case, the susceptors were allowed up to 99 minutes to attain the maximum temperature for the experiment. For phase IV, the particle size was reduced even further, and between 10 and 50 weight percent high purity 0.64 μm α-phase silicon carbide or 0.68 μm β-phase silicon carbide were incorporated into the composite sample. In this case, a full factorial statistical analysis was employed, with susceptors once again being heated in either air or nitrogen atmospheres. A set of samples were heated starting at 300 °C, and the temperature was increased by 25 °C increments until a significant increase in the heating rate was observed, and a transition was found at approximately 625 °C for both air and nitrogen. This was then used to determine the temperatures for heating further sets of samples. As a result, sets of composite samples were heated to 550 °C, 700 °C and 1100 °C.

## Sample Characterization

### "Green" Sample Characterization

Samples which had not been exposed to further heating after fabrication were characterized in a variety of different ways to determine what had changed in the samples upon microwave exposure. To begin with, x-ray diffraction (XRD) was performed on the starting powders, as well as cross-sections of cast samples to find what phases can be detected at that time. Particle size analysis was also performed to examine the particle size distributions of the starting powders. Scanning electron microscopy (SEM) was utilized to look at the microstructure of cast samples, and the shape of the silicon carbide

particles. Energy dispersive x-ray spectroscopy (EDX) was employed to look at the dispersion of elements within the composite, with specific interest in x-ray dot mapping. Thermogravimetric analysis/differential thermal analysis (TGA/DTA) was used to determine phase changes that occur within the composite samples as they are being heated, as well as to assist in identification of the temperature of transition to higher microwave heating rates.

**Processed Sample Characterization**

After undergoing heating cycles, samples were characterized using the same techniques as were used for the "green" sample characterization. These techniques include XRD, SEM, EDX, and TGA/DTA. Any differences detected between the heated samples and the "green" samples are of particular interest. In addition, the temperature versus time data collected during microwave heating was examined and compared.

## Characterization Methods

**X-Ray Diffraction (XRD)**

X-ray diffraction is a method for identifying the crystalline components in a sample material. When a crystalline sample material is bombarded by x-ray radiation, the crystal structure of the material acts as a diffraction grating with the atoms acting as scattering centers. A diagram of the required geometry for x-ray diffraction to occur is presented in Figure 3.4. Bragg's law describes this condition by:

$$n\lambda = 2d \sin\theta \quad \textbf{[3. 1]}$$

where n is a whole number of wavelengths, $\lambda$ is the wavelength of the incident x-ray radiation, d is the spacing between two adjacent planes of atoms, and $\theta$ is the angle of incidence and the angle of reflection. This spacing is characteristic of a given material.

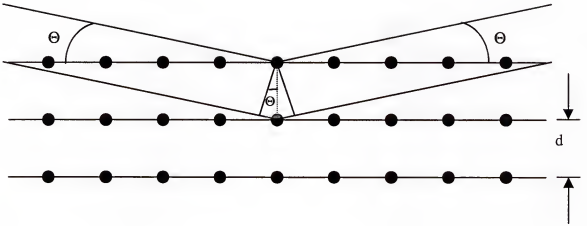


Figure 3.4. Conditions for x-ray diffraction. (adapted from [Sha92])

X-ray diffraction may be utilized to either determine the crystal structure of a known material, or it may be used to identify a more common material, provided that its structure has been previously tested and identified (and therefore already catalogued by the Joint Committee on Powder Diffraction Standards (JCPDS)). Each crystalline material will produce a characteristic diffraction pattern that is unique to that material. X-ray diffraction can therefore be used to identify the various crystalline phases that may comprise a sample by comparison with patterns on file. If the individual components can be tested, and known combinations of the components tested, x-ray diffraction can also be used as a quantitative technique. Unfortunately, small quantities of a single phase present in a sample may not exhibit sufficient intensity in the diffraction response to be identified, as they will become lost in the background. In addition, x-ray diffraction is only of limited usefulness for non-crystalline materials. Non-crystalline materials such as glasses only exhibit short-range order, and the diffraction pattern of such materials tends to be a broad peak. Identification of an unknown non-crystalline material is therefore not possible using this technique [Sha92, Cul78].

**Particle Sizing**

In the laboratory, particle size was measured using the enhanced laser diffraction technique. The Coulter LS 230 that was used is capable of measuring particle sizes in the range of 0.04-2000 μm. The particle size is determined by using the Fraunhofer and Mie theories of light scattering. These theories state that light will be scattered by small particles in a characteristic and symmetrical pattern. From the flux pattern of scattered light intensity in relation to the incident beam angle, the particle size distribution may be determined. A diffraction pattern of a bright spot (Airy disk) surrounded by dark and

bright rings of diminishing intensity would result from a dispersion of spherical particles of a single size. The scattering angle increases with distance from the center of the pattern. The particle size can be determined from this pattern from the principle that the distance to the first dark ring will increase with decreasing particle size. With more than one particle size, or a particle size distribution, the flux patterns will be superimposed on top of each other. Fortunately, the patterns obey the rule of linear superposition, but the instrument must be able to measure the pattern accurately enough that these patterns can be deconvoluted to individual particle sizes [Bec00a, Bec00b].

For most instruments, the accuracy of laser diffraction is reduced for sub-micron particles. By using polarization intensity differential scattering (PIDS), sub-micron particle sizes can be accurately determined. For PIDS, three wavelengths of light are polarized vertically and horizontally, and the differential intensity of the scattered light at the two polarizations is measured. Forty-two measurements are made at three wavelengths, two polarizations, and six scattering angles. The information detected using PIDS involves the same theory as the laser scattering, but enhances the resolution of the instrument for sub-micron particles [Bec00c].

**Scanning Electron Microscopy (SEM)**

Scanning electron microscopy, or SEM, is an ideal instrument for characterizing microstructural features of a material. The microscope uses a very focused electron beam with a spot diameter on the order of one micron to 10 nm. This spot is scanned across the surface of the sample material. The depth of field, D, which can be focused by an SEM, is much greater than for an optical microscope, so precisely polished surfaces are not as necessary. The depth of field can be maximized by reducing the divergence of the beam,

$\alpha$, or by reducing the magnification. A diagram of the depth of field and the region of effective focus are illustrated in Figure 3.5. Calculations of the maximum depth of field depending upon the magnification and the divergence of the beam are presented in Table 3.2. Magnifications of up to 100,000X are possible, but this is dependent upon the spot size that can be produced. The smaller the spot size, the greater the magnification which can be attained. Most SEMs can accelerate the electron beam to energies in the range of 1-40 keV. Higher voltages increase the probability of collecting enough signal from the sample surface to produce a good picture at high magnification [Sha92, Gol92].

The primary electrons emitted by the electron beam strike the surface of the sample, and this produces two different types of reactions which may be measured. One reaction that will occur is the production of secondary electrons ejected from the surface of the sample in reaction to the electron beam. This signal may be reproduced on either a television screen or a photograph. Differences in topography result in very different signal strengths being collected by the detector, and therefore show up very effectively on the television screen or photograph. The other reaction that will occur is some of the primary electrons from the electron beam will be scattered back to the detector. When the detector collects these backscattered electrons, the primary contrast mechanism is caused by the difference in atomic number of the elements or compounds being examined. As a result, the greater the atomic number difference, the greater the visible contrast when viewing a backscattered electron image. Unfortunately, aluminum and silicon are right next to each other on the periodic table, and consequently the backscattered electron image does not provide sufficient contrast between the two phases under study here [Sha92, Gol92].

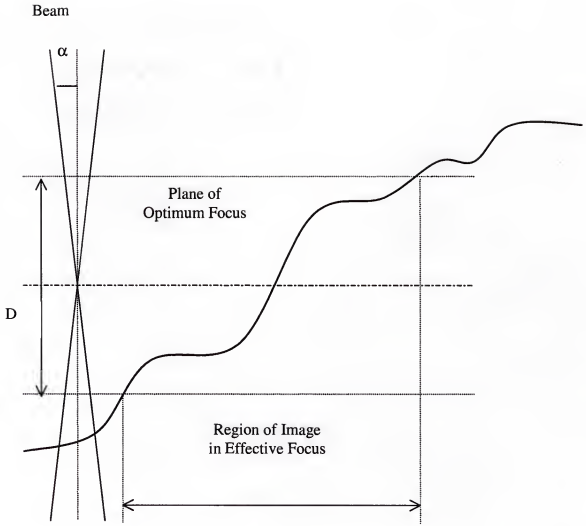


Figure 3.5. Illustration of depth of field attainable in an SEM image.
(adapted from [Gol92])

Table 3.2. Depth of focus based on magnification and divergence of the electron beam.

| Magnification | α (radians) | | |
|---|---|---|---|
| | $5 \times 10^{-3}$ | $1 \times 10^{-2}$ | $3 \times 10^{-2}$ |
| 10X | 4,000 | 2,000 | 670 |
| 50X | 800 | 400 | 133 |
| 100X | 400 | 200 | 67 |
| 500X | 80 | 40 | 13 |
| 1,000X | 40 | 20 | 6.7 |
| 10,000X | 4 | 2 | 0.67 |
| 100,000 | 0.4 | 0.2 | 0.067 |

(adapted from [Gol92])

**Energy Dispersive X-Ray Spectroscopy (EDX)**

In addition to the detection of secondary or backscattered electrons, characteristic x-rays emitted from the sample material may also be detected. When bombarded with an electron beam, characteristic x-rays may be emitted by the elements composing the sample material in reaction to the energy of the electron beam. An energy level diagram illustrating how the characteristic x-rays for an atom will be emitted from an excitation is shown in Figure 3.6. The energy of the x-rays that are emitted are characteristic of the particular element from which they came.

Therefore, by measuring the energy of the emitted electrons, the elements contained in the sample material can be determined. Unfortunately, this technique really only provides qualitative elemental information, and cannot specify how much of what element may be present. Techniques do exist to make semi-quantitative measurements; however, the accuracy of these techniques may depend upon the elements present. Semi-quantitative measurements are especially difficult for lighter elements mixed with heavier elements. In these cases, the characteristic x-rays emitted by the lighter elements may be absorbed by the heavier elements, thus reducing the amount of signal collected by the

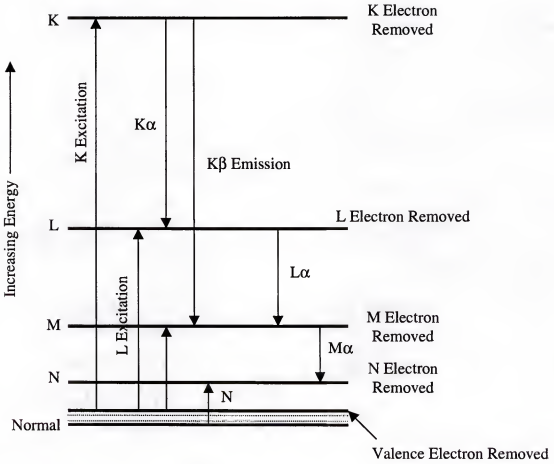


Figure 3.6. Atomic energy level diagram with characteristic x-ray emissions illustrated. (adapted from [Gol92])

detector from the lighter elements. As a result, a smaller amount of the lighter element than is actually present would be calculated due to the absorbed x-rays [Gol92].

Another use of energy dispersive x-ray spectroscopy is for x-ray dot mapping. If a picture is first taken using the secondary or backscattered electron signal, x-ray dot mapping can help to identify the elements and where they are located on this picture. As the electron beam scans across the surface of the sample material, x-rays associated with the presence of a particular element may be detected. Whenever a characteristic x-ray for the element of interest is detected, a dot in that location on the screen will appear. By scanning across the area several times, this may then be related to features evident in the secondary or backscattered electron picture. This procedure can then be repeated for every element of interest to give an idea of where particular elements or compounds may be located in the picture. Therefore, if for example, an agglomerate of aluminum oxide is present on a mound of silicon carbide, this could be identified by using x-ray dot mapping.

**Thermogravimetric Analysis/Differential Thermal Analysis (TGA/DTA)**

Thermogravimetric analysis or TGA measures the weight change of a sample relative to time or temperature. In this case, the data that was examined was that of weight change relative to temperature. The weight of a material may change as a result of evaporation, oxidation, or a variety of other reactions. Powdered samples should be used, as solid samples may be affected by factors such as porosity, defects, and surface condition. In addition, only very small quantities of sample should be used, as the probability of non-uniform temperature becomes more likely as the sample becomes larger. The factors affecting the TGA curve that will be recorded include both

instrumental factors as well as sample characteristics, which are presented in more detail in Table 3.3. One of the most important factors that will affect the recorded curve is the heating rate. The sample temperature will normally lag behind the furnace temperature, and this difference can be as great as 30 °C. High heating rates, vacuum, or fast-flowing atmospheres will exacerbate this temperature difference [ASM91, Bro88, Wen86].

Some of the applications of thermogravimetric analysis are thermal decomposition, corrosion, solid-state reactions, calcining of minerals, evaporation of liquids, pyrolysis, determining moisture content, rates of evaporation, reduction, or vaporization of a phase. To assist in precisely locating the temperature of a reaction, the TGA curve may be plotted with its derivative, the DTG curve, which may be either measured or calculated. However, sometimes identification of the activity of the curve may be assisted by simultaneous measurement of the DTA curve, as was done in these experiments [ASM91, Bro88, Wen86].

Differential thermal analysis, or DTA, measures the difference in temperature between the sample material and a reference material which are being heated simultaneously. When a reaction occurs, the temperature of the sample may lag behind

Table 3.3. Factors that influence the TGA curve.

| Instrumental Factors | Sample Characteristics |
|---|---|
| Furnace heating rate | Amount of sample |
| Recording speed | Solubility of evolved gases in sample |
| Furnace atmosphere | Particle size |
| Geometry of sample holder and furnace | Heat of reaction |
| Sensitivity of recording mechanism | Sample packing |
| Composition of sample container | Nature of the sample |
| | Thermal conductivity |

(adapted from [Wen86])

the reference material when events such as evaporation occur, or the temperature of the sample may increase when other types of reactions such as oxidation occur. The y-axis of the DTA curve may be either marked in terms of $\Delta T$, or more simply just with an endothermic or exothermic direction. The reference material must undergo no reactions throughout the temperature range of interest, must not react with the holder or thermocouple, and it should have similar thermal conductivity and heat capacity as the sample material. The DTA curve will be affected by some of the same factors as the TGA curve, with some additions, and these are all presented in Table 3.4 [Bro88, Fre88, Wen86].

Differential thermal analysis data may be used to gain information about nearly any type of chemical or physical reaction within a sample material. Some of these reactions include crystalline phase changes, vaporization, absorption, oxidation, reduction, decomposition, combustion, and others. A more complete list is presented in Table 3.5. It should be noted that some of these reactions may exhibit either an exothermic or endothermic peak, and this will be dependent on the material being tested [Wen86].

**Thermocouple**

The temperature for all of the experiments performed in this study was measured by thermocouple. A thermocouple measures temperature by the voltage produced at the junction of two dissimilar metal wires, where the joined end is subject to the temperature to be measured, and the other unjoined end is the cold end, which is at the reference temperature. The voltage induced between the two metals by the temperature difference is known as the Seebeck potential. Any two dissimilar metals which are subject to a

Table 3.4. Factors that influence the DTA curve.

| Instrumental Factors | Sample Characteristics |
|---|---|
| Furnace atmosphere | Particle size |
| Furnace size and shape | Thermal conductivity |
| Sample holder material | Heat capacity |
| Sample holder geometry | Packing density |
| Wire and bead size of thermocouple junction | Swelling or shrinkage of sample |
| Heating rate | Amount of sample |
| Speed and response of recording instrument | Effect of diluent |
| Thermocouple location in sample | Degree of crystallinity |

(adapted from [Wen86])

Table 3.5. Potential causes for DTA peaks.

| Phenomena | Enthalpic Change | |
|---|---|---|
| | Endothermic | Exothermic |
| Physical Phenomena | | |
| Crystalline transition | X | X |
| Fusion | X | |
| Vaporization | X | |
| Sublimation | X | |
| Adsorption | | X |
| Desorption | X | |
| Absorption | X | |
| Curie point transition | X | |
| Glass transition | Change of baseline, no peak | |
| Liquid crystal transition | X | |
| Heat capacity transition | Change of baseline, no peak | |
| Chemical Phenomena | | |
| Chemisorption | | X |
| Desolvation | X | |
| Dehydration | X | |
| Decomposition | X | X |
| Oxidative degradation | | X |
| Oxidation in gaseous atmosphere | | X |
| Reduction in gaseous atmosphere | X | |
| Redox reactions | X | X |
| Solid-state reaction | X | X |
| Combustion | | X |
| Polymerization | | X |
| Precuring (resins) | | X |
| Catalytic reactions | | X |

(adapted from [Wen86])

Table 3.6. Thermocouple systems and their recommended usage environments.

| Type | Common Name | Positive Element | Negative Element | Recommended Service Environment(s) | Max. Use Temp. |
|---|---|---|---|---|---|
| B | Platinum-Rhodium/ Platinum-Rhodium | 70 Pt-30 Rh | 94 Pt-6 Rh | Oxidizing | 1700 |
| | | | | Vacuum | |
| | | | | Inert | |
| E | Chromel/Constantan | 90 Ni-9 Cr | 44 Ni-55 Cu | Oxidizing | 870 |
| J | Iron/Constantan | Fe | 44 Ni-55 Cu | Oxidizing | 760 |
| | | | | Reducing | |
| K | Chromel/Alumel | 90 Ni-9 Cr | 94 Ni-Al, Mn, Fe, Si, Co | Oxidizing | 1260 |
| R | Platinum/ Platinum-rhodium | 87 Pt-13 Rh | Pt | Oxidizing | 1480 |
| | | | | Inert | |
| S | Platinum/ Platinum-rhodium | 90 Pt-10 Rh | Pt | Oxidizing | 1480 |
| | | | | Inert | |
| T | Copper/Constantan | Cu | 44 Ni-55 Cu | Oxidizing | 370 |
| | | | | Reducing | |

[Sha92]

temperature differential in this manner will produce a voltage. The metal combinations that are commonly used are preferred because the change in voltage tends to be fairly linear with temperature. The types of thermocouples which are most commonly used, and their preferred use conditions are summarized in Table 3.6.

The type of thermocouple that was used for these experiments was the chromel/alumel K-type thermocouple. The wires were insulated with Nextel fiber, and an Inconel overbraid surrounded the wires and the insulation. The wires of the thermocouple were grounded to the Inconel sheath, which allowed the thermocouple to be easily grounded to the microwave cavity. It should be noted that the maximum use temperature for the K-type thermocouple used in this experiment is listed as 1260 °C. However, this maximum use temperature also depends on other factors, such as the wire diameter. As the wire diameter becomes smaller, the maximum use temperature of the

thermocouple will decrease. In addition, at the maximum use temperature, the wires in the thermocouple may react with the atmosphere and/or crystallize, and this will alter the voltage produced between the two wires, and thus alter the temperature reading calculated from the voltage measured [Sha92, Ome95].

The grounding of the thermocouple was a critical factor, as this inhibited arcing between the thermocouple tip and the sample. When this did occur, arcing was easily identified by one or more of the following methods: crackling sounds, light emission, and/or anomalous temperature increases. If these signals were not caught in the midst of the experiment, the presence of arcing was clearly evident upon removal of the sample. Arcing of any kind caused the zirconia or alumina felt to draw away from the thermocouple tip. In other words, the heat discharge from the dielectric breakdown would cause the felt to sinter and densify in the area of the thermocouple tip. If this occurred, the heating run would have to be repeated.

# CHAPTER 4
# RESULTS

As was mentioned in the previous chapter, the experiment was performed in four different phases. The first phase looked at "coarse" and "fine" low-purity silicon carbide powder/high alumina cement composites of varying compositions. The second phase used either the hexagonal ($\alpha$) or the cubic ($\beta$) phases of a much smaller particle size and much higher purity silicon carbide. The third phase used the same types of silicon carbide powder as the second phase, but changed the experimental setup and included atmosphere of processing and maximum temperature as variables. In addition, statistical design was used to reduce the number of samples that needed to be tested. The fourth and final phase examined all of the variables as before with still smaller particles of silicon carbide. A full factorial design was used in this final phase of the experiment. This chapter will present the experimental results for each phase individually.

## Phase I

The objective of this phase of the experiment was to determine the variation in microwave heating rates of silicon carbide/high alumina cement composites as a function of weight percent and particle size of silicon carbide. The two types of silicon carbide that were incorporated into the high alumina cement for this part of the experiment were 1000 μm particle diameter "coarse" and 85 μm particle diameter "fine" silicon carbide. The amount of silicon carbide particles incorporated in the susceptors was varied from 10

to 50 weight percent. The effect of changing the weight percent of "coarse" silicon carbide particles in Figure 4.1 shows that as the weight percent of silicon carbide increased, the heating rate of the susceptor also increased, after the first few minutes. The effects of increasing the weight percent of silicon carbide appeared to diminish as more silicon carbide was added to the sample.

When tested, a sample of pure high alumina cement did not heat nearly as well as any of these composite samples. Unfortunately, due to the very low microwave absorption of the pure alumina cement sample, the temperature of the pure alumina cement could not be measured accurately while the microwave was operating. In this case, the lack of an absorbing load in the microwave cavity resulted in the thermocouple heating more than the sample. As a result, the pure high alumina cement sample was heated in the microwave for a set time, and then temperature was measured after the microwave was turned off. This was also done for a composite sample. The temperature of the composite sample was always higher than that of the pure high alumina cement.

Similarly, for the 85 μm diameter "fine" silicon carbide particles, as the amount of silicon carbide in the composite sample was increased, the heating rate tended to increase, as is evident in Figure 4.2. However, in this case, there was also a clear change in behavior between 30 and 40 weight percent silicon carbide. For 10, 20 and 30 weight percent composite samples, the slope of the curve drops off after approximately the first ninety seconds, or when the composite sample temperature reached between 200 and 300 °C. For the 40 and 50 weight percent composite samples, no such change in slope is observed, but instead this behavior more closely mimics that of the 1000 μm particles.

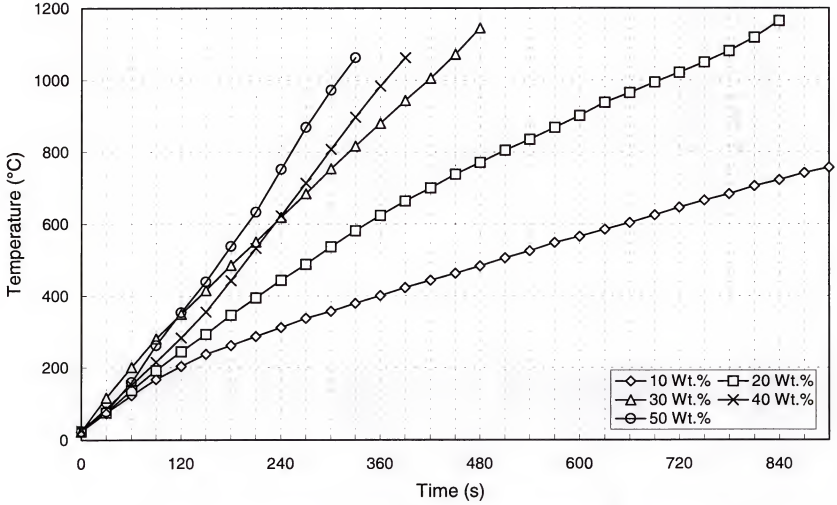


Figure 4.1. Heating rates of the susceptors using 1000 µm low-purity "coarse" silicon carbide particles.

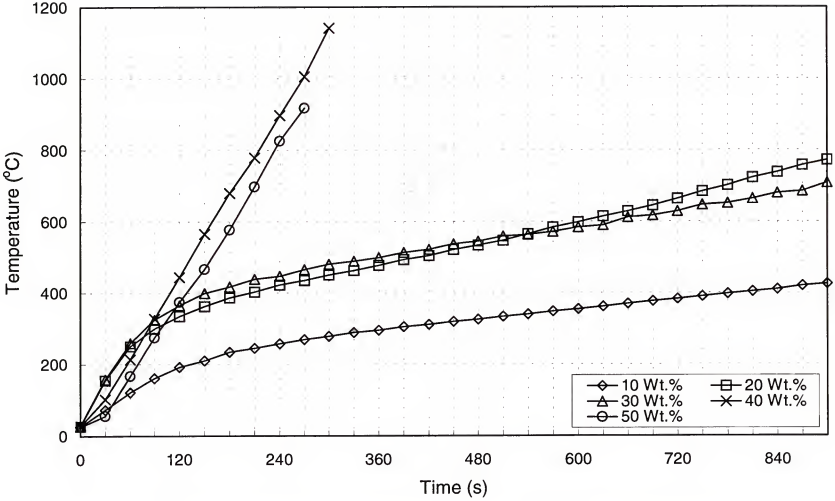


Figure 4.2. Heating rates of the susceptors using 85 μm low-purity "fine" silicon carbide particles.

For the composite samples containing between 10 and 30 weight percent silicon carbide, a dramatic difference was observed in the behavior of the two particle sizes. Figure 4.3 shows the difference in heating rates between three different susceptors, all containing 10 weight percent silicon carbide, but in different forms. The initial heating rate of all three samples is very similar; however, after the first ninety seconds, there is a very clear difference in behavior. The curve for the composite sample containing the 85 μm silicon carbide particles levels off, while that of the composite sample containing the 1000 μm particles does not. The composite sample containing half of each of the two different particle sizes of silicon carbide had a heating rate which fell between that of the two tested separately. Very similar behavior was observed for the composite samples containing 20 and 30 weight percent silicon carbide as well, as can be seen for the 30 weight percent sample in Figure 4.4. It may also be noted that the behavior of the composite sample made from a mixture of the two different particle sizes of silicon carbide tends to more closely follow the behavior of the composites made from the "coarse" silicon carbide particles.

However, this type of behavior was not observed for the higher weight percent silicon carbide composites samples. When the amount of silicon carbide in the material was increased to 40 weight percent silicon carbide, the heating rates measured were much more similar than they had been at lower percentages of silicon carbide. In fact, the heating rates of the 50 weight percent silicon carbide composite samples are nearly identical, as can be seen in Figure 4.5. This would be indicative of a change in behavior for the composite samples fabricated from the 85 μm silicon carbide particles.

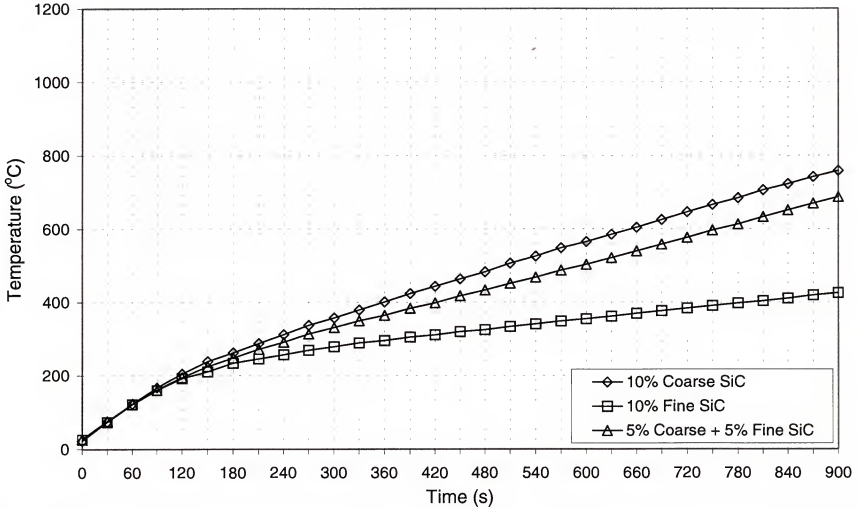


Figure 4.3. Heating rates of 10 weight percent silicon carbide composite samples containing different particle sizes of silicon carbide.

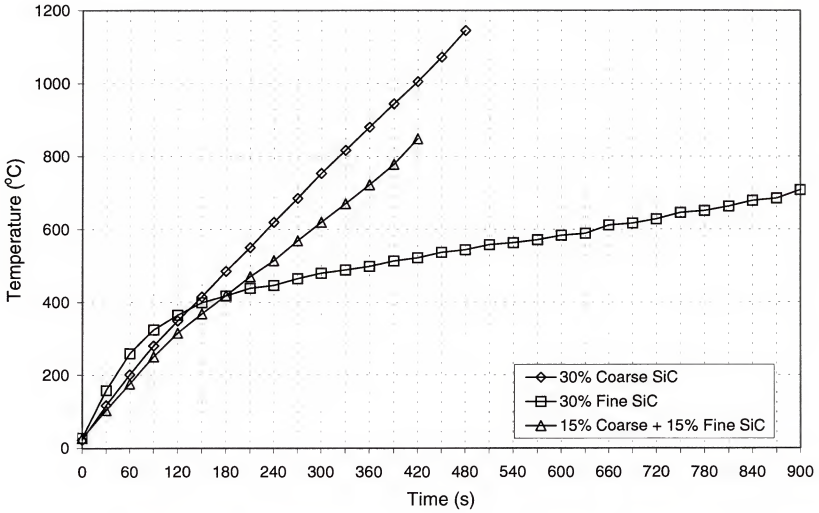


Figure 4.4. Heating rates of 30 weight percent silicon carbide composite samples containing different particle sizes of silicon carbide.

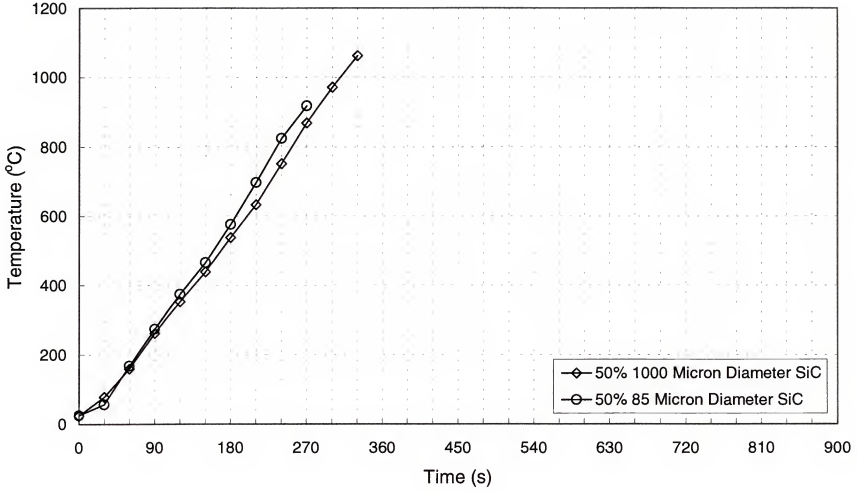


Figure 4.5. Heating rates of 50 weight percent silicon carbide composite samples containing different particle sizes of silicon carbide.

To put this in numerical rather than graphical terms, temperature measurements for the samples after 270 seconds of microwave heating are presented in Table 4.1. This time was chosen, as it was the maximum time for which a direct reading from the thermocouple was available for all samples. This table illustrates very clearly that as the silicon carbide content in the composite samples was increased, the amount of heating over a set time period increased. The data for the composite made with 40 weight percent 85 μm silicon carbide particles will be discussed in the next chapter. However, in every case, excluding approximately the initial 90 seconds of microwave heating, the heating rate for the composite samples was generally linear. During this initial heating stage, the composition of the composites appeared to be less critical, as they all seemed to heat at similar rates. Consequently, heating rates could be calculated from this section of the graphs.

Table 4.2 presents calculations of the steady state heating rates for the composite samples, which once again indicate that the heating rate increased as the silicon carbide content increased. This was also true for the composite samples made with half of each particle size of silicon carbide. The microwave heating rate of these susceptors appears to be dominated by the presence of the "coarse" 1000 μm particles of silicon carbide.

Table 4.1. Temperature after 270 seconds of microwave heating (°C).

| Weight Percent SiC | 1000 μm SiC Particles | 85 μm SiC Particles |
|---|---|---|
| 10 | 337 | 269 |
| 20 | 488 | 435 |
| 30 | 685 | 465 |
| 40 | 714 | 1005.5 |
| 50 | 869 | 918 |

Table 4.2. Steady state microwave heating rates of susceptors (°C/sec).

| Weight Percent SiC | 85 μm Particles | Half 85 μm + Half 1000 μm Particles | 1000 μm Particles |
|---|---|---|---|
| 10 | 0.242 | 0.661 | 0.755 |
| 20 | 0.531 | 1.00 | 1.31 |
| 30 | 0.377 | 1.76 | 2.20 |
| 40 | 3.75 | Not Available | 2.73 |
| 50 | 3.45 | Not Available | 3.24 |

**Phase II**

The objective of phase II of the experiment was to determine the variation in microwave heating rates of the silicon carbide/high alumina cement susceptors as a function of weight percent and phase of the silicon carbide. The two types of silicon carbide that were tested in this phase of the experiment were high purity 2 μm α-phase silicon carbide and 1 μm β-phase silicon carbide. Once again, the amount of silicon carbide particles incorporated into the composite samples was varied from 10 to 50 weight percent in increments of 10 weight percent.

Upon testing these samples, the first thing that was apparent was that a reaction took place sometime after the samples reached high temperature. The first indication of this reaction was a physical, visible change. The samples changed from a gray-green color and grainy or powdery texture to a dark gray color and a smoother, glassy-like texture with more mechanical strength. This reaction resulted in more efficient heating rates for the composite samples, as may be viewed in Figure 4.6, which clearly shows this effect for one set of composite samples. There is no overlap between the two profiles even when error bars are taken into account. This could be viewed with all compositions above 10 weight percent silicon carbide. To prove this reaction further, x-ray diffraction

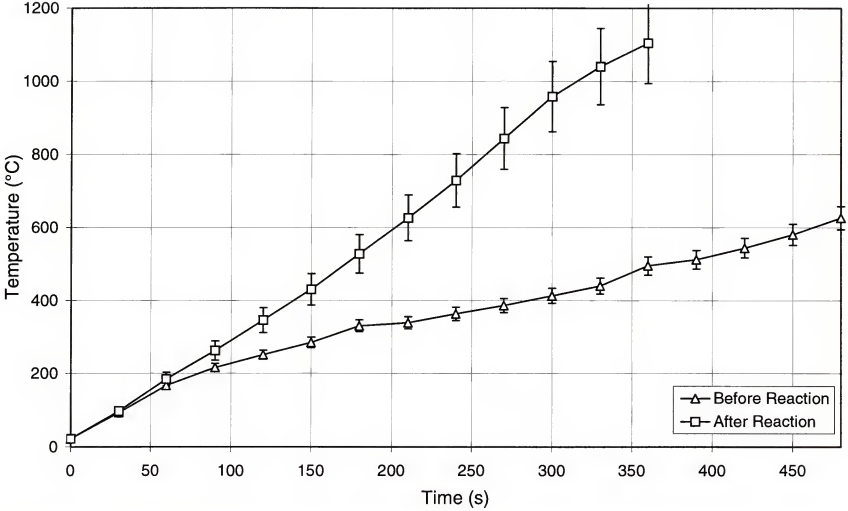


Figure 4.6. Heating profiles of 40 weight percent β-phase (1 μm) silicon carbide composite samples before and after reaction.

spectra were taken of 40 weight percent α- and β-phase silicon carbide composite samples. A single solid sample for each phase was first examined using XRD, and then each sample was heated and reacted in the microwave before being examined again. The before and after spectra for each of these samples respectively with the major peaks identified are presented in Figure 4.7 and Figure 4.8. The compounds that were detected in each sample before and after reaction are presented in Table 4.3. Not only does this show that very different compounds were detected for composite samples made with each of the different phases of silicon carbide, but also that the compounds detected changed significantly after the samples had been heated and reacted.

For the samples fabricated from the high alumina cement with α-phase silicon carbide, in general it was found that as the amount of silicon carbide in the susceptor was increased, the heating rate tended to increase. The heating profiles of these samples may be seen in Figure 4.9. Similar, but not identical behavior was observed for the composite susceptor samples fabricated using β-phase silicon carbide. The heating profiles for this set of samples may be seen in Figure 4.10. In addition, as in phase I for the "fine" 85 μm silicon carbide composite samples (see Figure 4.2), a definite transition is evident as the amount of silicon carbide in the composites is increased. However, in this case, the transition is not between 30 and 40 weight percent silicon carbide, but has shifted to between 10 and 20 weight percent silicon carbide.

In both cases, it may be seen that the heating rate for the 10 weight percent composite samples is much lower than for all of the other compositions. For the higher weight percent samples (20-50 wt.%), the heating rate is much higher. It may also be noted that the heating rate for the 30 weight percent silicon carbide composite sample is

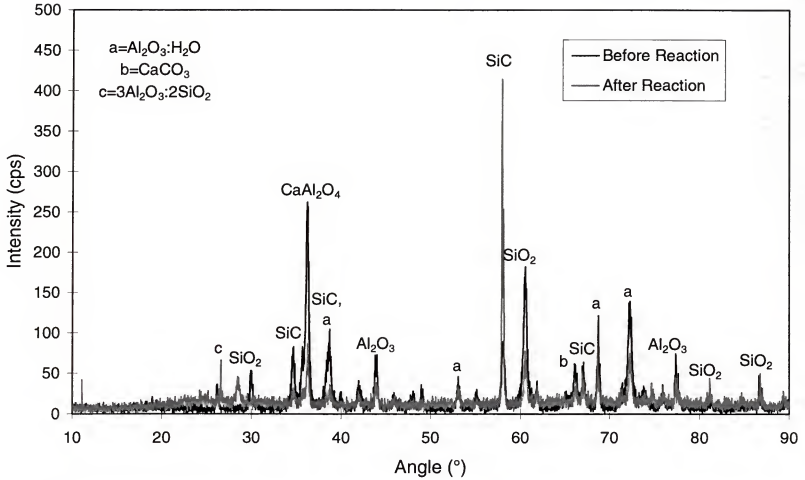


Figure 4.7. X-ray diffraction spectra for 40 weight percent α-phase (2 μm) silicon carbide composite samples before and after reaction.

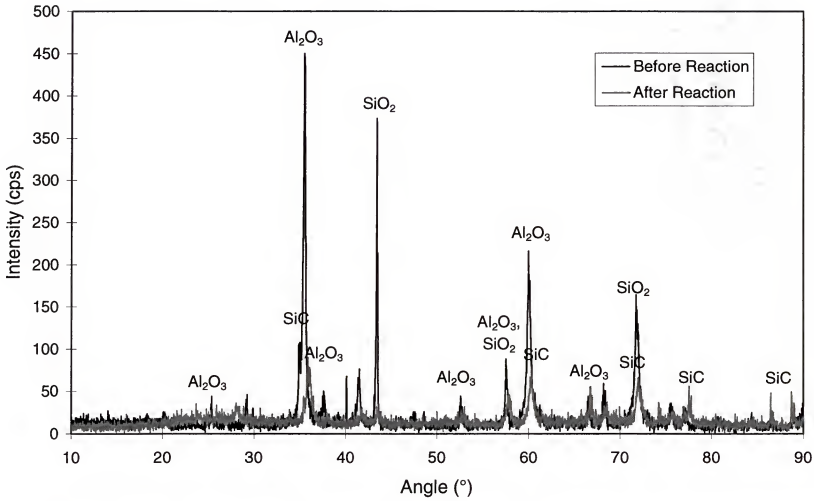


Figure 4.8. X-ray diffraction spectra for 40 weight percent β-phase (1 μm) silicon carbide composite samples before and after reaction.

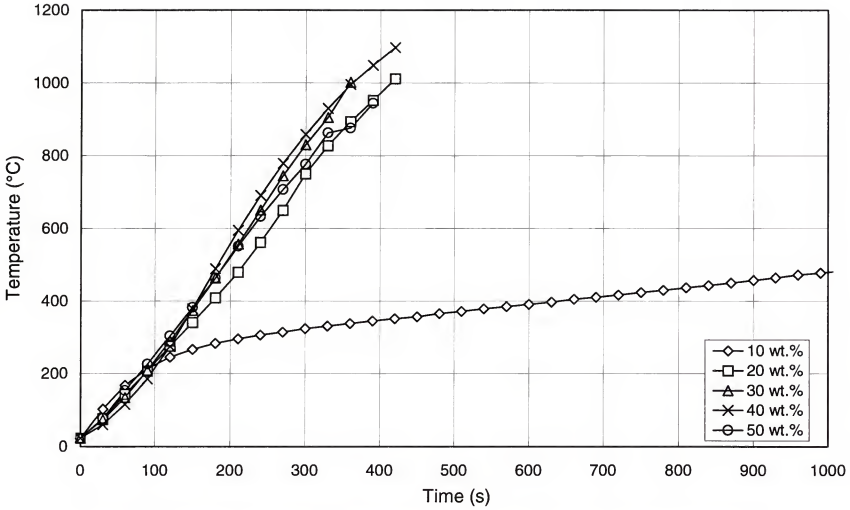


Figure 4.9. Heating profiles of 10-50 weight percent α-phase (2 μm) silicon carbide composite samples.

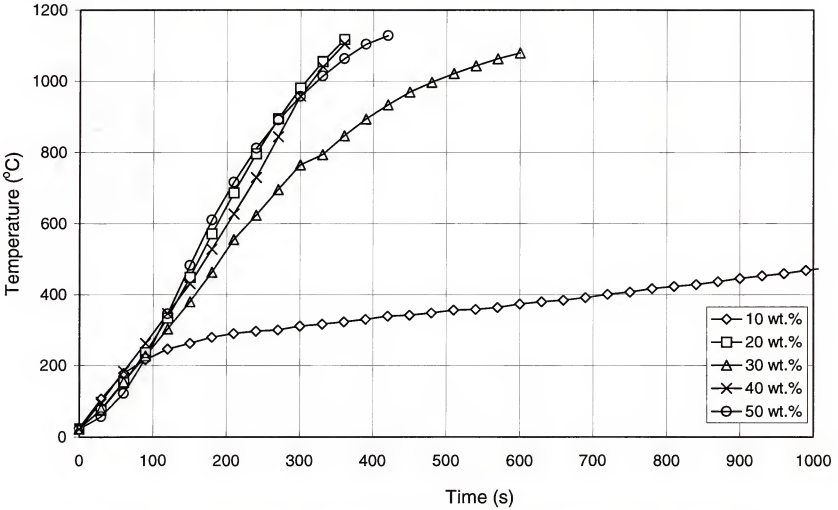


Figure 4.10. Heating profiles of 10-50 weight percent β-phase (1 μm) silicon carbide composite samples.

Table 4.3. Compounds detected by XRD in 40 weight percent silicon carbide composite samples.

| | Before Reaction | After Reaction |
|---|---|---|
| α-Phase Silicon Carbide | $Al_2O_3$<br>$Al_2O_3:H_2O$<br>$CaCO_3$<br>α-SiC<br>$SiO_2$<br>$CaAl_2O_4$ | α-SiC<br>$SiO_2$<br>$3Al_2O_3:2SiO_2$ |
| β-Phase Silicon Carbide | $Al_2O_3$<br>$SiO_2$<br>$5CaO:3SiO_2:2H_2O$<br>$Al(OH)_3$ | $Al_2O_3$<br>SiC |

Table 4.4. Steady state microwave heating rates of susceptors (°C/sec).

| | α-Phase Silicon Carbide | β-Phase Silicon Carbide |
|---|---|---|
| 10 Wt.% | 0.234 | 0.248 |
| 20 Wt.% | 2.43 | 3.15 |
| 30 Wt.% | 2.53 | 2.55 |
| 40 Wt.% | 2.49 | 3.08 |
| 50 Wt.% | 2.41 | 3.11 |

lower than for the 20 weight percent sample. Regardless of the lower heating rate for the 30 weight percent β-phase silicon carbide sample, it was found that the heating rates for the β-phase silicon carbide composite susceptor samples were higher than those for the α-phase silicon carbide composites. This may be seen graphically in Figure 4.11 - Figure 4.15. In Table 4.4, the steady-state heating rates for every sample is presented, where it is demonstrated numerically that the β-phase silicon carbide composite samples tended to have higher heating rates than the α-phase silicon carbide samples.

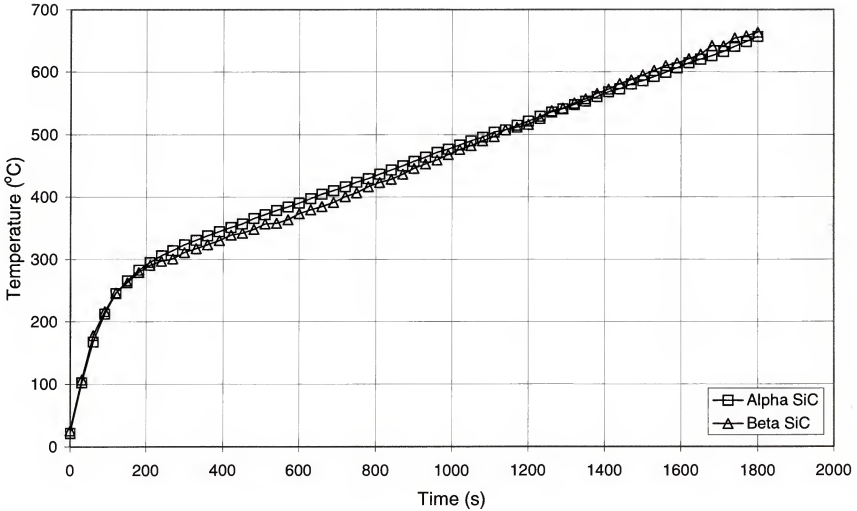


Figure 4.11. Heating profiles of 10 weight percent α- (2 μm) and β-phase (1 μm) silicon carbide composite samples.

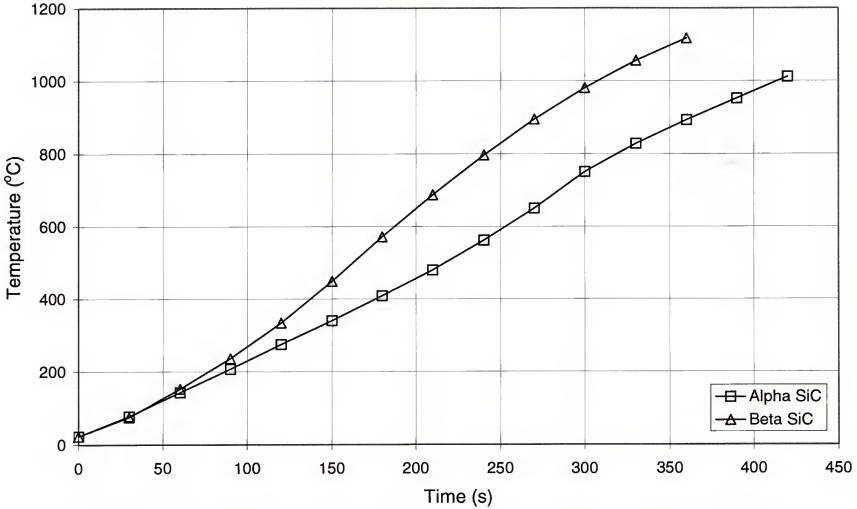


Figure 4.12. Heating profiles of 20 weight percent α- (2 μm) and β-phase (1 μm) silicon carbide composite samples.

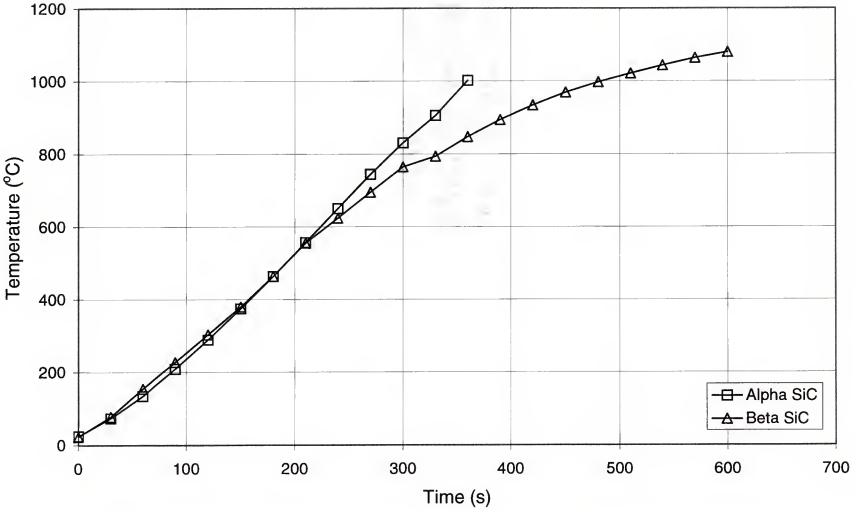


Figure 4.13. Heating profiles of 30 weight percent α- (2 μm) and β-phase (1 μm) silicon carbide composite samples.

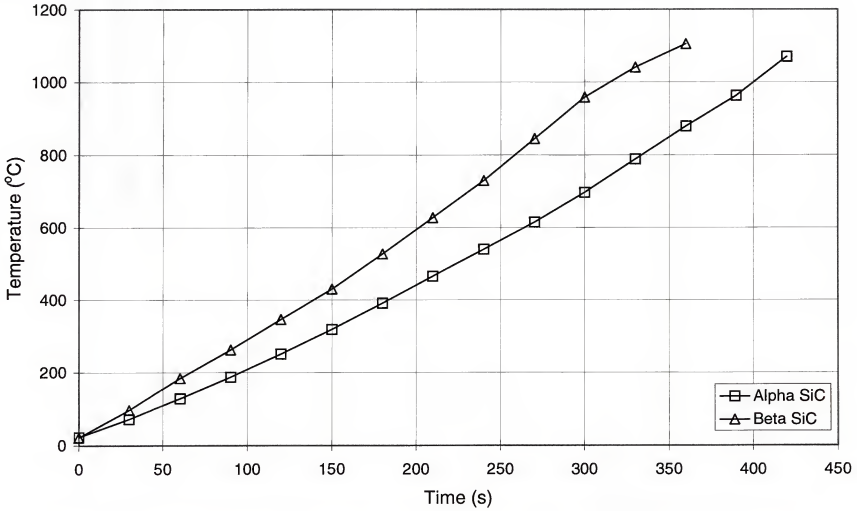


Figure 4.14. Heating profiles of 40 weight percent α- (2 μm) and β-phase (1 μm) silicon carbide composite samples.

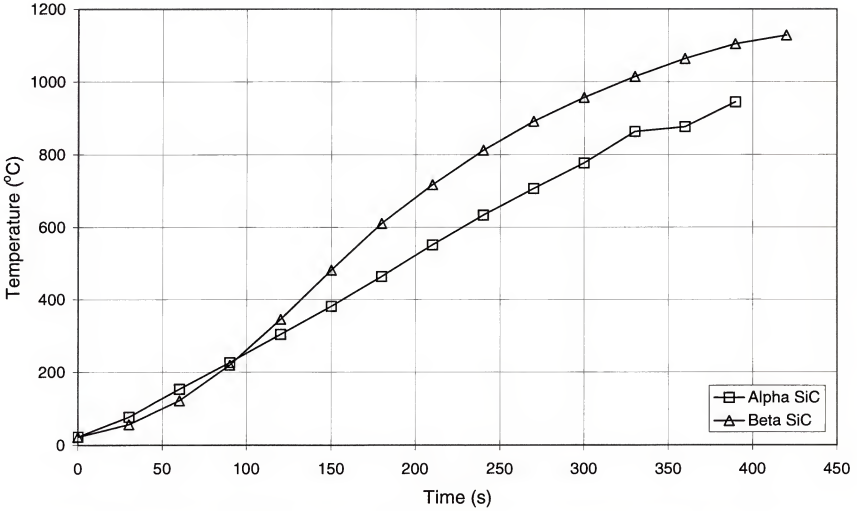


Figure 4.15. Heating profiles of 50 weight percent α- (2 μm) and β-phase (1 μm) silicon carbide composite samples.

**Phase III**

From phase II, it was determined that a reaction took place in the high alumina cement/silicon carbide composite samples upon reaching a certain temperature. Since a glassy phase appeared to form on the composites, it was proposed that oxidation of the silicon carbide might be causing the change in heating rate. Therefore, nitrogen was used to hinder oxidation for part of the experiment. As a result, the objective for this phase of the experiment was to examine the microwave heating rates as a function of atmosphere of processing, maximum temperature of processing, weight percent and phase of silicon carbide. The same high purity $\alpha$- and $\beta$-phase silicon carbides were used as in phase II, with composition again varying from 10 to 50 weight percent silicon carbide in increments of 10 weight percent. However, in this case, a fractional factorial statistical design was used, so that in this case, not every single sample composition and condition was created and tested as before. As a result, some information cannot be illustrated graphically, but only through the statistical calculations. To reduce error, the design was replicated three times. In addition, some of the low temperature composite samples were later heated to higher temperatures to increase the information obtained.

Once the temperature versus time data had been measured, the data was examined to create the statistical response values. These were calculated by determining the time required to increase the temperature of the composite from one temperature to another. From these response values, ANOVA (Analysis of Variance) linear regression was performed, and levels of significance were determined. The calculations and graphs were generated by inputting the data into the computer program DOE-PC IV, version 3.01. The higher the percentage, the greater is the certainty that the factor in question is an

important factor contributing toward the response value. Lower significance levels indicate that the factor in question may or may not be of importance, as it is not considerably greater than the experimental error, and therefore cannot be determined. Significance values above 90% are presented in the following tables. Dashes indicate that the value obtained for the level of significance was lower than 90%, and therefore could not be determined to be significant.

The temperature versus time data was analyzed in several different manners to obtain the maximum amount of information from the study. Because the behavior for some samples clearly changed as the temperature was increased, the response data was examined over individual temperature ranges. Therefore, if the mechanism controlling the microwave heating rate was affected by different factors over different temperature ranges, this could be detected. However, as there was no data available at higher temperatures for the samples run to 600 °C, the data for the low temperature samples and the high temperature samples were examined both together and separately.

To start with, the low temperature composite samples run to 600 °C were examined alone. The ANOVA results in Table 4.5 indicate that nearly all of the factors are clearly significant at every temperature range. In comparison to Table 4.5, where most factors are significant, in Table 4.6, it is evident that some factors only play a role in certain temperature regimes. For example, the type of silicon carbide in the composite was found to have significance only from 700 to 1100 °C. In fact, most of the factors can only be determined to be sporadically significant at higher temperatures only. What should be noted, however, is that some of this information may be influenced by the data that could not be obtained. As in previous phases of the experiment, the 10 weight

Table 4.5. Significance levels from ANOVA for composite samples run to 600 °C.

| | Temperature Range (°C) | | | |
|---|---|---|---|---|
| | 25-300 | 300 – 400 | 400 – 500 | 500 – 600 |
| Type of SiC (α or β) | 99.9+% | 99.9+% | - | 99.9+% |
| Wt.% SiC (10, 20, 30, 40, or 50 wt.%) | 99.9+% | 99.9+% | 99.9+% | 99.9+% |
| Interaction of Type of SiC and Wt.% SiC | - | 95.7 | 96.8 | 99.8 |
| Atmosphere (air or $N_2$) | 99.9+% | 99.6 | 98.5 | 99.9+% |
| Interaction of Type of SiC and Atmosphere | 99.9+% | 99.9+% | - | 99.9+% |
| Interaction of Wt.% SiC and Atmosphere | 99.9+% | 99.9+% | - | 99.9+% |

Table 4.6. Significance levels from ANOVA for composite samples run to 1200 °C.

| | Temperature Range (°C) | | | | | | | | |
|---|---|---|---|---|---|---|---|---|---|
| | 25–300 | 300–400 | 400–500 | 500-600 | 600-700 | 700-800 | 800-900 | 900–1000 | 1000–1100 |
| Type of SiC (α or β) | - | - | - | - | - | 95.8 | 90.9 | - | 90.3 |
| Wt.% SiC (10, 20, 30, 40, or 50 wt.%) | - | - | - | 90.6 | - | - | - | - | - |
| Interaction of Type of SiC and Wt.% SiC | - | - | 97.5 | - | - | 94.6 | - | 91.6 | 97.7 |
| Atmosphere (air or $N_2$) | - | - | - | - | - | 95.5 | 98.5 | - | - |
| Interaction of Type of SiC and Atmosphere | - | - | - | - | - | - | - | 91.4 | 96.9 |
| Interaction of Wt.% SiC and Atmosphere | - | - | - | - | - | 93.3 | - | 95.0 | 98.5 |

percent silicon carbide composite samples did not heat very rapidly, and information above 600-700 °C was not always available. Therefore, if we look back at Figure 4.9, for example, not very much difference was observed between the composites made with 20-50 weight percent silicon carbide, and thus even a small amount of error may inhibit many conclusions from being made.

Table 4.7 summarizes the ANOVA results when the data for all of the samples was combined. Consequently, the significance of the maximum processing temperature (600 or 1200 °C) could now be determined. And, when the responses of all these samples were put together, processing temperature and weight percent silicon carbide were significant over nearly the entire range of comparison.

However, the effects of some of the factors that were found to be important statistically may also be illustrated graphically using the raw temperature versus time data. For example, the effect of atmosphere is clearly demonstrated for two 40 weight percent β-silicon carbide composite samples in Figure 4.16, where one sample was microwave heated in air and one was microwave heated in nitrogen. The effect of

Table 4.7. Significance levels from ANOVA for all samples combined.

| | Temperature Range (°C/100) | | | |
|---|---|---|---|---|
| | 25 – 300 | 300 – 400 | 400 – 500 | 500 – 600 |
| Type of SiC (α or β) | - | - | - | - |
| Wt.% SiC (10, 20, 30, 40, or 50 wt.%) | 98.0 | 99.9+% | 99.9+% | 99.9+% |
| Interaction of Type of SiC and Wt.% SiC | - | - | 93.8 | 94.4 |
| Atmosphere (air or $N_2$) | - | - | 97.0 | 93.9 |
| Maximum Temperature (600 or 1200 °C) | - | 99.9 | 99.9+% | 99.9 |
| Interaction of Wt.% SiC and Maximum Temperature | - | - | 90.6 | 95.4 |

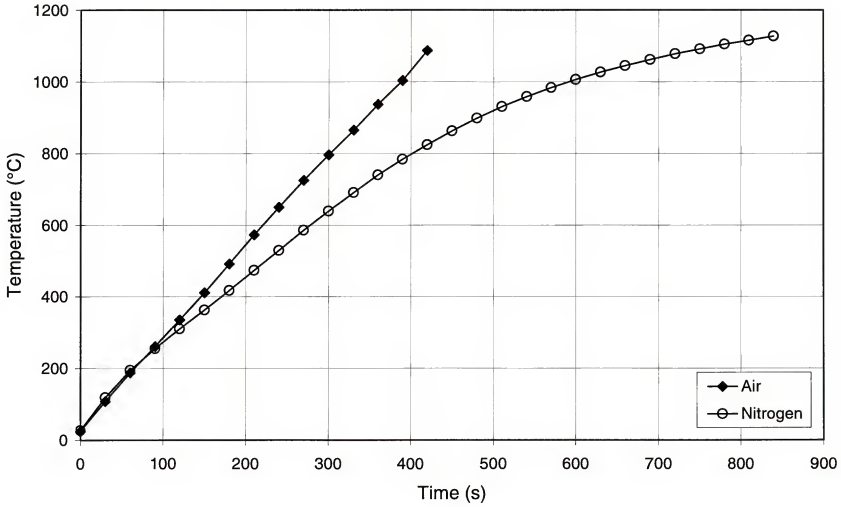


Figure 4.16. Forty weight percent β-phase (1 μm) silicon carbide composite samples heated to 1200 °C in air and nitrogen.

atmosphere for at least this sample composition is clear at temperatures above 400 °C, as the difference in slope of these two curves indicates.

From the work so far, indications of a reaction in the composite samples have been found. This can be explicitly demonstrated graphically by the difference between the initial and then subsequent heating cycles of a single composite sample. This is illustrated in Figure 4.17 for 20 weight percent α-phase silicon carbide composites. The data for the composite sample that was heated to only 600 °C is also presented here. The curve for the 600 °C composite was repeatable until the sample was heated further. At this point, a transition is indicated by an increase in slope. Subsequent runs then follow their own repeatable behavior, which is also shown in Figure 4.17. This increase in heating rate when heated above approximately 600 °C was found for composite samples of varying compositions and processed in different atmospheres, as shown in Figure 4.18 and Figure 4.19. However, it has also been determined that the reaction that takes place does not always happen immediately. In some instances, the reaction may continue over several microwave heating cycles before completion. Figure 4.20 illustrates one instance where the reaction progresses further with each subsequent heating cycle.

In addition to finding differences through the statistical analysis and the temperature versus time graphs, a difference in microstructure between samples was also observed depending on composition and processing. To obtain scanning electron micrographs of the composites, a cross section of each sample was cut using a low-speed diamond saw. All of the low temperature samples were relatively soft, and could be cut quickly; however, a lot of material in the vicinity of the blade was lost. In comparison, the high temperature composite samples were much harder, and could only be cut with a

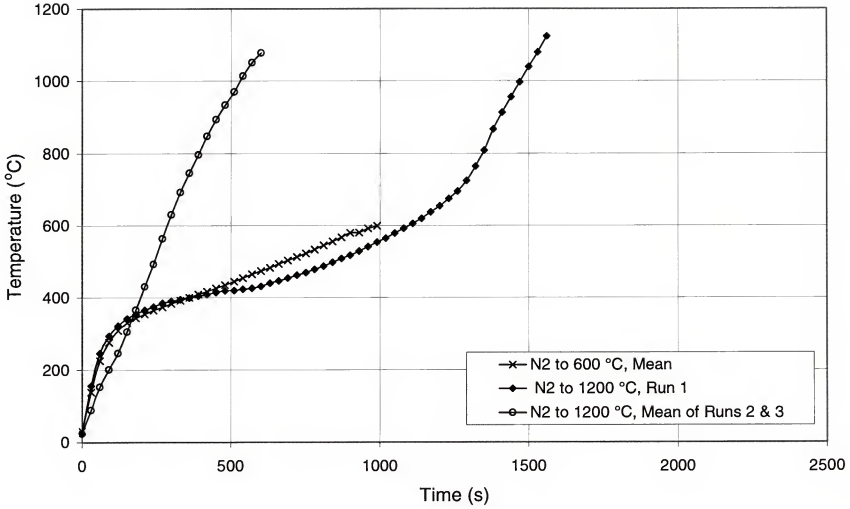


Figure 4.17. Twenty weight percent α-phase (2 μm) silicon carbide composite samples heated to 600 and 1200 °C in nitrogen.

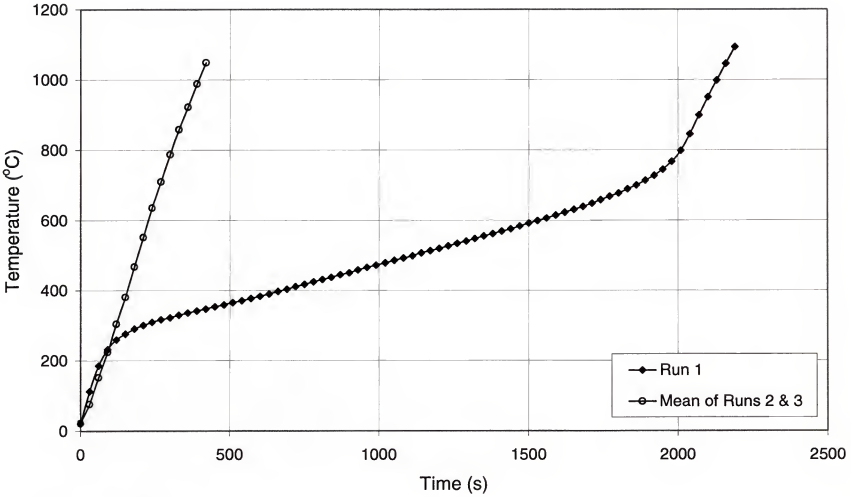


Figure 4.18. Twenty weight percent β-phase (1 μm) silicon carbide heated to 1200 °C in air.

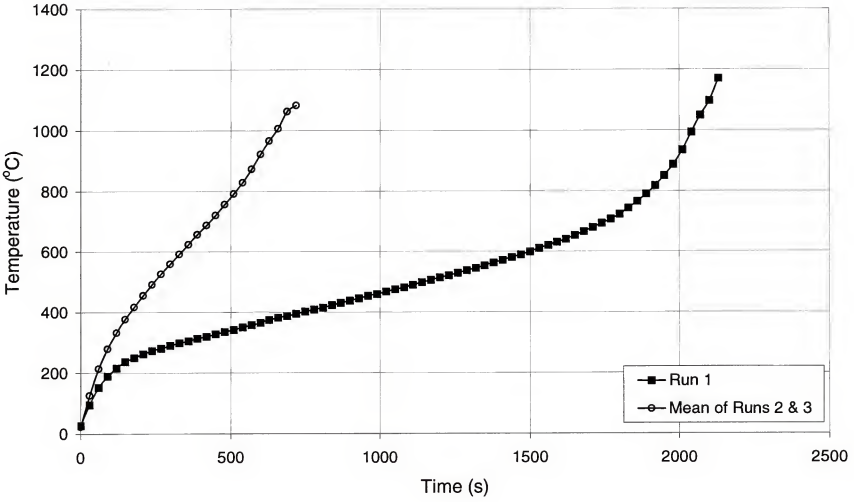


Figure 4.19. Thirty weight percent α-phase (2 μm) silicon carbide heated to 1200 °C in nitrogen.

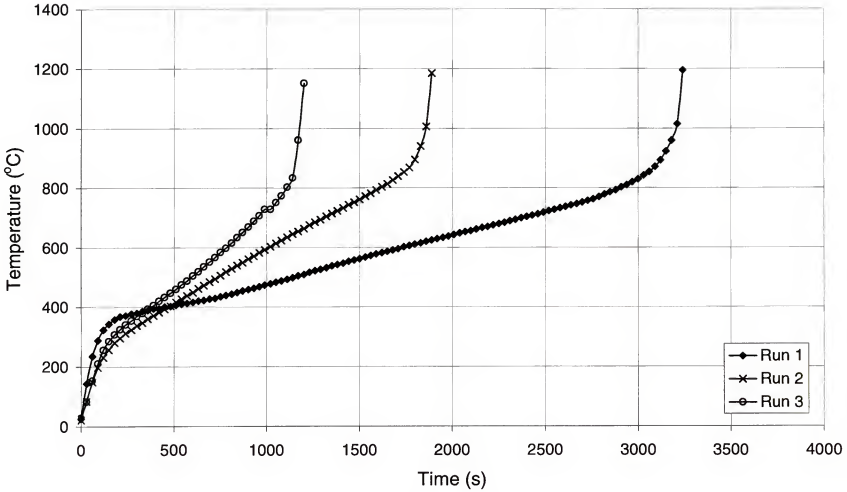


Figure 4.20. Ten weight percent β-phase (1 μm) silicon carbide composite samples heated to 1200 °C in nitrogen.

lot more difficulty. The sample cross-sectional surfaces were not polished to avoid having any phases potentially preferentially removed. Unfortunately, some of the composite samples heated to low temperatures (600 °C) could not be photographed in the SEM. To take a micrograph, the composites had to be cut which would prohibit their further use in the microwave. Some of the samples heated to low temperatures (600 °C) were later heated to higher temperatures (1200 °C), and this would not have been possible if they had been cut to examine the cross-section. All of the micrographs were taken at the maximum possible accelerating voltage that would still allow a picture to be taken with minimal charging effects. In some cases, the composite susceptor samples tended to charge, forcing the accelerating voltage to be reduced.

Figure 4.21 - Figure 4.23 show the cross-sectional micrographs for 10, 20, and 40 weight percent α-phase silicon carbide composite samples heated in air to 600 °C. The 50 weight percent α-phase silicon carbide sample could not be photographed because it was later heated to 1200 °C. For the samples heated in air to 600 °C, all have a rocky texture and no significant outstanding features. A somewhat flatter, but still rocky texture was found for the 10 weight percent α-phase silicon carbide composite sample heated to 600 °C in nitrogen, shown in Figure 4.24. Again, no significant outstanding features are observed.

In Figure 4.25, where a 50 weight percent β-phase silicon carbide composite sample was heated in nitrogen, a similar rocky microstructure was observed. X-ray dotmapping of this area was also performed, and this is presented in Figure 4.26. The SEM image of this area appears artificially flat in this figure due to charging of the area. Unfortunately, when detecting the x-rays from an area, higher voltages may be required

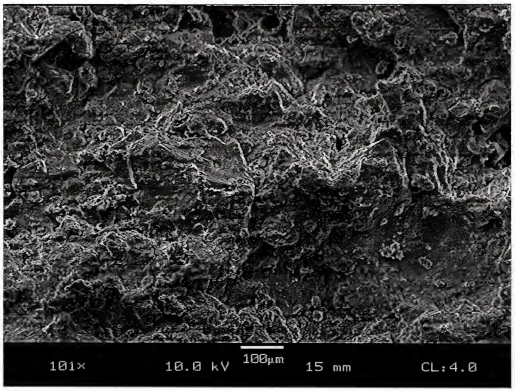


Figure 4.21. Ten weight percent α-phase (2 µm) silicon carbide composite samples heated to 600 °C in air.

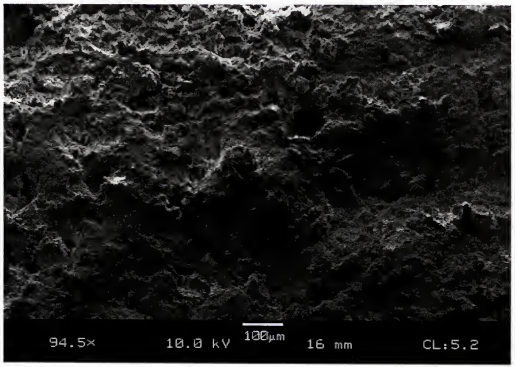


Figure 4.22. Twenty weight percent α-phase (2 µm) silicon carbide composite samples heated to 600 °C in air.

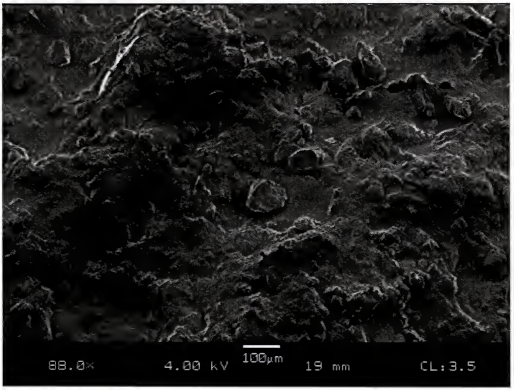


Figure 4.23. Forty weight percent α-phase (2 µm) silicon carbide composite samples heated to 600 °C in air.

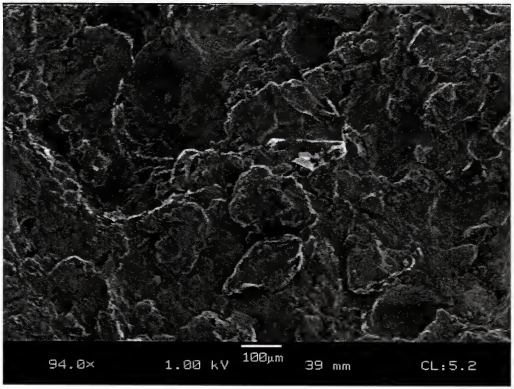


Figure 4.24. Ten weight percent α-phase (2 µm) silicon carbide composite samples heated to 600 °C in nitrogen.

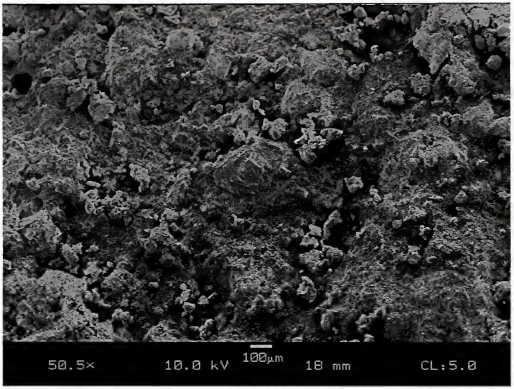


Figure 4.25. Fifty weight percent β-phase (1 µm) silicon carbide composite samples heated to 600 °C in nitrogen.

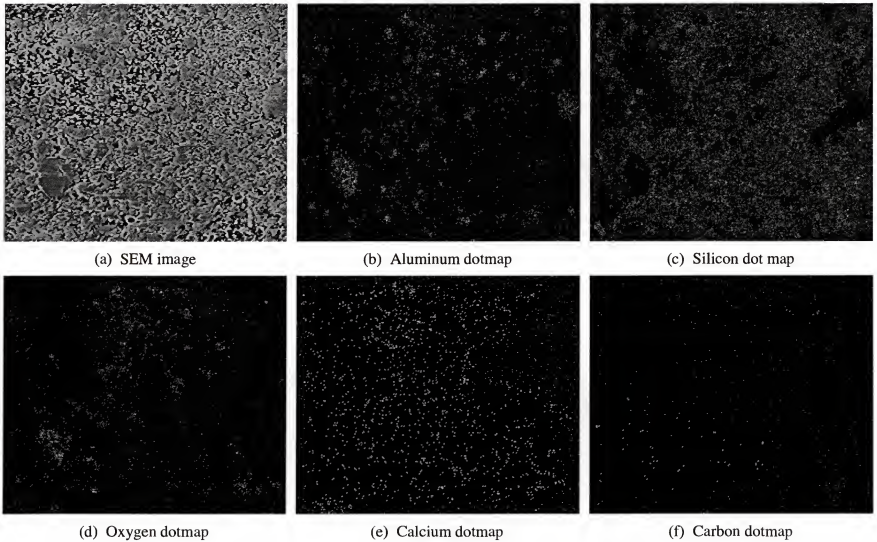

(a) SEM image (b) Aluminum dotmap (c) Silicon dot map

(d) Oxygen dotmap (e) Calcium dotmap (f) Carbon dotmap

Figure 4.26. X-ray dotmapping of 50 weight percent β-phase (1 μm) silicon carbide composite samples heated to 600 °C in nitrogen.

to obtain enough signal. This may result in too much signal being collected to obtain a good secondary electron picture, as it is in this case. Looking at these dotmaps, small pieces of aluminum oxide are apparent in places. In general, it can be concluded that the silicon carbide and high alumina cement are well mixed as they both appear throughout the material.

However, when a fracture surface of this same composite sample was examined in Figure 4.27, a very different microstructure was evident. When a fracture surface of a 30 weight percent β-phase silicon carbide composite sample heated to 600 °C in air was examined, crystals were also found, as shown in Figure 4.28. Even when fracture surfaces were examined, these crystals were not found in any α-silicon carbide sample. The x-ray dotmaps of each major constituent element in an area of the 30 weight percent β-phase silicon carbide composite sample with crystals are presented in Figure 4.29. Examination of the crystals demonstrates a calcium concentration at least five times higher than in other areas, when compared to the concentration shown in Figure 4.26. High oxygen concentrations are also present. It is clear that silicon makes up no part of these crystals, as the silicon dotmap shows the areas where the crystals are located as completely dark. From the elements found to be prevalent here, it is thought that the crystals that formed are calcite, forming off of an aluminum oxide or silicon carbide "seed crystal." Since both are hexagonal phases, aluminum oxide may also be present in combination with the calcium carbonate [Lid98].

Figure 4.30 and Figure 4.31 show a 40 weight percent β-phase silicon carbide composite sample and a 50 weight percent α-phase silicon carbide sample respectively heated to 1200 °C in air. These figures show much smoother, more glassy-like surfaces

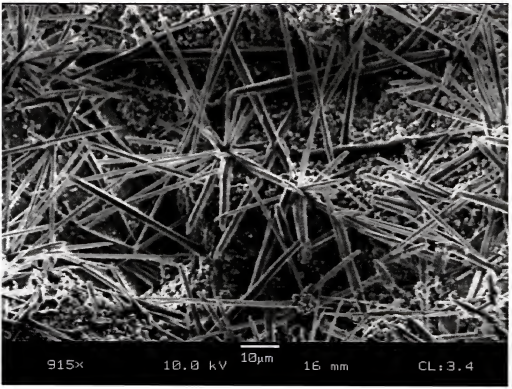


Figure 4.27. Fracture surface of 50 weight percent β-phase (1 µm) silicon carbide composite samples heated to 600 °C in nitrogen.

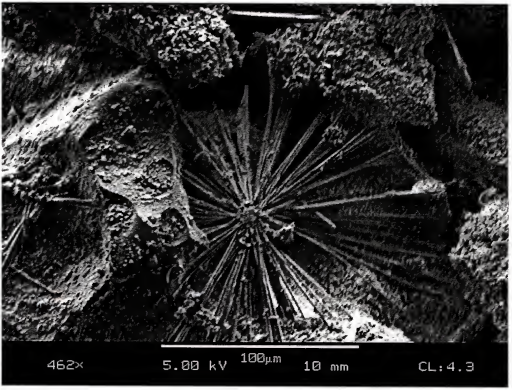


Figure 4.28. Fracture surface of 30 weight percent β-phase (1 µm) silicon carbide composite samples heated to 600 °C in air.

(a) SEM image

(b) Aluminum dotmap

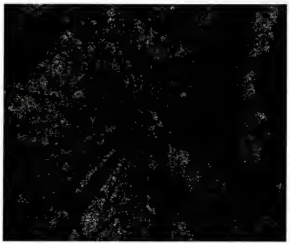

(c) Silicon dot map

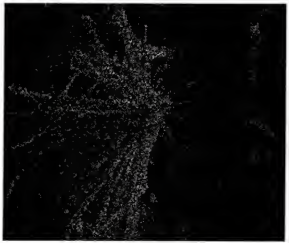

(d) Oxygen dotmap

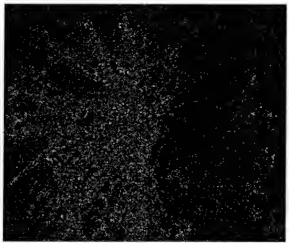

(e) Calcium dotmap

(f) Carbon dotmap

Figure 4.29. X-ray dot mapping of crystals found in 30 weight percent β-phase (1 μm) silicon carbide composite samples heated to 600 °C in air.

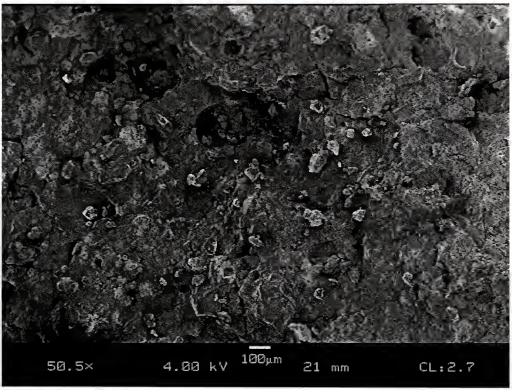


Figure 4.30. Forty weight percent β-phase (1 µm) silicon carbide composite samples heated to 1200 °C in air.

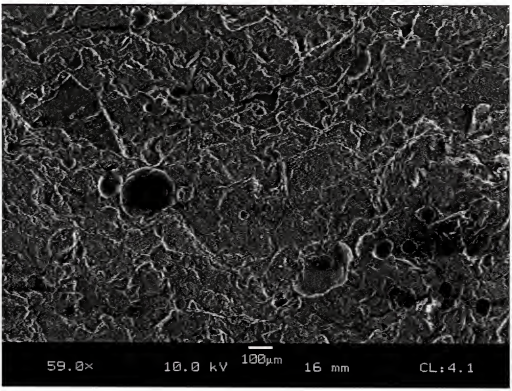


Figure 4.31. Fifty weight percent α-phase (2 µm) silicon carbide composite samples heated to 1200 °C in air.

than those found for the lower temperature samples. Similarly, in Figure 4.32 and Figure 4.33 which show 30 weight percent α-phase silicon carbide and 40 weight percent β-phase silicon carbide composite samples heated to 1200 °C in nitrogen, smoother, glassy-like surfaces are found. It may be noted that the crystals that were found in the low temperature β-phase silicon carbide composite samples were not found in any of these high temperature samples.

The micrographs of all of the low temperature and high temperature composite samples combined also helped to show the difference in hardness, if only by the difference in roughness of the cross-sectional surfaces. The low temperature samples tended to have a very rough surface, while the high temperature samples showed much smoother surfaces. This helped to confirm the impressions formed from the tactile texture as well as the behavior of the samples during cutting with the low-speed diamond saw. It also confirms that a reaction took place in the composite susceptor samples.

**Phase IV**

Now that phase III of the experiment demonstrated that the factors that were being tested were important, this was to be examined further in phase IV, and confirmed with more similar α- and β-phase silicon carbide particle sizes. It had also been proposed that with more similar particle size, the difference between the microwave heating rates of α- and β-silicon carbide composite samples might be more pronounced. It was clear from both phases II and III that a reaction did occur in the composites upon reaching a certain temperature, as well as proving that using a nitrogen atmosphere rather than air might affect this reaction. In this case, due to the limitations inherent with a fractional factorial design, a full factorial design was used, but the number of levels of composition

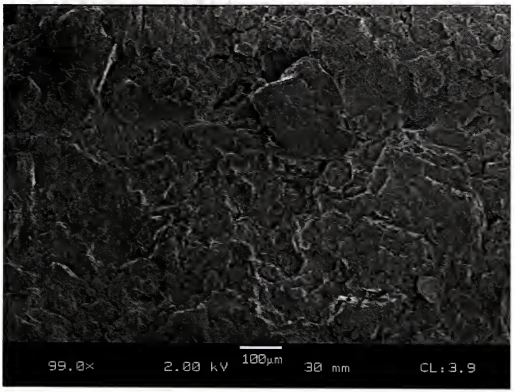


Figure 4.32. Thirty weight percent α-phase (2 µm) silicon carbide composite samples heated to 1200 °C in nitrogen.

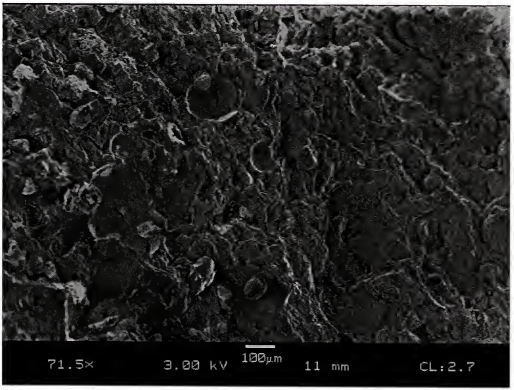


Figure 4.33. Forty weight percent β-phase (1 µm) silicon carbide composite samples heated to 1200 °C in nitrogen.

was reduced from five (10, 20, 30, 40, and 50 weight percent silicon carbide) to three (10, 30, and 50 weight percent silicon carbide), and the design was replicated five times. The reduction in the number of compositions to be tested was necessary to reduce the number of tests to be performed.

Since this set of experiments was designed to use $\alpha$- and $\beta$-phase silicon carbide particles that were of similar size, particle size analysis was performed. This confirmed that the particles were mostly at the particle size indicated, and that the distributions were similar. However, the instrument reported a peak at 2 $\mu$m for both phases of silicon carbide, which at first was thought to be possibly due to agglomeration. However, SEM of the powders showed that they did indeed contain some particles of approximately this size, as is seen in Figure 4.34 and Figure 4.35. The Alfrax 66 powder, as seen in Figure 4.36, contained a wide range of particle sizes, some in the submicron range, and others larger.

The first set of experiments in this section was designed to pinpoint the temperature at which the microwave heating rate would change irreversibly. By gradually increasing the maximum temperature reached by the composite sample, an estimate of the transition temperature could be obtained. The first step that was taken was to determine if possible, at what temperature the reaction took place using conventional heating methods. This was tested by running TGA/DTA on composite samples that had been prepared in the same manner as the microwave samples, and then were powdered. As has been discussed in the previous chapter, powdered samples will give more accurate peaks than solid samples in the TGA/DTA, as variables such as density, porosity, defects, or surface condition are reduced or eliminated. Silicon carbide

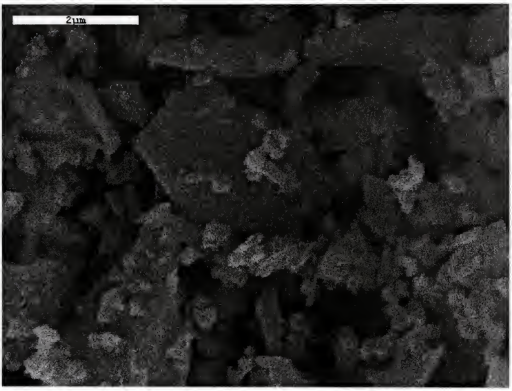


Figure 4.34. Micrograph of the α-phase (0.64 µm) silicon carbide powder from H.C. Starck.

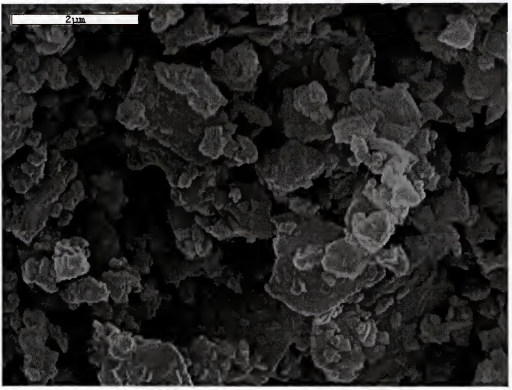


Figure 4.35. Micrograph of the β-phase (0.68 µm) silicon carbide powder from H.C. Starck.

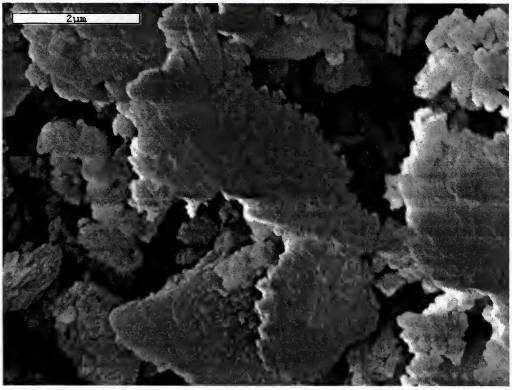


Figure 4.36. Micrograph of the Alfrax 66 high alumina cement powder.

composite samples containing 10, 30, or 50 weight percent α- or β-phase silicon carbide were tested in both flowing air and flowing nitrogen atmospheres. The rate of atmosphere flow was identical to that used in the microwave experiments.

Figure 4.37 and Figure 4.38 present the DTA results for 10 weight percent composite samples and each of the constituent materials heated in flowing air and flowing nitrogen, respectively. Although only the DTA is shown, the peaks were identified using both the DTA and the TGA data. In these figures, we see the endothermic peaks of water evaporation at approximately 100 °C, the dehydration of basic calcium carbonate (BCC) ($2CaCO_3 \bullet Ca(OH)_2 \bullet H_2O$) at approximately 300 °C to form basic calcium carbonate anhydride (BCCA), and the pyrolysis of calcite at approximately 800-825 °C [Mat95]. The exothermic peak representing crystallization of unstable calcium carbonate to calcite also appears in both figures; however, it is less distinct and at a lower temperature when heated in flowing nitrogen rather than flowing air [Mat95]. In addition, when the materials are heated in flowing air, two additional peaks are found. A slight exothermic peak occurs at about 700 °C, which is attributed to the decomposition of amorphous phases that tend to form during the formation of β-silicon carbide [Kha95]. It is also quite clear from comparison of the two figures that oxidation of the silicon carbide is inhibited by the presence of the flowing nitrogen, since the endothermic peak between 1050 and 1100 °C occurs only in the materials heated in flowing air [Ogb95].

Figure 4.39 and Figure 4.40 show the DTA results for 10, 30, and 50 weight percent α- and β-phase silicon carbide composite samples heated in flowing air. In both cases, it can be seen that as the amount of silicon carbide in the composite decreases (and

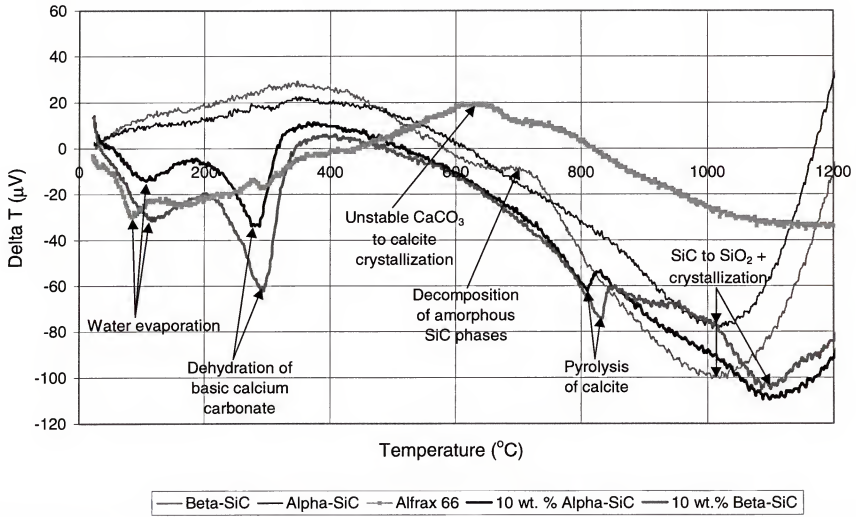


Figure 4.37. Differential thermal analysis of composite samples and their constituent materials heated in flowing air. (Silicon carbide from H.C. Starck).

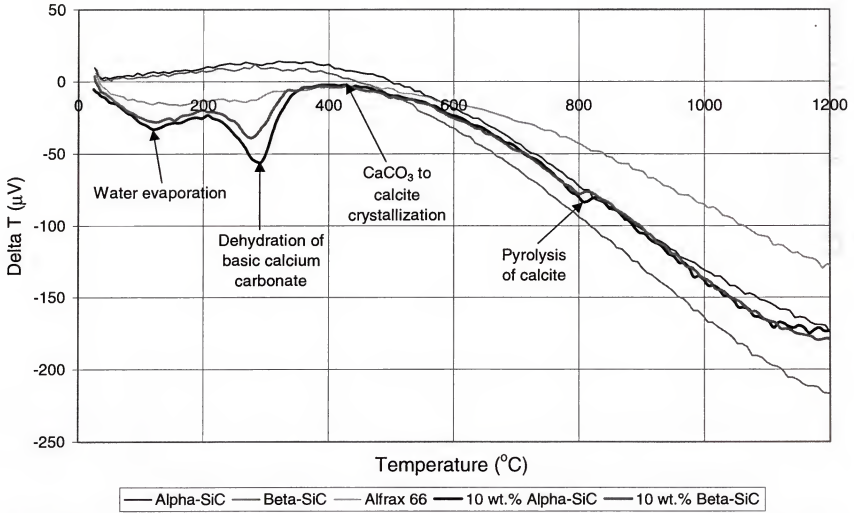


Figure 4.38. Differential thermal analysis of composite samples and their constituent materials heated in flowing nitrogen. (Silicon carbide from H.C. Starck).

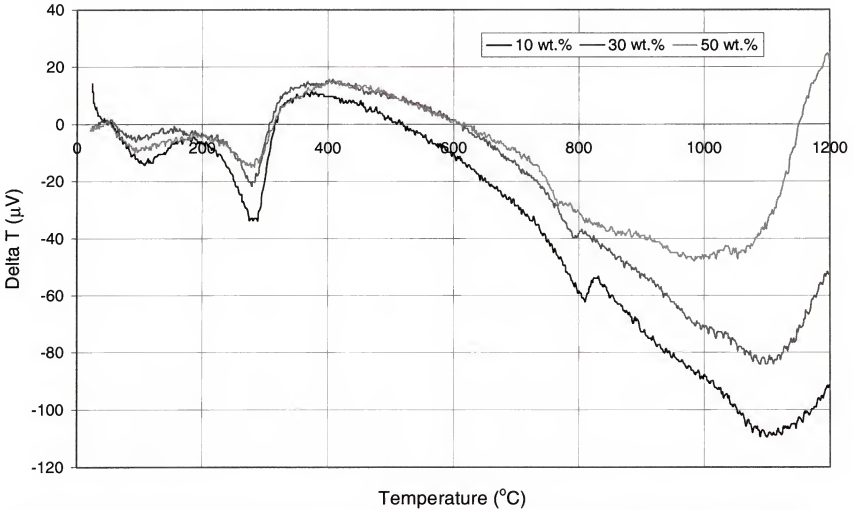


Figure 4.39. Differential thermal analysis of α-phase (0.64 μm) silicon carbide composite samples heated in flowing air.

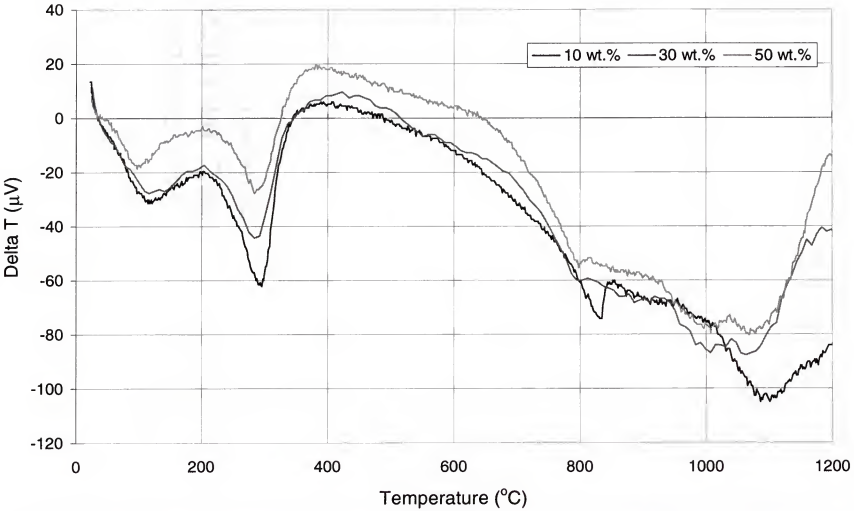


Figure 4.40. Differential thermal analysis of β-phase (0.68 μm) silicon carbide composite samples heated in flowing air.

therefore the amount of cement increases), that the amount of both physically and chemically bonded water increases. This is very clear by the increasing depth of the endothermic peaks at 100 and 300 °C, as well as by an increasing weight loss.* Additionally, the temperature at which calcite is pyrolyzed and at which silicon carbide is oxidized shifts depending upon the composition. For both of these reactions, the addition of more silicon carbide shifts the reaction to lower temperatures.

Similarly, Figure 4.41 shows the DTA results for α-phase silicon carbide composite samples heated in flowing nitrogen. In this case the composition does not appear to play a role in the amount of water evaporation, but does follow the trend of the samples run in flowing air (Figure 4.39 and Figure 4.40) in relation to the dehydration of basic calcium carbonate as well as the pyrolysis of calcite. However, in Figure 4.42, which presents the DTA for β-silicon carbide composites heated in flowing nitrogen, the temperature for pyrolysis of calcite does not appear to be significantly affected by the composition of the composite samples. The peaks occur in the same location for α- and β-phase silicon carbide composite samples, as is evident in Figure 4.43 and Figure 4.44 for 50 weight percent composite samples heated in air and nitrogen, respectively.

To confirm the identification of the peaks, a few samples were run through multiple heating cycles. In Figure 4.45, a composite sample of 30 weight percent α-phase silicon carbide was tested once, and then again several days later. It is clear that none of the low temperature peaks are present in the second test. In the second TGA/DTA test, only the endothermic peak for the oxidation of silicon carbide is evident.

---

* The weights of all of the samples prepared for TGA/DTA analysis were kept similar so that this could be compared.

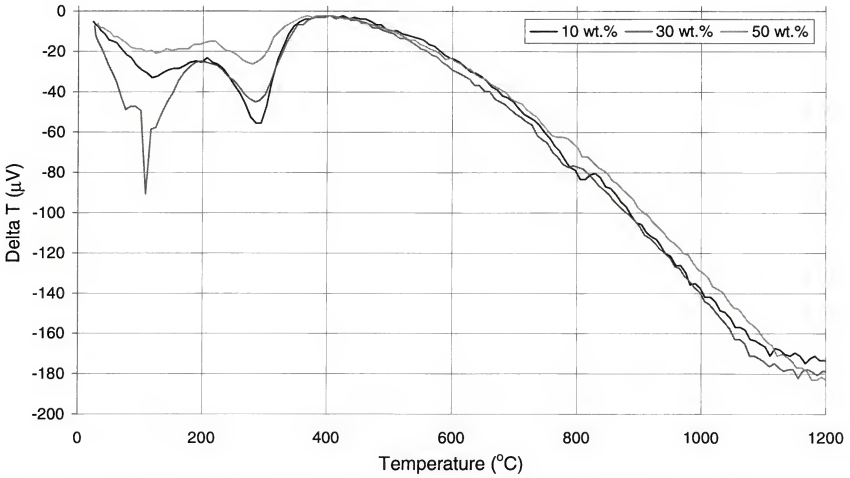


Figure 4.41. Differential thermal analysis of α-phase (0.64 μm) silicon carbide composite samples heated in flowing nitrogen.

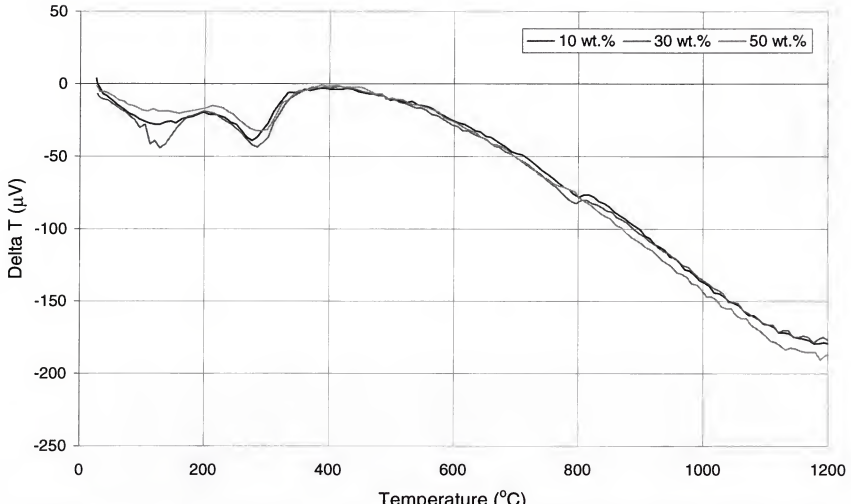


Figure 4.42. Differential thermal analysis of β-phase (0.68 μm) silicon carbide composite samples heated in flowing nitrogen.

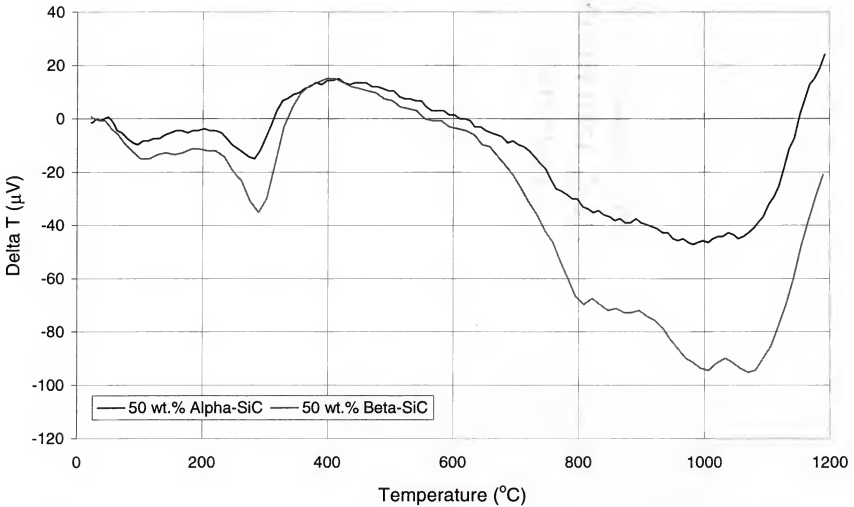


Figure 4.43. Differential thermal analysis of 50 weight percent α- (0.64 µm) and β-phase (0.68 µm) silicon carbide composite samples heated in flowing air.

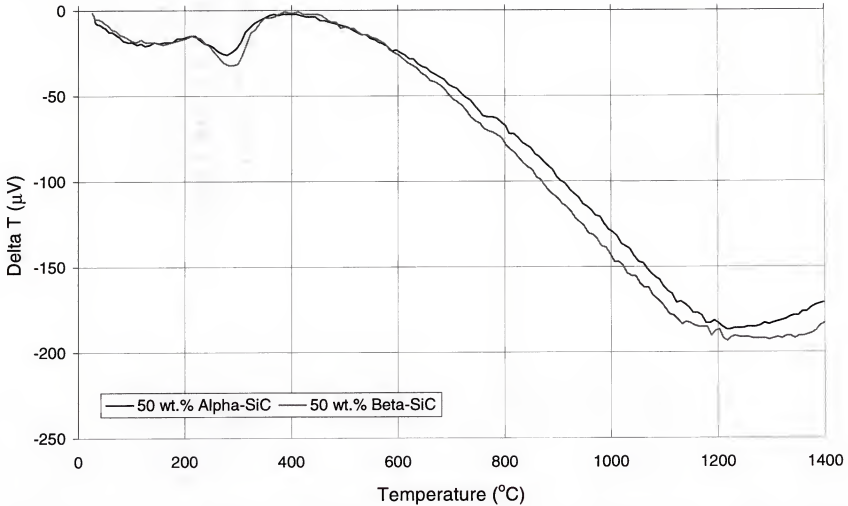


Figure 4.44. Differential thermal analysis of 50 weight percent α- (0.64 μm) and β-phase (0.68 μm) silicon carbide composite samples heated in flowing nitrogen.

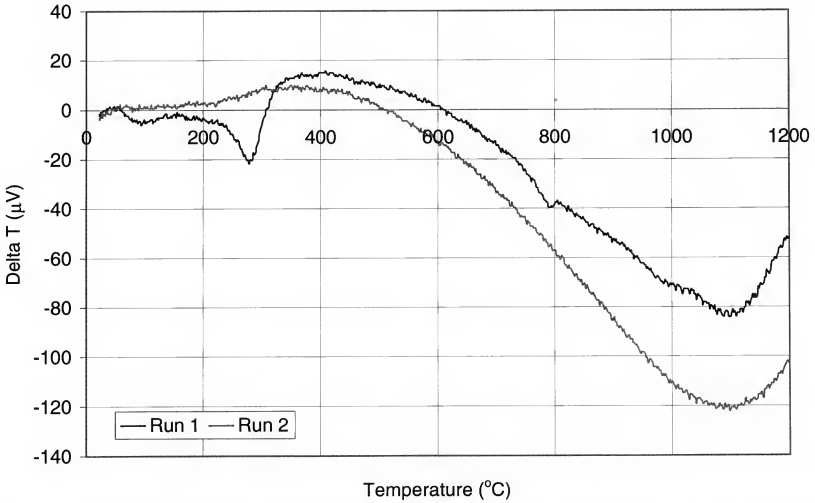


Figure 4.45. Differential thermal analysis of a 30 weight percent α-phase (0.64 μm) silicon carbide composite sample heated in flowing air through two heating cycles.

Figure 4.46 demonstrates that similar results were also found for β-phase silicon carbide composite samples, as well as for samples heated in flowing nitrogen.

From the TGA/DTA results, it was clear that excluding water evaporation, the first peak occurred at 300 °C. Consequently, this temperature was used as the starting point for testing for the microwave reaction. When the composites were microwave heated in flowing air, the transition was very clear, as demonstrated in Figure 4.47 for a 40 weight percent α-phase silicon carbide composite sample and in Figure 4.48 for a 20 weight percent β-silicon carbide composite sample. In Figure 4.47, the reaction appeared to occur gradually between 600 and 650 °C. On the other hand, in Figure 4.48, the reaction appeared to occur completely in the heating cycle up to 625 °C. In both of these figures, heating cycles to temperatures lower than 600 °C followed the same trend as at 600 °C, and heating cycles to temperatures above 650 °C followed the same trend as at 650 °C. All of the samples were heated above the transition temperature for several cycles to ensure that the reaction was complete. From these results, as well as for the other two compositions, it was determined that in flowing air the reaction in the microwave occurred at approximately 625 °C. It was also clear that the composition of the samples did not affect the temperature of the transition using microwave heating.

Similarly, Figure 4.49 and Figure 4.50 show a 40 weight percent α-phase silicon carbide composite sample and a 20 weight percent β-phase silicon carbide composite sample respectively, heated in flowing nitrogen. In this case, as is evident in Figure 4.49, the reaction is much less distinctly located at one particular temperature, but seems to occur gradually and be more spread out over a range of temperatures from 625-725 °C. Figure 4.50 also shows that the reaction was less distinct when the composite samples

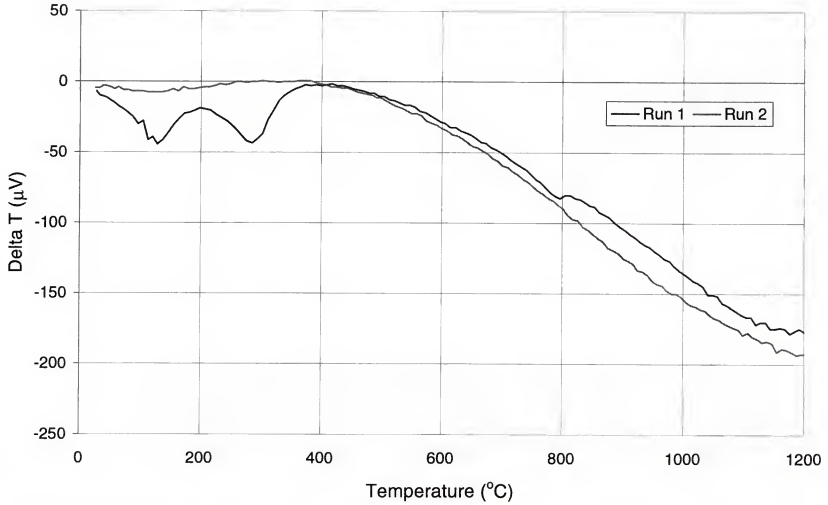


Figure 4.46. Differential thermal analysis of a 30 weight percent β-phase (0.68 μm) silicon carbide composite sample heated in flowing nitrogen through two heating cycles.

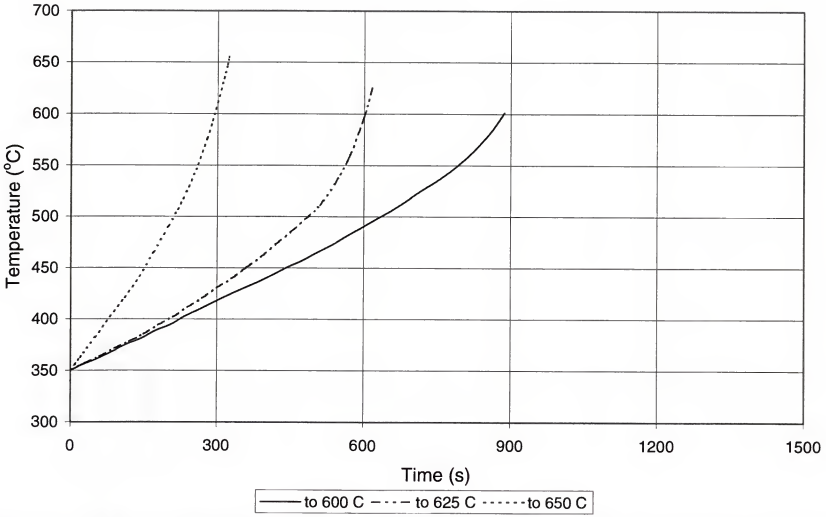


Figure 4.47. Forty weight percent α-phase (0.64 μm) silicon carbide composite sample gradually heated to higher temperatures in flowing air to find the microwave transition temperature.

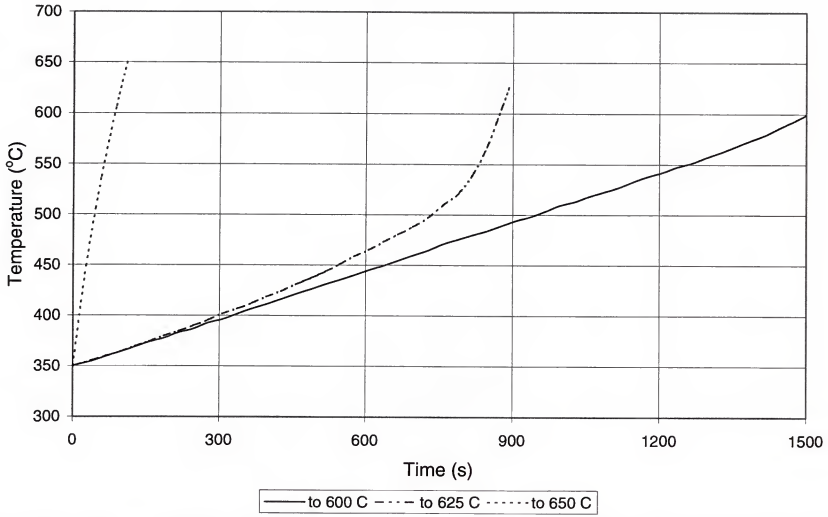


Figure 4.48. Twenty weight percent β-phase (0.68 μm) silicon carbide composite sample gradually heated to higher temperatures in flowing air to find the microwave transition temperature.

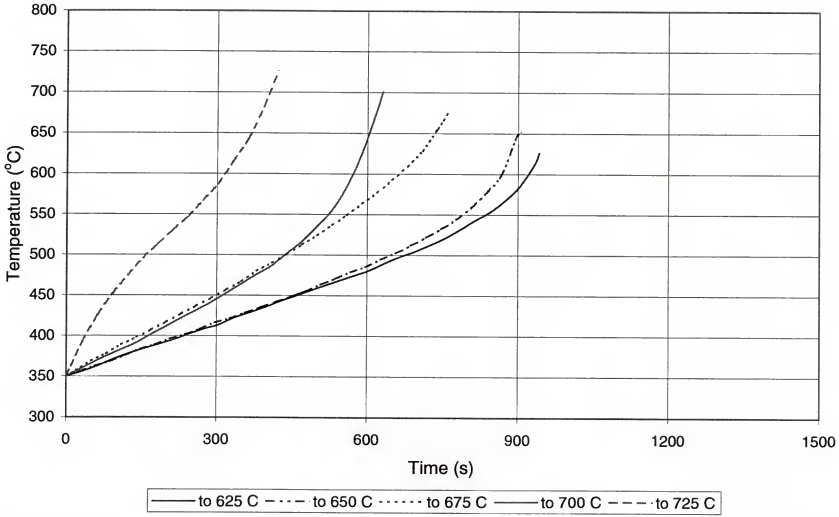


Figure 4.49. Forty weight percent α-phase (0.64 μm) silicon carbide composite sample gradually heated to higher temperatures in flowing nitrogen to find the microwave transition temperature.

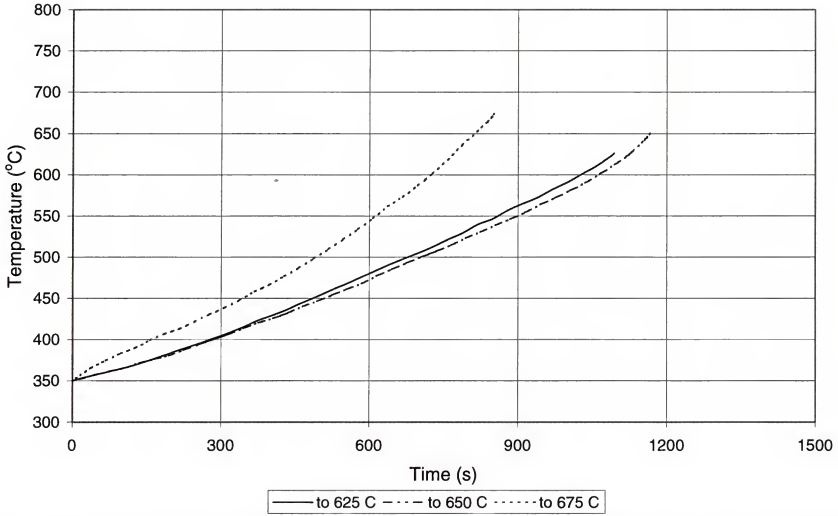


Figure 4.50. Twenty weight percent β-phase (0.68 μm) silicon carbide composite sample gradually heated to higher temperatures in flowing nitrogen to find the microwave transition temperature.

were heated in flowing nitrogen. This type of behavior was also observed for the 40 weight percent α-phase and the 20 weight percent β-phase composite samples. The best determination that could be made was that the reaction begins to occur at 625-650 °C. The ending point of the reaction appeared to be dependent upon the particular sample and its composition. Therefore, the temperature of the reaction was determined to begin at 625 °C, and tended to be complete by approximately 700 °C.

These experimentally measured heating rate transition temperatures were then utilized to determine the temperature to which the samples in the second part of the experiment would be heated. One set was heated to 75 °C below the transition temperature, and another set was heated to 75 °C above the transition temperature. Since it was determined that in both flowing air and flowing nitrogen, the reaction had at least begun by at least 625 °C, a set of low temperature composite samples was microwave heated to 550 °C, and another set of samples was microwave heated to 700 °C. Therefore, the composites heated to 550 °C should be completely unreacted, and the composites heated to 700 °C should be at least partially reacted. Another set of composite samples that was microwave heated to 1100 °C should be completely reacted. This final composite sample set would demonstrate if there was any significant difference in the microwave heating rate for samples heated significantly above the transition temperature and those that had been heated to just above the transition temperature.

The heating rates of all of the samples heated in flowing air are presented in Figure 4.51 - Figure 4.53. Each curve that is plotted in these figures represents the average of the five heating cycles that the sample experienced. The lower temperature portion of the curves has been omitted in these figures, as there was very little difference

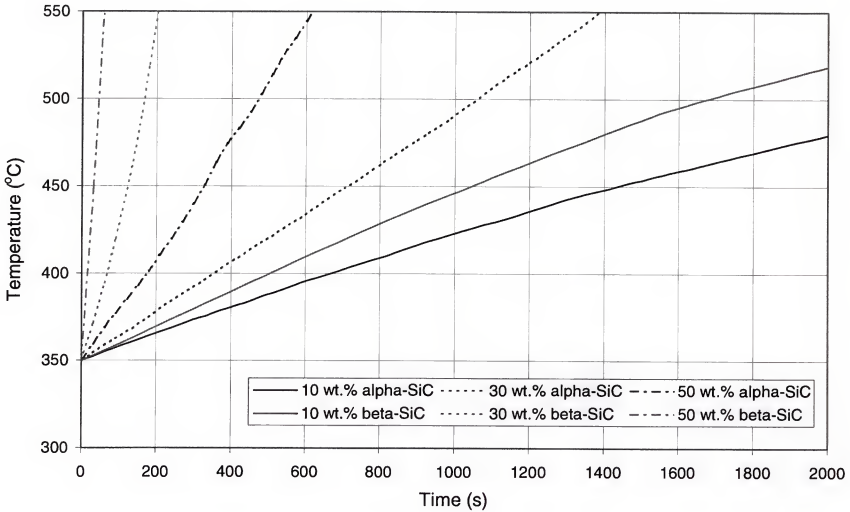


Figure 4.51. Microwave heating behavior of composite samples heated in flowing air to 550 °C. (Silicon carbide from H.C. Starck).

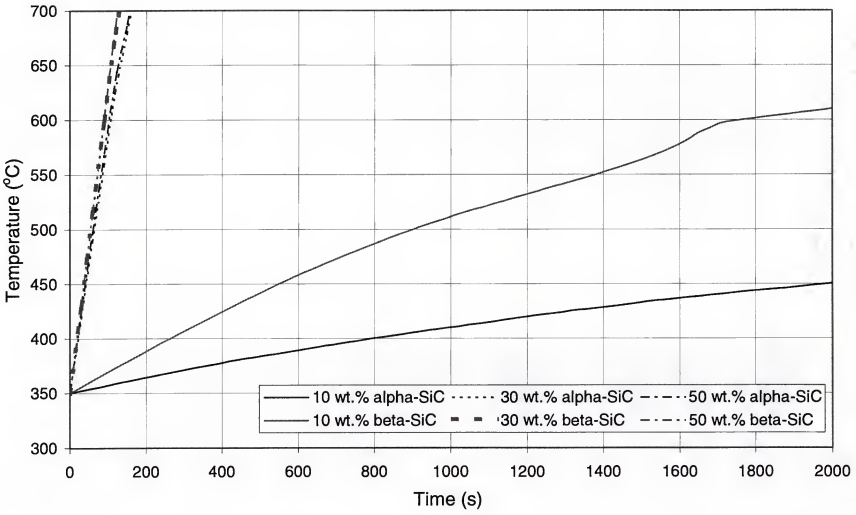


Figure 4.52. Microwave heating behavior of composite samples heated in flowing air to 700 °C. (Silicon carbide from H.C. Starck).

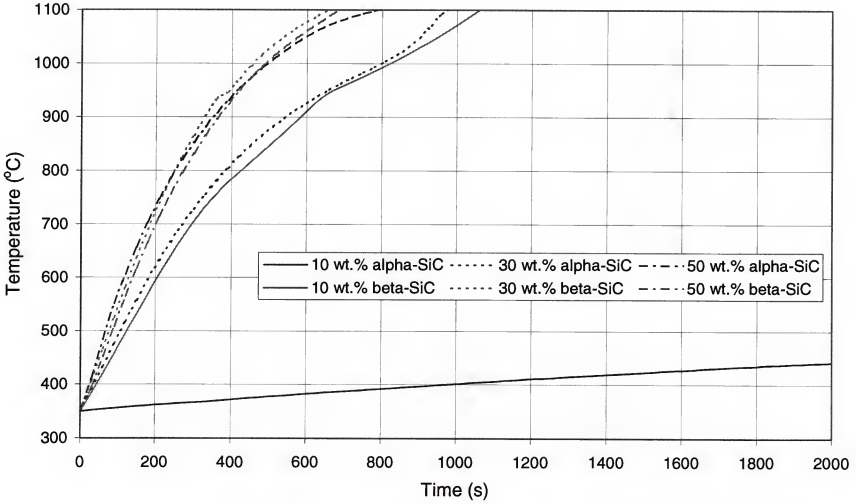


Figure 4.53. Microwave heating behavior of composite samples heated in flowing air to 1100 °C. (Silicon carbide from H.C. Starck).

in the heating rate until about 350 °C. This was similar to what had been found in previous phases of the experiment. Therefore, the data was transformed so that each curve would begin at 350 °C. A curve is plotted for every sample; however, in some cases where the composites were heated to 700 °C or 1100 °C, the individual curves are difficult to differentiate. On the other hand, in Figure 4.51, all of the curves can be easily differentiated from each other. Therefore, even before the statistical analysis, it can be determined that the weight percent of silicon carbide in the composite samples was more important at lower temperatures.

Figure 4.51 demonstrates that as before, the β-phase silicon carbide composite samples had faster heating rates than their α-phase counterparts. This trend was continued in Figure 4.52 for the samples heated to 700 °C, although this effect was decidedly less pronounced. This was not necessarily the case for the composites heated to 1100 °C in Figure 4.53, where the 50 weight percent α-phase silicon carbide composite heated more rapidly than the 30 and 50 weight percent β-phase composites over part of the heating cycle. However, the differences are slight and may be due only to experimental error. Figure 4.52 and Figure 4.53 also illustrate that the increase in silicon carbide content is much more significant between 10 and 30 weight percent than between 30 and 50 weight percent silicon carbide. To help distinguish between the different compositions for the composite susceptor samples heated to 700 and 1100 °C, the first few minutes of microwave heating are expanded in Figure 4.54 and Figure 4.55. However, as can be seen clearly in Figure 4.53, the heating rates of the composite samples did not necessarily remain constant over the entire temperature regime, but did change systematically with temperature.

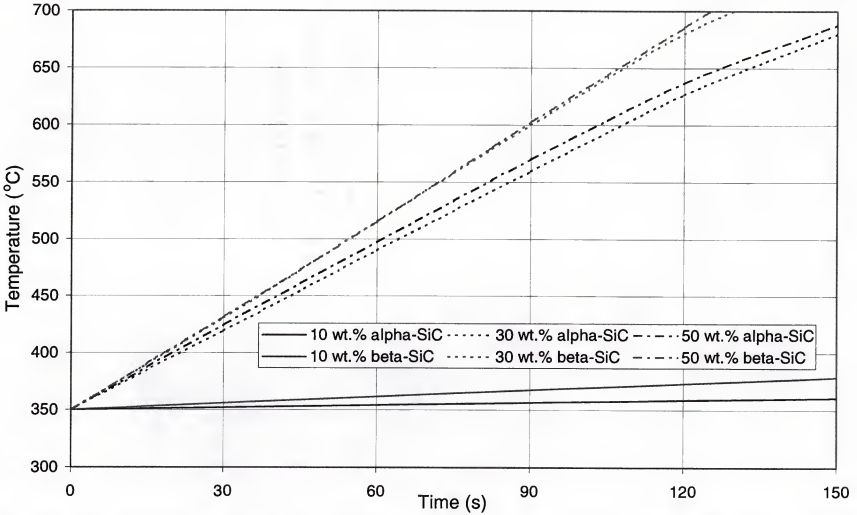


Figure 4.54. Magnified view of microwave heating behavior of composite samples heated in flowing air to 700 °C. (Silicon carbide from H.C. Starck).

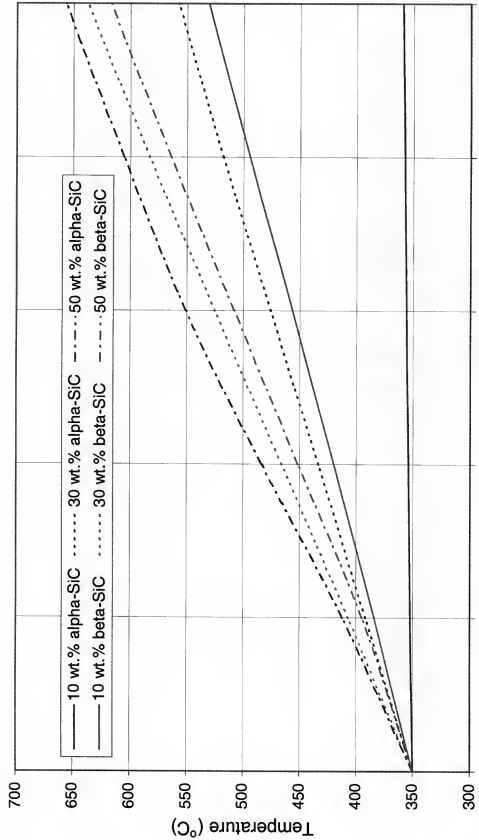


Figure 4.55. Magnified view of microwave heating behavior of composite samples heated in flowing air to 1100 °C. (Silicon carbide from H.C. Starck).

Heating behavior of the composite samples heated in flowing nitrogen may be viewed in Figure 4.56 - Figure 4.58, and are similar to those for flowing air. Once again, the most pronounced difference appeared between 10 and 30 weight percent silicon carbide, especially in the middle temperature range. Also, in Figure 4.56, the β-phase silicon carbide composites continued to heat more rapidly than the α-phase silicon carbide composite samples. In this case, however, the difference in heating rate between α- and β-phase composites was less pronounced than when the samples were heated in flowing air (Figure 4.51) rather than flowing nitrogen. For samples heated to 700 °C, (Figure 4.57) the curves showing the heating of the composites in flowing nitrogen were more individually distinguishable than they had been in flowing nitrogen. Clearly, as silicon carbide was added, the heating rate increased, and β-phase composites continued to heat more rapidly than α-phase composites. This was not necessarily found to be true for the composites heated to 1100 °C in flowing nitrogen, where all of the β-phase silicon carbide samples heated at a similar rate, with only small differences due to weight percent silicon carbide in the samples. On the other hand, for α-phase silicon carbide, the amount of silicon carbide continued to make a real difference in the heating behavior. Similarly to the composites heated in flowing air, the composites heated to high temperature in flowing nitrogen (Figure 4.58) demonstrated definite changes in the heating behavior as the temperature increased. Especially for the β-phase silicon carbide samples, the temperature would in some cases slowly drop, instead of increasing, after the composites had reached a temperature at some point above 1000 °C (usually 1030-1090 °C, depending upon the composition of the sample).

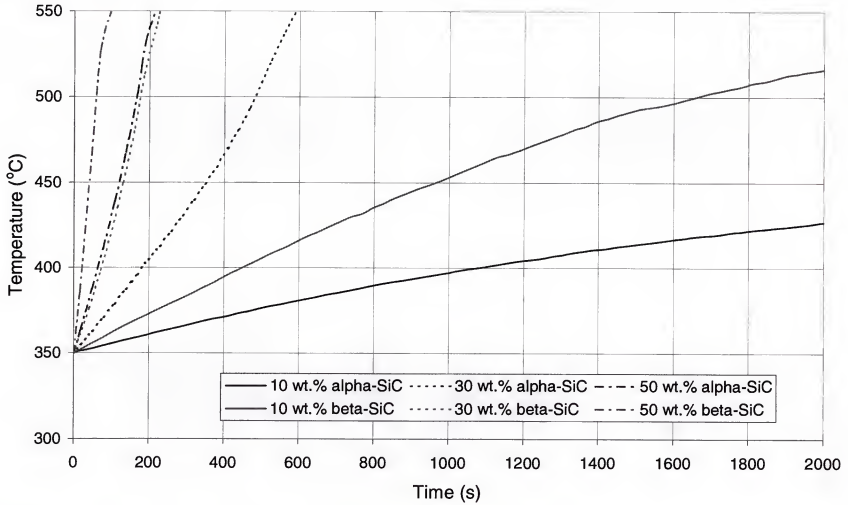


Figure 4.56. Microwave heating behavior of composite samples heated in flowing nitrogen to 550 °C. (Silicon carbide from H.C. Starck).

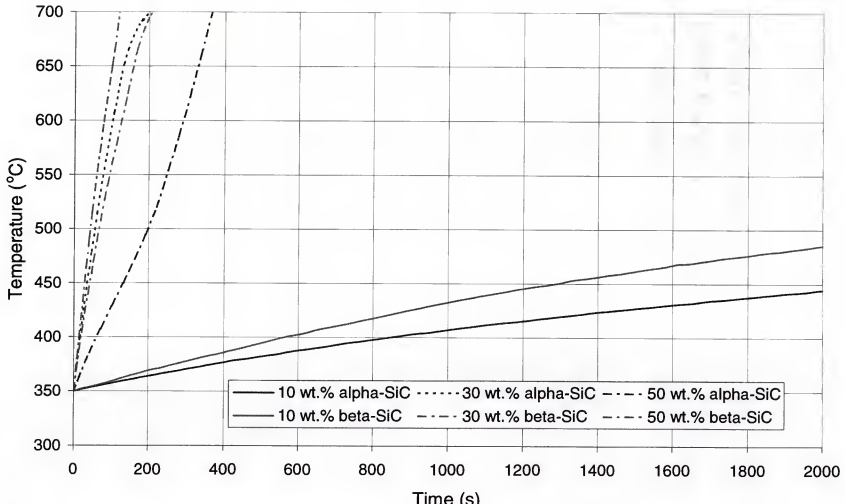


Figure 4.57. Microwave heating behavior of composite samples heated in flowing nitrogen to 700 °C. (Silicon carbide from H.C. Starck).

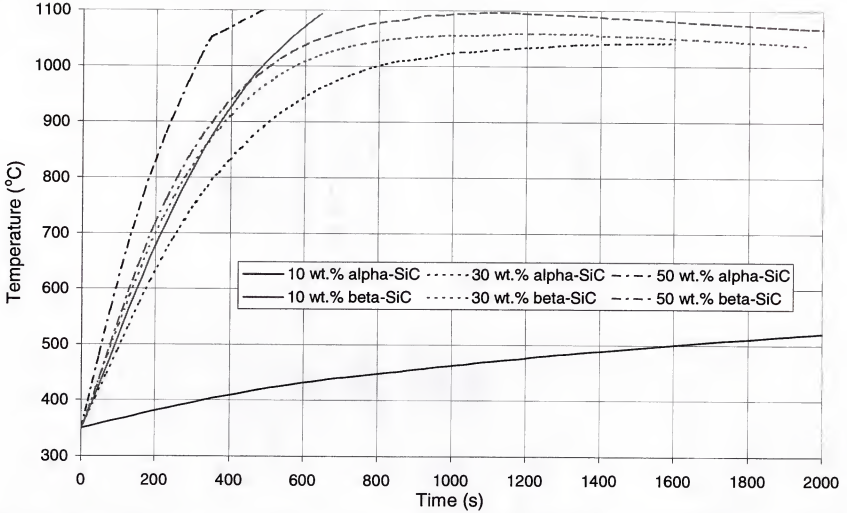


Figure 4.58. Microwave heating behavior of composite samples heated in flowing nitrogen to 1100 °C. (Silicon carbide from H.C. Starck).

Figure 4.59 - Figure 4.67 compare samples of a given weight percent silicon carbide heated in either flowing air or flowing nitrogen. A summary of whether a sample of given composition heated more rapidly in air or nitrogen is presented in Table 4.8. Figure 4.59 - Figure 4.61 show the differences in behavior for the composites heated to 550 °C for 10, 30, and 50 weight percent silicon carbide, respectively. At 10 weight percent α-phase silicon carbide, heating in air provided more rapid heating. However, at 30 and 50 weight percent α-phase silicon carbide, the composites heated in nitrogen consistently heated more rapidly than those heated in air. This same phenomenon was not observed for the β-phase silicon carbide composite samples, where regardless of the amount of silicon carbide in the composites, the heating rate in air or nitrogen remained about the same.

Table 4.8. Summary of heating rate behavior of composites as affected by presence of air or nitrogen, as determined from Figure 4.59 - Figure 4.67.

| | Heating Rates | | |
|---|---|---|---|
| | to 550 °C | to 700 °C | to 1100 °C |
| 10 Wt.% α-SiC | Air>Nitrogen | Air≈Nitrogen | Air<Nitrogen |
| 10 Wt.% β-SiC | Air≈Nitrogen | Air>Nitrogen | Air<Nitrogen |
| 30 Wt.% α-SiC | Air<Nitrogen | Air<≈Nitrogen | Air<≈Nitrogen |
| 30 Wt.% β-SiC | Air≈Nitrogen | Air≈>Nitrogen | Air>Nitrogen |
| 50 Wt.% α-SiC | Air<Nitrogen | Air>Nitrogen | Air<≈Nitrogen |
| 50 Wt.% β-SiC | Air≈Nitrogen | Air<≈Nitrogen | Air≈Nitrogen |

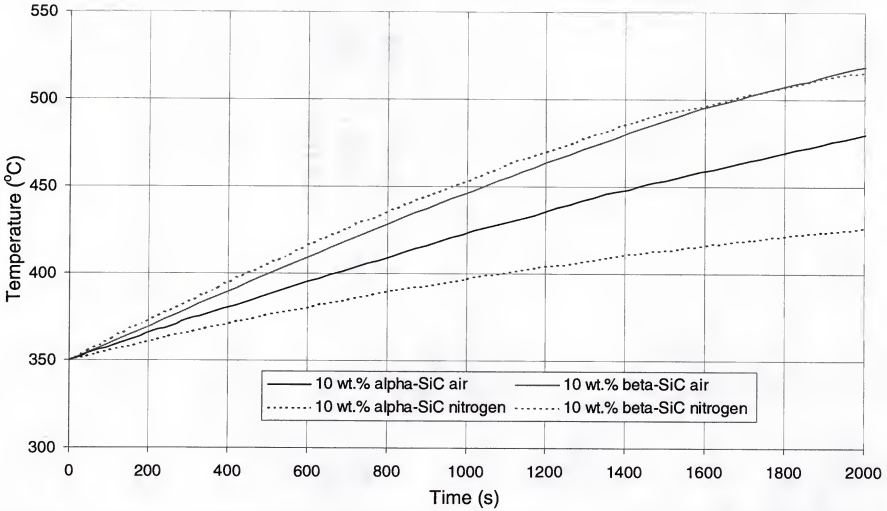


Figure 4.59. Ten weight percent silicon carbide composite samples heated to 550 °C in air and nitrogen. (Silicon carbide from H.C. Starck).

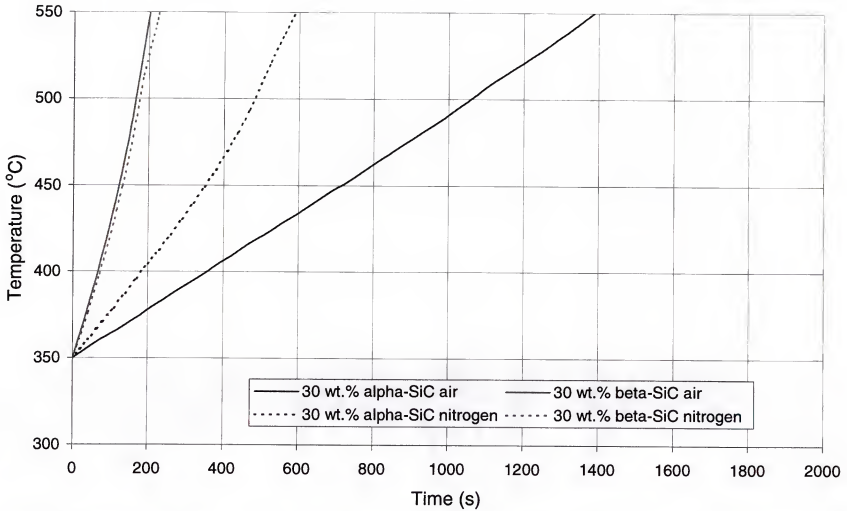


Figure 4.60. Thirty weight percent silicon carbide composite samples heated to 550 °C in air and nitrogen. (Silicon carbide from H.C. Starck).

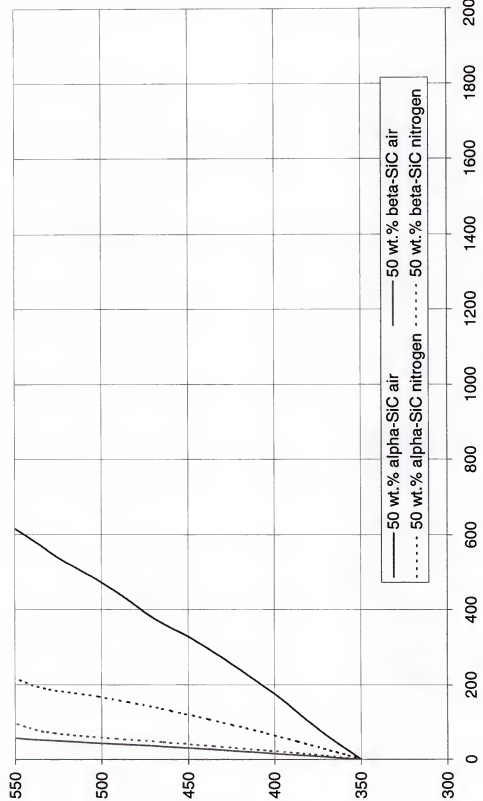


Figure 4.61. Fifty weight percent silicon carbide composite samples heated to 550 °C in air and nitrogen. (Silicon carbide from H.C. Starck).

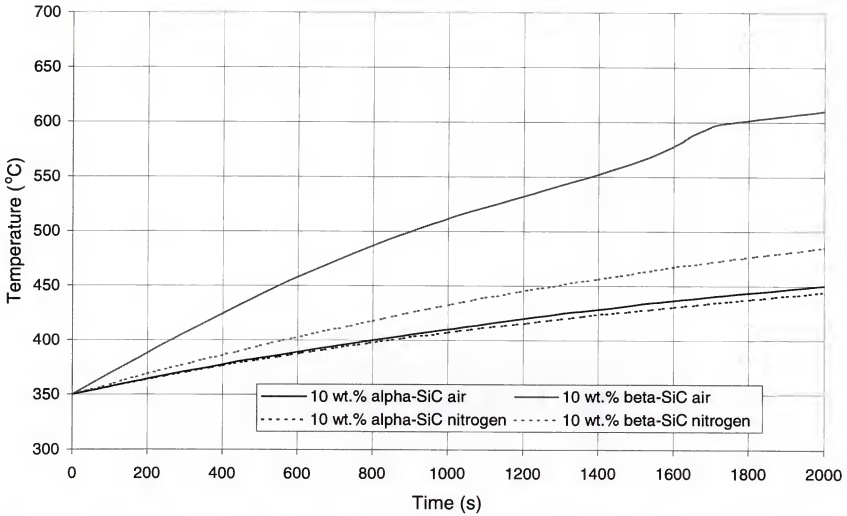


Figure 4.62. Ten weight percent silicon carbide composite samples heated to 700 °C in air and nitrogen. (Silicon carbide from H.C. Starck).

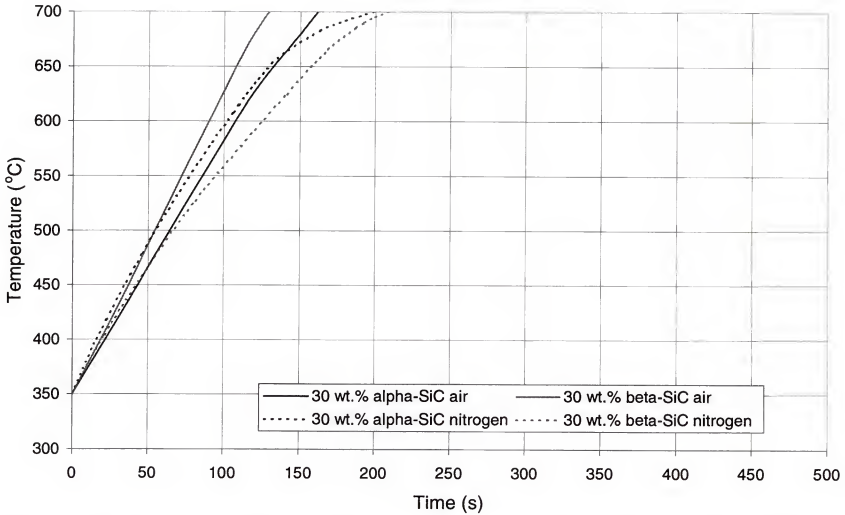


Figure 4.63. Thirty weight percent silicon carbide composite samples heated to 700 °C in air and nitrogen. (Silicon carbide from H.C. Starck).

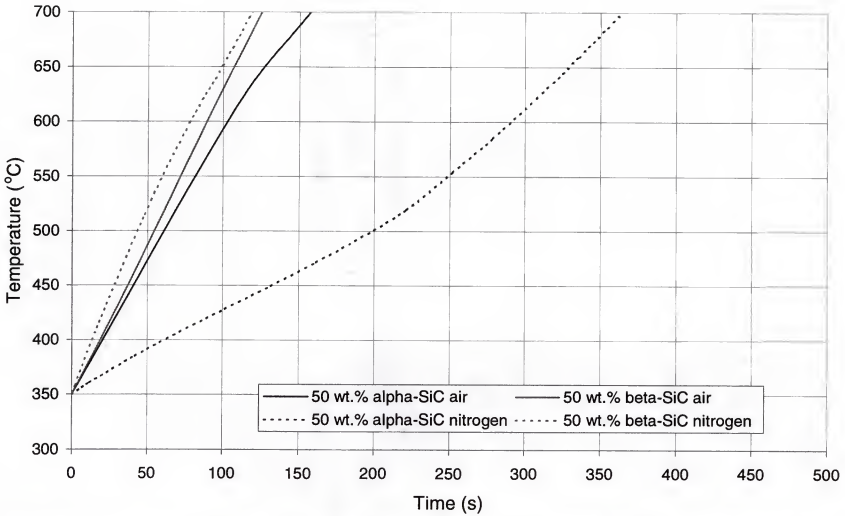


Figure 4.64. Fifty weight percent silicon carbide composite samples heated to 700 °C in air and nitrogen. (Silicon carbide from H.C. Starck).

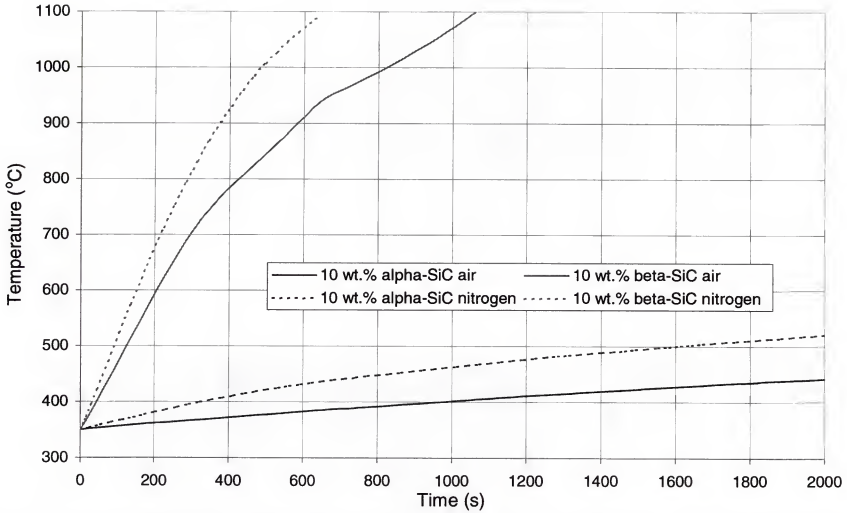


Figure 4.65. Ten weight percent silicon carbide composite samples heated to 1100 °C in air and nitrogen. (Silicon carbide from H.C. Starck).

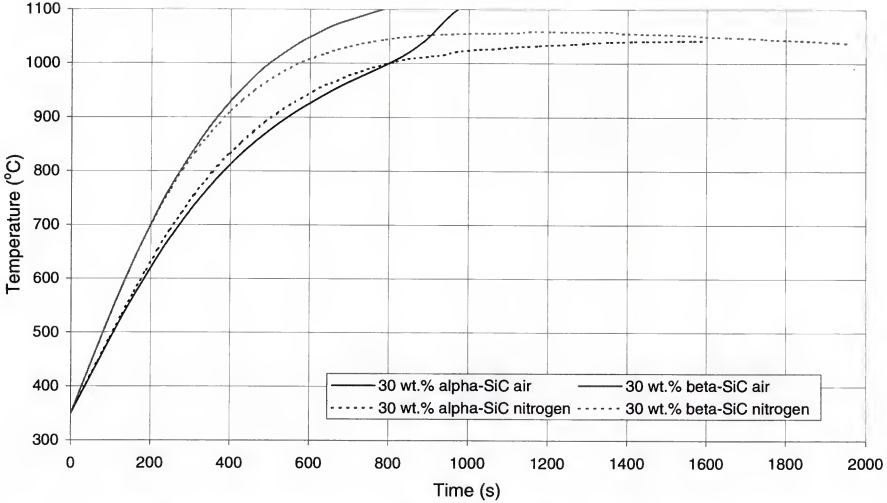


Figure 4.66. Thirty weight percent silicon carbide composite samples heated to 1100 °C in air and nitrogen. (Silicon carbide from H.C. Starck).

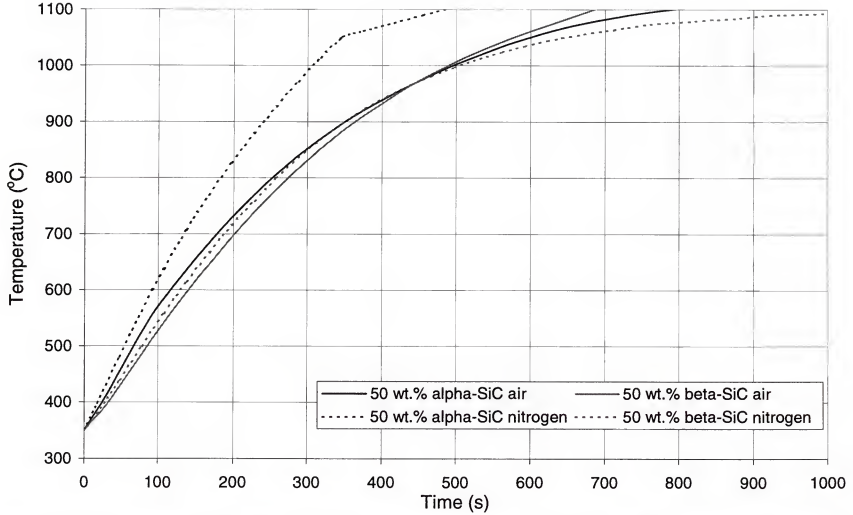


Figure 4.67. Fifty weight percent silicon carbide composite samples heated to 1100 °C in air and nitrogen. (Silicon carbide from H.C. Starck).

As the temperature increased, the behavior changed. Figure 4.62 - Figure 4.64 show heating comparisons for composite samples heated to 700 °C. In this case, which atmosphere was more conducive to a faster heating rate was extremely dependent upon composition. Figure 4.65 - Figure 4.67 summarize the effects of atmosphere on the composites for the samples heated to 1100 °C. For these samples, all of the α-phase silicon carbide composite samples heated more quickly in flowing nitrogen than in flowing air. This was not observed for the β-phase silicon carbide composite samples, whose behavior was once again more dependent upon composition.

Some general conclusions may be made from these graphs. The presence of nitrogen tended to inhibit microwave heating of the samples at high temperatures. However, the heating rates of these composites heated in nitrogen over the whole temperature range tended to be higher than if they had been heated in air. Overall, it is quite clear that the interaction of atmosphere with the composition plays an important role in the heating rate of the composite samples.

Table 4.9 summarizes the average heating rates of the composites heated in flowing air over specific temperature ranges. From this information, it can be determined that at low temperatures, as the amount of silicon carbide in the composite increased, the heating rate tended to increase. In addition, in agreement with phases II and III, in nearly every case, composite samples made with β-phase silicon carbide exhibited faster heating rates than those made with α-phase silicon carbide. As is also evident in Figure 4.53, the heating rates for the composite samples heated to 1100 °C tended to drop for most compositions as the susceptors were microwave heated above 700 °C. It should also be noted that for the 10 weight percent α-silicon carbide composite samples, they did not

Table 4.9. Heating rates of composite samples heated in flowing air depending upon temperature range. (°C/min.)

| Maximum Temperature of Sample (°C) | Temperature Range of Measurement (°C) | Sample Composition | | | | | |
|---|---|---|---|---|---|---|---|
| | | 10 wt.% α-SiC | 30 wt.% α-SiC | 50 wt.% α-SiC | 10 wt.% β-SiC | 30 wt.% β-SiC | 50 wt.% β-SiC |
| 550 | 350-550 | 3.64 | 9.55 | 21.1 | 6.36 | 59.7 | 186 |
| 700 | 350-550 | 2.16 | 119 | 143 | 9.34 | 165 | 183 |
| 1100 | 350-550 | 1.91 | 74.7 | 131 | 62.2 | 108 | 115 |
| 700 | 550-700 | 7.01 | 124 | 134 | 9.19 | 153 | 153 |
| 1100 | 550-700 | N.A. | 85.3 | 100 | 59.7 | 120. | 101 |
| 1100 | 700-900 | N.A. | 72.3 | 69.7 | 72.9 | 87.2 | 73.1 |
| 1100 | 900-1100 | N.A. | 30.2 | 30.6 | 80.4 | 50.7 | 28.9 |

Table 4.10. Heating rates of composite samples heated in flowing nitrogen depending upon temperature range. (°C/min.)

| Maximum Temperature of Sample (°C) | Temperature Range of Measurement (°C) | Sample Composition | | | | | |
|---|---|---|---|---|---|---|---|
| | | 10 wt.% α-SiC | 30 wt.% α-SiC | 50 wt.% α-SiC | 10 wt.% β-SiC | 30 wt.% β-SiC | 50 wt.% β-SiC |
| 550 | 350-550 | 2.68 | 20.1 | 56.6 | 6.69 | 53.4 | 155 |
| 700 | 350-550 | 1.81 | 132 | 42.9 | 2.60 | 110 | 198 |
| 1100 | 350-550 | 6.03 | 72.5 | 157 | 99.9 | 111 | 118 |
| 700 | 550-700 | N.A. | 104 | 112 | N.A. | 99.0 | 169 |
| 1100 | 550-700 | 3.19 | 73.9 | 164 | 92.7 | 104 | 132 |
| 1100 | 700-900 | N.A. | 55.0 | 121 | 75.3 | 74.3 | 78.9 |
| 1100 | 900-1100 | N.A. | 20.3 | 77.1 | 36.8 | 25.8 | 36.4 |

reach 1100 °C within the 6000 second imposed time limit. As a result, if the heating rates could not be obtained, they are listed in the table as not available (N.A.).

Table 4.10 summarizes the heating rate information the composites heated in flowing nitrogen. Generally, as the amount of silicon carbide in the composite increased, the heating rates increased in flowing nitrogen as well as in flowing air. With the exception of the 50 weight percent silicon carbide composites, β-phase silicon carbide samples tended to heat more quickly than α-phase silicon carbide composites. The drop

in heating rate as temperature increases is very evident for all compositions. As with the samples heated in air, the 10 weight percent α-phase silicon carbide composites had difficulty reaching the maximum temperature within the time limit. However, the 10 weight percent β-phase silicon carbide composites did not have this difficulty when they were allowed to heat up to 1100 °C in the very first heating cycle.

The heating rate data for all of these samples was then used to determine the statistical response values by ANOVA linear regression, and significance levels for each linear and quadratic factor were thus obtained for the composites heated in flowing air. As before, DOE-PC IV, version 3.01 was used to perform the calculations. In phase III, the quadratic terms could not be calculated due to the fractional factorial design, which design resulted in confounding of the quadratic terms. By using a full factorial design in this case, this problem was reduced. Some quadratic factors could still not be calculated due to confounding, and these are noted in the tables. Backwards elimination of factors that were found to be less than 75.0% significant was performed to increase the accuracy of the calculations. Only values of greater than 90% are presented in the table. Dashes in the table indicate that the value was lower than 90%, and thus the level of experimental error prohibited differentiation, meaning the factor could not be determined to be significant. Additionally, if a factor was not found to be at least 90% significant over any temperature range, it was eliminated altogether from the table.

Table 4.11 presents the calculated significance values for all of the samples heated in flowing air combined over specific temperature ranges. Up to 700 °C, all of the linear terms for weight percent silicon carbide, silicon carbide phase, and maximum processing temperature were found to be definitely significant, producing values of

Table 4.11. Significance levels of the factors for composites heated in flowing air as determined by ANOVA.

| Source | Temperature (°C) | | | |
|---|---|---|---|---|
| | 350-550 | 550-700 | 700-1100 | 350-1100 |
| Wt.% SiC (l) | 99.9+% | 99.9+% | - | 99.9+% |
| Wt.% SiC (q) | 99.9+% | 99.9+% | - | 99.9+% |
| SiC Phase ($\alpha$ or $\beta$) (l) | 93.7% | 99.1% | - | 90.0% |
| Maximum Temperature (550, 700 or 1100 °C) (l) | 99.9+% | 99.8% | N.A. | - |
| Maximum Temperature (550, 700 or 1100 °C) (q) | 99.9+% | - | N.A. | 96.8% |
| Interaction of Wt.% SiC (l) and SiC phase (l) | - | - | 98.7% | - |
| Interaction of Wt.% SiC (q) and SiC phase (l) | - | - | - | 99.9+% |

N.A. – Not applicable

nearly 100% in all but one case. Unfortunately, at higher temperatures, the level of error prohibited conclusions as to whether certain factors were or were not significant. However, it may be concluded that as the temperature increased, the mechanism controlling heating rate altered since the known significant factors changed with temperature, both in phase III as well as in this phase of the experiment. In addition to this, no significant difference in heating rate was found for the 700 and 1100 °C composite samples. This would indicate that no further reactions affecting the heating rate occurred at temperatures above 700 °C.

Table 4.12 summarizes the significant factors for the composite samples that were heated in flowing nitrogen. The phase of silicon carbide is noticeably missing from this table, as it could not be determined to be significant. However, it does make itself important in combination with the other factors involved. More noticeable is that the number of controlling factors is reduced as the temperature increases. The most factors

Table 4.12. Significance levels of the factors for composites heated in flowing nitrogen as determined by ANOVA.

| Source | Temperature (°C) | | | |
|---|---|---|---|---|
| | 350-550 | 550-700 | 700-1100 | 350-1100 |
| Wt.% SiC (l) | 99.9+% | 99.9+% | 90.5% | 99.9+% |
| Wt.% SiC (q) | 99.9+% | - | 99.7% | 99.9+% |
| Maximum Temperature (550, 700 or 1100 °C) (l) | 99.9+% | - | N.A. | - |
| Maximum Temperature (550, 700 or 1100 °C) (q) | 99.9+% | - | N.A. | 99.9+% |
| Interaction of Wt.% SiC (l) and SiC phase (l) | 99.7% | - | 99.4% | 99.7% |
| Interaction of Wt.% SiC (q) and SiC phase (l) | 99.9% | 99.9+% | - | 99.9% |
| Interaction of SiC Phase (l) and Maximum Temperature (q) | 95.3% | - | N.A. | 92.6% |
| Interaction of Wt.% SiC (l) and Maximum Temperature (l) | - | 98.9% | N.A. | 98.6% |
| Interaction of Wt.% SiC (l) and Maximum Temperature (q) | - | - | N.A. | 92.9% |
| Interaction of Wt.% SiC (q) and Maximum Temperature (q) | 99.9+% | - | N.A. | 99.9+% |
| Interaction of Wt.% SiC (l), SiC Phase (l), and Maximum Temperature (l) | 99.9+% | 99.9+% | N.A. | 99.9+% |
| Interaction of Wt.% SiC (l), SiC Phase (l), and Maximum Temperature (q) | 99.8% | - | N.A. | 99.5% |
| Interaction of Wt.% SiC (l), SiC Phase (q), and Maximum Temperature (q) | 99.5% | - | N.A. | - |
| Interaction of Wt.% SiC (q), SiC Phase (l), and Maximum Temperature (l) | - | 98.8% | N.A. | 98.7% |
| Interaction of Wt.% SiC (q), SiC Phase (l), and Maximum Temperature (q) | - | - | N.A. | 98.0% |

* could not be calculated due to confounding

are significant when only the low temperature regime or the entire temperature regime are considered. With the exception of weight percent silicon carbide, the significant factors shift with the temperature regime of interest. This would indicate that the heating mechanism changes as the temperature increases.

Table 4.13 contains all of the information about both sets of samples and analyzes the two different atmospheres together. It confirms again that the significant factors change with temperature when all samples are considered. As the graphs and data indicate, the presence of a nitrogen atmosphere definitely interacts with the other factors of interest. It also confirms the change in the significant factors with temperature. In addition, the weight percent of silicon carbide appears to be the most consistently significant factor throughout all of the analyses, both graphical and statistical, and therefore this is the factor that will be utilized to help predict the composite heating rate, depending upon the other conditions.

Table 4.13. Significance levels of the factors for all composites as determined by ANOVA.

| Source | Temperature (°C) | | | |
|---|---|---|---|---|
| | 350-550 | 550-700 | 700-1100 | 350-1100 |
| Processing Atmosphere (Air or Nitrogen) (l) | 99.4% | - | - | 99.9+% |
| SiC Phase (α or β) (l) | 99.4% | 99.9+% | - | - |
| Interaction of Atmosphere (l) and SiC Phase (l) | 91.9% | - | - | - |
| Wt.% SiC (l) | 99.9% | 99.9+% | - | 99.9+% |
| Wt.% SiC (q) | 99.9% | - | * | 99.9+% |
| Interaction of Atmosphere (l) and Wt.% SiC (l) | - | - | 99.7% | 96.3% |
| Interaction of Atmosphere (l) and Wt.% SiC (q) | 95.1% | - | * | 95.5% |
| Interaction of SiC Phase (l) and Wt.% SiC (l) | - | - | 95.2% | 98.2% |
| Interaction of SiC Phase (l) and Wt.% SiC (q) | 93.3% | - | * | - |
| Interaction of Atmosphere (l), SiC Phase (l), and Wt.% SiC (l) | - | - | 93.2% | - |
| Interaction of Atmosphere (l), SiC Phase (l), and Wt.% SiC (q) | - | - | * | 96.7% |
| Maximum Temperature (550, 700 or 1100 °C) (l) | - | - | - | 93.0% |
| Maximum Temperature (550, 700 or 1100 °C) (q) | 99.9+% | - | N.A. | 99.9+% |
| Interaction of Atmosphere (l) and Maximum Temperature (l) | - | - | N.A. | - |
| Interaction of Atmosphere (l) and Maximum Temperature (q) | 97.8% | - | N.A. | 99.8% |
| Interaction of Atmosphere (l), SiC Phase (l), and Maximum Temperature (q) | - | - | N.A. | 99.8% |
| Interaction of SiC Phase (l) and Maximum Temperature (q) | 95.8% | - | N.A. | - |
| Interaction of Wt.% SiC (l) and Maximum Temperature (l) | - | 99.9+% | N.A. | 99.9+% |
| Interaction of Wt.% SiC (l) and Maximum Temperature (q) | - | - | N.A. | 99.9+% |
| Interaction of Wt.% SiC (q) and Maximum Temperature (l) | - | - | N.A. | 90.1% |
| Interaction of Wt.% SiC (q) and Maximum Temperature (q) | 99.4% | - | N.A. | 99.9+% |
| Interaction of Atmosphere (l), Wt.% SiC (l) and Maximum Temperature (q) | - | - | N.A. | 98.1% |

Table 4.13—continued

| Source | Temperature (°C) | | | |
|---|---|---|---|---|
| | 350-550 | 550-700 | 700-1100 | 350-1100 |
| Interaction of SiC Phase (l), Wt.% SiC (l) and Maximum Temperature (l) | - | 99.9+% | N.A. | 99.9+% |
| Interaction of SiC Phase (l), Wt.% SiC (q) and Maximum Temperature (l) | - | 99.7% | N.A. | 99.9+% |
| Interaction of Atmosphere (l), Wt.% SiC (q) and Maximum Temperature (q) | 90.6% | - | N.A. | - |

* Due to confounding, the quadratic terms for the temperature regimes of 550-700 and 700-1100 °C could not be calculated.

# CHAPTER 5
# DISCUSSION

The main issue that brought about this study is the question of how can the behavior of these silicon carbide/high alumina cement composite susceptors be predicted? One of the main factors of interest (as well as significance) was how much silicon carbide should be incorporated? Unfortunately, the system contains various complicating factors that make this task difficult. However, by performing a systematic study of the behavior of the composite material, reasonable predictions can be made, provided certain other details are specified. This chapter examines the critical issues that must be controlled, the parameters that affect the heating rate of the composite susceptors, and how the heating rate can be predicted for a composite sample of a given composition.

## General Discussion

### Phase I

This phase of the experiment examined the effects of variation of silicon carbide weight percent and particle size on the composite samples. Clearly, the two different particle sizes contributed to a significant difference in behavior of the composite samples. The first set with 1000 μm particles showed a gradual increase in slope as the amount of silicon carbide was increased. This type of behavior, where the dielectric loss of the composites increases as the volume fraction of the lossy phase increases is predicted by

any of the dielectric mixing equations [2.28] – [2.33]. The second set with 85 μm particles also show this behavior, but with a sudden change from one slope to a much higher slope. The difference in heating rate between the 10-30 weight percent and the 40-50 weight percent composite samples made from these particles is probably due to particle-particle touching, thus essentially creating larger silicon carbide particles through percolation effects which will be discussed in more detail later. The composition differences between the two silicon carbide materials are minute. Both sets of particles were between 97 and 98% α-phase silicon carbide. The impurities were identical, similar in quantity (within a fraction of a percent), with the only significant difference known between the two sets being particle size. So, particle size apparently causes the observed differences in behavior.

The trends observed were reproducible. However, the exact numbers obtained were found to be dependent upon several factors. These included the insulation of the susceptor and preventing arcing from the thermocouple to the sample. Any heating cycles where arcing was observed were scrapped and retested. Finally, placement of the susceptor and housing within the microwave cavity was critical, even though the microwave had a mode stirrer. Therefore, the sample was always placed in the same location in the microwave cavity. However, even with all of these important factors to be considered, the trends were able to be reproduced time after time.

Some data variation was evident, where a sample with lower silicon carbide content may have exhibited an initial higher heating rate than a sample with a higher silicon carbide content. The variation was determined to be likely caused by particle settling in the sample, which would be affected by how much water was added to the

high alumina cement. Particle settling was especially a problem for the larger, and thus heavier, particles. At longer times for the 1000 μm particle samples, the lower heating rates found for the higher weight percent silicon carbide composites were only temporary, as composites with larger amounts of silicon carbide always reached the maximum temperature in less time. For the 85 μm particles, this was not always the case. However, when this was found, the differences were not very great, and the variations were most likely due to experimental error. Experimental error is also the likely cause of the variation in heating rate at the start of the runs, as seen in Figure 4.1, since the initial heating rate is very rapid, and the thermocouple is often caught playing a game of "catch-up." This very rapid heating as well as the small difference in heating rate with composition at the beginning of the heating cycle was part of the reason why the heating from room temperature to ~350 °C was generally excluded from the calculation of the heating rate of the composites.

When the composites containing smaller amounts of silicon carbide are examined, the heating rate differences seen in Figure 4.3 are striking. But, even more interesting are the samples made of half and half of each particle size. The behavior appears to be dominated by the presence of the 1000 μm silicon carbide particles, even though in a cross-section of the material, only a very small number of these particles are present. However, at high weight percent silicon carbide, the difference between the behavior of the 1000 μm and the 85 μm silicon carbide particles is very small. This would indicate that the mechanism controlling the 85 μm particles has changed to that which controls the 1000 μm particles. This may also confirm the theory that particle-particle contact is

controlling the behavior, creating essentially larger particles when enough of the "fine" particles are incorporated into the composite.

The heating rate of the susceptors was fairly linear after reaching 350 °C. The linear heating rates allowed the steady-state heating rate to be measured, and this was clearly dependent upon particle size. The heating rates of the composite samples are plotted in Figure 5.1. The heating rate data was then analyzed to create a best-fit equation for each particle size or combination of particle sizes. For the "coarse" 1000 μm particles, a linear equation easily followed the behavior by the equation:

$$Rate\left(\frac{^{\circ}C}{\text{min.}}\right) = 3.8342x + 7.8684 \quad \textbf{[5. 1]}$$

where x is the weight percent of silicon carbide contained in the composite. Similarly, equations of increasing complexity were calculated for the half and half composites and for the "fine" 85 μm composite samples in equations [5.2] and [5.3], respectively.

$$Rate\left(\frac{^{\circ}C}{\text{min.}}\right) = 0.1253x^2 - 1.7007x + 44.13 \quad \textbf{[5. 2]}$$

$$Rate\left(\frac{^{\circ}C}{\text{min.}}\right) = -0.0161x^3 + 1.554x^2 - 38.369x + 268.56 \quad \textbf{[5. 3]}$$

By using these equations, the time to increase the temperature by 600 °C, for example, for composites of varying compositions could be calculated, and these are presented for some compositions in Table 5.1. This table also demonstrates again that the composite samples with half of each particle size generally tend to follow the heating rate of the 1000 μm particles more closely. It is also clear that as the weight percent silicon carbide

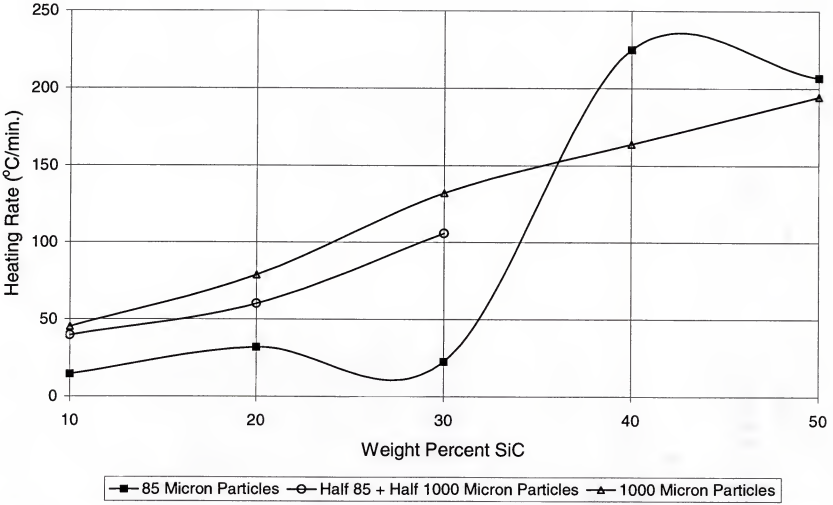


Figure 5.1. Heating rates of α-phase silicon carbide (1000 μm, 85 μm, and combination) composite samples as a function of weight percent silicon carbide.

Table 5.1. Calculated time (min.) required to raise the temperature of "coarse", "fine" and mixed silicon carbide composites by 600 °C, depending upon sample composition.

| Silicon Carbide Particle Size | Weight Percent Silicon Carbide | | | |
|---|---|---|---|---|
| | 15 | 25 | 35 | 45 |
| 1000 μm | 9.2 | 5.8 | 4.2 | 3.3 |
| 1000 μm mixed with 85 μm | 12.8 | 7.5 | 4.3 | 2.7 |
| 85 μm | 89.9 | 7.6 | 3.2 | 2.5 |

increased, the heating rate increased. By taking the equation [5.3], the turning point to higher heating rates may also be calculated. The point of inflection of this curve* (percolation threshold) should indicate where the heating rate increases most rapidly for the 85 μm silicon carbide composite samples. The point of inflection was calculated to occur at 32.2 weight percent silicon carbide. The calculation corroborates the information shown in the graphs, where the greatest change in heating rate was observed between 30 and 40 weight percent silicon carbide. To further pinpoint the transition, more compositions between 30 and 40 weight percent silicon carbide would need to be fabricated and tested.

* The point of inflection is defined as where the slope of the curve changes from concave up to concave down or vice versa. It is also the point of maximum or minimum slope of the curve. The point of inflection may be calculated from the second derivative of the equation.

**Major Results From Phase I**

Phase I of the study identified insulation of the composite susceptor sample, sample placement in the microwave cavity, and preventing arcing between the composite and the thermocouple to be critical factors that had to be controlled to obtain reproducible results. Generally, as the amount of silicon carbide in the composite was increased, the heating rate would also increase. It was also found that silicon carbide particle size had a distinct effect on the heating rates of the composites. The smaller silicon carbide particle composites exhibited an abrupt transition to higher heating rates as the amount of silicon carbide in the composites was increased, which is attributed to crossing the percolation threshold. Composites made with a combination of the two particle sizes tended to exhibit heating rates that were controlled by the presence of the larger silicon carbide particles. Heating rates of the composites were measured and used to create equations predicting the heating rate of a sample of any given composition. From one of these equations, the percolation threshold for the composites containing the 85 μm silicon carbide was calculated to occur at 32.2 weight percent silicon carbide.

**Phase II**

The silicon carbide particle size was reduced, purity was increased, and the phase of the silicon carbide particles was considered as a possible factor in the second part of the experiment. This time, the two types of silicon carbide were obtained from the same manufacturer; but the particle sizes were different. The α-phase silicon carbide particles were approximately 2 μm in diameter, and the β-phase silicon carbide particles were approximately 1 μm in diameter. These particles were of much higher purity, being 99.8% α-phase or β-phase silicon carbide respectively. Therefore, the behavior of the

composites can be truly attributed to the silicon carbide itself, rather than from potential effects of impurities.

As was stated in Chapter 4, from the combination of physical characteristics, heating rate, and x-ray diffraction spectra, it was clear that the samples underwent a reaction. Finding a reaction was not altogether unexpected, since the silicon carbide particles that were used were so small. The smaller size of the particles, and corresponding increase in surface area should make the particles more reactive due to the increase in energy required by the free surfaces. For the α-phase silicon carbide samples, before reaction the compounds detected consisted of SiC, $SiO_2$, and several other compounds that would be expected in a hydrated form of $Al_2O_3$ cement, as presented in Table 4.3. However, after reaction, only SiC and $SiO_2$ were still detected, and these had been joined by trace amounts of $3Al_2O_3{:}2SiO_2$. It appears that the $Al_2O_3$ and either SiC or $SiO_2$ reacted to form this phase. For the β-phase silicon carbide samples before reaction, only components of the high alumina ($Al_2O_3$/CaO) cement were detected, and these components did not match those found for the α-phase silicon carbide samples. In this case, after reaction, the SiC was easily detected, as well as $Al_2O_3$. It is thought that silicon carbide may not have been found before the reaction due to the testing of solid samples which may have examined an area in the XRD sample that contained a smaller than normal amount of silicon carbide.

However, the most likely explanation for some of the differences in the phases found is the manner in which the materials had to be tested. Small samples of the specific size required for the XRD equipment were specially made for this test. These samples were first examined in the XRD without any heating as solid samples. They

were then heated in the microwave, and examined again. Solid samples had to be used because powder samples react differently in the microwave field than a larger material. Using a solid, somewhat porous material can be examined with XRD, but it will at the very least diminish the intensity of the signal that is received, thus making the information more difficult to interpret [Cul78]. In addition, any inhomogeneities in the material (such as areas of higher cement concentration) may give misleading results, and this is more difficult to avoid when solid samples are used.

In both Figure 4.9 and Figure 4.10, it may be observed that the heating rate for the 10 weight percent silicon carbide samples was much lower than that of all of the other samples. The large difference in heating rates is again presumed to be caused by particle-particle touching and percolation effects for the higher weight percentages of silicon carbide. In Figure 4.10, the 30 weight percent composite sample exhibited a lower heating rate than the 20 weight percent sample. In this case, it is believed that the lower heating rate measured was caused by particle settling or inhomogeneous mixing of the particular sample. However, with the exception of the 30 weight percent β-phase silicon carbide result, the heating rates for the 20-50 weight percent α- or β-phase composite samples, respectively, are similar. The α-phase composite heating rates ranged from 2.41-2.53 °C/sec, and the β-phase composite heating rates ranged from 3.08-3.15 °C. Therefore, the amount of silicon carbide in the composite did not seem to affect the results significantly for compositions above 20 weight percent silicon carbide. It might be suggested, based on equation [2.45] that the change in specific heat with composition may be causing the heating rate differences that were observed. If it were the primary cause of the change in heating rate with composition, changes in the specific heat might

result in a fan of heating rates from 10-50 weight percent silicon carbide. This was not observed, thus implying that the specific heat of the samples is not the primary influence to the observed behavior. However, since the difference in specific heat of silicon carbide and alumina is small, not much of an effect might be observed in any event.* As will be discussed later, the minimal differences in heating rate for 20-50 weight percent silicon carbide composites is thought to be caused by the percolation threshold being crossed between 10 and 20 weight percent silicon carbide.

In any case, even with the low heating profile for the 30 weight percent β-phase silicon carbide composite sample, all samples containing β-phase silicon carbide exhibited higher heating rates than those containing α-phase silicon carbide did. It could be argued that perhaps the difference in heating rates between the two silicon carbide phases could be because the particles are two different sizes. But, phase I does not support this conclusion. In fact, the data indicates that a smaller particle size (the β-phase particles) tends to exhibit a lower heating rate. If the particle size is taken into account, since the β-phase silicon carbide particles were smaller, perhaps the difference in heating rates between the two phases would be even larger.

As in phase I, the composites tested in phase II generally tended to have a linear heating rate, with the exception of the 10 weight percent composites. However, even these composites showed a linear heating rate after reaching a certain temperature. Therefore, the heating rate over all or most of the temperature range could be examined.

---

* The specific heat of aluminum oxide is 0.775 J/(g K), [Lid98], and the specific heat of silicon carbide is 0.67 J/(g K). [Sai00]

These values were calculated and are presented in Table 4.4. These heating rates can then be plotted as a function of weight percent and phase of silicon carbide, as in Figure 5.2. As before, best-fit equations were developed from the heating rate data. For the α-phase silicon carbide composite samples, the heating rate may be estimated by:

$$Rate\left(\frac{^{\circ}C}{\text{min.}}\right) = 0.0103x^3 - 1.1263x^2 + 38.973x - 271.75 \quad \textbf{[5. 4]}$$

And, similarly for the β-phase silicon carbide composites:

$$Rate\left(\frac{^{\circ}C}{\text{min.}}\right) = 0.015x^3 - 1.6381x^2 + 56.048x - 396.8 \quad \textbf{[5. 5]}$$

where x is the weight percent silicon carbide incorporated into the composite sample. Using these equations to calculate the time required to increase the temperature by 600 °C, Table 5.2 is obtained. The β-phase silicon carbide composites heat more rapidly than their α-phase counterparts; however, the models for both silicon carbide phases indicate that beyond a certain point, the heating rates of the composites tend to decrease slightly before increasing again. Unfortunately, the transition to higher heating rates correlating to the percolation threshold could no longer be calculated from the polynomials obtained. In this case, due to the data available, the shape of the curve does not assist in determining the transition. At the low weight percentages involved in the transition (10-25 weight percent silicon carbide) the slope merely gradually decreases, with no point of inflection. Although the fit was quite good in both cases, this is an artifact of the polynomial.

**Major Results From Phase II**

Phase II identified that the composite susceptor samples underwent a reaction that resulted in higher heating rates. As in phase I, as the amount of silicon carbide in the

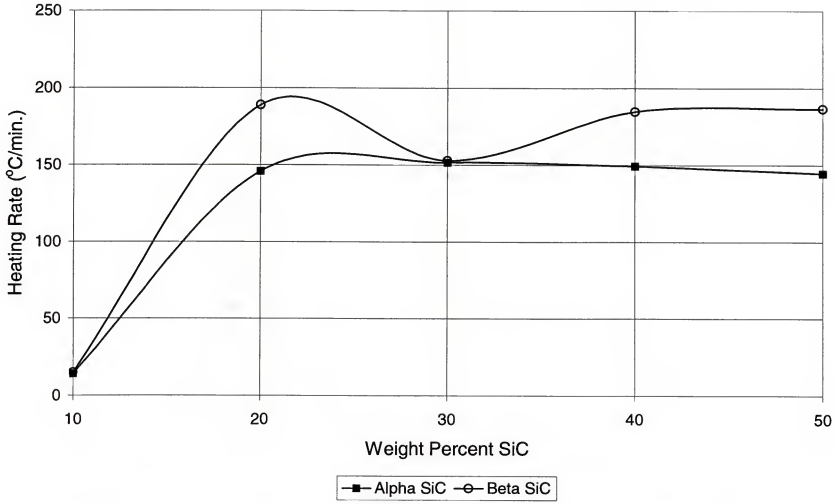


Figure 5.2. Heating rates of α- (2 μm) and β-phase (1 μm) silicon carbide composite samples as a function of weight percent silicon carbide.

Table 5.2. Calculated time (min.) required to raise the temperature of α- and β-phase silicon carbide composites by 600 °C, depending upon sample composition.

| Silicon Carbide Phase | Weight Percent Silicon Carbide | | | |
|---|---|---|---|---|
| | 15 | 25 | 35 | 45 |
| Alpha | 6.4 | 3.8 | 3.9 | 4.3 |
| Beta | 4.8 | 2.8 | 3.0 | 3.4 |

composites increased, the heating rate tended to increase. In addition, these composites again indicated that a percolation threshold had been crossed; however, the percolation threshold had dropped to a lower weight percent (between 10-20 weight percent) silicon carbide. Beta-phase silicon carbide composites tended to heat more rapidly than α-phase silicon carbide composites, even when the particle size was considered. Once again, the heating rates of the composites were measured, and equations were created to predict heating rates. However, the exact percolation threshold could not be calculated for these composites.

**Phase III**

This phase continued to use the same types of silicon carbide as in phase II, but the maximum temperature experienced by the samples and the processing atmosphere were added as variables. A reaction had been evident in phase II, and the influence of the reaction was examined further by heating one set of composite samples to only 600 °C. The addition of atmosphere required a change in the experimental setup, and this change prevented a direct comparison of these results with the previous experiments.

Because the heating behavior did not necessarily remain linear, especially for the composites heated in nitrogen, the ANOVA results had to be examined over specific temperature ranges. By examining the data over small temperature ranges, it could be assumed that the heating over that range approximated linear behavior so that the heating rate could be simply calculated from the slope. The statistical analysis results can also help us to understand some of the effects that occur in the composite samples due to composition or processing that are not obvious through the ANOVA tables or the heating curves presented in Chapter 4.

The statistical analysis also allows the creation of plots based on the information obtained. The four plots in Figure 5.3 of the interaction between the type of silicon carbide and atmosphere of processing help to illustrate some of the effects observed. In all of these interaction plots, it is clear that there is a difference in behavior. The crossing of the lines in Figure 5.3 indicates that there is an interaction between the two factors of type of silicon carbide and processing atmosphere. Dashed lines are used to indicate that no functional relationship exists between the points, since the factor of silicon carbide type is qualitative. The time required to increase the temperature of the composite samples in nitrogen is consistently greater for $\alpha$-phase composites than it is for $\beta$-phase composites. In other words, in a nitrogen atmosphere, the heating rate for $\beta$-phase composite samples is greater than it is for $\alpha$-phase samples. It can also be concluded that in an air atmosphere, the type of silicon carbide in the composite sample is not as important as it is in a nitrogen atmosphere.

In comparison, when examining the plots contained in Figure 5.4, which illustrate the interaction between weight percent of silicon carbide and atmosphere of processing,

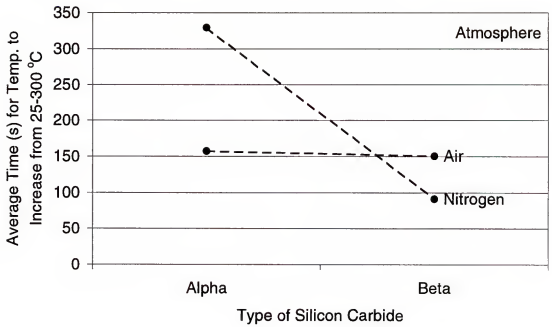


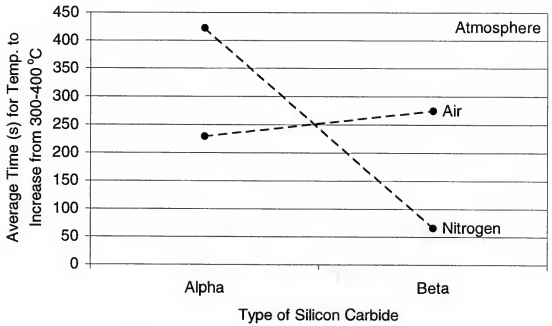


Figure 5.3. Plots of interaction of type of silicon carbide with atmosphere as a function of time (s) for temperature to increase a given amount from statistical data for composite samples heated to only 600 °C.

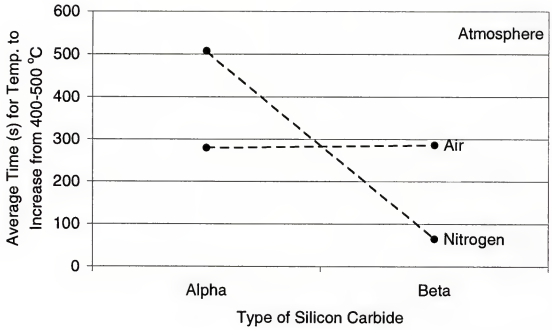


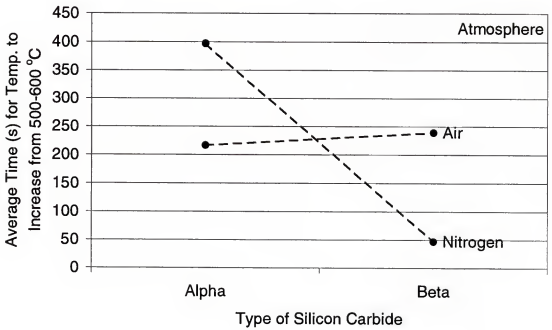


Figure 5.3—continued

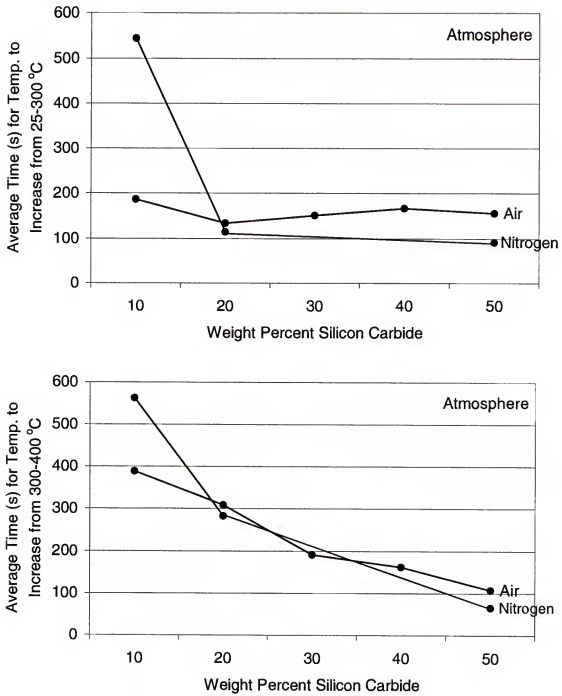


Figure 5.4. Plots of interaction of weight percent of silicon carbide with atmosphere as a function of time (s) for temperature to increase a given amount from statistical data for composite samples heated to only 600 °C.

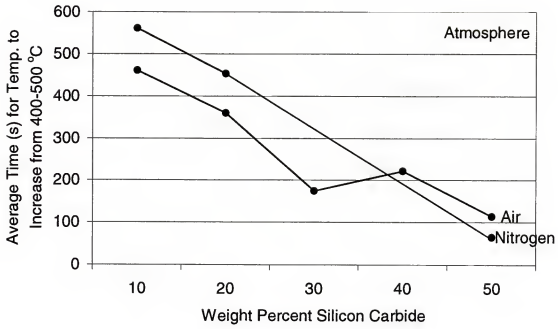


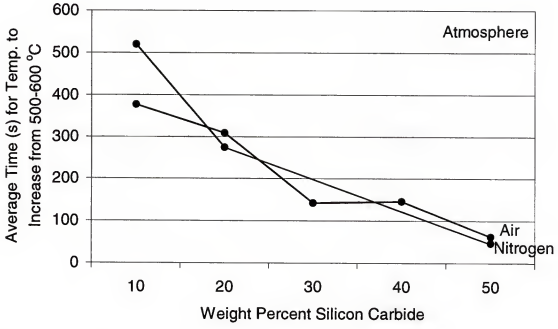


Figure 5.4—continued

the conclusions are a little less distinct. In this case, it may first be noted that points are not plotted for every composition. This is due to the fractional factorial design, where not every combination of conditions was tested. It may be noted that the 10 weight percent silicon carbide composite samples heated in nitrogen took more time to heat; or in other words, the composite samples heated in nitrogen had a lower heating rate than those heated in air. For compositions above 10 weight percent silicon carbide, it can be concluded that the difference between air and nitrogen heated composite samples is much less distinct, and no clear conclusion may be drawn except that an interaction between the two factors does occur.

The graphs in Figure 5.5 show the interaction (or lack thereof) between the type of silicon carbide and the atmosphere of processing for composites heated to 1200 °C. These show that excluding the first temperature regime of 25-300 °C, the β-phase silicon carbide composite samples tended to have either lower heating rates or nearly identical heating rates to the α-phase silicon carbide composites, as is indicated by the positive or flat slopes.

When the responses of all of the samples were combined, Figure 5.6 could be obtained. Figure 5.6 illustrates the interaction between the type of silicon carbide and the atmosphere of processing, and is very similar to Figure 5.3 for the samples heated to only 600 °C. As was evident in the previous experiments of phase II, the β-phase silicon carbide composite susceptor samples tended to heat more quickly than the α-phase composite susceptors. This effect was definitely much more pronounced for the samples heated in nitrogen. Figure 5.7 demonstrates the effects of both atmosphere and maximum temperature on the time required to increase the temperature. In all of these plots, and

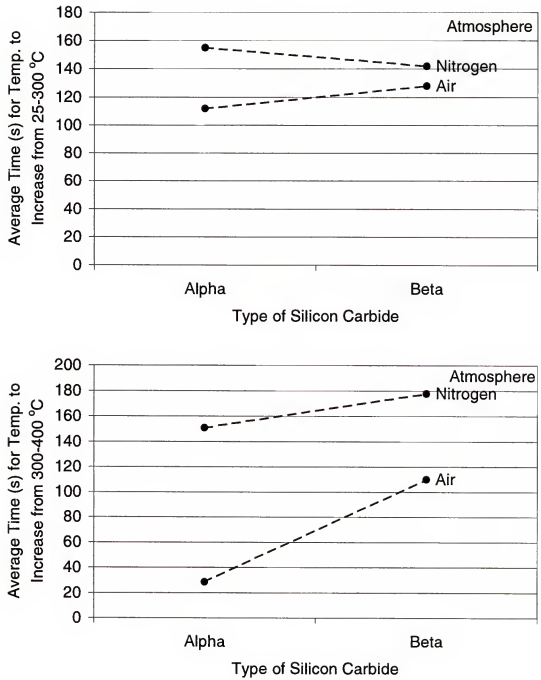


Figure 5.5. Plots of interaction of type of silicon carbide with atmosphere as a function of time (s) for temperature to increase a given amount from statistical data for composite samples heated to 1200 °C.

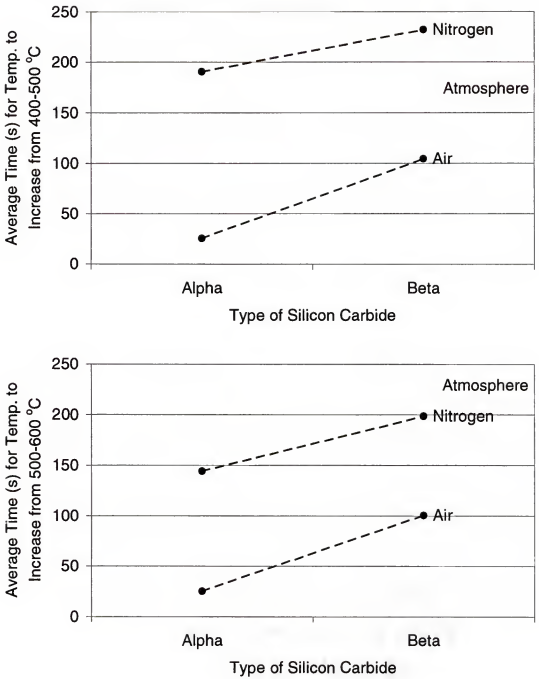


Figure 5.5—continued

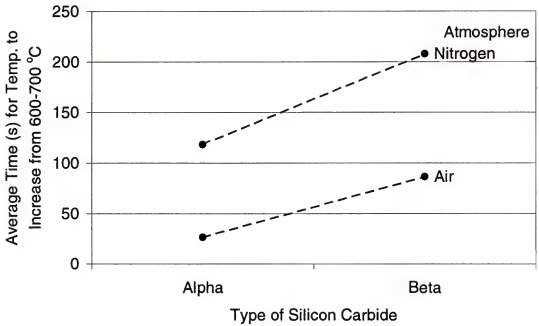


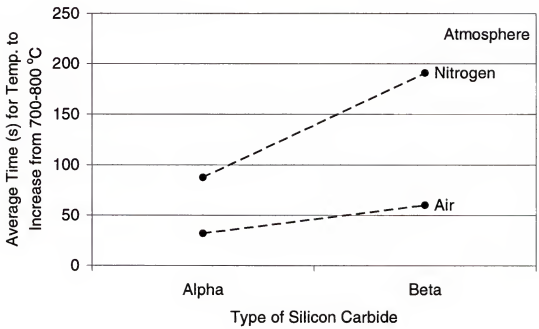


Figure 5.5—continued

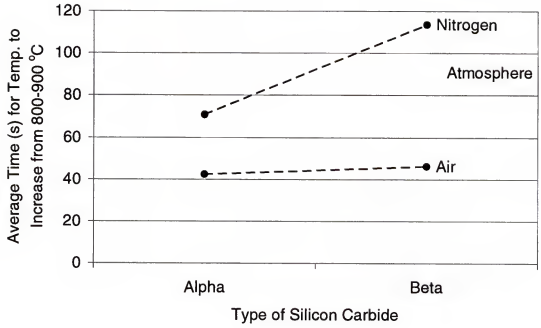


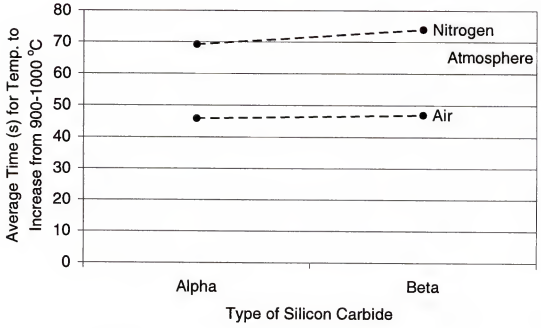


Figure 5.5—continued

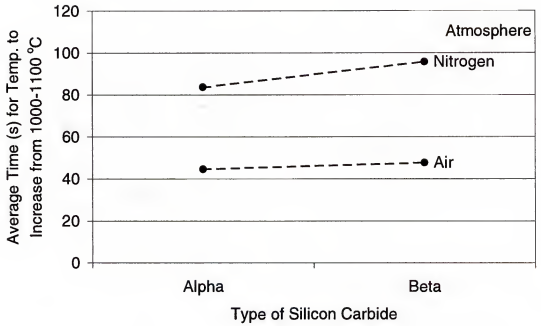


Figure 5.5—continued

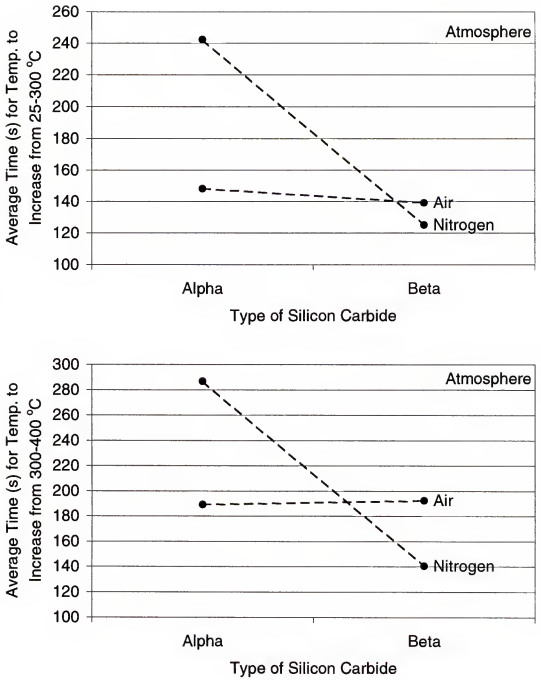


Figure 5.6. Plots of interaction of type of silicon carbide with atmosphere as a function of time (s) for temperature to increase a given amount from statistical data for all composite samples.

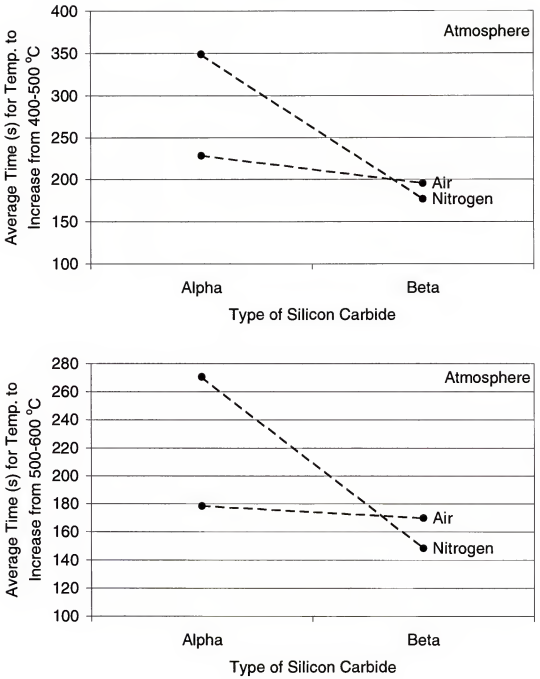


Figure 5.6—continued

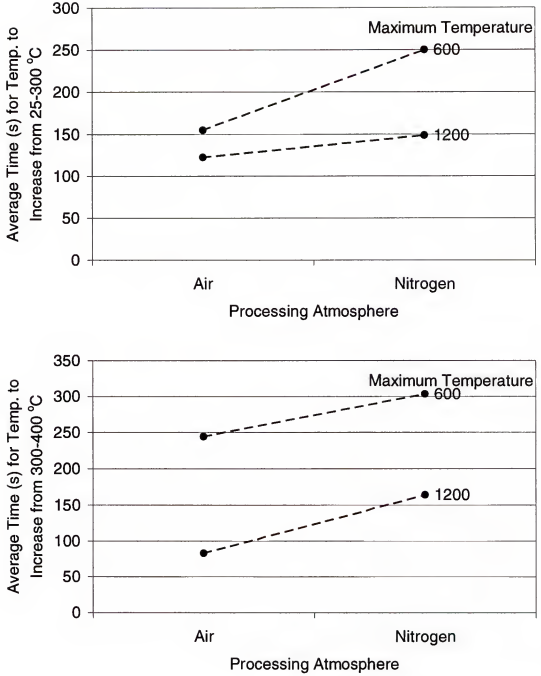


Figure 5.7. Plots of interaction of type of silicon carbide with atmosphere as a function of time (s) for temperature to increase a given amount from statistical data for all composite samples.

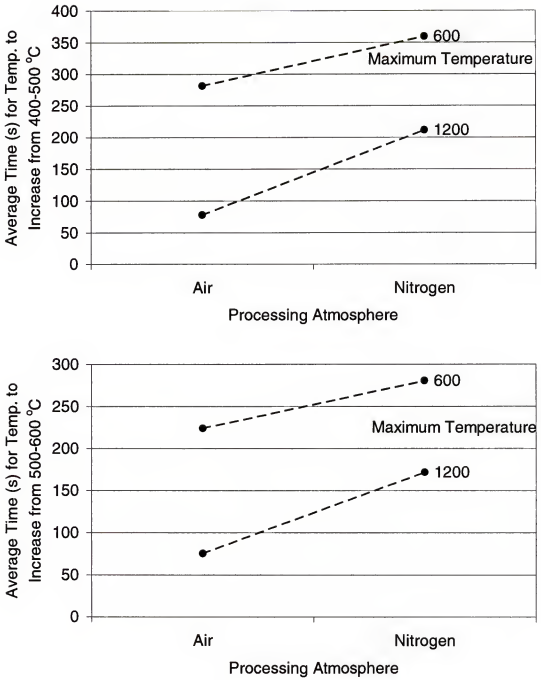


Figure 5.7—continued

therefore over the entire temperature regime from room temperature to 600 °C, the composites heat more quickly in air than in nitrogen, and the composites heated to 1200 °C heat more quickly than those heated to only 600 °C. Figure 5.8 shows the effects of the weight percent and type of silicon carbide on the heating of the composite samples. These graphs illustrate that the α-phase silicon carbide composites generally tend to heat more slowly than the β-phase silicon carbide composites, except at 20 weight percent silicon carbide. In addition, very little difference in heating is observed between the 50 weight percent α- and β-phase silicon carbide composite samples, as the means on all of the plots above 300 °C are essentially identical.

The heating curves and the statistical data clearly confirmed that the reaction that took place above 600 °C affected the heating rates of the composites. It was also found that the reaction did not always occur immediately upon reaching a given temperature. The micrographs helped to identify the reaction that occurred. The micrographs of the composite at low temperature definitely appeared qualitatively different than at high temperature. X-ray spectroscopy of any given sample at high temperature only showed that the material was well mixed, with no indication of what might be causing the abrupt change in heating rate when the composites reached a high enough temperature.

Originally, this was found to be the case as well for the low temperature samples. However, when fracture surfaces of β-phase silicon carbide composite samples heated to only 600 °C were examined, web-like crystal formations were discovered. The same samples that were examined, looking at the cut surfaces showed no trace of these formations. X-ray dotmapping identified the major components in these crystals to be calcium and oxygen. X-ray diffraction was not found to be useful in the identification of

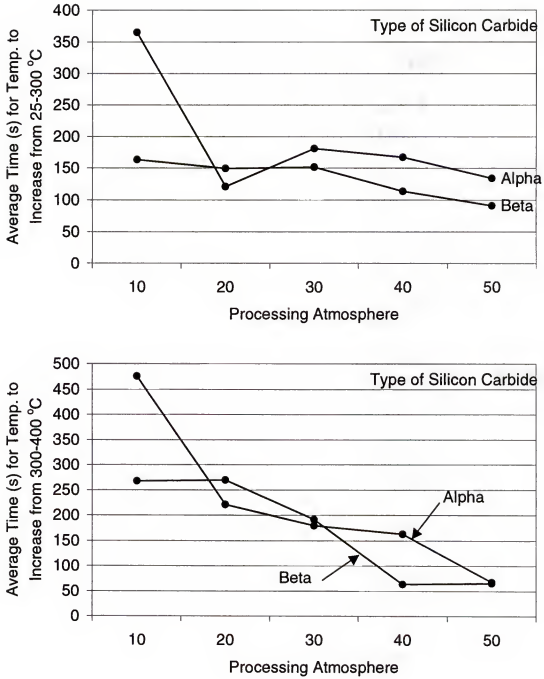


Figure 5.8. Plots of interaction of weight percent of silicon carbide with type of silicon carbide as a function of time (s) for temperature to increase a given amount from statistical data for all composite samples.

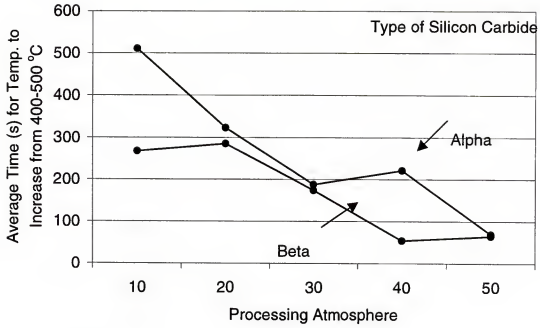


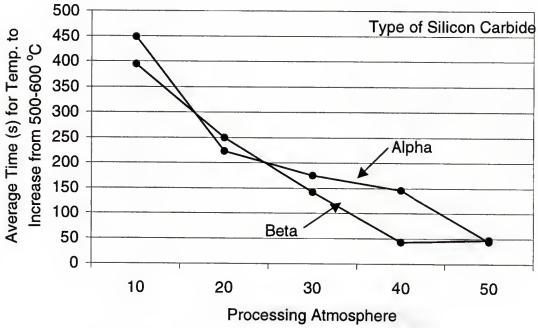


Figure 5.8—continued

the crystals as the amount of this phase present was minimal compared to that of the other phases in the composite. When the information from the x-ray dotmapping was put together with the TGA/DTA data taken in phase IV of the study, it was determined that these crystals are calcium carbonate in the form of calcite. The x-ray dotmap for carbon does not clearly show its presence in the crystals, but it must be considered that the x-ray signal emitted by carbon atoms is often absorbed by elements higher up on the periodic table. Therefore, the carbon signal is most likely merely being obscured by the presence of the other elements in the composite material. The crystals being calcium carbonate also explains why the crystals could not be found on any of the cut surfaces as calcium carbonate is soluble in water [Lid98]. As a result, the cutting process itself would tend to remove these crystals, thus preventing their detection.

That these crystals were not found in the silicon carbide samples heated to 1200 °C supports the calcite crystal identification. The crystallization of calcium carbonate to calcite begins at 370 °C. In addition, calcite decomposition begins in earnest between 600 and 800 °C, with a dependency on atmosphere [Mat95]. The decomposition of calcium carbonate would help to explain the transition above 600 °C. The decomposition of calcite to calcium oxide not only occurs over the right temperature range, but it is not a reversible reaction. It is hypothesized that the calcium oxide formation changes the thermal conductivity of the cement, leading to higher heating rates. The effects of thermal conductivity of the cement on the heating rate will be discussed in more detail later in the chapter.

**Major Results From Phase III**

A fractional factorial statistical design was employed to determine which factors were significant over specific temperature ranges where the heating rates could be considered essentially linear. For composites heated to only 600 °C, an interaction between silicon carbide phase and processing atmosphere is evident. An interaction between weight percent silicon carbide and processing atmosphere was also identified. For samples heated to higher temperature (1200 °C), an interaction between silicon carbide phase and processing atmosphere was no longer apparent. No interaction was found between processing atmosphere and maximum temperature for all of the samples analyzed concurrently; however, heating rates were found to be higher for composites heated in air as well as for composites heated to 1200 °C. An interaction was found between silicon carbide type and weight percent silicon carbide.

Phase III examined the reaction that had been identified in phase II further. Examination of scanning electron micrographs of cross-sections of the composite samples identified a difference in appearance between composites heated to 600 °C and composites heated to 1200 °C. X-ray spectroscopy (EDX) of composites heated to 1200 °C showed that the composites were indeed well-mixed. The EDX together with the TGA/DTA examination of the composites heated to 600 °C identified crystal formations on fracture surfaces that were calcium carbonate.

**Phase IV**

Phase IV examined the same factors as the previous parts of the study, but reduced the particle size further, and had more similar $\alpha$- and $\beta$-phase silicon carbide particle sizes and distributions. The heating rate transition in both air and nitrogen was

pinpointed to begin to occur at approximately 625 °C. The transition was identified in part due to the TGA/DTA data that was obtained. Before attempting to identify the peaks that were found, it was first determined that the peaks were not simply artifacts caused by the combination of the two components of the composites. This was proven by calculating what the DTA curve would be without any interactions between silicon carbide and Alfrax 66. This was done by averaging the data for α-phase silicon carbide and Alfrax 66 that were tested individually in air. The original data can be seen in Figure 4.37, and the calculated 50/50 composite data is presented in Figure 5.9. Therefore, since peaks found for the composite were not observed in the calculated curve, it was concluded that the additional TGA/DTA peaks that were observed for the composite samples must be attributed to interactions between the phases.

The heating rate results in this phase of the study confirmed what had been observed previously. As before, the heating rates of the composite samples tended to increase as greater amounts of silicon carbide particles were incorporated. Composites made with β- rather than α-phase silicon carbide continued to tend to heat more rapidly. This confirmed that the effects seen in phase II were not merely due to the difference in α- and β-phase silicon carbide particle sizes. Percolation effects were observed with the threshold occurring between 10 and 30 weight percent silicon carbide. From the results shown in Figure 4.51 - Figure 4.53 and Figure 4.56 - Figure 4.58, it may be concluded that the reaction was complete in the composite samples heated to 700 °C. The composites heated to 1100 °C behaved similarly to those heated to 700 °C, but the higher temperatures also appeared to affect the heating rate of the materials.

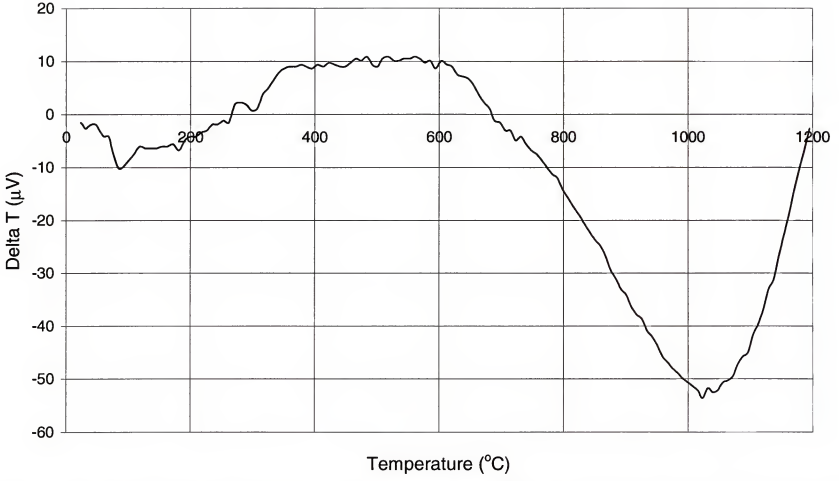


Figure 5.9. Calculated differential thermal analysis curve in air using 100% α-phase silicon carbide and 100% Alfrax 66 curves (see Figure 4.37) to predict the curve for a 50 weight percent silicon carbide/50 weight percent Alfrax 66 composite if no interactions occurred between the phases.

However, contrary to the original premise, the presence of a nitrogen atmosphere did not always assist in attaining higher heating rates. It is clear from comparison of the TGA/DTA results that heating in a nitrogen atmosphere did inhibit oxidation of the silicon carbide. The suppression of silicon carbide oxidation does appear to be beneficial for α-phase silicon carbide composites. At low temperatures, the presence of nitrogen resulted in more rapid heating rates, possibly because it would promote decomposition of the calcium carbonate [Mat95]. On the other hand, it appears that oxygen in the atmosphere, and the corresponding production of glassy phases in the β-silicon carbide composites appears to be beneficial to maintaining rapid high temperature heating rates in the composites. The glassy phase is likely due to the creation of aluminosilicate phases and/or calcium aluminosilicate phases that may promote the preferred transport path. This effect can be clearly observed in Figure 5.10, which presents the interaction of silicon carbide phase and atmosphere as a function of the high temperature heating rate. However, results such as this as well as the statistical data reinforce the idea that the factors that control the heating rate change depending upon the temperature regime of interest.

As in phases I and II, the heating rates for the different weight percents silicon carbide were calculated using information obtained over the entire range of heating. These results could then be plotted to help predict what the heating rates would be for other compositions. The heating rates as a function of weight percent silicon carbide heated to 550, 700, and 1100 °C in air for α- and β-phase silicon carbide composites are presented in Figure 5.11 - Figure 5.13. Similarly, plots of the heating rates for the composites heated in nitrogen are presented in Figure 5.14 - Figure 5.16. A set of best-fit

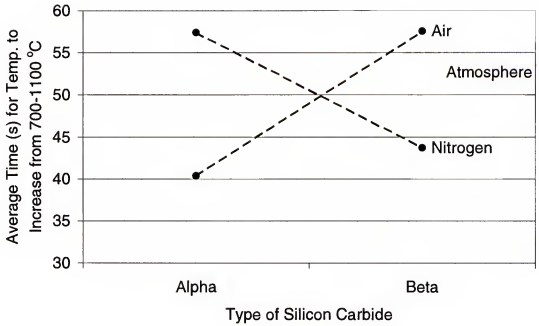


Figure 5.10. Plot of interaction of type of silicon carbide with atmosphere as a function of the heating rate at high temperature. (Silicon carbide from H.C. Starck).

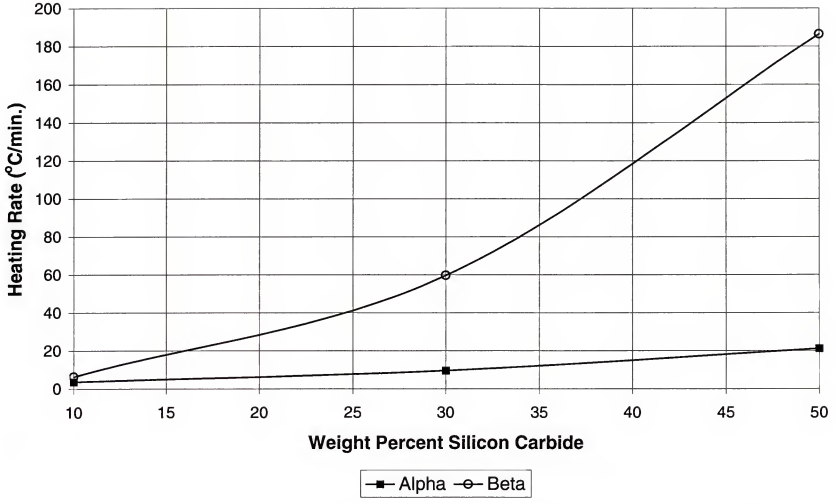


Figure 5.11. Heating rates of α- (0.64 μm) and β-phase (0.68 μm) silicon carbide composite samples as a function of weight percent silicon carbide for composites heated to 550 °C in air.

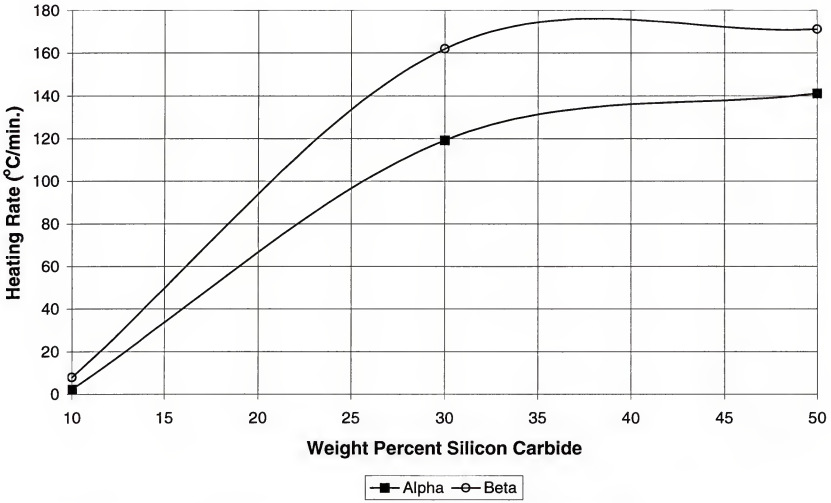


Figure 5.12. Heating rates of α- (0.64 μm) and β-phase (0.68 μm) silicon carbide composite samples as a function of weight percent silicon carbide for composites heated to 700 °C in air.

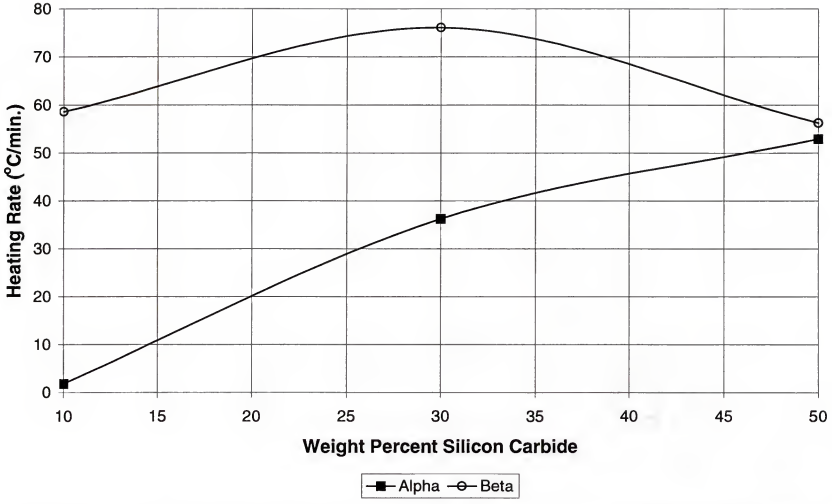


Figure 5.13. Heating rates of α- (0.64 μm) and β-phase (0.68 μm) silicon carbide composite samples as a function of weight percent silicon carbide for composites heated to 1100 °C in air.

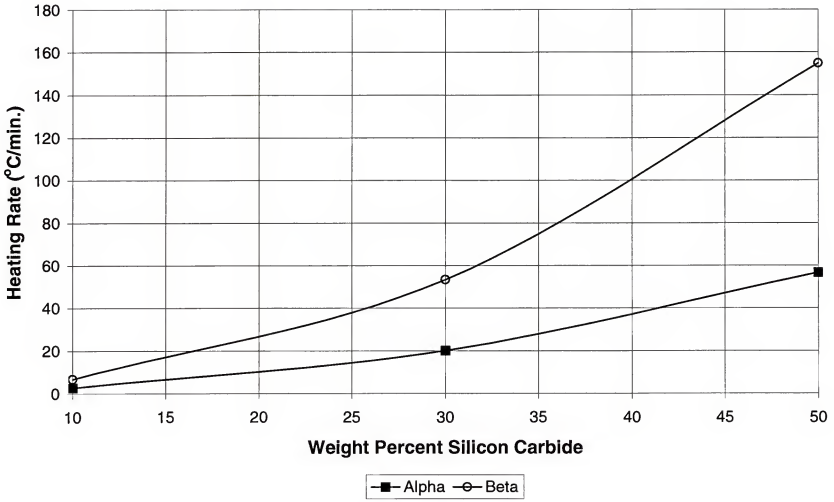


Figure 5.14. Heating rates of α- (0.64 μm) and β-phase (0.68 μm) silicon carbide composite samples as a function of weight percent silicon carbide for composites heated to 550 °C in nitrogen.

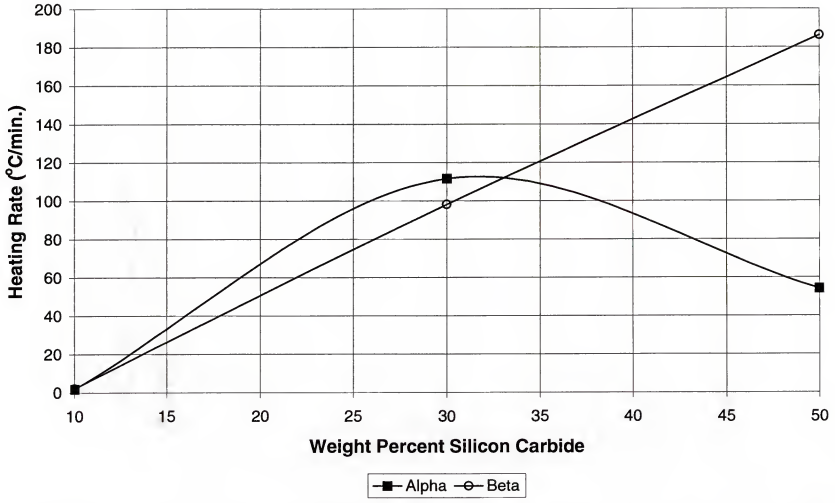


Figure 5.15. Heating rates of α- (0.64 μm) and β-phase (0.68 μm) silicon carbide composite samples as a function of weight percent silicon carbide for composites heated to 700 °C in nitrogen.

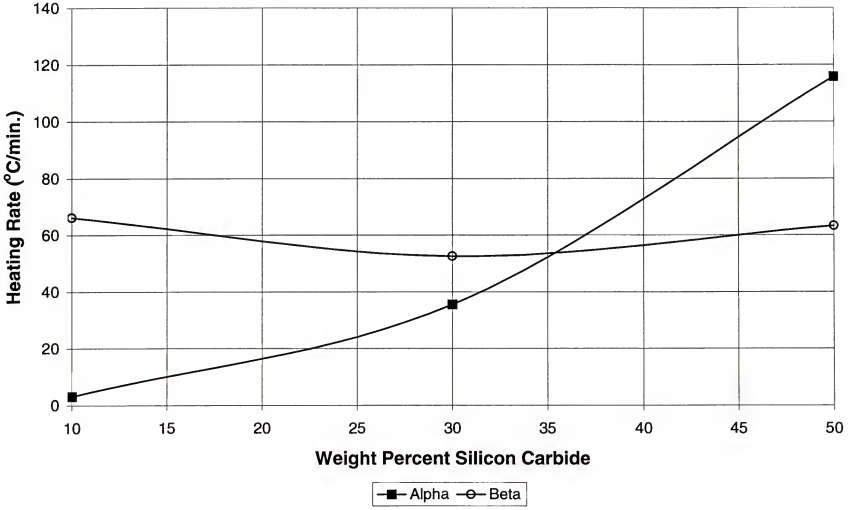


Figure 5.16. Heating rates of α- (0.64 μm) and β-phase (0.68 μm) silicon carbide composite samples as a function of weight percent silicon carbide for composites heated to 1100 °C in nitrogen.

equations was developed so that the heating rates could be predicted given the composition, atmosphere and maximum temperature of processing. These equations are presented in Table 5.3, where x is the weight percent silicon carbide in the composite. Similarly to phase II, the data available prohibited a calculation of the percolation threshold. However, observation of the heating curves in chapter 4 make it clear that the threshold lies between 10 and 30 weight percent silicon carbide for both α- and β-phase silicon carbide composite samples.

**Major Results from Phase IV**

The heating rate transition due to reaction in both air and nitrogen was ascertained to begin at approximately 625 °C. The reaction was ascertained to be complete for the samples heated to 700 °C. TGA/DTA results validated the identification of the crystals found in phase III as calcium carbonate. This phase of the experiment confirmed the results found in previous phases, as the heating rate continued to increase as more silicon carbide was incorporated into the composites, β-phase silicon carbide composites heated

Table 5.3. Calculated heating rate equations of composites as a function of weight percent silicon carbide.

| Processing Atmosphere | Type of Silicon Carbide | Maximum Temperature | $Rate\left(\frac{°C}{min.}\right) =$ | |
|---|---|---|---|---|
| Air | Alpha | 550 | $0.0071x^2 + 0.0132x + 2.7993$ | **[5. 6]** |
| | | 700 | $-0.1188x^2 + 10.601x - 91.901$ | **[5. 7]** |
| | | 1100 | $-0.0222x^2 + 2.6101x - 22.059$ | **[5. 8]** |
| | Beta | 550 | $0.0918x^2 - 1.0048x + 7.2299$ | **[5. 9]** |
| | | 700 | $-0.1812x^2 + 14.952x - 123.43$ | **[5. 10]** |
| | | 1100 | $-0.0466x^2 + 2.7375x + 35.888$ | **[5. 11]** |
| Nitrogen | Alpha | 550 | $0.0238x^2 - 0.0784x + 1.0867$ | **[5. 12]** |
| | | 700 | $-0.2089x^2 + 13.848x - 115.8$ | **[5. 13]** |
| | | 1100 | $0.0598x^2 - 0.7718x + 4.8674$ | **[5. 14]** |
| | Beta | 550 | $0.0683x^2 - 0.3978x + 3.8302$ | **[5. 15]** |
| | | 700 | $-0.0101x^2 + 5.2065x - 48.845$ | **[5. 16]** |
| | | 1100 | $0.0304x^2 - 1.8976x + 82.109$ | **[5. 17]** |

more rapidly than α-phase composites, and percolation effects were observed. The percolation threshold occurred between 10 and 30 weight percent silicon carbide. At high temperature, an interaction between type of silicon carbide and processing atmosphere was evident graphically, although the level of error was too great to determine this statistically. Nitrogen atmospheres tended to produce higher heating rates. However, a nitrogen atmosphere tended to produce lower heating rates at higher temperatures for β-phase silicon carbide composites. From the heating rates, equations describing the predicted heating rates for samples of any composition or processing conditions were determined.

## Specific Issues

During the course of the study, several questions were identified that needed to be answered. First, why is there a difference in heating rate as the silicon carbide particle size is changed? Second, what causes the sudden increase in heating rate as the amount of silicon carbide in the composites is increased, and why is it not observed for the largest silicon carbide particle composites? Third, what is the effect of calcium carbonate? Fourth, how does the processing atmosphere affect the system? These issues will be addressed in the following sections.

### Particle Size Behavior

The first issue that shall be addressed is the cause of the difference in heating rates with silicon carbide particle size. The difference in heating rates for the low silicon carbide content composite samples in Figure 4.3 is dramatic. The large difference in heating rate can be explained by a model that was developed based on this work [Pel00]. The model is based upon heat generation and heat transfer in a composite material where

the particle size of the lossy material is varied while holding the total mass of the lossy phase constant. It describes the behavior of the composites that were studied when particle-particle touching is not a factor. The model developed is nonlinear, preventing an exact solution of the equations. However, by simplifying with several assumptions, an asymptotic theory was developed. The main required assumptions and considerations are as follows [Pel00]:

1. The Biot number, which describes the relative strengths of conduction and convection, is small. Or, in other words, heat conduction is greater than heat convection, which assumption will be true with a well-insulated sample.
2. The samples are well insulated.
3. The thermal contact conductance (between particle and matrix) is small. In other words, the silicon carbide particles are not in perfect thermal contact with the alumina cement. This assumes that heat transfer across a silicon carbide particle is more rapid than heat transfer from a silicon carbide particle to the alumina cement matrix. This should be especially true in a composite such as silicon carbide/alumina cement since porosity and grain boundaries are also factors preventing perfect contact between the particle and the cement.
4. The particles (silicon carbide) are uniformly distributed throughout the matrix (high alumina cement). This was observed to be true by x-ray dotmapping of cross-sections of some of the composite samples.
5. All particles are completely embedded in the matrix. This assumption allows neglect of heat loss from the particles to the atmosphere. Observation of experimental samples shows this to be essentially true.

6. No two particles are in direct contact. This assumption allows neglect of heat transfer from silicon carbide particle to silicon carbide particle.
7. The electric field is known, and has constant amplitude in the cement and in the particles, respectively. This is valid as long as the sample size is smaller than the wavelength of the incident radiation.
8. Changes of the silicon carbide particle radius will not alter the electric field of the particles, and the change in the electric field in the cement should be minute. This should be true for dilute mixtures [Pel00].

Assumptions five and six allow the equations that are developed to be simplified. These assumptions are valid provided that the mixture is sufficiently dilute, so that these heat transfer contributions would be significantly smaller than the contributions from heat loss from the cement to the atmosphere and heat transfer between silicon carbide particles. If the rate of temperature increase is developed from the principles of equations [2.41] and [2.45], then the following equation is obtained:

$$\rho c \frac{\partial T}{\partial t'} = \kappa \nabla'^2 T + \frac{|E|^2}{2} \zeta(T) \quad \textbf{[5. 18]}$$

ρ = Density
c = Specific Heat
T = Temperature
t' = Time
κ = Thermal conductivity (this is a function of temperature, as well)
|E| = Electric field intensity (internal)
ζ(T) = Effective electrical conductivity as a function of temperature

If equation [5.18] is then defined individually for both the cement and the particles of silicon carbide, then the boundary conditions may be defined as follows. Unless otherwise noted, the subscript c refers to the cement, and the subscript p refers to the

properties of any given particle of silicon carbide. First, energy is lost at the surface of the sample by radiative and conductive heat loss, leading to the condition:

$$\kappa_c \frac{\partial T_c}{\partial n'} + h(T_c - T_A) + s\varepsilon(T_c^4 - T_A^4) = 0 \textbf{[5. 19]}$$

n' = The outward unit normal to the surface of the sample
h = Convective heat transfer coefficient
s = Stefan-Boltzmann constant
ε = Emissivity
$T_A$ = Ambient temperature

A similar equation for the energy lost by the silicon carbide particles is not necessary because of assumption five that all of the silicon carbide particles are embedded in the matrix so that the silicon carbide particles only transfer heat to the cement matrix. Next applying the assumption of imperfect thermal contact between the cement and the particles:

$$\kappa_p \frac{\partial T_p}{\partial n_p'} = \kappa_c \frac{\partial T_c}{\partial n_c'} \textbf{[5. 20]}$$

$$\kappa_p \frac{\partial T_p}{\partial n_p'} = -k_p (T_p - T_c) \textbf{[5. 21]}$$

k = thermal contact conductance of each boundary region

To develop a series of equations, dimensionless scaled variables were employed. Then, when the boundary conditions are applied (equations [5.19], [5.20], [5.21]), a series of nonlinear partial differential equations are obtained.* Since these equations cannot be

* For more information on these equations and their derivation, please see [Pel00].

explicitly solved, an asymptotic theory was developed to allow a solution to be calculated by transforming the equations to a series of nonlinear ordinary differential equations. This theory assumes that the power absorbed is of the same order of magnitude as power lost, that convection and radiation are weighted equally, the composite is well insulated, and that it is easier to transport heat through a particle than it is through the particle surface. These assumptions allow the equations to then be reduced to two equations. But first, the scaled parameters must be defined as follows:

$\theta = \dfrac{T_c - T_A}{T_A}$ = Dimensionless cement temperature increase **[5. 22]**

$\phi = \dfrac{T_p - T_A}{T_A}$ = Dimensionless particle temperature increase **[5. 23]**

$\tau = Bt = B\left(\dfrac{\kappa_c t'}{\rho_c c_c L^2}\right)$ = Scaled time variable **[5. 24]**

$B = \dfrac{hL}{\kappa_c}$ = Biot number **[5. 25]**

L = Weighted sample dimension

$p = \dfrac{E_0^2 \sigma_c L}{2hT_A}$ = Non-dimensional power **[5. 26]**

$E_0$ = Reference electric field amplitude (used to scale the electric field to a dimensionless variable)
$\sigma$ = Electrical conductivity

$\beta = \dfrac{B}{B_p}$ **[5. 27]**

$$B_p = \frac{k_p L}{\kappa_p} \textbf{[5. 28]}$$

$$\gamma = \frac{\kappa_c}{\kappa_p} = \text{Relative thermal conductivity } \textbf{[5. 29]}$$

$$\mu = \frac{\rho_p c_p}{\rho_c c_c} = \text{Relative heat capacity } \textbf{[5. 30]}$$

$$\delta = \frac{\sigma_c}{\sigma_p} = \text{Relative electrical conductivity } \textbf{[5. 31]}$$

$$L(\theta) = \theta + R[(\theta + 1)^4 - 1] = \text{Composite length as a function of temperature } \textbf{[5. 32]}$$

$$R = \frac{s\varepsilon T_A^3}{h} = \text{Radiative Biot number } \textbf{[5. 33]}$$

After formulating the equations for temperature evolution in the constituent materials (cement and silicon carbide) and simplification, two equations are obtained:

$$V_c \frac{d\theta_0}{d\tau} = pV_c f(\theta_0) - S_c L(\theta_0) + \frac{\beta S_p}{\gamma}(\phi_0 - \theta_0) \textbf{[5. 34]}$$

and

$$\mu V_p \frac{d\phi_0}{d\tau} = \frac{pV_p \gamma}{\delta} - \beta S_p(\phi_0 - \theta_0) \textbf{[5. 35]}$$

** $\theta_0$ and $\phi_0$ are developed from the assumption of solutions in the form of power-series expansions in the form of:

$$\theta \sim \theta_0 + B\theta_1 + \ldots \qquad \text{and} \qquad \phi \sim \phi_0 + B\phi_1 + \ldots$$

$V_c$ = total volume of the cement
$V_p$ = total volume of all of the particles
$f(\theta_0) = \exp(a\theta_0)$*
$S_c$ = Total surface area of the cement
$S_p$ = Total surface area of all of the particles

Then, if it is assumed that the temperature should be a weighted average of the silicon carbide particle and cement temperatures, using an equation similar to [2.35], where

$$T_{composite} = \frac{V_c\theta_0 + \mu V_p \phi_0}{V_c + \mu V_p} \quad \textbf{[5. 36]}$$

Under steady state conditions, equations [5.34] and [5.35] must both equal zero. This leads to the development of another equation for the mean sample temperature from the combination of equations [5.34], [5.35], and [5.36]:

$$T_{composite} = \theta_0 + \left(\frac{\mu V_p}{V_c + \mu V_p}\right)\left(\frac{pV_p\gamma}{\delta\beta S_p}\right) \quad \textbf{[5. 37]}$$

or

$$T_{composite} = \theta_0 + \left(\frac{\mu V_p}{V_c + \mu V_p}\right)\left(\frac{p\gamma}{3\delta\beta}\right)r \quad \textbf{[5. 38]}$$

where r is the radius of the particle. If equation [5.38] is then plotted as a function of time (remember that $\theta$, and thus $\theta_0$ is a function of time), Figure 5.17 may be obtained [Pel00]. Figure 5.17 appears very similar to the results that were obtained experimentally, such as in Figure 4.3 and Figure 4.4. The model equation [5.38] was

---

* This is based on the assumption that the electrical conductivity of the cement is a strong function of temperature, and is typically exponential. [Pel00, Wes63] The variable "a" is a constant.

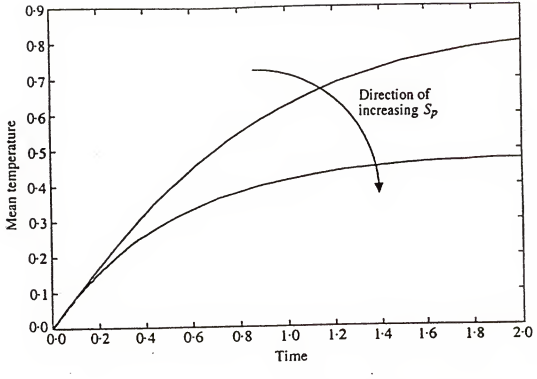


Figure 5.17. Mean composite temperature calculated from equation [5.38] as a function of time as the silicon carbide particle radius, $r_p$, and resulting particle surface area, $S_p$, is varied, assuming that the embedded particles do not touch and the mass fraction is held constant. [Pel00]

found to follow the experimental behavior up until the percolation threshold was crossed. The weight percent silicon carbide leading to crossing the percolation threshold depended on the silicon carbide particle size, as will be discussed later. The model did not explain behavior for any sample above 40 weight percent silicon carbide.

Analysis of the model indicates that if the silicon carbide particle and the cement were in perfect thermal contact, then the variation with regards to the particle diameter would disappear. In the limit of perfect thermal contact, the temperature of the particle ($\phi$) and the temperature of the cement ($\theta$) should be identical. Going back to [5.36], this leads to the conclusion that the temperature of the composite could be calculated simply from the temperature of the cement, which is not dependent on the particle size. To summarize, the model equation [5.38] confirms that the difference in behavior observed between the large and small silicon carbide particles is in essence a geometric effect that is dependent upon the particle size of the silicon carbide. It also suggests that the observed behavior is caused by imperfect thermal contact between the alumina cement and the silicon carbide, indicating that the bonding between the two phases is a critical parameter.

**Percolation Theory**

The model presented in equation [5.38] does help to explain the behavior at low weight percentages of silicon carbide (below the percolation threshold), depending upon silicon carbide particle size. However, it does not explain the changes that occur at higher silicon carbide content for any given particle size. Studies have shown that in a heterogeneous system of a conducting material embedded in an insulator, the dielectric properties depend upon the amount of conducting phase [Lux93]. Many theories tend to

base their description of these properties on the principle that there are no preferred pathways within the material. Unfortunately, the results from this study show that this description is inadequate for the composite under examination.

Percolation theory, however, assumes that the material in question does have preferred transport paths. A schematic illustrating the concept of percolation as the volume fraction is increased is presented in Figure 5.18. In this illustration, a 2-dimensional lattice is randomly filled. When two adjacent sites are occupied, a pathway becomes available between these sites. When a complete pathway is formed from one side to the other, the percolation threshold is crossed. With ten to thirty percent of the available sites are filled, as in Figure 5.18a-c, there is no clear preferred pathway. It can be seen that a complete path is only formed when forty percent of the available sites are filled. However, if the consideration of what constituted adjacent sites were altered to include diagonals, the percolation threshold could be reduced to a lower level. When preferred transport paths do exist (such as in Figure 5.18d), a distinct change will occur. Some properties of the composite will suddenly switch from being more like the properties of the matrix material (alumina cement) to more like the properties of the filler material (silicon carbide particles) when the amount of filler material is increased very slightly. When this transition occurs, it is known as the percolation threshold.

In this study, the primary response of the material that was measured was the temperature increase with time. It is well documented that the heating rate is dependent upon the dielectric properties of the material (see equations [2.42-2.45]). Recent studies have proven that the complex permittivity (see equation [2.20]) is highly dependent upon the amount of conducting filler material in an insulator/conductor composite.

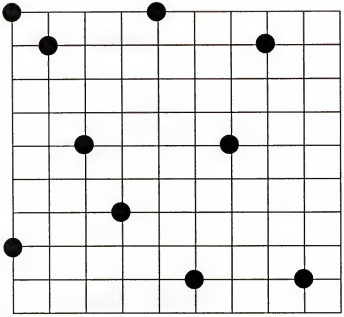

(a). Ten percent of available sites filled.

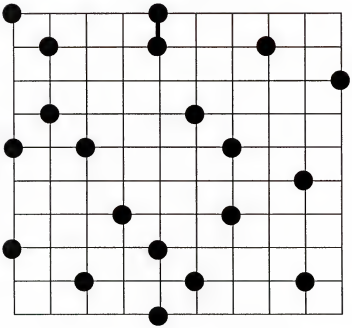

(b). Twenty percent of available sites filled.

Figure 5.18. Illustration of how percolation would occur on a small randomly filled 2-dimensional lattice. A path is available from one site to another when neighboring sites are occupied, as indicated by bold lines. As more of the available sites are filled, eventually (at 40%, part d), a pathway from one side of the lattice to the other is created. The creation of this pathway represents the onset of percolation.

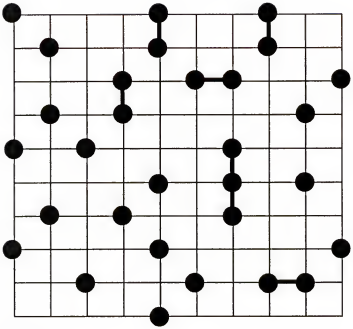

(c). Thirty percent of available sites filled.

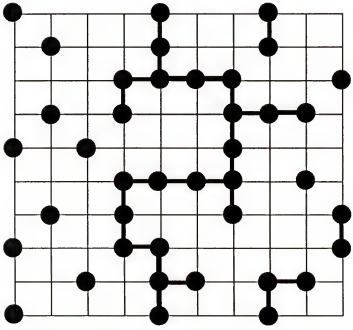

(d). Forty percent of available sites filled.

Figure 5.18—continued

Additionally, these composites which contain amounts of the conducting phase above a given fraction tend to show a frequency dependent imaginary permittivity that tends to be indicative of bulk DC conduction* [You00]. Evidence of bulk DC conduction helps to justify the use of percolation models, many of which have been focused on percolation relating to DC conductivity.

The electrical conductivity is also dependent upon the dielectric properties, as in equations [2.28] and [2.29]. By combining equations [2.44] and [2.45], it is clear that the heating rate is dependent upon the conductivity as well. Many studies have been performed examining percolation and the electrical conductivity of insulator/conductor composites. These have found that the electrical conductivity of insulator/conductor composites undergoes a drastic increase as the percolation threshold is crossed. The increase in conductivity as the volume fraction of conducting phase is increased is shown schematically in Figure 5.19 [You00, Lux93]. In this figure, the percolation threshold would be considered to occur at approximately 0.04 - 0.07 volume fraction conducting phase. Percolation studies such as these on conductivity can be related to the dielectric heating rate. The basic types of proposed percolation models include statistical percolation models, thermodynamic percolation models, geometrical percolation models, and structure-oriented percolation models.

Within the general categories of models, there were two groups. One set of models was designed to predict the electrical conductivity based on percolation theory,

---

* The electrical conductivity is directly related to the imaginary permittivity (dielectric loss factor, $\varepsilon''$) by equation [2.26]. When the imaginary permittivity decreases as frequency increases, this is indicative that
(continued next page)

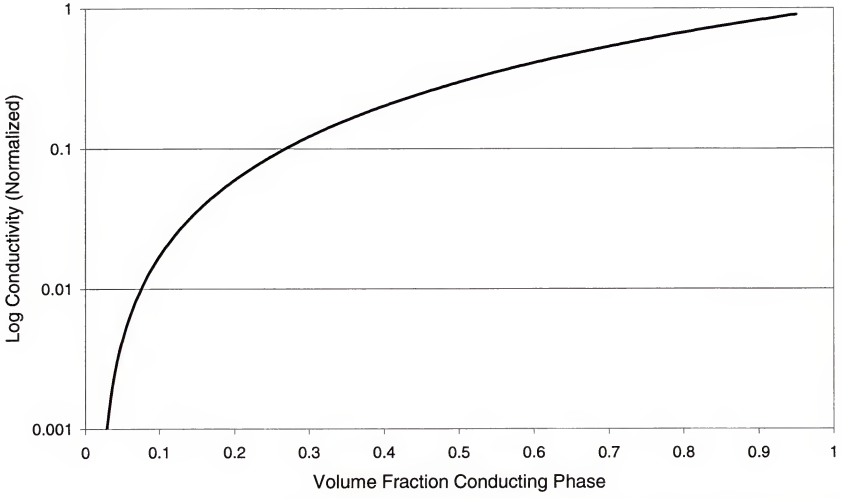


Figure 5.19. Schematic showing how the conductivity of an insulator/conductor composite would increase as the volume fraction of conducting phase is increased when percolation occurs in the composite. [based on data from Lux93]

and the other set was designed to predict the percolation threshold. The models designed to predict the percolation threshold were of particular interest. Since it was clear from the experimental data that the size of the silicon carbide particles altered the location of the percolation threshold, this limited the scope of the models examined further to those that considered the particle size as a factor in the calculation.

After examination of the remaining models, geometric and thermodynamic percolation models were studied in more detail. The geometric models tended to assume that the diameter of the insulating particles was much larger than the diameter of the conducting particles. These models also assumed that the conducting particles would create a thin surface layer surrounding the insulating particles. However, particle size analyses showed that in the silicon carbide/high alumina cement system, this assumption was not true, and that the silicon carbide particles may be either similar in size or larger than the alumina cement particles. Although these models were tested to calculate the percolation threshold, the calculation disagreed with the experimental results by at least 20%. Further calculations determined that the model from the literature that showed the best fit was a thermodynamic percolation model developed by Sumita et al [Lux93].

Sumita and co-workers developed a model based on an interfacial free energy, and the concept that a network will form once the interfacial free energy has reached a level that is independent of the contents of the mixture (the universal free energy). This was also the first attempt to include the effects of interactions between the two phases in

---

the conductivity is not frequency dependent. The electrical conductivity will not be frequency dependent when bulk DC conduction occurs.

the percolation model. According to their model, if the interfacial free energy is low, percolation will occur at higher volume concentrations than if the interfacial free energy is high. Sumita's study focused on an insulating polymer mixed with carbon black particles. The equation that they obtained is as follows:

$$\frac{1-V_c}{V_c} = \frac{3}{g^* R}\left\{\left[\gamma_c + \gamma_p - 2(\gamma_p \gamma_c)^{1/2}\right]\left(1 - e^{-ct/\eta}\right) + K_0 e^{-ct/\eta}\right\} \quad \textbf{[5. 39]}$$

where $V_c$ is the volume percolation concentration, $g^*$ is the universal interfacial free energy, R is the particle radius, $\gamma_c$ is the surface tension of the carbon black, $\gamma_p$ is the surface tension of the polymer, c is a constant of speed for the evolution of the interfacial free energy, t is time of mixing of the two components, $\eta$ is the viscosity of the polymer mixture during the mixing process, and $K_0$ is the interfacial free energy at time zero. These studies found that smaller particles of the carbon black resulted in a lower percolation threshold, consistent with equation [5.39]. This is exactly the behavior that was seen in this study for smaller particles of silicon carbide in alumina cement, as can be seen by comparing Figure 4.2 and Figure 4.53, for example [Lux93].

If it is assumed that for the alumina cement/silicon carbide system the surface tension parameters, the speed of interfacial free energy evolution, time of mixing, viscosity during mixing, and interfacial free energy at time zero are identical, and only the particle diameter changes, then the following equation for the onset of percolation, $V_c$, is obtained:

$$\frac{1-V_c}{V_c} = \frac{1}{AR} \quad \textbf{[5. 40]}$$

where A is a parameter that combines the surface tension, speed of interfacial free energy evolution, time of mixing, and interfacial free energy at time zero. This assumption is an oversimplification, of course, as all of these parameters will not remain the same for every particle size, but it does allow us to obtain a picture of the transition across the percolation threshold, as shown in Figure 5.20 with an arbitrary choice of A=0.01. Figure 5.20 indicates that the results of this model generally follow the trend observed in this study for the behavior of the percolation threshold. It was attempted to estimate a value for A using the calculated value for the percolation threshold in phase I. When this calculation was performed, the percolation thresholds for the 1000 μm and the 1 μm silicon carbide particles were calculated to occur at ~85% and ~0.5% respectively. The calculation for the 1000 μm particles may be correct, as this composition could not be tested, as explained in Chapter 3. Unfortunately, the calculation for the 1 μm particles definitely does not match the experimental data, indicating that perhaps too many assumptions had been made.

However, Sumita's model, for example, assumes that the particles are spherical. This is not the case in most real systems. In addition, crystallization of the matrix is excluded from consideration in the model, as well as new phases forming at the particle/matrix boundaries. The XRD and SEM data suggest that both of these effects occur in the silicon carbide/alumina cement system. Limitations of the model such as these would also help to account for its inability to accurately predict the percolation thresholds that were observed experimentally. It also indicates that factors such as these cannot be neglected in future models. However, it does support the conclusion that the particle size will affect the percolation threshold.

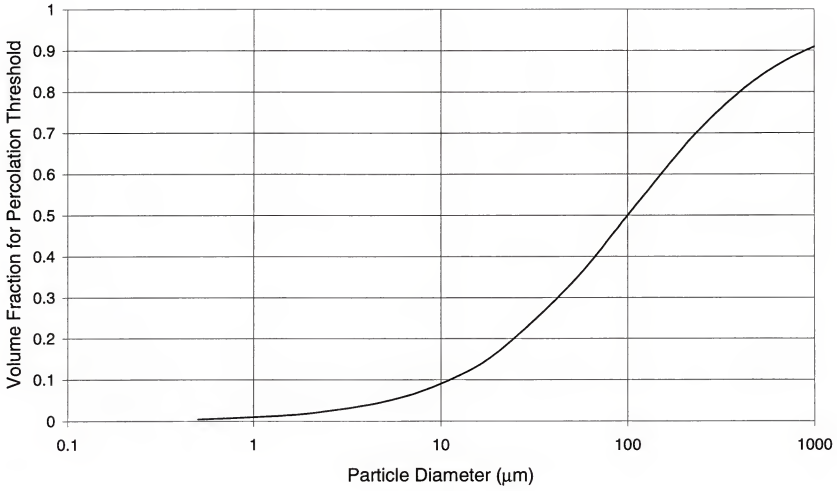


Figure 5.20. Determination of percolation threshold using equation [5.40], and an arbitrary choice of A as 0.01.

To demonstrate the potential importance of particle shape with percolation, calculations were performed estimating the maximum distance attainable between embedded silicon carbide particles in alumina cement. It was assumed that only two particles were present in the composite, and that the composite and particle shapes were identical. This composite could be looked at as only a small piece of a larger whole that contains N particles. The two shapes considered were spherical and cubical, and the locations of the embedded particles in the composite are shown in Figure 5.21. The particle size was also considered, using three of the particle sizes that were employed experimentally, at 1000, 85 and 1 μm particle diameters. The amount of silicon carbide in the composite was set at 10, 20, 30, 40, or 50 weight percent silicon carbide. The volume fraction of silicon carbide was then calculated by

$$V_{f,SiC} = \frac{V_{SiC}}{V_{composite}} = \frac{m_{f,SiC} / \rho_{SiC}}{\frac{m_{f,SiC}}{\rho_{SiC}} + \frac{1 - m_{f,SiC}}{\rho_{cement}}} \quad \textbf{[5. 41]}$$

where $V_{f,\,SiC}$ is the volume fraction of silicon carbide, $V_{SiC}$ is the total volume of the silicon carbide, $V_{composite}$ is the total volume of the composite, $m_{f,\,SiC}$* is the mass fraction of silicon carbide, and $\rho_{SiC}$ and $\rho_{cement}$ are the densities of the silicon carbide and the cement, respectively. When experimental densities of the composite are used, the volume fraction of silicon carbide was found by:

---

* The mass fraction silicon carbide can be simply calculated from the weight percent silicon carbide by dividing by 100.

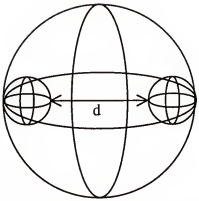


a. Spherical composite containing two particles.

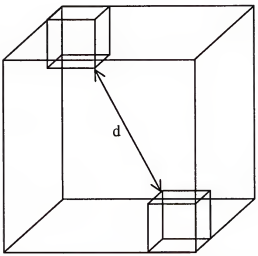


b. Cubical composite containing two particles.

Figure 5.21. Conditions used for determining nearest neighbor distances as a function of volume percent silicon carbide. The volume fraction occupied by the smaller particles remains constant. The particle separation, d, used for the calculations is denoted as well.

$$V_{f,SiC} = \frac{V_{SiC}}{V_{composite}} = \frac{m_{f,SiC} \Big/ \rho_{SiC}}{1 \Big/ \rho_{composite}} = \frac{m_{f,SiC}\rho_{composite}}{\rho_{SiC}} \quad \textbf{[5. 42]}$$

The size of the overall composite was allowed to vary, and this could be calculated from the combination of particle size and volume fraction of particles. Because of the assumptions made about the geometry of the material, negative numbers were calculated in some cases for larger volume fractions of silicon carbide. The negative numbers only meant that the particles would definitely be touching, and these numbers were changed to zero.

Table 5.4 and Table 5.5 use these geometric models to show the calculated differences in the maximum distance between particles as a function of weight percent and particle size of silicon carbide using the theoretical densities of alumina (3.965 g/cm$^3$) and silicon carbide (3.217 g/cm$^3$). These calculations help to illustrate the importance of particle morphology on only geometric considerations of the percolation threshold. However, the real system is not a perfect 100% dense mixture of alumina and silicon carbide. In the real system, porosity is likely also a factor. Therefore, a second set of calculations was performed using the experimentally measured densities of the composites in phase IV, and these are presented in Table 5.6 and Table 5.7. The experimental densities were calculated from measurements of the bulk densities taken from all of the samples tested in phase IV. These average densities were then used to set up a simple equation for the density for any mass fraction of silicon carbide given by:

$$\rho_{composite}\left(\frac{g}{cm^3}\right) = 0.9 * m_{f,SiC} + 2.2 \quad \textbf{[5. 43]}$$

Table 5.4. Particle separation distance between two spherical particles of silicon carbide in a spherical composite using theoretical densities.

| 2 Spherical Particles | | |
|---|---|---|
| Weight Percent SiC | Particle Radius (μm) | Particle Separation Distance (μm) |
| 10 | 1000 | 1106 |
| | 85 | 94.02 |
| | 1 | 1.106 |
| 20 | 1000 | 82.81 |
| | 85 | 7.039 |
| | 1 | 0.08281 |
| 30 | 1000 | 0 |
| | 85 | 0 |
| | 1 | 0 |
| 40 | 1000 | 0 |
| | 85 | 0 |
| | 1 | 0 |
| 50 | 1000 | 0 |
| | 85 | 0 |
| | 1 | 0 |

Table 5.5. Particle separation distance between two cubical particles of silicon carbide in a cubical composite using theoretical densities.

| 2 Cubical Particles | | |
|---|---|---|
| Weight Percent SiC | Particle Radius (μm) | Particle Separation Distance (μm) |
| 10 | 1000 | 2044 |
| | 85 | 173.7 |
| | 1 | 2.044 |
| 20 | 1000 | 1371 |
| | 85 | 116.5 |
| | 1 | 1.371 |
| 30 | 1000 | 1048 |
| | 85 | 89.08 |
| | 1 | 1.048 |
| 40 | 1000 | 847.0 |
| | 85 | 72.00 |
| | 1 | 0.8470 |
| 50 | 1000 | 706.0 |
| | 85 | 60.01 |
| | 1 | 0.7060 |

Table 5.6. Particle separation distance between two spherical particles of silicon carbide in a spherical composite using experimental densities.

| 2 Spherical Particles | | |
|---|---|---|
| Weight Percent SiC | Particle Radius (μm) | Particle Separation Distance (μm) |
| 10 | 1000 | 2248 |
| | 85 | 191.1 |
| | 1 | 2.248 |
| 20 | 1000 | 1031 |
| | 85 | 87.71 |
| | 1 | 1.031 |
| 30 | 1000 | 463.0 |
| | 85 | 39.36 |
| | 1 | 0.4630 |
| 40 | 1000 | 120.0 |
| | 85 | 10.20 |
| | 1 | 0.1200 |
| 50 | 1000 | 0 |
| | 85 | 0 |
| | 1 | 0 |

Table 5.7. Particle separation distance between two cubical particles of silicon carbide in a cubical composite using experimental densities.

| 2 Cubical Particles | | |
|---|---|---|
| Weight Percent SiC | Particle Radius (μm) | Particle Separation Distance (μm) |
| 10 | 1000 | 2796 |
| | 85 | 237.6 |
| | 1 | 2.796 |
| 20 | 1000 | 1995 |
| | 85 | 169.6 |
| | 1 | 1.995 |
| 30 | 1000 | 1621 |
| | 85 | 137.8 |
| | 1 | 1.621 |
| 40 | 1000 | 1395 |
| | 85 | 118.6 |
| | 1 | 1.395 |
| 50 | 1000 | 1243 |
| | 85 | 105.7 |
| | 1 | 1.243 |

The silicon carbide particles themselves were still assumed to be 100% dense. The separation distances were then calculated by the following set of equations:

Two Spherical Particles: $$d = 2*\left(\frac{2r^3}{V_{f,SiC}}\right)^{1/3} - 4r \quad \textbf{[5. 44]}$$

Two Cubical Particles: $$d = \left[\sqrt{3}*\left\{\left(\frac{2x^3}{V_{f,SiC}}\right)^{1/3} - x\right\}^2\right]^{1/2} \quad \textbf{[5. 45]}$$

where d is the particle separation, r is the silicon carbide particle diameter, and x is the length of one side of a cubical silicon carbide particle.

Some conclusions may be made based upon these calculations. First, that the choice of particle shape alters the calculated particle separation. The spherical shape and the cubical shape give very different values for the particle separation distance. Second, that generally, as the particle size is decreased, the particle separation distance also decreases. This conclusion could then be applied to a composite containing N particles, and implies that as more particles are included in the system, the particle separation distance decreases. Third, assuming that porosity has a negative effect on the transport mechanisms in the material, the large differences in these calculations using experimental density rather than theoretical density indicate that porosity may be an important, but often neglected parameter.

Unfortunately, data such as this illustrate some of the difficulties in accurately predicting the percolation threshold, and shows why current models are only qualitatively informative. Most models assume that percolation is independent of particle shape and size. The results of this study emphasize that this assumption is not accurate in a real

system, and that an accurate model of this system must include particle shape, size and porosity.

**Other Issues**

The issues of the effects of calcium carbonate and of atmosphere will be addressed concurrently as there is some interaction between them. Crystals of calcium carbonate crystals were found in scanning electron micrographs of the silicon carbide/alumina cement composite samples that had been heated only to low temperature, and were not found in composites heated to higher temperatures. The disappearance of the crystals was attributed to the pyrolysis of calcium carbonate to calcium oxide. The pyrolysis of calcium oxide has been found to occur at lower temperatures in a nitrogen atmosphere. The change in temperature with atmosphere has been attributed to the reduction or elimination of carbon dioxide gas. When the level of carbon dioxide in the oven is reduced, this leads to a greater driving force towards the evolution of carbon dioxide from the calcium carbonate, dropping the pyrolysis reaction to a lower temperature [Mat95].

However, the atmosphere dependence of the pyrolysis temperature of calcium carbonate is only part of the issue. The other question is why the pyrolysis of calcium carbonate leads to more rapid heating rates in the composite. This question will be examined by using the model relating to the silicon carbide particle size, where equation [5.38] demonstrated the change in heating rate with particle size.

A variety of parameters make up this equation in addition to the size of the silicon carbide particle, including the thermal conductivity of the cement. The pyrolysis of calcium carbonate crystals found within the composite is believed to cause an increase in

the heating rate. The thermal conductivity of calcium carbonate is quite low at only ~1 W/m-K. On the other hand, the thermal conductivity of calcium oxide is significantly higher at 16 W/m-K [Lid98]. If equations [5.27] and [5.25] are inserted into equation [5.38], it may be seen that

$$T_{composite} \propto \kappa_c \quad \textbf{[5. 46]}$$

From the thermal conductivity information, it is suggested that the decomposition of calcium carbonate should increase the thermal conductivity of the cement. According to equation [5.46], increasing the thermal conductivity of the cement is equivalent to increasing the temperature of the composite at a given time. Therefore, an increase in thermal conductivity of the cement results in an increase in the heating rate of the composite.

Another effect that was observed experimentally was the difference in heating rate between α- and β-phase silicon carbide composites. The β-phase silicon carbide composites tended to exhibit consistently higher heating rates than α-phase silicon carbide composites. It is not yet absolutely known what is the source of this difference, but some potential causes may be postulated. The two phases have different crystal structures, which will exhibit different properties. Therefore, the dielectric loss factor of β-phase silicon carbide may be greater than α-phase silicon carbide. This is supported in part by the difference in the room temperature mobility of the electrons, which is 4000 $cm^2/V\text{-}s$ for β-phase silicon carbide, and is 400 $cm^2/V\text{-}s$ for α-phase silicon carbide [Lid98]. In addition to this, the β-phase is not truly stable at room temperature, and thus will have a higher free energy than the α-phase. It is possible that in an effort to reduce

the free energy, β-phase silicon carbide particles will bond more strongly to the alumina cement, and thus improve the thermal contact conductance.

# CHAPTER 6
# SUMMARY AND CONCLUSIONS

Before beginning this study, it was known that the susceptor composite of silicon carbide/high alumina cement was very useful for microwave processing other materials. By using this composite for microwave hybrid heating, both ordinary and unique materials have the potential to be fabricated. The use of a susceptor such as this one can help to produce a more even temperature distribution across a material being microwave heated. This composite of silicon carbide particles embedded in high alumina cement only needed to be better characterized to enhance its applicability to more systems. This goal was accomplished in this study.

Chapter 1 introduced the goal of the study and the parameters of interest. Chapter 2 gave background material on microwave theory and types of microwave behavior. Chapter 3 discussed the experimental procedures used throughout the study, as well as important issues regarding any equipment that was used to obtain information. Chapter 4 presented the results of each phase of the study. Chapter 5 examined these results further, as well as modeling and explaining the behavior that was observed.

During the course of the study, the factors affecting the heating rate of the composites were identified. These factors included the silicon carbide particle size, the weight percent silicon carbide in the composite, the silicon carbide phase, the processing atmosphere, and the maximum temperature experienced by the composite. In addition to

these parameters regarding fabrication and treatment of the composite, it was found that insulation and placement of the composite in the microwave needed to be controlled to obtain reproducible results. Preventing arcing between the sample and the thermocouple was also an important consideration.

Statistical design was employed to determine the significance of the factors of interest, which included silicon carbide particle size, silicon carbide phase, amount of silicon carbide in the composite, processing atmosphere, and maximum temperature experienced by the composite. Each of these factors was found to be significant, although some were found significant only in combination with other factors. Therefore, none of the factors could be excluded from examination, as they all played some role in the microwave heating behavior of the composites, which in some cases was primarily an interaction effect. The factors were each significant over specific temperature ranges, and which factors were significant tended to change depending upon the temperature range of concern.

The amount of silicon carbide in the composite was definitely found to be a significant factor affect the heating rates of the composites over a wide range of temperature. One of the goals of this research was to be able to better predict the heating rate of these susceptors, so that better choices could be made when they are used for processing of other materials. Therefore, equations were created that predict the heating rate of the composite samples, depending upon sample composition and heating conditions.

As the weight percent silicon carbide in the composite was increased, at one point a dramatic increase in the heating rate was found as the silicon carbide content was

slightly increased. This was explained by percolation theory, which suggests the presence of a preferred pathway in the composite. The dielectric properties of a material are dependent upon the electrical conductivity, which in conductor/insulator composites has been found to be affected by preferred transport pathways in the material. The percolation threshold, which is identified by the volume fraction of conducting phase where a preferred pathway first becomes available, is dependent upon the silicon carbide particle size, and this was found experimentally. As the silicon carbide particle size is reduced, the interfacial free energy of the particles will increase and the particle separation distance will decrease. The distance between particles was examined, as it is related to the percolation threshold. It was determined that the geometry of the particles and the composites definitely affects the calculated distance between particles, indicating that particle size and shape assumed in a percolation model is of vital importance. The porosity (and consequently density) of the composite also directly affects the distance between particles, and thus is likely to shift the percolation threshold.

However, weight percent silicon carbide was not the only factor that was important, as silicon carbide particle size was found to alter the heating rate of the composites, especially at lower weight percent silicon carbide. Therefore, this behavior was mathematically modeled. The model was consistent with experimental results, and it suggests that bonding between the silicon carbide particle and the alumina cement is critical towards determining the heating rate of the composite. It also found that if the mass fraction of silicon carbide was held constant while the particle size was reduced that the heating rate of the composite would also decrease, resembling experimental results.

In addition, a reaction in the composites was identified. This reaction resulted in higher heating rates being observed. Using SEM, x-ray dotmapping, and TGA/DTA, the reaction was identified as the pyrolysis of calcium carbonate to form calcium oxide. Studies have shown that this reaction may occur at lower temperatures in a nitrogen atmosphere due to lack of carbon dioxide. In the microwave, the heating rate increase attributed to the formation of calcium oxide was found to begin in both air and nitrogen atmospheres at approximately 625 °C, and was complete by 700 °C. A hypothesis as to the cause of the heating rate increase with the formation of calcium carbonate was postulated.

The major findings of this study into the microwave behavior of silicon carbide/high alumina cement are discussed in detail in the preceding chapters and are summarized here.

1. Silicon carbide/high alumina cement composites can be tailored to provide a wide range of heating rates.
2. As the amount of silicon carbide in the composite increased, the heating rate tended to increase. The effects observed were explained by a combination of dielectric mixing equations, a heat transfer model and percolation theory.
3. The silicon carbide particle size had a definite effect on the heating rate of the composites. Mathematical modeling of this behavior showed that the particle size effect was due to imperfect thermal contact between the silicon carbide particle and the cement matrix. As the silicon carbide particle size was reduced, the percolation threshold was also reduced to a lower silicon carbide volume fraction due to changes in the particle separation distance. For composites that were below the percolation

threshold, as the silicon carbide particle size was reduced, the heating rate was also reduced when the total amount of silicon carbide was held constant.

4. A significant increase in the heating rates of the composites was attributed to the pyrolysis of calcium carbonate to form calcium oxide. This increase is credited to the increase in thermal conductivity as calcium oxide is produced from calcium carbonate. According to the mathematical model, an increase in thermal conductivity of the cement matrix results in an increase in the heating rate of the composite.
5. A nitrogen processing atmosphere tended to result in higher composite heating rates than an air atmosphere, most likely due to the suppression of oxidation of silicon carbide.
6. Beta-phase silicon carbide composites tended to heat more rapidly than alpha-phase silicon carbide composites. This could not yet be verified by statistics, but was observed in the experiments. This difference cannot yet be definitely explained, but it does illustrate the importance of structure on the dielectric heating of the composites.

# CHAPTER 7
# SUGGESTIONS FOR FUTURE WORK

This is the first study on composites used for microwave hybrid heating. The system of silicon carbide/high alumina cement composite susceptors was determined to be more complicated than might be thought at first glance. Unfortunately, this meant that not every avenue could be pursued in this study, and some of these areas are presented here.

Some of the results of this study need to be examined in further detail. Some of the parameters that require further examination include particle size distribution, particle purity, and a more in-depth study of atmosphere and silicon carbide phase. With more experiments, the true difference between $\alpha$- and $\beta$-phase silicon carbide could be determined. Also, with more statistical design and analysis, equations containing more of the essential parameters could be developed. In addition to further dissection of the results obtained in this study, it is thought that the reactions occurring in the microwave may be shifted to lower temperature, or may be entirely different than in a conventional furnace. Therefore, it has been proposed to study composites heated in a conventional furnace in a similar manner, then comparing microstructures. Additionally, composites that have been heated to higher temperature conventionally could be heated in the microwave to determine if the same heating rates are obtained as for composites that have only been microwave heated.

## REFERENCES


[Ahm88] Iftikhar Ahmad, G. T. Chandler and D. E. Clark, "Processing of Superconducting Ceramics Using Microwave Energy," in Microwave Processing of Materials, (eds. W. H. Sutton, M. H. Brooks, and I. J. Chabinsky), Materials Research Society Symposium Proceedings, Vol. 124, Materials Research Society, Pittsburgh, pp. 239-245 (1988).

[Ahm91] Iftikhar Ahmad and David E. Clark, "Effect of Microwave Heating on Solid State Reactions of Ceramics," in Microwaves: Theory and Application in Materials Processing, (eds., D. E. Clark, F. D. Gac, and W. H. Sutton), Ceramic Transactions, Vol. 21, American Ceramic Society, Westerville, OH, pp. 605-612 (1991).

[Ahm92] Iftikhar Ahmad, Richard Silberglitt, W. Murray Black, Hussamaldin S. Sa'Adaldin and Joel D. Katz, "Microwave Joining of Silicon Carbide Using Several Different Approaches," in Microwave Processing of Materials III, (eds. R. L. Beatty, W. H. Sutton, and M. F. Iskander), Materials Research Society Symposium Proceedings, Vol.269, Materials Research Society, Pittsburgh, pp. 271-276 (1992).

[Al-A91] Salwan Al-Assafi, Iftikhar Ahmad, Zakaryae Fathi, and David E. Clark, "Microwave Joining of Ceramics," in Microwaves: Theory and Application in Materials Processing, (eds., D. E. Clark, F. D. Gac, and W. H. Sutton), Ceramic Transactions, Vol. 21, American Ceramic Society, Westerville, OH, pp. 515-521 (1991).

[Al-A92] Salwan Al-Assafi and David E. Clark, "Microwave Joining of Ceramics: A Study on Joining Alumina Both Directly and with Alumina Gel," in Microwave Processing of Materials III, (eds. R. L. Beatty, W. H. Sutton, and M. F. Iskander), Materials Research Society Symposium Proceedings, Vol.269, Materials Research Society, Pittsburgh, pp. 335-340 (1992).

[And91] Octavio M. Andrade, "Microwave Industrial, Scientific and Medical Applications in Brazil," in Microwave Processing of Materials II (eds. W. B. Snyder, Jr., W. H. Sutton, M. F. Iskander and D. L. Johnson) Materials Research Society Symposium Proceedings, Vol. 189, Materials Research Society, Pittsburgh, pp. 27-38 (1991).

[And92] Octavio M. Andrade, Magdy F. Iskander, and Shane Bringhurst, "High Temperature Broadband Dielectric Properties Measurement Techniques," in Microwave Processing of Materials III, (eds. R. L. Beatty, W. H. Sutton, and M. F. Iskander), Materials Research Society Symposium Proceedings, Vol.269, Materials Research Society, Pittsburgh, pp. 527-539 (1992).

[Ara93] M. Arai, J. G. P. Binner, G. E. Carr, and T. E. Cross, "High Temperature Dielectric Property Measurements of Engineering Ceramics," in Microwaves: Theory and Application in Materials Processing II, (eds. D. E. Clark, W. R. Tinga, and J. R. Laia, Jr.), Ceramic Transactions, Vol. 36, American Ceramic Society, Westerville, OH, pp. 483-492 (1993).

[ASM91] ASM International Handbook Committee, Engineered Materials Handbook, Volume 4: Ceramics and Glasses, ASM International, USA, 1991.

[Ato98] Duangduen Atong and D. E. Clark, "Synthesis of TiC-$Al_2O_3$ Composites Using Microwave-Induced Self-Propagating High Temperature Synthesis," Ceramic Engineering and Science Proceedings, Vol. 19, no. 4, pp. 415-421 (1998).

[Bar95] W. R. Barron, "Principles of Infrared Thermometry," The Temperature Handbook, Omega Engineering, Stamford, pp. Z-49-Z-52 (1995).

[Bat95] J. Batt, J. G. P. Binner, T. E. Cross, N. R. Greenacre, M. G. Hamlyn, R. M. Hutcheon, W. H. Sutton, and C. M. Weil, "A Parallel Measurement Programme in High Temperature Dielectric Property Measurements: An Update," in Microwaves: Theory and Application in Materials Processing III, (eds. D. E. Clark, D. C. Folz, S. J. Oda, and R. Silberglitt), Ceramic Transactions, Vol. 59, American Ceramic Society, Westerville, OH, pp. 243-250 (1995).

[Bec00a] Beckman Coulter, Inc., "COULTER LS Series Laser Diffraction Particle Size Analyzers," http://www.beckmancoulter.com/coulter/PC/SS000096.asp, October 6, 2000.

[Bec00b] Beckman Coulter, Inc., "Enhanced Laser Diffraction," http://www.beckmancoulter.com/coulter/PC/SS000104.ASP, October 6, 2000.

[Bec00c] Beckman Coulter, Inc., "Patented PIDS technology for unsurpassed resolution," http://www.beckmancoulter.com/coulter/PC/pids.asp, October 6, 2000.

[Ber93] H. E. Berek and E. M. Jensen, "Electric Field Strength/Power Density and Temperature Measurements in an Electromagnetic Field," in Microwaves: Theory and Application in Materials Processing II, (eds. D. E. Clark, W. R. Tinga, and J. R. Laia, Jr.), Ceramic Transactions, Vol. 36, American Ceramic Society, Westerville, OH, pp. 511-516 (1993).

[Bes91] Eric Bescher and John D. Mackenzie, "Microwave Heating of Cermets," in Microwaves: Theory and Application in Materials Processing, (eds., D. E. Clark, F. D. Gac, and W. H. Sutton), Ceramic Transactions, Vol. 21, American Ceramic Society, Westerville, OH, pp. 557-563 (1991).

[Bin92] J. G. P. Binner, I. A. Al-Dawery, C. Aneziris and T. E. Cross, "Use of the Inverse Temperature Profile in Microwave Processing of Advanced Ceramics," in Microwave Processing of Materials III, (eds. R. L. Beatty, W. H. Sutton, and M. F. Iskander), Materials Research Society Symposium Proceedings, Vol.269, Materials Research Society, Pittsburgh, pp. 357-362 (1992).

[Boo93] A. Boonyapiwat, Z. Fathi, D. C. Folz, and D. E. Clark, "Repair of Glass by Sol-Gel Coating Using Either Conventional or Microwave Heating," in Microwaves: Theory and Application in Materials Processing II, (eds. D. E. Clark, W. R. Tinga, and J. R. Laia, Jr.), Ceramic Transactions, Vol. 36, American Ceramic Society, Westerville, OH, pp. 341-349 (1993).

[Boo94] A. Boonyapiwat, J. J. Mecholsky, Jr., and D. E. Clark, "Repair of Glass by Sol-Gel Coating and Heating with Microwave or Conventional Techniques," Ceramic Engineering and Science Proceedings, Vol. 15, no. 5, pp. 1011-1018 (1994).

[Boo95] A. Boonyapiwat and D. E. Clark, "Nucleation and Crystal Growth of $Li_2O{\cdot}2SiO_2$ in a Microwave Field," in Microwaves: Theory and Application in Materials Processing III, (eds. D. E. Clark, D. C. Folz, S. J. Oda, and R. Silberglitt), Ceramic Transactions, Vol. 59, American Ceramic Society, Westerville, OH, pp. 505-514 (1995).

[Boo97] John H. Booske, Reid F. Cooper, Samuel A. Freeman, Binshen Meng, Kirill I. Rybakov, and Vladimir E. Semenov, "Thermal and Nonthermal Interactions Between Microwave Fields and Ceramics," in Microwaves: Theory and Application in Materials Processing IV, Ceramic Transactions, Vol. 80, American Ceramic Society, Westerville, OH, pp. 143-151 (1997).

[Bro88] Michael E. Brown, Introduction to Thermal Analysis: Techniques and Applications, Chapman and Hall, New York, 1988.

[Bru88] Ralph W. Bruce, "New Frontiers in the Use of Microwave Energy: Power and Metrology," in Microwave Processing of Materials, (eds. W. H. Sutton, M. H. Brooks, and I. J. Chabinsky), Materials Research Society Symposium Proceedings, Vol. 124, Materials Research Society, Pittsburgh, pp. 3-15 (1988).

[Bru91] Ralph W. Bruce, "Activation Energies for the Dielectric Loss Factor/AC Conductivity of Some Polycrystalline Ceramics," in Microwaves: Theory and Application in Materials Processing, (eds., D. E. Clark, F. D. Gac, and W. H. Sutton), Ceramic Transactions, Vol. 21, American Ceramic Society, Westerville, OH, pp. 107-116 (1991).

[Bru96] R. W. Bruce, A. W. Fliflet, D. Lewis, III, R. J. Rayne, B. A. Bender, L. K. Kurihara, G. -M. Chow, and P. E. Schoen, "Microwave Sintering of Pure and Doped Nanocrystalline Alumina Compacts," in Microwave Processing of Materials V, (eds. M. F. Iskander, J. O. Kiggans, Jr., and J.-C. Bolomey), Materials Research Society Symposium Proceedings, Vol. 430, Materials Research Society, Pittsburgh, pp. 139-144 (1996).

[Byk96] Y. Bykov, A. Eremeev, and V. Holoptsev, "Influence of Specific Absorbed Microwave Power on Activation Energy of Densification in Ceramic Materials," in Microwave Processing of Materials V, (eds. M. F. Iskander, J. O. Kiggans, Jr., and J.-C. Bolomey), Materials Research Society Symposium Proceedings, Vol. 430, Materials Research Society, Pittsburgh, pp. 385-390 (1996).

[Cam92] Isidoro E. Campisi, Lynda K. Summers, Keith E. Finger and Anne M. Johnson, "Microwave Absorption by Lossy Ceramic Materials," in Microwave Processing of Materials III, (eds. R. L. Beatty, W. H. Sutton, and M. F. Iskander), Materials Research Society Symposium Proceedings, Vol.269, Materials Research Society, Pittsburgh, pp. 157-162 (1992).

[Car91] Joseph A. Carpenter, Jr., "Dielectric Property Measurements and Data," in Microwaves: Theory and Application in Materials Processing, (eds., D. E. Clark, F. D. Gac, and W. H. Sutton), Ceramic Transactions, Vol. 21, American Ceramic Society, Westerville, OH, pp. 477-487 (1991).

[Cla91] D. E. Clark and D. C. Folz, "Microwave Processing Activities at the University of Florida," in Microwaves: Theory and Application in Materials Processing, (eds., D. E. Clark, F. D. Gac, and W. H. Sutton), Ceramic Transactions, Vol. 21, American Ceramic Society, Westerville, OH, pp. 29-34 (1991).

[Cla94] D. E. Clark, D. C. Folz, R. L. Schulz, Z. Fathi, A. D. Cozzi, A. Boonyapiwat, P. Komarenko, R. DiFiore and C. B. Jones, "Microwave Processing at the University of Florida," in Microwave Processing of Materials IV, (eds. M. F. Iskander, R. J. Lauf, and W. H. Sutton), Materials Research Society Symposium Proceedings, Vol. 347, Materials Research Society, Pittsburgh, pp. 489-500 (1994).

[Cla96] David E. Clark and W. H. Sutton, "Microwave Processing of Materials," Annual Review of Materials Science, (eds. Matthew Tirrell, Elton N. Kaufmann, Joseph A. Giordmaine, and John B. Wachtman, Jr.), Vol. 26, Annual Reviews Inc., Palo Alto, CA, pp. 299-331 (1996).

[Cla97] David E. Clark, Willard H. Sutton, and David A. Lewis, "Microwave Processing of Materials," in Microwaves: Theory and Application in Materials Processing IV, (eds. D. E. Clark, W. H. Sutton, and D. A. Lewis), Ceramic Transactions, Vol. 80, American Ceramic Society, Westerville, OH, pp. 61-96 (1997).

[Coz91] A. D. Cozzi, D. K. Jones, Z. Fathi, and D. E. Clark, "Microstructural Evolution of $YBa_2Cu_3O_{7-x}$ Using Microwave Energy," in Microwaves: Theory and Application in Materials Processing, (eds., D. E. Clark, F. D. Gac, and W. H. Sutton), Ceramic Transactions, Vol. 21, American Ceramic Society, Westerville, OH, pp. 357-364 (1991).

[Coz94] A. D. Cozzi, D. E. Clark, W. D. Porter, and O. B. Cavin, "Potential Interlayer Materials for the Microwave Joining of Alumina," Ceramic Engineering and Science Proceedings, Vol. 15, no. 5, pp. 1036-1043 (1994).

[Coz95] A. D. Cozzi, D. E. Clark, M. K. Ferber, and V. J. Tennery, "Apparatus for the Joining of Ceramics Using Microwave Energy," in Microwaves: Theory and Application in Materials Processing III, (eds. D. E. Clark, D. C. Folz, S. J. Oda, and R. Silberglitt), Ceramic Transactions, Vol. 59, American Ceramic Society, Westerville, OH, pp. 389-396 (1995).

[Coz96a] A. D. Cozzi, D. E. Clark, and M. K. Ferber, "Microwave Joining of High-Purity Alumina," Ceramic Engineering and Science Proceedings, Vol. 17, no.3, pp. 155-162 (1996).

[Coz96b] Alex D. Cozzi, Theory and Application of Microwave Joining, Ph.D. Dissertation, University of Florida, 1996.

[Coz97a] Alex D. Cozzi, Mattison K. Ferber, and David E. Clark, "Microwave Joining of Alumina Ceramics," in Microwaves: Theory and Application in Materials Processing IV, (eds. D. E. Clark, W. H. Sutton, and D. A. Lewis), Ceramic Transactions, Vol. 80, American Ceramic Society, Westerville, OH, pp. 465-474 (1997).

[Coz97b] A. D. Cozzi, Theory & Application of Microwave Joining, Ph.D. Dissertation, University of Florida, (1997).

[Cul78] B. D. Cullity, Elements of X-Ray Diffraction, Second Edition, Addison-Wesley Publishing Company, Inc., Reading, Massachusetts, 1978.

[Dad96] D. Dadon, D. Gershon, Y. Carmel, K. I. Rybakov, R. Hutcheon, A. Birman, L. P. Martin, J. Calame, B. Levush, and M. Rosen, "Observation of an Electromagnetically Driven Temperature Wave in Porous Zinc Oxide During Microwave Heating," in Microwave Processing of Materials V, (eds. M. F. Iskander, J. O. Kiggans, Jr., and J.-C. Bolomey), Materials Research Society Symposium Proceedings, Vol. 430, Materials Research Society, Pittsburgh, pp. 507-512 (1996).

[Dal90] R. C. Dalton, I. Ahmad, and D. E. Clark, "Combustion Synthesis Using Microwave Energy," Ceramic Engineering and Science Proceedings, Vol. 11, no. 9-10 pt. 2, pp. 531-541 (1990).

[Dar95] Greg Darby, D. E. Clark, Robert Di Fiore, Diane Folz, Rebecca Schulz, Attapon Boonyapiwat, and David Roth, "Temperature Measurement During Microwave Processing," in Microwaves: Theory and Application in Materials Processing III, (eds. D. E. Clark, D. C. Folz, S. J. Oda, and R. Silberglitt), Ceramic Transactions, Vol. 59, American Ceramic Society, Westerville, pp. 515-522 (1995).

[Dar96] G. J. Darby, R. R. Di Fiore, R. L. Schulz, and D. E. Clark, "Microwave Processing of $Al_2O_3$-$ZrO_2$ Composites," Ceramic Engineering and Science Proceedings, Vol. 17, no. 3, pp. 147-156 (1996).

[Dav94] Pamela Davis, Jon Binner, Tom Cross and John Fernie, "The Role of Glassy Grain Boundary Phases in the Microwave Joining of Alumina," in Microwave Processing of Materials IV, (eds. M. F. Iskander, R. J. Lauf, and W. H. Sutton), Materials Research Society Symposium Proceedings, Vol. 347, Materials Research Society, Pittsburgh, pp. 655-660 (1994).

[Dé91a] Arindam Dé, Iftikhar Ahmad, E. Dow Whitney and David E. Clark, "Effect of Green Microstructure and Processing Variables on the Microwave Sintering of Alumina," in Microwave Processing of Materials II (eds. W. B. Snyder, Jr., W. H. Sutton, M. F. Iskander and D. L. Johnson) Materials Research Society Symposium Proceedings, Vol. 189, Materials Research Society, Pittsburgh, pp. 283-288 (1991).

[Dé91b] Arindam Dé, Iftikhar Ahmad, E. Dow Whitney and David E. Clark, "Microwave (Hybrid) Heating of Alumina at 2.45 GHz: I. Microstructural Uniformity and Homogeneity," in Microwaves: Theory and Application in Materials Processing, (eds., D. E. Clark, F. D. Gac, and W. H. Sutton), Ceramic Transactions, Vol. 21, American Ceramic Society, Westerville, OH, pp. 319-328 (1991).

[Dé91c] Arindam Dé, Iftikhar Ahmad, E. Dow Whitney and David E. Clark, "Microwave (Hybrid) Heating of Alumina at 2.45 GHz: II. Heating Rates and Particle Size," in Microwaves: Theory and Application in Materials Processing, (eds., D. E. Clark, F. D. Gac, and W. H. Sutton), Ceramic Transactions, Vol. 21, American Ceramic Society, Westerville, OH, pp. 329-339 (1991).

[DiF95a] R. R. Di Fiore and D. E. Clark, "Microwave Joining of Zinc Sulfide," in Microwaves: Theory and Application in Materials Processing III, (eds. D. E. Clark, D. C. Folz, S. J. Oda, and R. Silberglitt), Ceramic Transactions, Vol. 59, American Ceramic Society, Westerville, OH, pp. 381-387 (1995).

[DiF95b] R. R. Di Fiore and D. E. Clark, "Microwave Processing of Silica Sol-Gels," Ceramic Engineering and Science Proceedings, Vol. 16, no. 5, pp. 1089-1096 (1995).

[DiF96] R. R. Di Fiore and D. E. Clark, "Microwave Processing of Redox Ceramic-Metal Composites," in Microwave Processing of Materials V, (eds. M. F. Iskander, J. O. Kiggans, Jr., and J.-C. Bolomey), Materials Research Society Symposium Proceedings, Vol. 430, Materials Research Society, Pittsburgh, pp. 101-106 (1996).

[DiF97] R. R. Di Fiore and D. E. Clark, "Microwave Induced Reduction/Oxidation of Powders to Form Ceramic-Metal Composites," Ceramic Engineering and Science Proceedings, Vol. 18, no. 4B, pp. 557-562 (1997).

[DiF98] R. R. Di Fiore and D. E. Clark, "Microwave-Induced Decomposition of Ceramic Oxides to Form Unique Composites," Ceramic Engineering and Science Proceedings, Vol. 19, no. 4, pp. 517-523 (1998).

[Dis97] L. A. Dissado and R. M. Hill, "What Form of Motion Gives Rise to Dielectric Response at Microwave Frequencies?" in Microwaves: Theory and Application in Materials Processing IV, (eds. D. E. Clark, W. H. Sutton, and D. A. Lewis), Ceramic Transactions, Vol. 80, American Ceramic Society, Westerville, OH, pp. 99-106 (1997).

[Drz91] L. T. Drzal, K. J. Hook, and R. K. Agrawal, "Enhanced Chemical Bonding at the Fiber-Matrix Interphase in Microwave Processed Composites," in Microwave Processing of Materials II (eds. W. B. Snyder, Jr., W. H. Sutton, M. F. Iskander and D. L. Johnson) Materials Research Society Symposium Proceedings, Vol. 189, Materials Research Society, Pittsburgh, pp. 449-454 (1991).

[Fan91a] Y. Fang, D. K. Agrawal, D. M. Roy and R. Roy, "Rapid Sintering of Hydroxyapatite Ceramics by Microwave Processing." in Microwaves: Theory and Application in Materials Processing, (eds., D. E. Clark, F. D. Gac, and W. H. Sutton), Ceramic Transactions, Vol. 21, American Ceramic Society, Westerville, OH, pp. 349-356 (1991).

[Fan93] Y. Fang, D. K. Agrawal, D. M. Roy, and R. Roy, "Microwave Sintering of Calcium Strontium Zirconium Phosphate Ceramics," in Microwaves: Theory and Application in Materials Processing II, (eds. D. E. Clark, W. R. Tinga, and J. R. Laia, Jr.), Ceramic Transactions, Vol. 36, American Ceramic Society, Westerville, OH, pp. 109-114 (1993).

[Fan91b] Glenn E. Fanslow, "Microwave Enhancement of Chemical and Physical Reactions," in Microwave Processing of Materials II (eds. W. B. Snyder, Jr., W. H. Sutton, M. F. Iskander and D. L. Johnson) Materials Research Society Symposium Proceedings, Vol. 189, Materials Research Society, Pittsburgh, pp. 43-48 (1991).

[Fat91] Z. Fathi, I. Ahmad, J. H. Simmons, D. E. Clark, and A. R. Lodding, "Surface Modification of Sodium Aluminosilicate Glasses Using Microwave Energy," in Microwaves: Theory and Application in Materials Processing, (eds., D. E. Clark, F. D. Gac, and W. H. Sutton), Ceramic Transactions, Vol. 21, American Ceramic Society, Westerville, OH, pp. 623-629 (1991).

[Fat92] Z. Fathi, D. E. Clark, and R. Hutcheon, "Surface Modification of Ceramics Using Microwave Energy," in Microwave Processing of Materials III, (eds. R. L. Beatty, W. H. Sutton, and M. F. Iskander), Materials Research Society Symposium Proceedings, Vol.269, Materials Research Society, Pittsburgh, pp. 347-351 (1992).

[Fat93] Z. Fathi, D. C. Folz, D. E. Clark, and R. Hutcheon, "Surface Modification of Sodium Aluminosilicate Glasses Using Microwave Energy II," in Microwaves: Theory and Application in Materials Processing II, (eds. D. E. Clark, W. R. Tinga, and J. R. Laia, Jr.), Ceramic Transactions, Vol. 36, American Ceramic Society, Westerville, OH, pp. 333-340 (1993).

[Fat94] Zakaryae Fathi, Surface Modification of Sodium Aluminosilicate Glasses Using Microwave Energy, Ph.D. Dissertation, University of Florida, 1994.

[Fat64] E. Fatuzzo and P. R. Mason, "A Two-Impedance Method for Measuring the Microwave Dielectric Constant of Liquids," Journal of Scientific Instruments, Vol. 41, pp. 694-695 (Nov. 1964).

[Fre88] H. Frederickssson, "Interpretation and Use of Cooling Curves (Thermal Analysis), ASM Handbook, Volume 15: Casting, ASM International, USA, 1988.

[Fre93] S. A. Freeman, J. H. Booske, R. F. Cooper, B. Meng, J. Kieffer, and B. J. Reardon, "Studies of Microwave Field Effects on Ionic Transport in Ionic Crystalline Solids," in Microwaves: Theory and Application in Materials Processing II, (eds. D. E. Clark, W. R. Tinga, and J. R. Laia, Jr.), Ceramic Transactions, Vol. 36, American Ceramic Society, Westerville, OH, pp. 213-220 (1993).

[Fre94] John Freim, Joanna McKittrick, Joel Katz, and Kurt Sickafus, "Phase Transformation and Densification Behavior of Microwave Sintered $\gamma$-$Al_2O_3$," in Microwave Processing of Materials IV, (eds. M. F. Iskander, R. J. Lauf, and W. H. Sutton), Materials Research Society Symposium Proceedings, Vol. 347, Materials Research Society, Pittsburgh, pp. 525-530 (1994).

[Gar95] Richard S. Garard, "Controlling and Understanding the Variables: Key to Commercializing Microwave Processing of Advanced Materials," in Microwaves: Theory and Application in Materials Processing III, Ceramic Transactions, Volume 59, American Ceramic Society, Westerville, OH, pp. 29-32 (1995).

[Gar96] J. A. Gardner, M. V. Rao, Y. L. Tian, O. W. Holland, G. Kelner, J. A. Freitas, Jr., and I. Ahmad, "Microwave Annealing of Ion Implanted 6H-SiC," in Microwave Processing of Materials V, (eds. M. F. Iskander, J. O. Kiggans, Jr., and J.-C. Bolomey), Materials Research Society Symposium Proceedings, Vol. 430, Materials Research Society, Pittsburgh, pp. 641-646 (1996).

[Gol92] Joseph I. Goldstein, Dale E. Newbury, Patrick Echlin, David C. Joy, A. D. Romig, Jr., Charles E. Lyman, Charles Fiori, and Eric Lifshin, Scanning Electron Microscopy and X-Ray Microanalysis: A Text for Biologists, Materials Scientists, and Geologists, second edition, Plenum Press, New York, 1992.

[Gre93] Daniel J. Grellinger and Mark A. Janney, "Temperature Measurement in a 2.45 GHz Microwave Furnace," in Microwaves: Theory and Application in Materials Processing II, (eds. D. E. Clark, W. R. Tinga, and J. R. Laia, Jr.), Ceramic Transactions, Vol. 36, American Ceramic Society, Westerville, OH, pp. 529-538 (1993).

[Gre95] D. J. Grellinger, J. H. Booske, S. A. Freeman, and R. F. Cooper, "Processing Parameters Influencing the Sintering of Alumina in a Conventional and 14 GHz Microwave Furnace," in Microwaves: Theory and Application in Materials Processing III, (eds. D. E. Clark, D. C. Folz, S. J. Oda, and R. Silberglitt), Ceramic Transactions, Vol. 59, American Ceramic Society, Westerville, OH, pp. 465-471 (1995).

[Ham97] Michael G. Hamlyn, Neil A. Hart, and Nigel G. Evans, "A Combined Microwave and Electric Radiant Heating System for Firing Ceramics," in Microwaves: Theory and Application in Materials Processing IV, (eds. D. E. Clark, W. H. Sutton, and D. A. Lewis), Ceramic Transactions, Vol. 80, American Ceramic Society, Westerville, OH, pp. 555-562 (1997).

[Hen90] L.L. Hench and J.K. West, Principles of Electronic Ceramics, John Wiley & Sons, New York, 1990.

[Ho88] Yung Shou Ho and John J. Kramer, "Microwave Dielectric Properties of Metal Filled Particulate Composites," in Microwave Processing of Materials, (eds. W. H. Sutton, M. H. Brooks, and I. J. Chabinsky), Materials Research Society Symposium Proceedings, Vol. 124, Materials Research Society, Pittsburgh, pp. 161-166 (1988).

[Hut92] R. M. Hutcheon, M. S. De Jong, F. P. Adams, P. G. Lucuta, J. E. McGregor and L. Bahen, "RF and Microwave Dielectric Measurements to 1400 °C and Dielectric Loss Mechanisms," in Microwave Processing of Materials III, (eds. R. L. Beatty, W. H. Sutton, and M. F. Iskander), Materials Research Society Symposium Proceedings, Vol.269, Materials Research Society, Pittsburgh, pp. 541-551 (1992).

[Hut95a] R. M. Hutcheon, F. P. Adams and M. S. De Jong, "What is the Best Microwave Absorber?," in Microwaves: Theory and Application in Materials Processing III, (eds. D. E. Clark, D. C. Folz, S. J. Oda, and R. Silberglitt), Ceramic Transactions, Vol. 59, American Ceramic Society, Westerville, OH, pp. 215-225 (1995).

[Hut95b] R. M. Hutcheon, P. Hayward, B. H. Smith and S. B. Alexander, "High Temperature Dielectric Constant Measurement - Another Analytical Tool for Ceramic Studies?," in Microwaves: Theory and Application in Materials Processing III, (eds. D. E. Clark, D. C. Folz, S. J. Oda, and R. Silberglitt), Ceramic Transactions, Vol. 59, American Ceramic Society, Westerville, OH, pp. 235-242 (1995).

[Isk88] Magdy F. Iskander, "Medical and Biological Applications of Electromagnetic Techniques—A Relevant Experience to the Microwave Processing of Materials Research," in Microwave Processing of Materials, (eds. W. H. Sutton, M. H. Brooks, and I. J. Chabinsky), Materials Research Society Symposium Proceedings, Vol. 124, Materials Research Society, Pittsburgh, pp. 69-119 (1988).

[Isk91] Magdy F. Iskander, "Computer Modeling and Numerical Techniques for Quantifying Microwave Interactions With Materials," in Microwave Processing of Materials II (eds. W. B. Snyder, Jr., W. H. Sutton, M. F. Iskander and D. L. Johnson) Materials Research Society Symposium Proceedings, Vol. 189, Materials Research Society, Pittsburgh, pp. 149-171 (1991).

[Isk93] Magdy F. Iskander, "Modeling the Microwave Process -- Challenges and New Directions," in Microwaves: Theory and Application in Materials Processing II, (eds. D. E. Clark, W. R. Tinga, and J. R. Laia, Jr.), Ceramic Transactions, Vol. 36, American Ceramic Society, Westerville, OH, pp. 167-187 (1993).

[Jan91] M. A. Janney, C. L. Calhoun, and H. D. Kimrey, "Microwave Sintering of Zirconia-8 Mol % Yttria," in Microwaves: Theory and Application in Materials Processing, (eds., D. E. Clark, F. D. Gac, and W. H. Sutton), Ceramic Transactions, Vol. 21, American Ceramic Society, Westerville, OH, pp. 311-318 (1991).

[Jan92] Mark A. Janney, Hal D. Kimrey, and James O. Kiggans, "Microwave Processing of Ceramics," in Microwave Processing of Materials III, (eds. R. L. Beatty, W. H. Sutton, and M. F. Iskander), Materials Research Society Symposium Proceedings, Vol. 269, Materials Research Society, Pittsburgh, pp. 173-185 (1992).

[Jan93] Mark A. Janney, Mitchell L. Jackson, and Hal D. Kimrey, "Microwave Sintering of $ZrO_2$ - 12 Mol% $CeO_2$," in Microwaves: Theory and Application in Materials Processing II, (eds. D. E. Clark, W. R. Tinga, and J. R. Laia, Jr.), Ceramic Transactions, Vol. 36, American Ceramic Society, Westerville, OH, pp. 101-108 (1993).

[Joh91] D. Lynn Johnson, "Microwave Processing of Ceramics at Northwestern University," in Microwaves: Theory and Application in Materials Processing, (eds., D. E. Clark, F. D. Gac, and W. H. Sutton), Ceramic Transactions, Vol. 21, American Ceramic Society, Westerville, OH, pp. 17-28 (1991).

[Joh93] D. Lynn Johnson, Daniel J. Skamser, and Mark S. Spotz, "Temperature Gradients in Microwave Processing: Boon and Bane," in Microwaves: Theory and Application in Materials Processing II, (eds. D. E. Clark, W. R. Tinga, and J. R. Laia, Jr.), Ceramic Transactions, Vol. 36, American Ceramic Society, Westerville, OH, pp. 133-146 (1993).

[Kat88] J. D. Katz, R. D. Blake, J. J. Petrovic and H. Sheinberg, "Microwave Sintering of Boron Carbide," in Microwave Processing of Materials, (eds. W. H. Sutton, M. H. Brooks, and I. J. Chabinsky), Materials Research Society Symposium Proceedings, Vol. 124, Materials Research Society, Pittsburgh, pp. 219-226 (1988).

[Kat91] J. D. Katz, R. D. Blake, and V. M. Kenkre, "Microwave Enhanced Diffusion?," in Microwaves: Theory and Application in Materials Processing, (eds., D. E. Clark, F. D. Gac, and W. H. Sutton), Ceramic Transactions, Vol. 21, American Ceramic Society, Westerville, OH, pp. 95-105 (1991).

[Kat92] Joel D. Katz, "Microwave Sintering of Ceramics," Annual Review of Materials Science, (eds. Robert A. Huggins, Joseph A. Giordmaine, and John B. Wachtman, Jr.), Annual Reviews Inc., Palo Alto, CA, pp. 153-170 (1992).

[Ken91] V. M. Kenkre, "Theory of Microwave Interactions with Ceramic Materials," in Microwaves: Theory and Application in Materials Processing, (eds., D. E. Clark, F. D. Gac, and W. H. Sutton), Ceramic Transactions, Vol. 21, American Ceramic Society, Westerville, OH, pp. 69-80 (1991).

[Kha95] B. V. Khaenko, E. V. Prilutskii, A. A. Mikhailik, M. V. Karpets, and A. V. Krainikov, "Phase State and Crystal Structure of Products Obtained by Reaction of SiC with $SiO_2$," Inorganic Matter, Vol. 31, n. 3, pp. 304-309 (1995).

[Kig93] J. O. Kiggans, T. N. Tiegs, H. D. Kimrey, and C. E. Holcombe, "Processing of Complex Sintered Reaction-Bonded Silicon Nitride Parts by Microwave Heating," in Microwaves: Theory and Application in Materials Processing II, (eds. D. E. Clark, W. R. Tinga, and J. R. Laia, Jr.), Ceramic Transactions, Vol. 36, American Ceramic Society, Westerville, OH, pp. 269-276(1993).

[Kig94] J. O. Kiggans, T. N. Tiegs, H. D. Kimrey, and Jon-Paul Maria, "Studies on the Scale-Up of the Microwave Assisted Nitridation and Sintering of Reaction-Bonded Silicon Nitride," in Microwave Processing of Materials IV, (eds. M. F. Iskander, R. J. Lauf, and W. H. Sutton), Materials Research Society Symposium Proceedings, Vol. 347, Materials Research Society, Pittsburgh, pp. 71-76 (1994).

[Kim91] H. D. Kimrey, J. O. Kiggans, M. A. Janney, and R. L. Beatty, "Microwave Sintering of Zirconia-Toughened Alumina Composites," in Microwave Processing of Materials II (eds. W. B. Snyder, Jr., W. H. Sutton, M. F. Iskander and D. L. Johnson) Materials Research Society Symposium Proceedings, Vol. 189, Materials Research Society, Pittsburgh, pp. 243-255 (1991).

[Kin76] W. D. Kingery, H. K. Bowen, and D. R. Uhlmann, Introduction to Ceramics, Second Edition, John Wiley & Sons, Inc., New York, 1976.

[Koh95] Michael T. K. Koh, Rajiv K. Singh and David E. Clark, "Temperature Distribution Considerations During Microwave Heating of Ceramics," in Microwaves: Theory and Application in Materials Processing III, (eds. D. E. Clark, D. C. Folz, S. J. Oda, and R. Silberglitt), Ceramic Transactions, Vol. 59, American Ceramic Society, Westerville, OH, pp. 313-322 (1995).

[Kom94] P. Komarenko and D. E. Clark, "Synthesis of $Ti_3SiC_2$-based Materials Using Microwave Initiated SHS," Ceramic Engineering and Science Proceedings, Vol. 15, no. 5, pp. 1028-1035 (1994).

[Lee95] Ki-Yong Lee, Eldon D. Case, Jes Asmussen, Jr., and Marvin Siegel, "Sintering of Alumina Ceramics in a Single Mode Cavity Under Automated Control," in Microwaves: Theory and Application in Materials Processing III, (eds. D. E. Clark, D. C. Folz, S. J. Oda, and R. Silberglitt), Ceramic Transactions, Vol. 59, American Ceramic Society, Westerville, OH, pp. 473-480 (1995).

[Lei97] K. S. Leiser, R. R. Di Fiore, A. D. Cozzi, and D. E. Clark, "Microwave Heating Rates of Silicon Carbide/Alumina Cement Susceptors," Ceramic Engineering and Science Proceedings, Vol. 18, no. 4, pp. 551-556 (1997).

[Lei98] K. S. Leiser, and D. E. Clark, "Effects of Silicon Carbide Structure on the Microwave Properties of Silicon Carbide/Alumina Cement Susceptors," Ceramic Engineering and Science Proceedings, Vol. 19, no. 4, pp. 367-372 (1998).

[Lei99] K. S. Leiser and D. E. Clark, "Investigation of Microwave Behavior of Silicon Carbide/High Alumina Cement Composites," Ceramic Engineering and Science Proceedings, Vol. 20, no. 3, pp. 103-109 (1999).

[Lei00] K. S. Leiser and D. E. Clark, "Microwave Behavior of Silicon Carbide/High Alumina Cement Composites," in Microwaves: Theory and Application in Materials Processing V, Ceramic Transactions, American Ceramic Society, Westerville, OH, to be published.

[Lid98] David R. Lide, editor-in-chief, CRC Handbook of Chemistry and Physics, 79th edition 1998-1999, CRC Press, Boston, 1998.

[Lux93] F. Lux, "Review: Models Proposed to Explain the Electrical Conductivity of Mixtures Made of Conductive and Insulating Materials," Journal of Materials Science, Vol. 28, n.2, pp. 285-301 (1993).

[Mat95] I. Matsushita, J. Nakanishi, T. Kono, T. Sekita, T. Ashida, and I. Nakabayashi, "Effect of Atmosphere on the Pyrolysis Process of Basic Calcium Carbonate," Journal of the Ceramic Society of Japan, Vol. 103, n. 3, pp. 240-244 (1995).

[McG88] S. L. McGill, J. W. Walkiewicz, and G. A. Smyres, "The Effects of Power Level on the Microwave Heating of Selected Chemicals and Minerals," in Microwave Processing of Materials, (eds. W. H. Sutton, M. H. Brooks, and I. J. Chabinsky), Materials Research Society Symposium Proceedings, Vol. 124, Materials Research Society, Pittsburgh, pp. 247-252 (1988).

[Men95] Binshen Meng, John Booske, Reid Cooper, and Benjamin Klein, "Microwave Absorption in Ionic Crystalline Ceramics With Various Concentrations of Point Defects," in Microwaves: Theory and Application in Materials Processing III, (eds. D. E. Clark, D. C. Folz, S. J. Oda, and R. Silberglitt), Ceramic Transactions, Vol. 59, American Ceramic Society, Westerville, OH, pp. 177-184 (1995).

[Mer95] John Merchant, "Infrared Temperature Measurement Theory and Application," The Temperature Handbook, Omega Engineering, Stamford, pp. Z-53-Z-56 (1995).

[Mer91] Jason Mershon, "Accurate High Temperature Measurements in Microwave Environments," in Microwaves: Theory and Application in Materials Processing, (eds., D. E. Clark, F. D. Gac, and W. H. Sutton), Ceramic Transactions, Vol. 21, American Ceramic Society, Westerville, OH, pp. 641-646 (1991).

[Met83] A. C. Metaxas and R. J. Meredith, Industrial Microwave Heating, Peter Peregrinus, London, UK, 1983.

[Moo91] Edmund H. Moore, Iftikhar Ahmad and David E. Clark, "Microwave Thermogravimetric Analyzer, (MTGA)," in Microwaves: Theory and Application in Materials Processing, (eds., D. E. Clark, F. D. Gac, and W. H. Sutton), Ceramic Transactions, Vol. 21, American Ceramic Society, Westerville, OH, pp. 675-681 (1991).

[Moo93a] Edmund H. Moore, David E. Clark, and Ronald Hutcheon, "Removal of Polymethyl Methacrylate Binder from Alumina Using Conventional and/or Microwave Heating," in Microwaves: Theory and Application in Materials Processing II, (eds. D. E. Clark, W. R. Tinga, and J. R. Laia, Jr.), Ceramic Transactions, Vol. 36, American Ceramic Society, Westerville, OH, pp. 325-332 (1993).

[Moo93b] Edmund H. Moore, Removal of Polymethyl Methacrylate from Alumina Compacts Using Microwave Energy, Ph.D. Dissertation, University of Florida, 1993.

[Mor91] R. Moreno, P. Miranzo, J. Requena, J. S. Moya, J. Mollá and A. Ibarra, "Effect of Powder Characteristics on Dielectric Properties of Alumina Compacts," in Microwaves: Theory and Application in Materials Processing, (eds., D. E. Clark, F. D. Gac, and W. H. Sutton), Ceramic Transactions, Vol. 21, American Ceramic Society, Westerville, OH, pp. 225-233 (1991).

[New91] R. E. Newnham, S. J. Jang, Ming Xu, and Frederick Jones, "Fundamental Interaction Mechanisms Between Microwaves and Matter," in Microwaves: Theory and Application in Materials Processing, (eds., D. E. Clark, F. D. Gac, and W. H. Sutton), Ceramic Transactions, Vol. 21, American Ceramic Society, Westerville, OH, pp. 51-67 (1991).

[New93] J. D. Newman, L. Walsh, R. Evans, T. Tholen, O. M. Andrade, M. F. Iskander and K. J. Bunch, "Experimental Validation of Numerical Simulations of the Microwave Sintering Process," in Microwaves: Theory and Application in Materials Processing II, (eds. D. E. Clark, W. R. Tinga, and J. R. Laia, Jr.), Ceramic Transactions, Vol. 36, American Ceramic Society, Westerville, OH, pp. 229-237 (1993).

[Oda88] S. J. Oda and I. S. Balbaa, "Microwave Processing at Ontario Hydro Research Division," in Microwave Processing of Materials, (eds. W. H. Sutton, M. H. Brooks, and I. J. Chabinsky), Materials Research Society Symposium Proceedings, Vol. 124, Materials Research Society, Pittsburgh, pp. 303-309 (1988).

[Ogb95] Linus U.J.T. Ogbuji and M. Singh, "High-Temperature Oxidation Behavior of Reaction-Formed Silicon Carbide Ceramics," Journal of Materials Research, Vol. 10, n.12, pp. 3232-3240 (1995).

[Ome95] Omega Engineering, The Temperature Handbook, Omega Engineering, Stamford, p. Z-42 (1995).

[Pal88] David Palaith, Richard Silberglitt, Carl C. M. Wu, Richard Kleiner, and E. Laurence Libelo, "Microwave Joining of Ceramics," in Microwave Processing of Materials, (eds. W. H. Sutton, M. H. Brooks, and I. J. Chabinsky), Materials Research Society Symposium Proceedings, Vol. 124, Materials Research Society, Pittsburgh, pp. 255-266 (1988).

[Pel00] John A. Pelesko and Gregory A. Kriegsmann, "Microwave Heating of Ceramic Composites," IMA Journal of Applied Mathematics (Institute of Mathematics and Its Applications) Vol.64, n. 1, pp.39-50 (2000).

[Por92] M. Willert-Porada, T. Gerdes, S. Vodegel, "Metallorganic and Microwave Processing of Cermets," in Microwave Processing of Materials III, (eds. R. L. Beatty, W. H. Sutton, and M. F. Iskander), Materials Research Society Symposium Proceedings, Vol.269, Materials Research Society, Pittsburgh, pp. 205-210 (1992).

[Ric92] David W. Richerson, Modern Ceramic Engineering: Properties, Processing, and Use in Design, Second Edition, Marcel Dekker, Inc., New York, 1992.

[Rob46] S. Roberts and A. von Hippel, "A new Method for Measuring Dielectric Constant and Loss in the Range of Centimeter Waves," Journal of Applied Physics, Vol.17, n.7, 1946.

[Sai00] Carborundum (a part of Saint Gobain Industrial Ceramics), "Silicon Carbide Structural Ceramics," http://www.saintgobainsemi.com/brochure/Carbo%20Structural/HEXOLOY.html , November 13, 2000.

[Sam94] M. Samandi and M. Doroudian, "Plasma Assisted Microwave Sintering and Joining of Ceramics," in Microwave Processing of Materials IV, (eds. M. F. Iskander, R. J. Lauf, and W. H. Sutton), Materials Research Society Symposium Proceedings, Vol. 347, Materials Research Society, Pittsburgh, pp. 605-615 (1994).

[Sch95] James P. Schaffer, Ashok Saxena, Stephen D. Antolovich, Thomas H. Sanders, Jr., and Steven B. Warner, The Science and Design of Engineering Materials, Richard D. Irwin, Inc., Chicago, 1995.

[Sch91] R. L. Schulz, Z. Fathi, D. E. Clark, and G. G. Wicks, "Microwave Processing of Simulated Nuclear Waste Glass," in Microwaves: Theory and Application in Materials Processing, (eds., D. E. Clark, F. D. Gac, and W. H. Sutton), Ceramic Transactions, Vol. 21, American Ceramic Society, Westerville, OH, pp. 451-458 (1991).

[Sch93a] R. L. Schulz, D. C. Folz, D. E. Clark, and G. G. Wicks, "Microwave Destruction/Vitrification of Electronic Components," in Microwaves: Theory and Application in Materials Processing II, (eds. D. E. Clark, W. R. Tinga, and J. R. Laia, Jr.), Ceramic Transactions, Vol. 36, American Ceramic Society, Westerville, OH, pp. 81-88 (1993).

[Sch93b] R. L. Schulz, D. E. Clark, R. M. Hutcheon, and G. G. Wicks, "Microwave Processing of Simulated Nuclear Waste Glass II," in Microwaves: Theory and Application in Materials Processing II, (eds. D. E. Clark, W. R. Tinga, and J. R. Laia, Jr.), Ceramic Transactions, Vol. 36, American Ceramic Society, Westerville, OH, pp. 89-97 (1993).

[Sch94] R. L. Schulz, D. C. Folz, D. E. Clark, and G. G. Wicks, "Microwave Energy for Waste Remediation Applications," in Microwave Processing of Materials IV, (eds. M. F. Iskander, R. J. Lauf, and W. H. Sutton), Materials Research Society Symposium Proceedings, Vol. 347, Materials Research Society, Pittsburgh, pp. 401-406 (1994).

[Sha92] James F. Shackelford, Introduction to Materials Science for Engineers, Macmillan Publishing Company, New York, 1992.

[Sil91] Richard Silberglitt, David Palaith, W. Murray Black, H. S. Sa'adaldin, Joel D. Katz, and Rodger D. Blake, "Investigation of Interlayer Materials for the Microwave Joining of SiC," in Microwaves: Theory and Application in Materials Processing, (eds. D. E. Clark, F. D. Gac, and W. H. Sutton), Ceramic Transactions, Vol. 21, American Ceramic Society, Westerville, OH, pp. 487-495 (1991).

[Ska94] Daniel J. Skamser and D. Lynn Johnson, "Simulation of Hybrid Heating," in Microwave Processing of Materials IV, (eds. M. F. Iskander, R. J. Lauf, and W. H. Sutton), Materials Research Society Symposium Proceedings, Vol. 347, Materials Research Society, Pittsburgh, pp. 325-330 (1994).

[Smi92] Ray L. Smith, Magdy F. Iskander, Octavio Andrade, and Hal Kimrey, "Finite-Difference Time-Domain (FDTD) Simulation of Microwave Sintering in Multimode Cavities," in Microwave Processing of Materials III, (eds. R. L. Beatty, W. H. Sutton, and M. F. Iskander), Materials Research Society Symposium Proceedings, Vol.269, Materials Research Society, Pittsburgh, pp. 47-52 (1992).

[Sol93] L. Solymar and D. Walsh, Lectures on the Electrical Properties of Materials, Fifth Edition, Oxford University Press, New York, 1993.

[Ste94] Dale F. Stein, Richard H. Edgar, Magdy F. Iskander, D. Lynn Johnson, Sylvia M. Johnson, Chester G. Lob, Jane M. Shaw, Willard H. Sutton, Ping K. Tien, and Thomas E. Munns, "Microwave Processing - An Emerging Industrial Technology," in Microwave Processing of Materials IV, Materials Research Society Symposium Proceedings, Vol.347, Materials Research Society, Pittsburgh, pp. 3-7 (1994).

[Sut88] W.H. Sutton, "Microwave Firing of High Alumina Castables," in Microwave Processing of Materials, (eds. W. H. Sutton, M. H. Brooks, and I. J. Chabinsky), Materials Research Society Symposium Proceedings, Vol. 124, Materials Research Society, Pittsburgh, pp. 287-295 (1988).

[Sut89] Willard H. Sutton, "Microwave Processing of Ceramic Materials," Ceramic Bulletin, Vol. 68, no.2, pp. 376-386 (1989).

[Sut92] Willard H. Sutton, "Microwave Processing of Ceramics - An Overview," in Microwave Processing of Materials III, (eds. R. L. Beatty, W. H. Sutton, and M. F. Iskander), Materials Research Society Symposium Proceedings, Vol.269, Materials Research Society, Pittsburgh, pp. 3-20 (1992).

[Sut93] Willard H. Sutton, "Key Issues in Microwave Process Technology," in Microwaves: Theory and Application in Materials Processing II, (eds. D. E. Clark, W. R. Tinga, and J. R. Laia, Jr.), Ceramic Transactions, Vol. 36, American Ceramic Society, Westerville, OH, pp. 3-18 (1993).

[Tho95] J. R. Thomas, Jr., "Importance of Dielectric Properties in Modeling of Microwave Sintering of Ceramics," in Microwaves: Theory and Application in Materials Processing III, (eds. D. E. Clark, D. C. Folz, S. J. Oda, and R. Silberglitt), Ceramic Transactions, Vol. 59, American Ceramic Society, Westerville, OH, pp. 297-304 (1995).

[Thu92] Jacques Thuéry, Microwaves: Industrial, Scientific, and Medical Applications, Artech House, Boston, 1992.

[Tie93] T. N. Tiegs, K. L. Ploetz, J. O. Kiggans, and R. L. Yeckley, "Crystallization of Grain Boundary Phases in Silicon Nitride with Low Additive Contents by Microwave Annealing," in Microwaves: Theory and Application in Materials Processing II, (eds. D. E. Clark, W. R. Tinga, and J. R. Laia, Jr.), Ceramic Transactions, Vol. 36, American Ceramic Society, Westerville, OH, pp. 259-267 (1993).

[Tin88] Wayne R. Tinga, "Fundamentals of Microwave-Material Interactions and Sintering," in Microwave Processing of Materials, (eds. W. H. Sutton, M. H. Brooks, and I. J. Chabinsky), Materials Research Society Symposium Proceedings, Vol. 124, Materials Research Society, Pittsburgh, pp. 33-43 (1988).

[Tin93a] Wayne R. Tinga, "Microwave Material Interactions and Process Design Modeling," in Microwaves: Theory and Application in Materials Processing II, (eds. D. E. Clark, W. R. Tinga, and J. R. Laia, Jr.), Ceramic Transactions, Vol. 36, American Ceramic Society, Westerville, OH, pp. 29-43 (1993).

[Tin93b] Wayne R. Tinga and Willard H. Sutton, "Key Issues in Microwave Processing, Research and Commercialization - An Open Forum," in Microwaves: Theory and Application in Materials Processing II, (eds. D. E. Clark, W. R. Tinga, and J. R. Laia, Jr.), Ceramic Transactions, Vol. 36, American Ceramic Society, Westerville, OH, pp. 45-49 (1993).

[Tip91] Paul A. Tipler, Physics for Scientists and Engineers, Third Edition, Volume 2, Worth Publishers, New York, 1991.

[Tuc92] James Tucker, Ray Smith, Magdy F. Iskander, and Octavio M. Andrade, "Dynamic Model for Calculating Heating Patterns During Microwave Sintering," in Microwave Processing of Materials III, (eds. R. L. Beatty, W. H. Sutton, and M. F. Iskander), Materials Research Society Symposium Proceedings, Vol.269, Materials Research Society, Pittsburgh, pp. 61-67 (1992).

[Vol93] Dieter Vollath, "Some Activities of Microwave Processing of Ceramics in Germany," in Microwaves: Theory and Application in Materials Processing II, (eds. D. E. Clark, W. R. Tinga, and J. R. Laia, Jr.), Ceramic Transactions, Vol. 36, American Ceramic Society, Westerville, OH, pp. 147-156 (1993).

[von54a] Arthur von Hippel, editor, Dielectric Materials and Applications, Technology Press of MIT, Boston, 1954.

[von54b] Arthur von Hippel, Dielectrics and Waves, Wiley, New York, 1954.

[Vos91] W. A. Geoffrey Voss and H. K. Kua, "Model-Informed Microwave Processing of Materials," in Microwave Processing of Materials II (eds. W. B. Snyder, Jr., W. H. Sutton, M. F. Iskander and D. L. Johnson) Materials Research Society Symposium Proceedings, Vol. 189, Materials Research Society, Pittsburgh, pp. 3-14 (1991).

[Wen86] Wesley Wm. Wendlandt, Thermal Analysis, 3rd edition, John Wiley and Sons, New York, 1986.

[Wes99] J. K. West and D. E. Clark, "Microwave Absorption by Materials: Theory and Application," Ceramic Engineering and Science Proceedings, Vol. 20, to be published (1999).

[Wes63] W. B. Westphal, "Dielectric constant and loss measurements on high-temperature materials," Laboratory for Insulation Research Technical Report, MIT, October, 1963.

[You00] I.J. Youngs, "Dielectric Measurements and Analysis for the Design of Conductor/Insulator Artificial Dielectrics," IEE Proceedings: Science, Measurement and Technology, Vol. 147, n. 4, pp. 202-208 (2000).

[Zho93] J. P. Zhong, Z. Fathi, G. P. LaTorre, D. C. Folz and D. E. Clark, "Microwave Densification of Porous Silica Gel," in Microwaves: Theory and Application in Materials Processing II, (eds. D. E. Clark, W. R. Tinga, and J. R. Laia, Jr.), Ceramic Transactions, Vol. 36, American Ceramic Society, Westerville, OH, pp. 157-164 (1993).

[Zho94] J. P. Zhong, Z. Fathi, G. P. LaTorre, D. C. Folz, and D. E. Clark, "Microwave Condensation and Densification of Porous Silica Gel," Ceramic Engineering and Science Proceedings, Vol. 15, no. 5, pp. 1003-1010 (1994).

## BIOGRAPHICAL SKETCH

Kristie Sue Leiser was born November 3, 1973, in Mountain View, California. She attended Pioneer High School in San Jose, California, and graduated as valedictorian of her class. In the fall of 1991, she began attendance at the Univeristy of California, Los Angles, where she was very active in student organizations such as Tau Beta Pi, ASM/TMS, and the Engineering Society of the University of California. She graduated summa cum laude with a B.S. degree in Materials Engineering in March 1995. In the fall of 1995, she enrolled in the graduate program in the Department of Materials Science and Engineering at the University of Florida. She is a member of Tau Beta Pi, Keramos, the American Ceramic Society, and the National Institute of Ceramic Engineers.

I certify that I have read this study and that in my opinion it conforms to acceptable standards of scholarly presentation and is fully adequate, in scope and quality as a dissertation for the degree of Doctor of Philosophy.

David E. Clark, Chair
Professor of Materials Science and Engineering

I certify that I have read this study and that in my opinion it conforms to acceptable standards of scholarly presentation and is fully adequate, in scope and quality as a dissertation for the degree of Doctor of Philosophy.

E. Dow Whitney
Professor of Materials Science and Engineering

I certify that I have read this study and that in my opinion it conforms to acceptable standards of scholarly presentation and is fully adequate, in scope and quality as a dissertation for the degree of Doctor of Philosophy.

Hassan El-Shall
Associate Professor of Materials Science and Engineering

I certify that I have read this study and that in my opinion it conforms to acceptable standards of scholarly presentation and is fully adequate, in scope and quality as a dissertation for the degree of Doctor of Philosophy.

Christopher D. Batich
Professor of Materials Science and Engineering

I certify that I have read this study and that in my opinion it conforms to acceptable standards of scholarly presentation and is fully adequate, in scope and quality as a dissertation for the degree of Doctor of Philosophy.

J. Eric Enholm
Professor of Chemistry

This dissertation was submitted to the Graduate Faculty of the College of Engineering and to the Graduate School and was accepted as partial fulfillment of the requirements for the degree of Doctor of Philosophy.

May 2001

M. J. Ohanian
Dean, College of Engineering

Winfred M. Phillips
Dean, Graduate School